(2)

PIEZOELECTRIC AND ELECTROSTRICTIVE MATERIALS FOR TRANSDUCER APPLICATIONS

Period February 1, 1990 to January 31, 1991

Annual Report

VOLUME II

OFFICE OF NAVAL RESEARCH
Contract No. N00014-89-J-1689

L. E. Cross
R. E. Newnham
A. S. Bhalla
J. P. Dougherty
J. H. Adair
V. K. Varadan
V. V. Varadan

PENNSTATE

1855

THE MATERIALS RESEARCH LABORATORY
UNIVERSITY PARK, PA

SECURITY CLASSIFICATION OF THIS PAGE

REPORT DOCUMENTATION PAGE

Form Approved OMB No. 0704-0188

1a. REPORT SECURITY CLASSIFICATION	1b. RESTRICTIVE MARKINGS
2a. SECURITY CLASSIFICATION AUTHORITY	3. DISTRIBUTION/AVAILABILITY OF REPORT Reproduction in whole or in part is permitted for any purpose of the United States Governmer
2b. DECLASSIFICATION/DOWNGRADING SCHEDULE	
4. PERFORMING ORGANIZATION REPORT NUMBER(S) N00014-89-J-1689	5. MONITORING ORGANIZATION REPORT NUMBER(S)
6a. NAME OF PERFORMING ORGANIZATION Materials Research Laboratory 6b. OFFICE SYMBOL (If applicable)	7a. NAME OF MONITORING ORGANIZATION
6c. ADDRESS (City, State, and ZIP Code) The Pennsylvania State University University Park, PA 16802	7b. ADDRESS (City, State, and ZIP Code)
8a. NAME OF FUNDING/SPONSORING ORGANIZATION 8b. OFFICE SYMBOL (If applicable)	9. PROCUREMENT INSTRUMENT IDENTIFICATION NUMBER
8c. ADDRESS (City, State, and ZIP Code)	10. SOURCE OF FUNDING NUMBERS PROGRAM ELEMENT NO. / PROJECT NO. / TASK NO. / WORK UNIT ACCESSION NO

11. TITLE (Include Security Classification)
Piezoelectric and Electrostrictive Materials for Transducer Applications

12. PERSONAL AUTHOR(S)
L.E. Cross, R.E. Newnham, A.S. Bhalla, J.P. Dougherty, J.H. Adair, V.K. Varadan, V.V. Varadar

13a. TYPE OF REPORT	13b. TIME COVERED	14. DATE OF REPORT (Year, Month, Day)	15. PAGE COUNT
ANNUAL	FROM 2/1/90 TO 1/31/91		

16. SUPPLEMENTARY NOTATION

17. COSATI CODES			18. SUBJECT TERMS (Continue on reverse if necessary and identify by block number)
FIELD	GROUP	SUB-GROUP	

19. ABSTRACT (Continue on reverse if necessary and identify by block number)

SEE REVERSE SIDE OF PAGE.

20. DISTRIBUTION/AVAILABILITY OF ABSTRACT ☐ UNCLASSIFIED/UNLIMITED ☐ SAME AS RPT. ☐ DTIC USERS	21. ABSTRACT SECURITY CLASSIFICATION
22a. NAME OF RESPONSIBLE INDIVIDUAL	22b. TELEPHONE (Include Area Code) / 22c. OFFICE SYMBOL

DD Form 1473, JUN 86 Previous editions are obsolete. SECURITY CLASSIFICATION OF THIS PAGE

ABSTRACT

This report documents work carried out in the Materials Research Laboratory of the Pennsylvania State University over the second year of a three year program on "Piezoelectric and Electrostrictive Materials for Transducer Applications" sponsored under grant No. N00014-89-J-1689 from the Office of Naval Research.

Highlights of the year's activity include: Participation of a number of senior faculty in program to better define the role of ferroelectrics in "smart materials" and the manner in which these developing interests will impact the needs for transducers as both actuators and sensors. New progress has been made with the flextensional (moonie) type structures and with the evolution of the 1 : 3 composites towards commercial development as large area actuators.

The year has seen major advance in the understanding of the relaxor type ferroelectrics which are most useful as dielectrics and electrostrictors. It has become clear that the original superparaelectric model is only a first approximation valid for the very high temperature behaviour and that in fact both the Lead magnesium niobate and the PZT materials are close analogues of the magnetic spin glasses. Interaction between the polar micro-regions leads to a Vogel-Fulcher like slowing down and freezing, and provides understanding of the micros to macrodomain transitions, the hysteretic behaviour and the coupled elastic responses.

An essential component of the program is the excellent capability in synthesis and processing which has been developed to provide the many new compositions and controlled microstructures which are essential for the proper understanding of the properties.

The report gives a brief narrative description of the researches which are more fully documented in the published papers of the technical appendices.

PIEZOELECTRIC AND ELECTROSTRICTIVE MATERIALS FOR TRANSDUCER APPLICATIONS

Period February 1, 1990 to January 31, 1991

Annual Report

VOLUME II

OFFICE OF NAVAL RESEARCH
Contract No. N00014-89-J-1689

APPROVED FOR PUBLIC RELEASE -- DISTRIBUTION UNLIMITED

L. E. Cross
R. E. Newnham
A. S. Bhalla
J. P. Dougherty
J. H. Adair
V. K. Varadan
V. V. Varadan

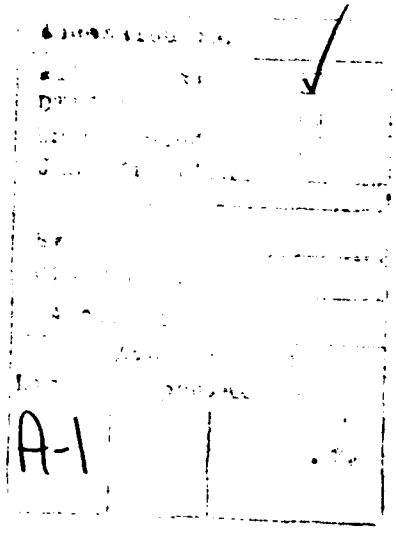

TABLE OF CONTENTS

APPENDICES

Volume I

General Summary Papers

1. R.E. Newnham and W. Huebner, "Electroceramics," Science of Advanced Materials, Chapter 9 (1990).

2. L. Eric Cross, "Polarization Controlled Ferroelectric High Strain Actuators (1990).

3. R.E. Newnham and S. Trolier-McKinstry, "Crystals and Composites," J. Appl. Cryst. 23, 447-457 (1990).

TABLE OF CONTENTS
(continued)

Smart Materials

4. R.E. Newnham and G.R. Ruschau, "Smart Electroceramics," J. Am. Ceram. Soc. 74 (3), 463-480 (1991).

5. R.E. Newnham, "Tunable Transducers: Nonlinear Phenomena in Electroceramics," National Institute of Standards and Technology Special Publication 804, Chemistry of Electronic Ceramic Materials, Proceedings of the International Conference held in Jackson, WY, August 17-22, 1990, issued January 1991.

6. D. Damjanovic and R.E. Newnham, "Electrostrictive and Piezoelectric Materials for Actuator Applications," A Section in Chapter 5 - Intelligent Materials Systems, ASME/NASA Monograph on Flight-Vehicle Materials, Structures and Dynamics Technologies - Assessment and Future Directions. Edited by Ahmed K. Noor and Samuel L. Venneri.

7. W.Y. Pan, C.Q. Dam, Q.M. Zhang and L.E. Cross, "Large Displacement Transducers Based on Electric Field Forced Phase Transitions in the Tetragonal $(Pb_{0.97}La_{0.02})(Ti,Zr,Sn)O_3$ Family of Ceramics," J. Appl. Phys. 66 (12), 6014-6023 (1989).

Composite Materials

8. Q.C. Xu, J.R. Belsick, S. Yoshikawa and R.E. Newnham, "Piezoelectric Composites with High Sensitivity and High Capacitance for Use at High Pressures," Materials Research Laboratory, The Pennsylvania State University, University Park, PA 16802.

9. A.S. Bhalla and R.Y. Ting, "Hydrophone Figure of Merit," Sensors and Materials 4, 181-185 (1989).

10. K.A. Hanner, A. Safari, R.E. Newnham and J. Runt, "Thin Film 0-3 Polymer/Piezoelectric Ceramic Composites : Piezoelectric Paints," Ferroelectrics 100, 255-260 (1989).

11. G.S. Lee, S. Kim and T.R. Shrout, "Fabrication of 0-3 Piezoelectric-Glass Composites," Sensors and Materials 2 (1), 7-15 (1990).

12. M.G. Grewe, T.R. Gururaja, T.R. Shrout and R.E. Newnham, "Acoustic Properties of Particle/Polymer Composites for Ultrasonic Transducer Backing Applications," IEEE Transactions on Ultrasonics, Ferroelectrics, and Frequency Control 37 (6), 506-514 (1990).

13. A.R. Ramachandran, Q.C. Xu, L.E. Cross and R.E. Newnham, "Passive Piezoelectric Damping," Presented at IEEE Ultrasonics Symposium (UFFC), Honolulu, Hawaii (December 1-7, 1990).

TABLE OF CONTENTS
(continued)

TABLE OF CONTENTS
(continued)

APPENDICES

Volume II

Electrostriction/Relaxor Ferroelectrics (continued)

Optical Studies

TABLE OF CONTENTS
(continued)

Optical Studies (continued)

37. D.A. McHenry, J. Giniewicz, S.J. Jang A. Bhalla and T.R. Shrout, "Optical Properties of Hot Pressed Relaxor Ferroelectrics," Ferroelectrics 93, 351-359 (1989).

38. G.R. Fox, J.K. Yamamoto, D.V. Miller, L.E. Cross and S.K. Kurtz, "Thermal Hysteresis of Optical Second Harmonic in Paraelectric $BaTiO_3$," Materials Letters 9 (7, 8), 284-288 (1990).

Preparative Studies

39. A.D. Hilton+, C.A. Randall*, D.J. Barber+ and T.R. Shrout*, "The Influence of Processing on Dielectric Properties of PMN:PT Based Ceramics." +Department of Physics, University of Essex, Colchester, United Kingdom; *Materials Research Laboratory, The Pennsylvania State University, University Park, PA 16802.

40. W.R. Xue, W.A. Schulze and R.E. Newnham, "Effects of Sm_2O_3 and Gd_2O_3 + Nd_2O_3 on Electromechanical Properties of $PbTiO_3$ Ceramics," J. Am. Ceram. Soc. 73 (6) 1783-84 (1990).

41. P. Ravindranathan, S. Komaraneni, A.S. Bhalla, L.E. Cross and R. Roy, "Solution-Sol-Gel Processing of Lead Magnesium Niobate Thin Films," Ferroelectrics Letters 12 ,29-34 (1990).

42. P. Papet, J. P. Dougherty and T.R. Shrout, "Particle and Grain Size Effects on the Dielectric Behaviour of the Relaxor Ferroelectric $Pb(Mg_{1/3}Nb_{2/3})O_3$," J. Mater. Res. 5 (12), 2902-2909 (1990).

43. J.T. Fielding, Jr., S.J. Jang and T.R. Shrout, "Thermal Degradation of Relaxor-Based Piezoelectric Ceramics," Materials Research Laboratory, The Pennsylvania State University, University Park, PA 16802.

44. N. Kim, S.J. Jang and T.R. Shrout, "Relaxor Based Fine Grain Piezoelectric Materials," Materials Research Laboratory, The Pennsylvania State University, University Park, PA 16802.

45. F.G. Jones, C.A. Randall, S.J. Jang and T.R. Shrout, "Preparation in Characterization of Indium Based Complex Perovskites - $Pb(In_{1/2}Nb_{1/2})O_3$ (PIN), $Ba(In_{1/2}Nb_{1/2})O_3$ (BIN), and $Ba(In_{1/2}Ta_{1/2})O_3$ (BIT)," Ferroelectrics Letters 12, 55-62 (1990).

46. T.R. Shrout, "Conventionally Prepared Submicron Electro-Ceramic Powders by Reactive Calcination," National Institute of Standards and Technology Special Publication 804, Chemistry of Electronic Ceramic Materials, Proceedings of the International Conference held in Jackson, WY, August 17-22, 1990, issued January 1991.

TABLE OF CONTENTS
(continued)

Preparative Studied (continued)

Miscellaneous Papers

ELECTROSTRICTION/RELAXOR FERROELECTRICS (continued)

APPENDIX 27

Accept. Phys. Rev. B

A DIPOLAR GLASS MODEL FOR LEAD MAGNESIUM NIOBATE

Dwight Viehland, J. F. Li, S. J. Jang, L. Eric Cross*

Materials Research Labratory, Pennsylvania State University

University Park, Pa. 16802

Manfred Wuttig

Engineering Materials Program, University of Maryland

College Park, Md. 20742

The static polarization of lead magnesium niobate relaxors has been studied using a standard Sawyer-Tower circuit. The square to slim loop hysteresis transition was phenomenologically modelled by modifying Neel's equation for the magnetization of a superparamagnet (1) to a similar relationship for a superparaelectric. A temperature dependent internal dipole field was included to account for cluster interactions. The slim loop polarization curves were found to scale to $E/(T-T_f)$, where E is the electric field and T_f a freezing temperature. A glassy character was subsequently proposed to exist in the zero field cooled state with local dipole fields between superparaelectric moments controlling the kinetics of the polarization reversals and the freezing process. Recent quasielastic neutron scattering results (2) have been interpreted to support this model.

I. INTRODUCTION

Lead Magnesium Niobate (PMN) is a relaxor ferroelectric. Relaxors are characterized by a dispersion of the dielectric permittivity, and an inability to sustain a macroscopic polarization until temperatures significantly below the permittivity maximum (T_{max}). Burns (3,4) has shown that a local polarization exists to temperatures far above T_{max} indicating that the local symmetry is lower than the global. Randall (5) and Harmer (6) have shown in PMN that there is a partitioning on the nanometer scale into clusters which are chemically ordered and disordered. Cross (7) suggested that the size of these cluster is such that the polarization may be thermally reversible, analogous to superparamagnetism (1). He has recently proposed that a coupling between polar clusters controls the kinetics of the polarization fluctuations and the development of a frustration near a freezing temperature (T_f), similar to spin glasses (8). T_f was determined by analyzing the frequency dispersion of T_{max} with the Vogel-Fulcher relationship, and was shown to agree with the temperature at which a stable remanent polarization collapsed. Similar phenomenological modelling has been used in spin glasses (9,10).

In the zero field cooled (ZFC) state the structure of a relaxor appears cubic indicating that the scale of the polar behavior is smaller than the coherence length of x-rays, however in the field cooled (FC) state the structure appears rhombohedral. Optical microscopy reveals no domain structure in the ZFC state, but normal micron-sized domains are observed in the FC state. Cross (11) has investigated the field dependence of the dielectric and elastic responses. He found the maximum nonlinearities near T_f. Bokov and Myl'nikova (12) and Smith (13) have previously investigated the static polarization. They found a large hysteresis at lower temperatures, but with increasing temperature it decreased; i.e. the so-called square to slim loop transition.

Spin glasses are magnetic systems which cannot establish long range magnetic ordering in the ZFC state due to some form of a chemical or structural inhomogeneity. The glassy behavior is believed to arise due to competing interactions between magnetic moments resulting in a freezing of the magnetization reversals below a characteristic temperature (T_f). Freezing has been shown to occur due to random fields between clusters (14,15) and a competition between ferromagnetic and antiferromagnetic exchanges (16,17). The FC state exhibits behavior resembling a normal ferromagnet below T_f, i.e. irreversibility and hysteresis (18).

II. EXPERIMENTAL PROCEDURE and RESULTS

The samples used in this study were PMN ceramics with 10 at.% PT (PMN-10PT). They were prepared as described by Pan and Cross (19). The samples were free of ageing as described by Pan (19), were free of pyrochlore as described by Shrout (20), they were of dimensions 1cm x 0.5cm x 0.03cm, and were electroded with gold. The hysteresis loops were measured as a function of temperature using a standard Sawyer and Tower circuit. Measurements were made between 150 and -50°C on cooling. The samples were allowed to equilibrate for 30 minutes at each temperature. The cycling frequency was 50 Hz, and the maximum bias applied was 20 kV/cm. To decrease the low frequency impedance, a large capacitance (10 μF) was placed in series with the sample.

Static polarization curves are shown in Figures 1(a)-(d) at measurement temperatures of -50, 10, 50, and 110°C respectively. The experimental data are the closed circles, and the solid line is a phenomenological model which will be presented. The square to slim loop hysteresis transition is evident in the figures. The polarization behavior became hysteretic near and below T_{max}. The saturation polarization was approximately 20 C/m^2 at lower temperatures. It was not possible to drive the sample into saturation at higher temperatures because breakdown

occurred. Above 25°C the remanence was so small that determination of the coercive field was difficult, but at lower temperatures it increased rapidly.

III. DISCUSSION

In systems consisting of nano-scale ferromagnetic or ferroelectric clusters the thermal energy of the particle can strongly influence the macroscopic magnetic or polar properties. These clusters are designated as superparamagnetic or superparaelectric, respectively. The magnetic behavior with no anisotropy can be described by a Langevian function, but real systems have an anisotropy which acts as an energy barrier for reorientation as originally proposed by Neel (1). The polarization behavior of an ensemble of uniform non-interacting clusters having uniaxial symmetry can be described by equation 1 (1);

$$p = \mathrm{Tanh}\left[\frac{EP}{kT}\right] \qquad (1)$$

where p is the reduced polarization, E the electric field, P the moment of the cluster, and kT the thermal energy. A consequence of equation 1 is that the polarization curves at different temperatures should superimpose when plotted against E/T, the analogous behavior has been observed for numerous superparamagnets (21,22,23). The implication of the superposition is that at higher temperatures it takes more electrical energy to align the moments against the thermal energy. The slim-loop hysteresis curves of PMN-10PT did not superimpose when plotted against E/T as shown in Figure 2, p is obviously more strongly temperature dependent. This may be a reflection of interactions between polar regions. Interactions might be accounted for by including a phenomenological freezing temperature. T_f has been previously estimated as 18°C for PMN-10PT (8). The polarization curves plotted as a function of $E/(T-T_f)$ are shown in Figure 3. It is obvious that the polarization curves nearly superimpose.

Interactions between superparamagnetic clusters have been reported to alter magnetization curves. Local internal Lorentz fields have been used to obtain an understanding of the magnetic behavior in these systems (24,25). A relationship for a superparaelectric cluster having rhombohedral symmetry including an internal dipole field is given in equation 2;

$$p = \frac{\sinh\left[\frac{P(E+\alpha p)}{kT}\right]}{\cosh\left[\frac{P(E+\alpha p)}{kT}\right] + 3\cosh\left[\frac{P\cos 70(E+\alpha p)}{kT}\right]} \quad (2)$$

where p is the reduced polarization, and α the internal field. The hysteresis curves were modelled by a nonlinear least squares fitting to equation 2, shown as the solid lines in Figures 1(a)-(d). The fitting was done by allowing the temperature changes to be absorbed by α. P can be approximated as $P_S V$, where P_S is the saturation polarization and V the cluster volume. P_S is approximately 20 C/m^2, and the cluster diameter has been found to be between 20 and 50 A^o (5,6). Assuming an average diameter of $35A^o$, P can be estimated as $5x10^{-25}$ C-cm. A normalized internal bias ($\gamma=P\alpha/kT$) as a function of temperature is shown in Figure 4. The reduced remanent polarization (p_r) can be approximated by setting E=0 in equation 2. Nonzero solutions for p_r will only exist when $\gamma>4$ which occurred between 10 and 20^oC. p_r as a function of temperature is shown as the inset of Figure 4. The temperature dependence of p_r was calculated by using the experimental values for γ, but close to T_f γ was determined by interpolation. These results are consistent with the experimental polarization (8,12).

The magnetization and polarization of spin and dipole glasses are known to be irreversible below T_f (18,26,27,28). The irreversibility is believed to arise due to the onset of nonergodicity. In particular if Sawyer-Tower measurements are made hystersis is observed (18,28). This hystersis has been shown to decrease with

temperature (29), somewhat similar to PMN. The scaling of the polarization to $E/(T-T_f)$ in PMN-10PT is strongly suggestive of a glassy mechanism, whereas the polarization equation of state was derived for a rhombohedral superparaelectric moment. Binder and Young (17) have suggested that interacting superparamagnetic moments should be treated as spin glasses. It is proposed that the polarization of the relaxor is glassy due to interactions between superparaelectric moments. In the ZFC state, the lack of macroscopic polarization indicates that the moments freeze into random orientations devoid of long range order. Local dipole fields may try to polarize neighboring moments over a distance of a correlation length, as illustrated in Figure 5. But if the dispersion in the fields is larger than the average field, long range ordering is impossible. In the FC state the moments freeze into ordered configurations, charateristic of a normal ferroelectric. A somewhat similar superpara-glassy model has been proposed for $K_{1-x}Li_xTaO_3$ (KTL), for x=0.026 (27).

Recent quasielastic neutron scattering (QES) results (2) on PMN revealed a temperature dependent correlation length (λ) similar to spin glasses (30), shown in Figure 6. Near 400°K, λ was 50 A° which is approximately equal to the cluster size observed by TEM (4,5). In the temperature interval below 225°K, λ was nearly temperature independent with a maximum value of 200 A°. This data can be interpreted to support the hypothesis that relaxors are interacting superparaelectric moments. The scale of λ supports the argument that the glassy character arises due to random fields between moments on the mesoscopic level. The agreement of λ with the average size of the clusters at higher temperatures supports the argument that the moments are decoupled from each other behaving as ideal superparaelectrics. On cooling λ increased supporting the model of a temperature dependent internal field which couples the moments more strongly. For comparison T_f has been estimated to be 217°K by analyzing the dispersion of T_{max} using the

Vogel-Fulcher relationship, shown as the solid line in the inset of Figure 6. This is close in temperature to the saturation of λ, a strong broadening of the relaxation time distribution (31), and the collapse of the remanent polarization. This indicates that the saturation of λ at 200 A^o may occur by the system freezing into local configurations of moment orientations, possibly by balancing the average orientation of nearest and next nearest neighbors effectively charge compensating the local polarization.

Various reasons have been proposed to explain the existence of short range order in dipolar glasses. The glassy behavior in KTL is believed to arise by a coupling of the Li defect structure to a soft mode lowering the local symmetry and stabilizing ferroelectric clusters (32,33). In KCl:OH^-, OH^- dipoles are believed to exist which have six orientations; local dipole fields are believed to couple the moments resulting in glassy behavior (34). The low temperature phases of RbH_2PO_4 (RDP) and $(NH_4)H_2PO_4$ (ADP) are ferro- and anti-ferroelectric, respectively; frustrated interactions are believed to lead to glassy behavior in their solid solution (RADP) (35). PMN is probably a normal ferroelectric which cannot establish long range polar order due to gross inhomogeneities, i.e. the partioning (phase seperation) on the nanometer scale (5,6). Local polarization may form where allowed by this "fossil chemistry" via local ferroelectric transitions, dipole fields between moments then subsequently lead to glassy behavior.

V. CONCLUSION

Static polarization curves for PMN were parameterized using a superparaelectric model which included an internal dipole field. Local randomly orientated dipole fields between superparaelectric moments are believed to exist in the zero field cooled state leading to a freezing of the polarization fluctuations. A dipole glass model for relaxors was subsequently proposed.

ACKNOWLEDMENTS

This work has been supported in full by contracts adminstered through the Office of Naval Research. Acknowledgement must also be expressed to Dr. S. Vakhrushev for the use of his published data.

* Also in the Electrical Engineering Department

REFERENCES

1) L. Neel, Compt. Rend. Acad. Sci. **228**, 664 (1949).

2) S. Vakhrushev, B. Kvyatkovsky, A. Naberezhnov, N. Okuneva, B. Topervers, Ferroelectrics **90**, 173 (1989).

3) G. Burns, F. Dacol, Sol. State Com. **48**, 10, 853 (1983).

4) G. Burns, F. Dacol, Sol. State Com. **58**,9, 567 (1986).

5) C. Randall, A. Bhalla, T. Shrout, L. E. Cross, J. Mat. Sci. **29**, 5 (1990).

6) J. Chen, H. Chan, M. Harmer, J. Am. Cer. Soc. **72**, 593 (1989).

7) L. E. Cross, Ferroelectrics **76**, 241 (1987).

8) D. Viehland, S. Jang, M. Wuttig, L. Cross, J. Appl. Phys. **68**, 2916 (1990).

9) J. Tholence, J. Appl. Phys. **50**, 7369 (1979).

10) J. Tholence, Sol. State Com. **35**, 113 (1980).

11) D. Viehland, S. Jang, M. Wuttig, L. Cross, Accept. into J. Appl. Phys.

12) V. Bokov, I. Myl'nikova, Sov. Phys. Sol. State **3**, 3 (1960).

13) James W. Smith, PhD Dissertation, The Pennsylvania State University (1967).

14) P. Nozav, V. Sechovsky, V. Kambersky, J. Mag. and Magnetic Mat. **69**, 71 (1987).

15) A. Morgownik, J. Mydosh, Phys. Rev. B **24**, 5277 (1981).

16) S. Kirkpatrick, D. Sherrington, Phys. Rev. B **17**, 4384 (1978).

17) S. Edwards, P. W. Anderson, J. Phys. F **5**, 765 (1975).

18) K. Binder, A. Young, Rev. Mod. Phys. **58**, 4, 860 (1986).

19) W. Pan, Q. Jiang, L.E. Cross, J. Am. Cer. Soc. 71, C-17 (1988).

20) S. Swart, T. Shrout, Mat. Res. Bull. **17**, 1245 (1982).

21) W. Henkelom, J. Brodeder, L. Van Reijen, J. Chim. Phys. **32**, 3 (1958).

22) M. Mayer, E. Vogt, Z. Naturforsh **79**, 334 (1952).

23) C. Bean, I. Jacobs, J. Appl. Phys. **27**, 1448 (1950).

24) E. Vogt, W. Henning, A. Hahn, "Bericte Arbeitsgemeimschaft Ferromagnetismus 1958", page 43.

25) F. Luborsky, P. Lawerence, J. Appl. Phys. **32**, suppl. 231S (1961).

26) K. Lyons, Pl Fleury, T. Negran, H. Carter, Phys. Rev. B **36**, 2465 (1987).

27) U. Hochli, P. Kofel, M. Maglione, Phys. Rev. B **32**, 4546 (1985).

28) J. Prejan, M. Joliclerc, P. Monad, J. Phys. **41**, 427 (1980).

29) S. Senoussi, J. Phys. **45**, 315 (1984).

30) G. Aeppli., S. Shapiro, H. Maletta, R. Birgeneau, H. Chen, J. Appl. Phys. **55**, 1629 (1984).

31) N. Yushin, Proceedings of Ferroelektrizitat 1988, 102, Halle, GDR.

32) G. Samara, Jap. J. Appl. Phys. **24**, supl. 24-2, 80 (1985).

33) B. Vugmeister, M. Glinchuck, Sov. Phys. JETP **52**, 3, 482 (1980).

34) M. Klein, C. Held, E. Zuroff, Phys. Rev. B **13**, 8, 3576.

35) E. Courtens, T. Rosenbaum, S. Nagler, P. Horn, Phys. Rev. B **29**, 515 (1984).

LIST OF FIGURES

Figure 1. Polarization curves at various temperatures. The solid points are the experimental data and the solid line is the curve fitting to equation 2. Figures (a)-(d) are at measurement temperatures of -50, 10, 50, and 110°C respectively.

Figure 2. Reduced polarization plotted as a function of the temperature normalized electric field at various temperatures. The arrow visually illustrates the direction of increasing temperature. The polarization curves shown are at temperatures of 39, 48, 54, 59, 69, 86, 110°C.

Figure 3. Reduced polarization at various temperatures plotted as a function of $E/(T-T_f)$ where T_f is the freezing temperature. The polarization curves shown are at temperatures of 39, 48, 54, 59, 69, 86, 110°C.

Figure 4. Reduced internal field ($\gamma=P\alpha/kT$) as a function of temperature where T_f is the freezing temperature. The inset shows the reduced remanent polarization (p_r) as a function of temperature as calculated from equation 3.

Figure 5. The correlation length as determined by quasielastic neutron scattering as a function of temperature where T_f is the freezing temperature. This data is taken from Vakrushev (2). The inset shows the modelling of the frequency dependence of the temperature of the dielectric relaxation with the Vogel-Fulcher relationship where the solid points are the experimental data and the solid line is the curve fitting.

Figure 6. Proposed model for freezing in PMN where E is a local internal dipole field which acts to couple the polar clusters. The open circles represent the polar clusters.

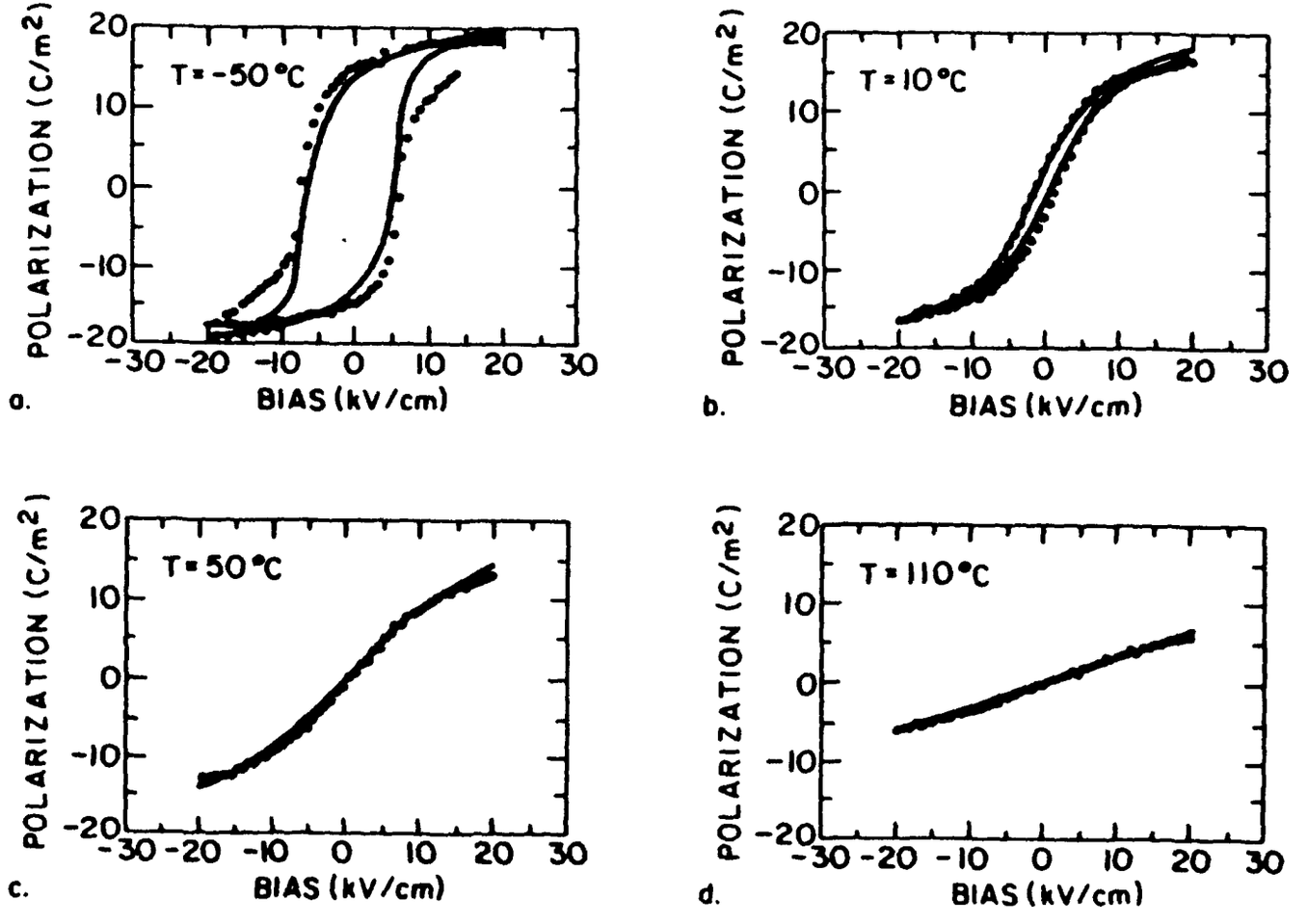
T = -50 °C
T = 10 °C
T = 50 °C
T = 110 °C
POLARIZATION (C/m²)
BIAS (kV/cm)
20
10
0
-10
-20
-30 -20 -10 0 10 20 30
a.
b.
c.
d.

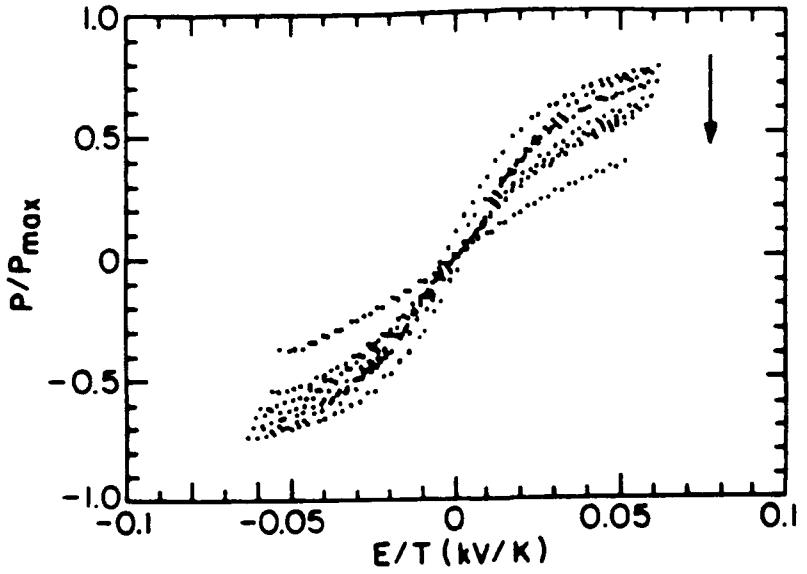
1.0
0.5
0
-0.5
-1.0
P/P_max
-0.1
-0.05
0
0.05
0.1
E/T (kV/K)

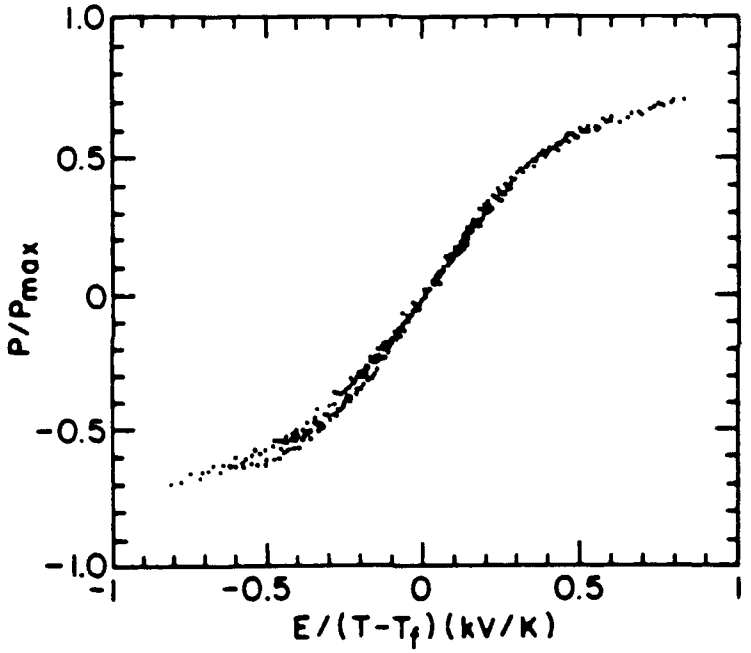
1.0
0.5
0
-0.5
-1.0
P/P_max
-1
-0.5
0
0.5
1
E/(T-T_f) (kV/K)

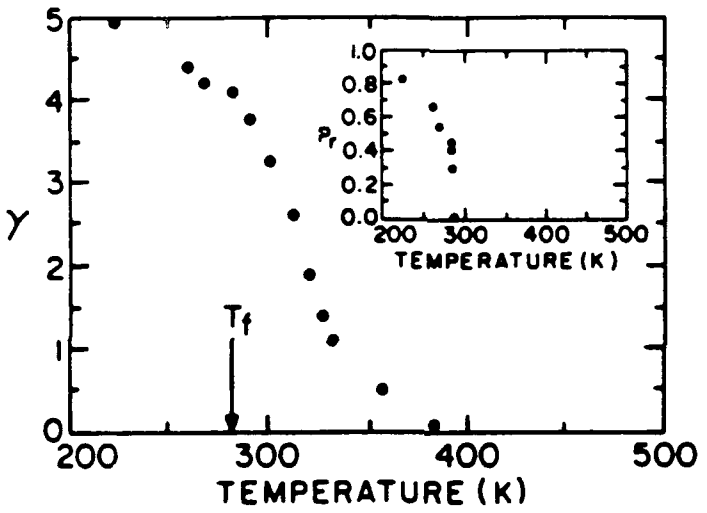
5
4
3
2
1
0
Y
200
300
400
500
TEMPERATURE (K)
T_f
1.0
0.8
0.6
0.4
0.2
0.0
P_r
200
300
400
500
TEMPERATURE (K)

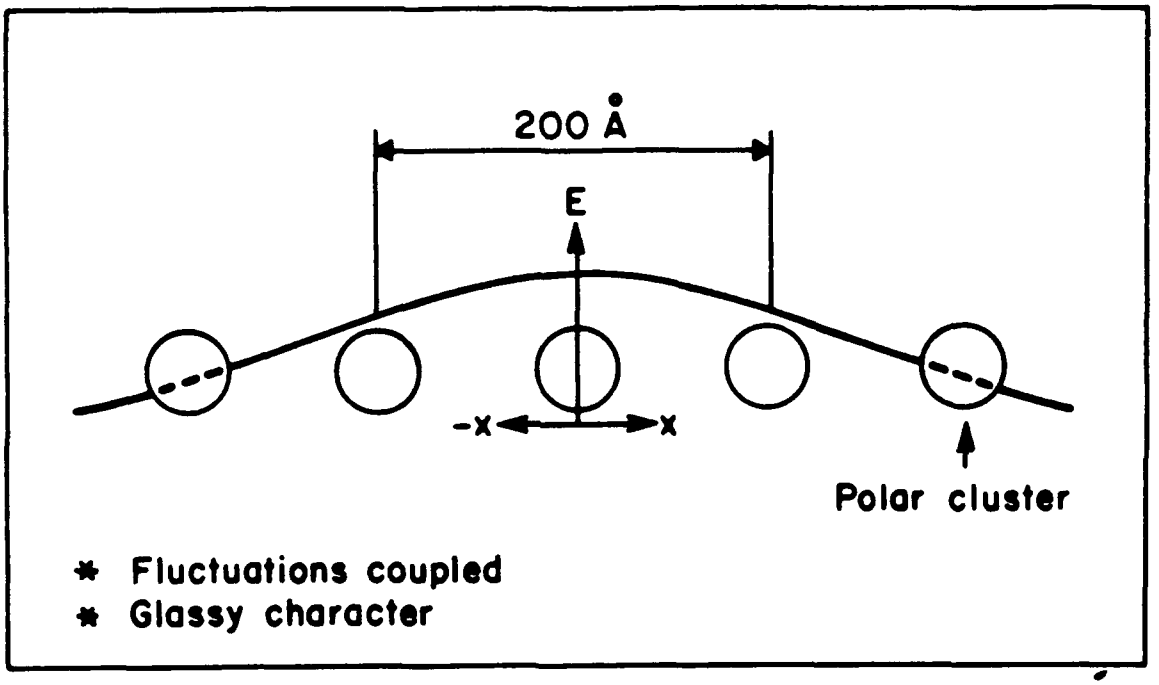

* Fluctuations coupled
* Glassy character

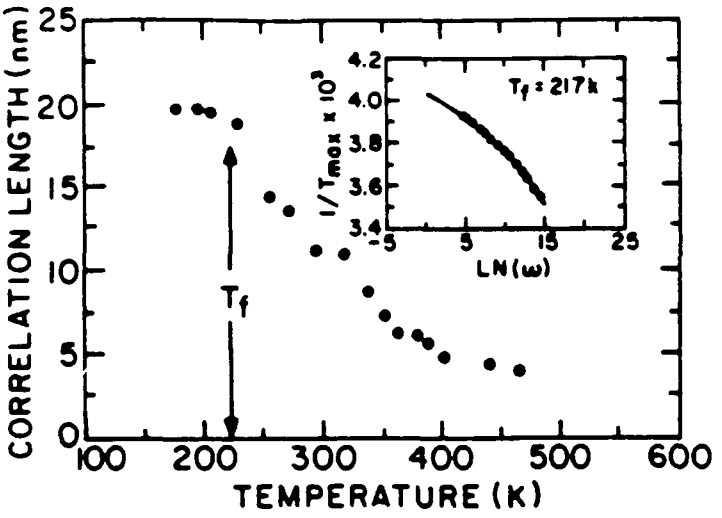
CORRELATION LENGTH (nm)
25
20
15
10
5
0
100
200
300
400
500
600
TEMPERATURE (K)
T_f
$1/T_{max} \times 10^3$
4.2
4.0
3.8
3.6
3.4
-5
5
15
25
LN(ω)
T_f = 217k

APPENDIX 28

Accept. Phil. Mag. B

ANELASTIC RELAXATION AND INTERNAL STRAIN IN LEAD MAGNESIUM NIOBATE RELAXORS

Dwight Viehland, S. J. Jang, L. Eric Cross*

Materials Research Laboratory, Pennsylvania State University

University Park, Pa. 16802

Manfred Wuttig

Dept. of Materials and Nuclear Engineering, University of Maryland

College Park, Md. 20742

ABSTRACT

Non-linear internal friction measurements have been carried out on lead magnesium niobate with 10 atomic% lead titanate. The purpose of these measurements was to investigate the field dependence of the elastic and anelastic responses, and to determine how the response depends on the amplitude of an applied stress. The linear elastic response was found to stiffen at all bias levels with the maximum electroelastic coupling occurring near the Vogel-Fulcher freezing temperature. A strong frequency dependence of the kinetics of the anelastic relaxation was found at low measurement frequencies. These data are compared to recent high frequency results. The existence of an inhomogeneous internal strain has been found from the line broadening of the (220) and (321) diffraction peaks. On application of an electrical field the internal strain is relieved by the development of a macrostrain which is shown to be the electrostrictive strain. It is proposed that the local electrostrictive strains are dynamic in nature and are at the origin of the anelastic relaxation. Strong elastic non-linearities, both an elastic softening and hardening under stress, have also been observed. These results are interpreted as a stress activation of the internal deformation process.

I. INTRODUCTION

Lead magnesium niobate (PMN) is a classic relaxor ferroelectric. Relaxors are ferroelectric materials which exhibit a diffuse phase transformation in which there is a strong frequency dispersion of the dielectric response at temperatures near the permittivity maximum (T_{max}). On heating from a poled state the remanent polarization is known to collapse at temperatures significantly below the permittivity maximum (Bokov and Myl'nikova 1960). The depolarization under an electric field is known to occur over a broader temperature interval (Xi, Zhilli, and Cross 1983). An RMS polarization, as calculated from the index of refraction, is known at temperatures far above T_{max} (Burns and Dacol 1983) which shows that a local polarization exists to much higher temperatures than that which a macroscopic polarization can be sustained. Smolenski's (Smolenski and Agranovska 1960) original model of relaxors was based on the concept of local variations of the transition temperature due to compositional heterogeneity. Randall (Randall and Bhalla 1989) more recently has observed contrast on the nanoscale in PMN using TEM which he believed to be due to short-range chemical ordering. Cross (Cross 1987) has proposed that local polar regions form where allowed by this short range chemical order, i.e. the so called "fossil chemistry", by a lowering of the local symmetry through ferroelectric distortions. He has further proposed that the frequency dispersion arises due to a thermal activation of the direction of spontaneous polarization, analogous to superparamagnetism. The frequency dispersion of T_{max} has recently been found to exhibit a Vogel-Fulcher type freezing (Viehland, Jang, Wuttig, and Cross 1990a), and the freezing temperature was found to correlate with the collapse of the remanent polarization.

Relaxors are known to have a large electrostrictive strain (Jang 1979), and to be strong non-linear materials electrically (Shrout 1980) (Glass 1969). The phenomena underlying the dielectric relaxation then might also be reflected into the

elastic properties. Yushin (Yushin, Smironova, Dorogortsev, Smirnov and Galayamov 1987) has recently investigated the anelastic response of PMN in the megahertz regime. He found that the magnitude and kinetics of the relaxation were frequency independent. Elastic non-linearities have been previously known to arise from domain wall motion (Wuttig and Lin 1983) and nucleation (Anning and Wuttig 1984). In general, these elastic non-linearities are believed to be a macroscopic reflection of a strain driven microscopic deformation process. The purpose of this work was to investigate the anelastic response in the low frequency regime and to determine if the response is dependent on the magnitude of the applied stress, i.e. elastically non-linear.

II. EXPERIMENTAL PROCEDURE

The elastic properties were studied using a non-linear internal friction technique developed by Wuttig and Suzuki (Anning, Suzuki, and Wuttig 1982). A diagram of the experimental apparatus is given in Figure 1. The technique uses a long thin vibrating reed which is externally driven through the natural resonance by a magnetic gradient acting on a small permanent magnet attached to the reed. The mechanical response of the reed to the driving force was measured capacitively by pick-up capacitors using a technique developed by Tomboulian (Tomboulian 1961). The samples were driven into the non-linear regime which resulted in asymmetric resonance curves. Measurements were made using increasing and decreasing frequency sweeps to obtain the complete asymmetry of the resonance curves. The resonance curves were then analyzed using a non-linear least squares fit to an empirical response relationship developed by Nayfeh (Nayfeh 1979) given in equation 1;

$$\omega = \omega_0 + \frac{3}{8}\left(\frac{\alpha a^2}{\omega_0}\right) \pm \frac{1}{2}\sqrt{\left(\frac{K}{\omega_0 a}\right)^2 - \delta^2} \qquad (1)$$

where ω_o represents the resonance frequency, α the non-linear elastic constant, δ the linear anelastic constant (damping), K the external excitation, and a the RMS amplitude of vibration of the sample.

Resonance curves were measured as a function of temperature on heating between 250 and 420°K, with resonance frequencies of approximately 10, 100, and 400 Hz. Measurements were done as a function of bias, the bias levels used were 0, 1, 2, 3, 4, 5, 6, 7, 8, 10, 12, and 15 KV/cm. X-ray line broadening measurements were also done using a position sensitive detector to supplement the data base. Measurements were made as a function of bias on the (200), (220), and (321) peaks at 25 and 0°C. The dielectric constant and polarization were also measured as a function of temperature for comparison using standard techniques.

The samples used in this study were PMN ceramics with 0 and 10 at% PT (PMN-10PT). They were prepared as described by Pan and Cross (Pan, Jiang, and Cross 1988). The samples were free of ageing as described by Pan, were free of pyrochlore as described by Shrout (*Swartz and Shrout* 1982), and were electroded with gold. Stoichiometric ageing free samples were used to avoid a potential complication of the relaxation mechanism by a time varying defect structure. Supplementary measurements were also done on La-modifed lead zirconate titanate (PLZT) with Zr/Ti ratio of 65/35 and a La content of 9 atomic%. The PLZT samples were donated by Honeywell Inc. of Bloomington, Minnesota.

III. RESULTS

Sample resonance curves are given in Figures 2.a-2.d for PMN-10PT at 270, 292, 310 and 340°K, respectively. Each Figure contains resonance curves under bias levels of 0, 5, and 10 KV/cm. These curves were chosen to illustrate the field dependence of the resonance curves at various temperatures. An electrical field increased the resonance frequency, and decreased the mechanical losses. At lower temperatures the resonance curve characterized a linear oscillator. As the

temperature was increased the resonance curve bent to lower frequencies with increasing displacement (elastically soft under stress), and on a further increment of the temperature the resonance curve bent to higher frequencies with increasing displacement (elastically hard under stress). The effect of a DC bias was to decrease the magnitude of the nonlinearity.

IV. DISCUSSION

The insertion of any local distortion into a crystalline lattice produces internal strains. Anelastic behavior is a manifestation of the relaxational kinetics of this internal deformation process. In PMN the anelastic response can be anticipated to reflect the kinetics of the polarization fluctuations which can couple the applied stress to the internal strain through the electrostriction. The elastic stiffness of PMN over a wide range of temperatures is illustrated in Figure 3. The elastic stiffness started to soften around 600°K which is close to the temperature of the onset of local polarization as originally shown by Burns (Burns and Dacol 1983). The implication is that the insertion of polarization into the prototypic phase softens the lattice, via the electrostriction. The agreement of the temperature of the maximum in the 100 Hz elastic softening with the temperature of the 100 Hz permittivity maximum, shown in Figure 4, illustrates that the relaxational processes in both responses does have a common origin. The dielectric relaxation has been shown to be glassy due to interactions between superparaelectric moments (Viehland, Jang, Wuttig, and Cross 1990a). The implication is that the anelastic relaxation may also be glassy due to local electrostictive strain fields.

Figures 5(a)-(d) illustrate the field dependence of the stiffness at various temperatures. The points in these figures are the experimental data, and the solid line is the curve fitting to equation 2;

$$c(E) = c(0) + \beta E^2 + \eta E^4 \qquad (2)$$

where c is the elastic stiffness, and β and η are the fourth and sixth order electoelastic couplings respectively. The experimental data was modelled using a nonlinear least squares fitting to equation 2, solving for β and η. β as a function of temperature is shown in Figure 6. The maximum electroelastic nonlinearities occurred near 15°C. The freezing temperature has been estimated to be 18°C by modelling the frequency dependence of T_{max} using the Vogel-Fulcher relationship (Viehland, Jang, Wuttig and Cross 1990a) which is close to the temperature of the maximum electroelastic nonlinearities. The modelling of the dielectric relaxation is shown as the inset of Figure 6. These results indicate that the local electrostrictive strains are dynamical in nature and undergo a Vogel-Fulcher type freezing corresponding to the freezing of the polarization fluctuations. This can be interpreted to mean that the polarization fluctuations do not occur within a rigid framework, but rather inside of a soft framework which deforms in response to the polarization fluctuations. The maximum nonlinearities in the electroelastic response, then, occurs near the freezing temperature where a DC biasing field can most effectively repopulate the states. Yushin (Yushin 1988) has reported a similar anomaly in the electroacoustic behavior near 210°K for PMN in the zero field cooled state.

An electrical field stiffened the elastic response at all bias levels. If the softening of the linear elastic stiffness is solely related to the introduction of polarization into the lattice, then application of an electrical field should further soften the lattice because it would stabilize more polarized regions. A possible explanation of this discrepancy is that the inhomogeneity in the internal strain field, both in the frozen and dynamical states, enhances the deformation mechanism. Consequently on application of an electrical field the lattice stiffens as the randomness of the strain field is destroyed. The elastic behavior of PMN may be similar to the orientational glassy state proposed for $(KBr)_{1-x}(KCN)_x$ (Knorr,

Volkmann, and Loidl 1986) (Knorr 1987) in which quadrupolar interactions between elastic dipoles leads to a freezing of the anelastic response. It is proposed here that quadrupolar interactions between polar clusters in PMN contribute to the freezing process, and that the corresponding frustration is partially orientational in nature. The main difference between the glassy response in PMN and $(KBr)_{1-x}(KCN)_x$ is the scale of the inhomogeneity in the strain field. In relaxors this scale is on the order of 50-100 A^o (Randall and Bhalla 1989) (Chen, Chan, and Harmer 1989), where as in $(KBr)_{1-x}(KCN)_x$ it is several unit cells. The glassy contribution to the elastic softening consequently would be expected to be much less for PMN than for $(KBr)_{1-x}(KCN)_x$, which is experimentally observed. In the tungsten bronze family of relaxors, an electrical field has been found to soften the lattice (Shrout 1980). The difference in the elastic behavior of the PMN family of relaxors and the tungsten bronzes, can be understood by the differences in their structures. The structure of the tungsten bronzes are prototypic tetragonal with only two ferroelectric domain states. Consequently the interaction of the electrostrictive deformation with an applied stress does not reveal any internal strain. PMN is rhombohedral having non-180^o variants which can contribute to an inhomogeneous internal strain if the cluster moments freeze in a random manner.

The (220) diffraction peak for PMN-10PT at various bias levels is shown in Figure 7(a) and (b) at 25 and 0^{o}C, respectively. The width of the peak decreased and the peak shifted to lower 2θ values with increasing bias. Upon removal of the field the width and the peak position returned to the unbiased values at 25^{o}C, but remained at the biased values at 0^{o}C. These results support the model of an inhomogeneity in the local strain field which has an instability to an applied bias. The inability of the inhomogeneity to recover after removal of the bias below the freezing temperature gives further evidence of the dynamical nature of the local electrostrictive strains above T_f. The shifting of the peak position shows that a

macrostrain develops from the inhomogeneous internal strain during electrification. The shift in the peak position ($\Delta 2\theta$) was approximately 0.1^{o} between 0 and 10 KV/cm. The lattice strain associated with this shift can be approximated by equating the Bragg relationships at both biases and solving for $\Delta d/d_1$ as given in equation 3;

$$\varepsilon = \frac{\Delta d}{d_1} = 1 - \frac{\sin(2\theta_1)}{\sin(2\theta_1+\Delta 2\theta)} \qquad (3)$$

where ε is the lattice strain, d_1 and d_2 are the lattice constant under 0 and 15 KV/cm respectively, and Δd is defined as d_1-d_2. $\Delta d/d_1$ can then be approximated as $5x10^{-4}$ which is comparable to the electrostrictive strain (Jang 1979). This shows that the large electrostrictive strains in these materials are not due to induced polarization, but rather to the relief of the internal strain by the development of a macrostrain. Hysteresis then occurs in the field dependence of the strain behavior below T_f.

The 100 Hz internal friction as a function of bias at T_f is shown in Figures 8. The maximum field dependence was also found near T_f. The internal friction initially increased until 3 KV/cm, then decreased upon further increment of the field. The coexistence of both dielectric and anelastic relaxation requires that the piezoelectric response (d33) must also be dispersive (Nowick and Heller 1965), which has recently been observed (Pan, Gu, Taylor, and Cross 1989). The maximum response and strongest relaxation in d33 were also observed near this threshold bias (3KV/cm). This means that at the threshold bias a small applied stress can most effectively repopulate the equivalent variants, consequently the mechanical losses are maximum. The threshold bias can be interpreted to mean that in the unelectrified state the orientations of the superparaelectric moments are not completely random, but rather there are local equilibrium configurations of moment orientations as previously proposed from the field dependence of the dielectric response (Viehland, Jang, Wuttig, and Cross 1990b). A small bias then acts to

override these configurations, enhancing the fluctuation kinetics and the magnitude of the relaxation. It is probable that the short range ordering in these configurations is determined in part by the local electrostrictive strain fields. Khachaturyan (Khachaturyan and Shatalov 1969) has previously shown that local strain fields between inclusion can lead to short range ordering of their "elastic dipoles". At bias levels above threshold, the internal friction decreased probably because of the relief of the internal strain and the longer range nature of the dipolar interactions.

The effective third order elastic constant of PMN as a function of temperature under zero bias is illustrated in Figure 9. The maximum softening of this constant occurred slightly below the temperature of the 100 Hz permittivity maximum. The maximum bending of the resonance curve under stress at T_{max} in the unelectrified state can be estimated to be 1 Hz (see Figure 2(c)) which is approximately 0.8%. This translates into a 1.5% decrease in the elastic energy by the nonlinearities. This contribution is not small in consideration of the inhomogeneous nature of the applied stress. It is obvious that the elastic softening occurs when the frequency of the polarization fluctuations nearly coincides with the driving frequency of the AC stress field. The maximum elastic softening probably occurs when the polarization can most effectively respond to the biasing strain. Below this temperature, the fluctuations are essentially frozen with respect to the time scale of the measurement. The natural elastic hardening, consequently, is observed at higher temperatures when the kinetics of the deformation process becomes much faster than the applied AC stress. The softening of the elastic response shows that the kinetics of the internal deformation process can be driven by an applied AC stress. Higher order elastic constants usually characterize the stress dependence of the velocity of an elastic wave and/or the nonlinear interactions between "elastic dipoles" (Wallace 1970). It is proposed that the microscopic origins of the softening arises due to interactions between cluster moments, both dipolar and quadrapolar, which in part

control the kinetics of the deformation process. A potential well diagram which illustrates the effect of an applied stress along a (111) variant is shown in Figure 10. If T<Tmax the applied stress lowers the activation energy by γ_p, consequently the repopulation kinetics along the axis of the stress is enhanced and the elastic response is soft . If T>Tmax the applied stress is shown to push against the walls of the wells, consequently the elastic response is hard. The third order elastic constant under 5 KV/cm is also illustrated in Figure 9(a). An electrical field decreased the softening and increased the temperature of its maximal response. The third order elastic constant as a function of bias at the temperature of the permittivity maximum is shown in Figure 9(b). The elastic response is essentially linear under 10 KV/cm. The reason for the decrease in the magnitude of the elastic softening can be understood as a reflection of the decrease in the inhomogeneity of the local strain fields on electrification. Consequently the deformation process is less stress sensitive and the magnitude of the softening of the lattice under stress decreases.

The internal friction of PMN has been reported to be frequency independent between 5 and 50 MHz (Yushin, Smironova, Dorogortsev, Smirnov, and Galayamov 1987). The internal friction of PMN at various frequencies between 100 Hz and 50 MHz is shown in Figure 10(a). The maximum loss and temperature of its half maximum value are plotted as a function of frequency in Figure 10(b). It is obvious that the kinetics of the relaxational process is temperature dependent in only the low frequency regime, whereas the magnitude of the relaxation is relatively frequency independent. A possible explanation for this behavior is that the thermal fluctuations of the local electrostrictive strains cannot follow above a certain frequency. Further evidence for such behavior in relaxors can be found in the temperature dependence of the line broadening of the diffraction peaks in PLZT-8.7 (Darlington 1989). These results are illustrated in Figures 11(a)-(c). The broadening of the (200) peak starts near the onset of local polarization, and seems

to saturate near 560°K. Where as the broadening of the (220) and (321) peaks continuously increases between approximately 560 and 250°K. This shows that the inhomogeneity in the strain field associated with the volume deformation saturates when an inhomogeneity in the shear deformation ((220) and (321) peaks) starts to develop. A possible explanation is that at high temperatures near the onset of reversible polarization, the rhombohedral strain of the individual ferroelectric distortions is largely suppressed due to their emergence in an elastically stiff matrix. The matrix is soft dielectrically (high permittivity) so that polarization can occur, but elastically the rhombohedral variants are cubically clamped. Consequently the strain fields associated with the volume deformation is inhomogeneous and static. At lower temperatures, as the kinetics of the polarization fluctuations slow down due to the build up of correlations, the polar regions may be able to lower their free energy by deforming in a correlated manner which preserves the cubic dimensions. Inversion of the polarization leaves the elastic environment unchanged, but the rotation of the polarization involves rearrangements of the local elastic minima. The free energy may then be lowered by allowing the local strain fields to become dynamic, consequently an inhomogeneity in the shear strain develops. The implication is that the anelastic and dielectric relaxation time distributions do not need to be equivalent, but rather varying differences between the two may occur as a function of temperature or frequency depending on whether the polarization is free to deform or clamped. At lower temperatures near T_f the relaxation time distributions would be very similar. For comparison the Vogel-Fulcher freezing temperature of PLZT-9 has been estimated as 265°K which is close in agreement with the temperature of the saturation in the broadening of the (220) and (321) peaks.

A model of a temperature dependent relaxation time spectrum is presented in Figure 12(a) for the anelastic response. A model previously proposed for the

dielectric response is shown in Figure 12(b) for comparison (Viehland, Jang, Wuttig, and Cross 1990a). These models are not quantitative, but are qualitatively consistent with the experimental observations. The isothermal width for both spectra is shown to become very broad near T_f with the mean value (τ_{ave}) approaching the macroscopic time regime. Relaxation is also shown to exist to temperatures significantly below T_f as a reflection of the size dispersion of the moments. Above T_f the isothermal widths of the relaxation time spectrums continuously sharpens with increasing temperature. The shortest relaxation time (τ_{min}) for the anelastic relaxation is shown to approach a critical frequency (τ_{clamp}) at which point the anelastically active orientations are becoming inaccessible to the polarization due to the stiffening of the matrix. This frequency is shown to be much lower than the Debye frequency (τ_d). Upon further increment of the temperature τ_{ave} and τ_{max} are shown to approach τ_{clamp} for the anelastic response. The maximum value of the distribution is shown to be relatively frequency independent to reflect the weak frequency dependence of the relaxation magnitude. The maximum value of the distribution for the anelastic response is shown to be smaller than that for the dielectric response to illustrate the relative magnitudes of their respective losses.

IV. CONCLUSION

Evidence for a Vogel-Fulcher type freezing of the anelastic response has been found. It has subsequently been proposed that the freezing process in relaxors is partially controlled by randomly orientated local electrostrictive strain fields. The existence of an internal strain which decreases on electrification has been confirmed by line broadening of the (220) diffraction peak. The frequency dependence of the anelastic relaxation has also been investigated. It has been found that the kinetics of the anelastic relaxation is substantially different than the dielectric relaxation at higher frequencies. A softening of the elastic response to the amplitude of the applied stress has also been found which was explained as a stress activation of the internal deformation process.

ACKNOWLEDGMENTS

This work has been supported in full by contracts adminstered through the Office of Naval Research. Recognition and appreciation must be given to Drs. N. Yushin and C. Darlington for the use of their published data. Further appreciation is expressed to Drs. Jacques J. Van der Klink and Gerhard Barsch for providing references and ideas.

REFERENCES

Anning, A., Wuttig, M., J. Phys. Chem. Solids **45**, 481 (1984).

Anning, A., Suzuki, T., Wuttig, M., J. Appl. Phys. **53**, 10, 6797 (1982).

Bokov, V., Myl'nikova, I., Sov. Phys. Sol. State **3**, 3 (1960).

Burns, G., Dacol., F., Sol. State Com. **48** (10), 853 (1983).

Chen, J., Chan, H., Harmer, M., J. Am. Cer. Soc. **72**, 593 (1989).

Cross, L., Ferroelectrics **76**, 241 (1987).

Darlington, C., Phys. Stat. Sol. (a) **113**, 63 (1989).

Glass, A., J. Appl. Phys. **40** (12), 4699 (1969).

Jang, S., PhD Dissertation, The Pennsylvania State University, 1979.

Knorr, K., Volkmann, U., Loidl, A., Phys. Rev. Lett. **57** (20), 2544 (1986).

Knorr, K., Proceedings of 7th Conf. of Condensed Mat. Div. of European Phys. Soc., Pisa, Italy 1987.

Khachaturyan, A., Shatalov, G., Sov. Phys. Sol. State **11** (1), 118 (1969).

Nayfeh, A., NONLINEAR OSCILLATIONS (page 166), J. Wiley and Son (1979).

Nowick, B., Heller, W., Advan. Phys. **14**, 101 (1965).

Pan, W., Jiang, Q., Cross, L., J. Am. Cer. Soc. **71** (1988).

Pan, W., Gu, W., Taylor, D., Cross, L., Jap. J. Appl. Phys **28** (4), 653 (1989).

Randall, C., Bhalla, A., Shrout, T., Cross, L., 7th Internal Meeting of Ferroelectricity, Saurbrucken, FRG (1989).

Shrout, T., PhD Dissertation, The Pennsylvania State University, 1980.

Smolenski, G., Agranovska, A., Sov. Phys. Sol. State **1**, 1429 (1960).

Swartz, S., Shrout, T., Mat. Res. Bull. **17**, 1245 (1982).

Tomboulian, R., IBM Research Report, RC-396 (1961).

Viehland, D., Jang, S., Wuttig, M., Cross, L., To be published in J. Appl. Phys. Sept. 1990.

Viehland, D., Jang, S., Wuttig, M., Cross, L., Submitted to J. Appl. Phys.

Wallace, D., Sol. State Phys. **25**, 302 (1970).

Wuttig, M., Lin, C., Acta Met. 1117 (1983).

Xi, Y., Zhilli, C., Cross, L., Ferroelectrics **54**, 163 (1983).

Yushin, N., Smironova, E., Dorogortsev, S., Smirnov, S., Galayamov, G., Sov. Phys. Sol. State **29** (10), 1693 (1987).

Yushin, N., Proceedings of Ferroelektrizitat 1988, 102, Halle, GDR.

LIST OF FIGURES

temperatures where ϵ is the RMS value of the stress and γ_p the change in the activation energy.

Figure 11. (a) Mechanical damping of PMN as a function of temperature at various frequencies. The frequencies shown are 0.1 and 2.3 KHz, and 7, 10, 20, and 50 MHz. The MHz data was taken from Yushin (2). (b) Maximum of the internal friction (Q^{-1}_{max}) and temperature of its half maximum value as a function of the measurement frequency for PMN-10PT.

Figure 12. X-ray diffraction peaks as a function of temperature for PLZT-8.7 (65/35) taken from Darlington (28) where T_B is the Burn's temperature and T_f the freezing temperature. (a) the (200) peak, (b) the (220) peak, and (c) the (321) peak.

Figure 13. Diagram illustrating the proposed temperature dependent relaxation time spectrum where $G(\tau)$ is the number of micro-polar regions having a relaxation time τ. (a) Anelastic distribution, (b) dielectric distribution.

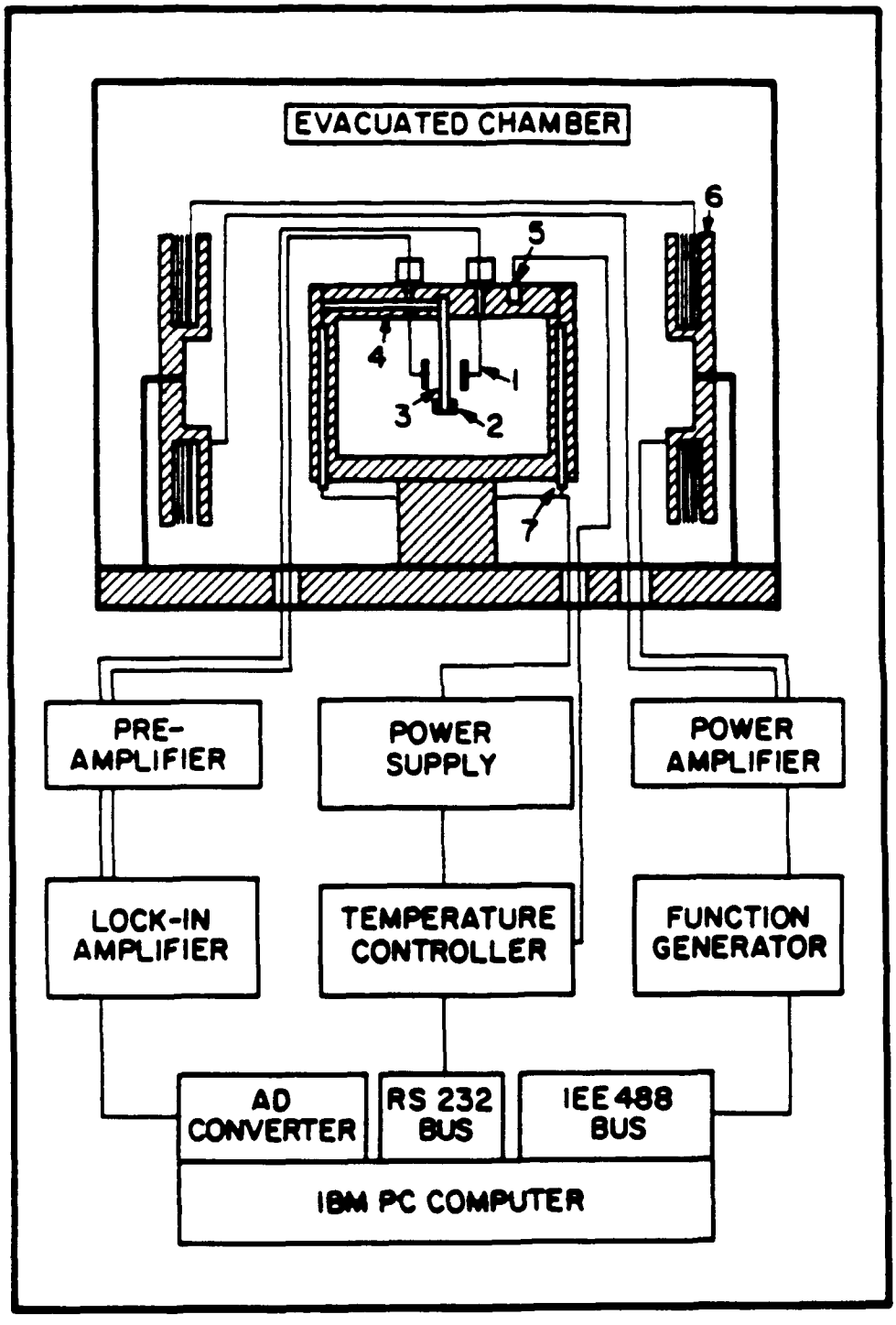
EVACUATED CHAMBER
6
5
4
1
3
2
7
PRE-
AMPLIFIER
POWER
SUPPLY
POWER
AMPLIFIER
LOCK-IN
AMPLIFIER
TEMPERATURE
CONTROLLER
FUNCTION
GENERATOR
AD
CONVERTER
RS 232
BUS
IEE 488
BUS
IBM PC COMPUTER

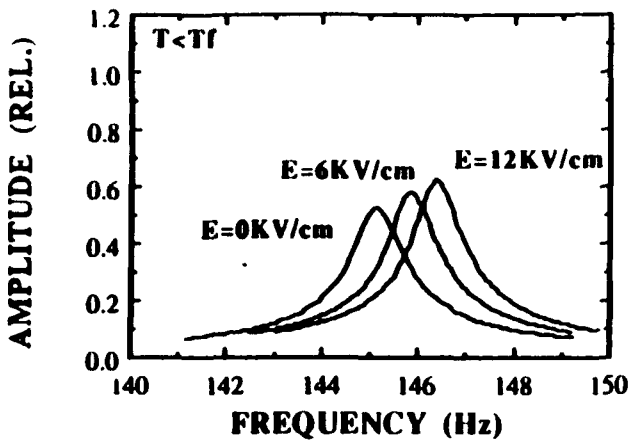
T<Tf
E=0KV/cm
E=6KV/cm
E=12KV/cm
AMPLITUDE (REL.)
FREQUENCY (Hz)
1.2
1.0
0.8
0.6
0.4
0.2
0.0
140
142
144
146
148
150

a.

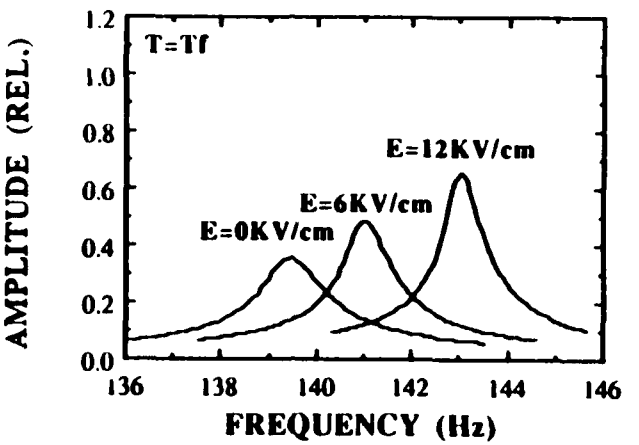
T=Tf
E=0KV/cm
E=6KV/cm
E=12KV/cm
AMPLITUDE (REL.)
FREQUENCY (Hz)
1.2
1.0
0.8
0.6
0.4
0.2
0.0
136
138
140
142
144
146

b.

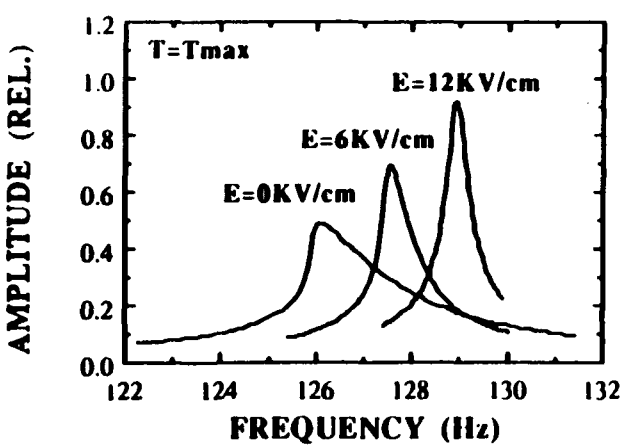
T=Tmax
E=0KV/cm
E=6KV/cm
E=12KV/cm
AMPLITUDE (REL.)
FREQUENCY (Hz)
1.2
1.0
0.8
0.6
0.4
0.2
0.0
122
124
126
128
130
132

c.

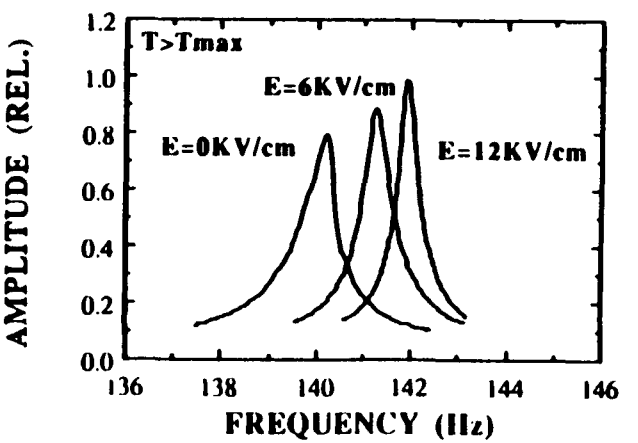
T>Tmax
E=0KV/cm
E=6KV/cm
E=12KV/cm
AMPLITUDE (REL.)
FREQUENCY (Hz)
1.2
1.0
0.8
0.6
0.4
0.2
0.0
136
138
140
142
144
146

d.

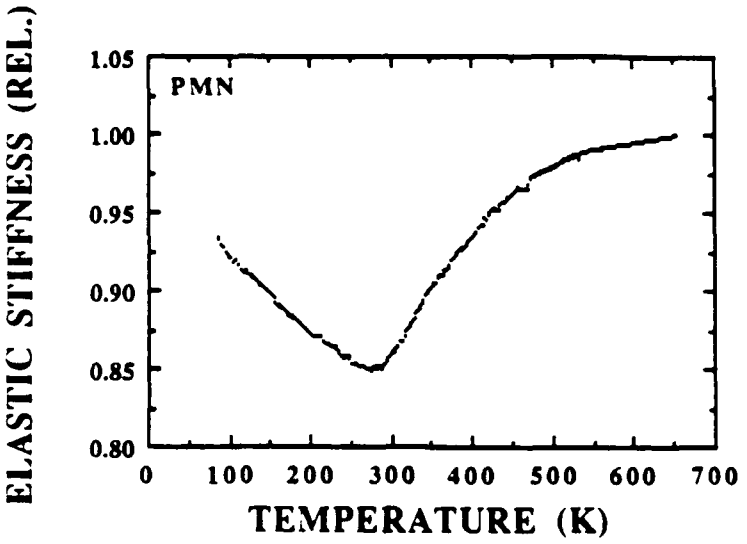
ELASTIC STIFFNESS (REL.)
PMN
1.05
1.00
0.95
0.90
0.85
0.80
0
100
200
300
400
500
600
700
TEMPERATURE (K)

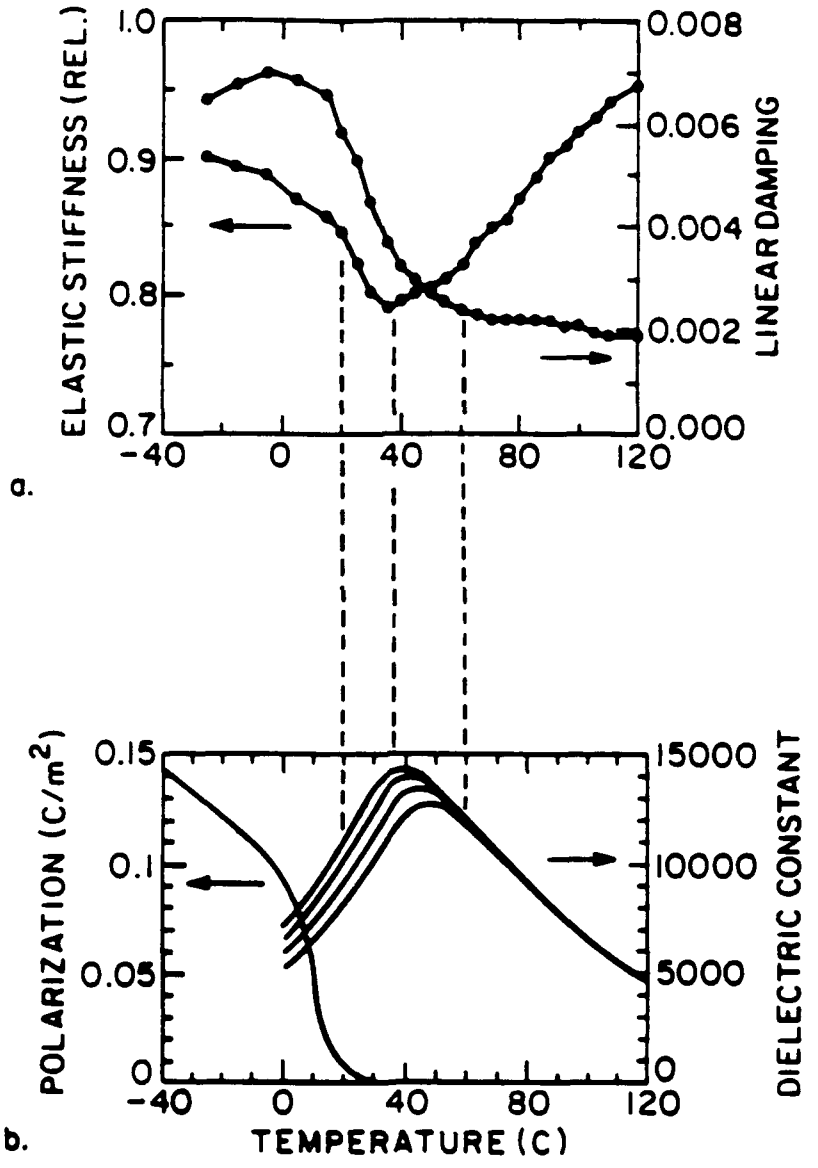
ELASTIC STIFFNESS (REL.)
1.0
0.9
0.8
0.7
0.008
0.006
0.004
0.002
0.000
LINEAR DAMPING
-40
0
40
80
120
a.
POLARIZATION (C/m²)
0.15
0.1
0.05
0
15000
10000
5000
0
DIELECTRIC CONSTANT
-40
0
40
80
120
TEMPERATURE (C)
b.

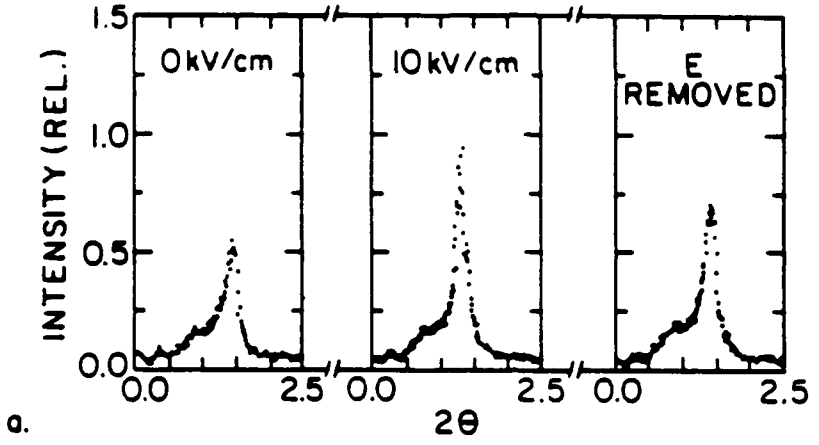
1.5
1.0
0.5
0.0
INTENSITY (REL.)
0 kV/cm
10 kV/cm
E
REMOVED
0.0
2.5
0.0
2.5
0.0
2.5
2θ

a.

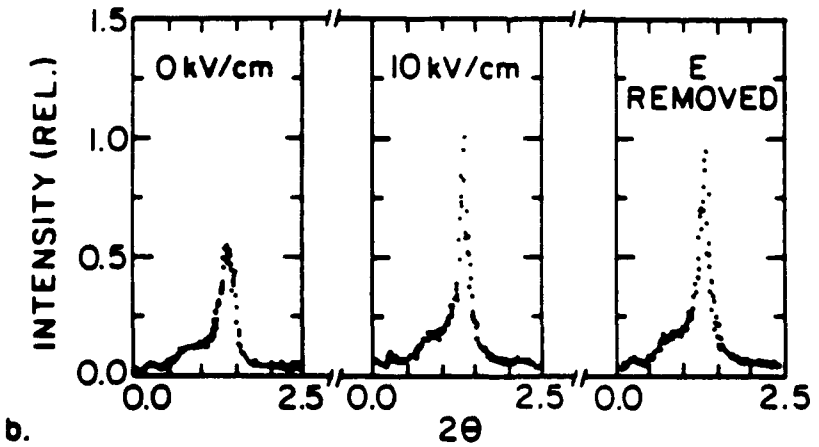
1.5
1.0
0.5
0.0
INTENSITY (REL.)
0 kV/cm
10 kV/cm
E
REMOVED
0.0
2.5
0.0
2.5
0.0
2.5
2θ

b.

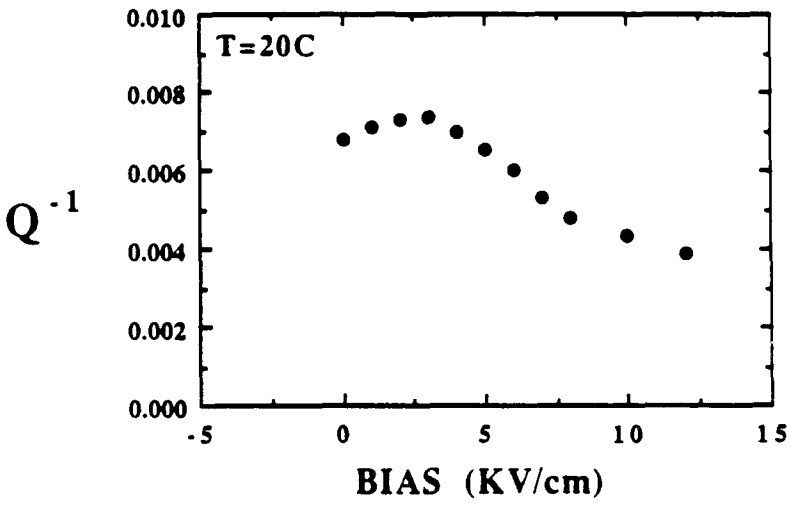
T=20C
0.010
0.008
0.006
0.004
0.002
0.000
-5
0
5
10
15
Q-1
BIAS (KV/cm)

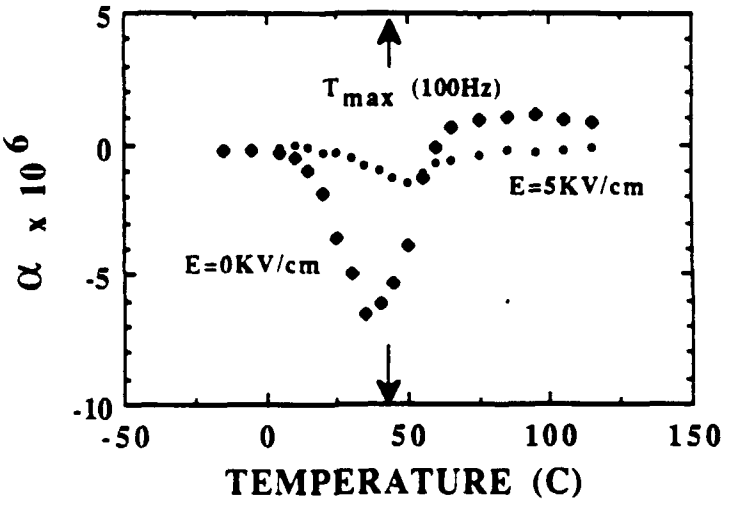
5
0
-5
-10
-50
0
50
100
150
α x 10^6
T_max (100Hz)
E=5KV/cm
E=0KV/cm
TEMPERATURE (C)

a.

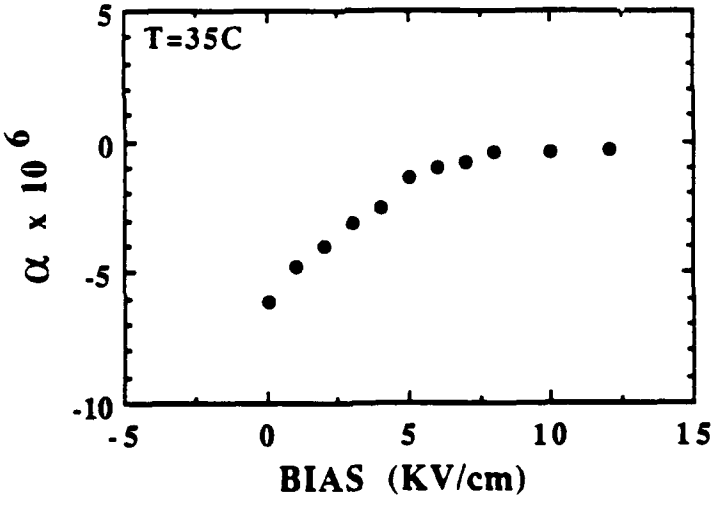
5
0
-5
-10
-5
0
5
10
15
α x 10^6
T=35C
BIAS (KV/cm)

b.

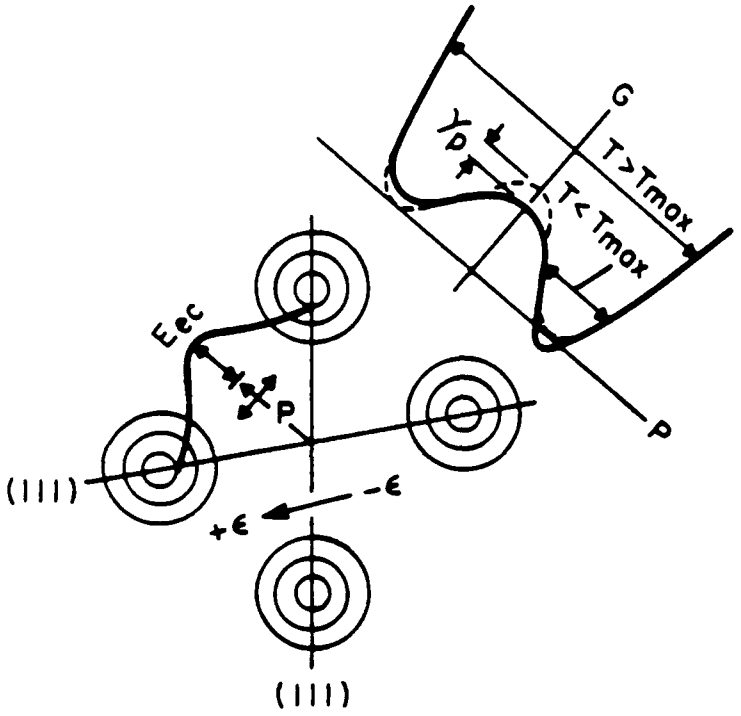
G
T>Tmax
T<Tmax
P
Eec
P
(111)
-ε
+ε
(111)

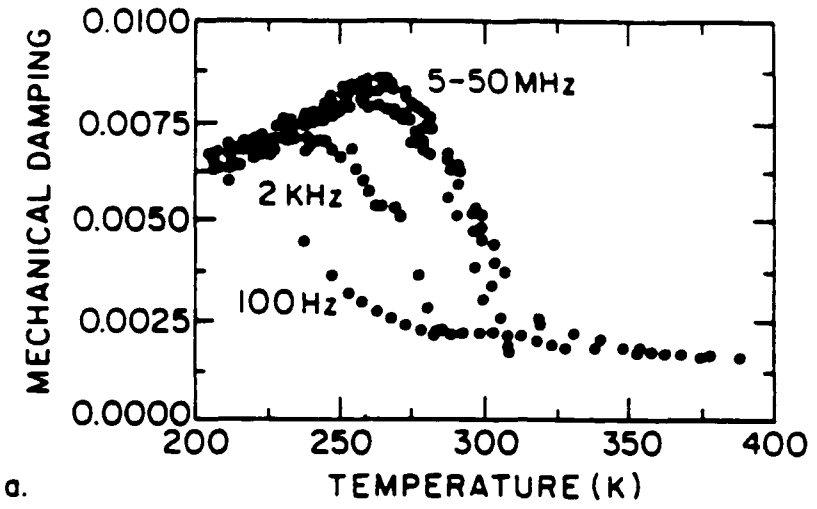
MECHANICAL DAMPING
0.0100
0.0075
0.0050
0.0025
0.0000
5-50 MHz
2 KHz
100 Hz
200
250
300
350
400
TEMPERATURE (K)

a.

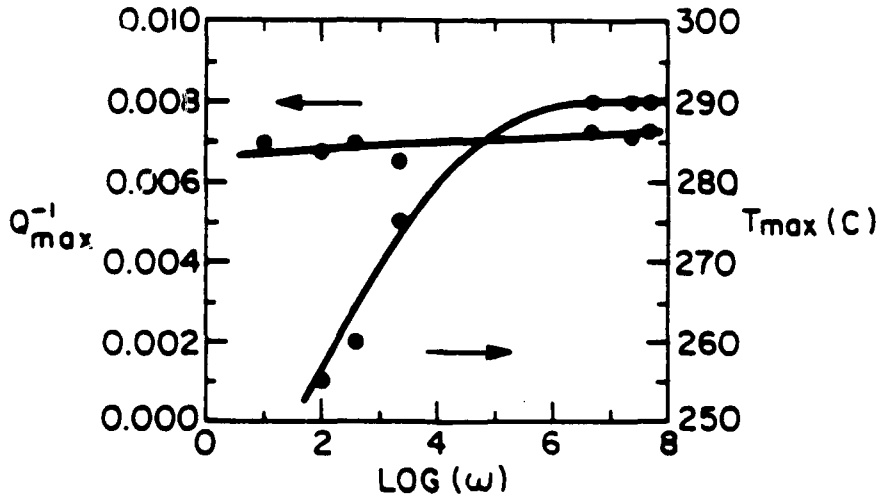
0.010
0.008
0.006
0.004
0.002
0.000
Q^{-1}_{max}
300
290
280
270
260
250
Tmax (C)
0
2
4
6
8
LOG (ω)

b.

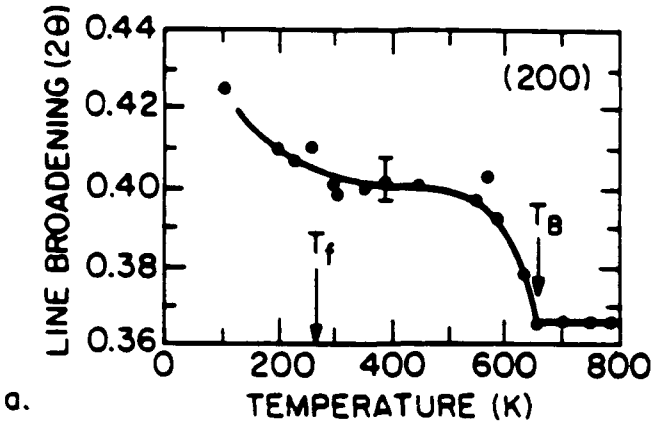
LINE BROADENING (2θ)
0.44
0.42
0.40
0.38
0.36
(200)
T_B
T_f
0
200
400
600
800
TEMPERATURE (K)

a.

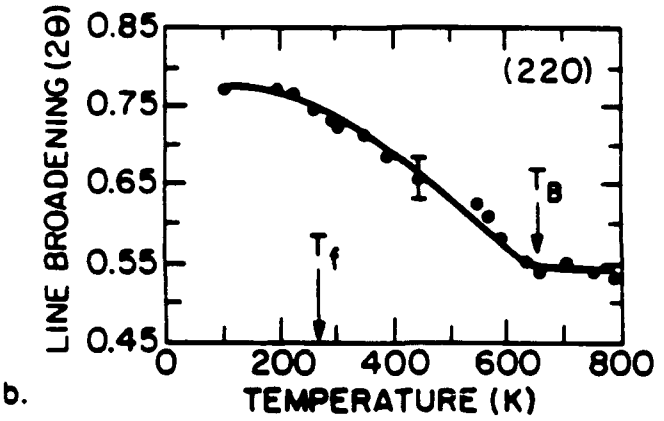
LINE BROADENING (2θ)
0.85
0.75
0.65
0.55
0.45
(220)
T_B
T_f
0
200
400
600
800
TEMPERATURE (K)

b.

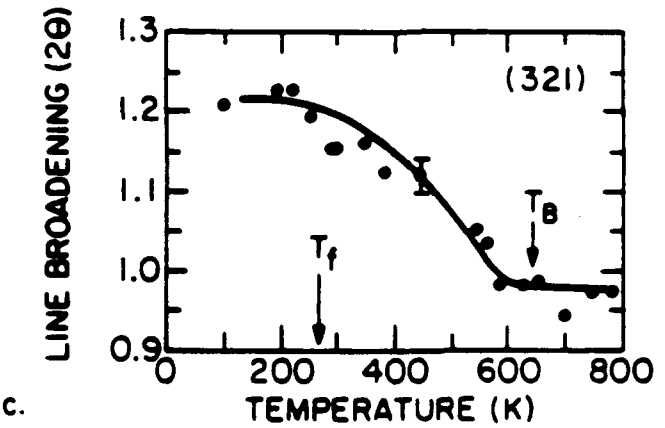
LINE BROADENING (2θ)
1.3
1.2
1.1
1.0
0.9
(321)
T_B
T_f
0
200
400
600
800
TEMPERATURE (K)

c.

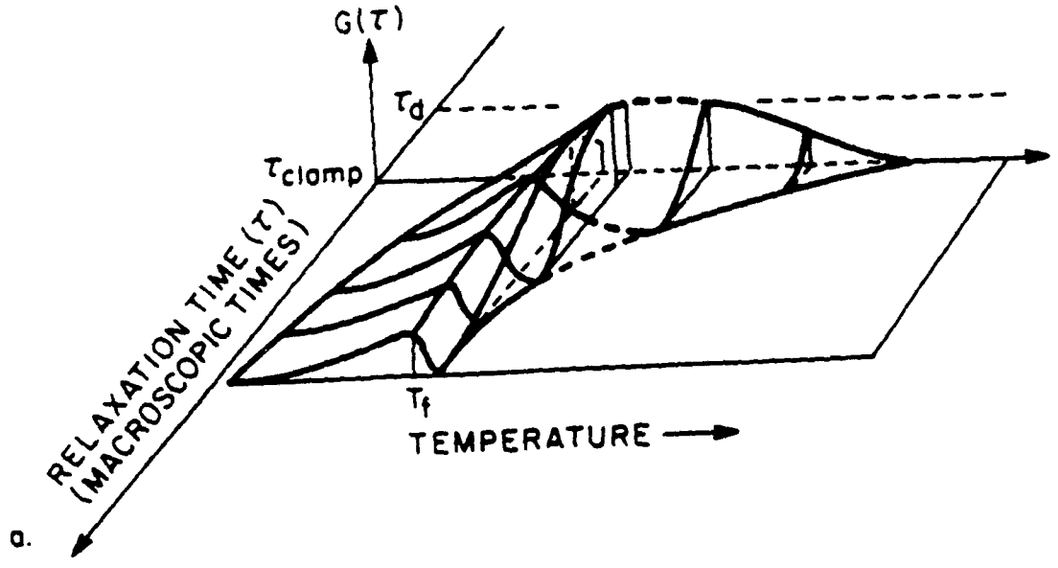
G(τ)
τd
τclamp
RELAXATION TIME (τ)
(MACROSCOPIC TIMES)
Tf
TEMPERATURE

a.

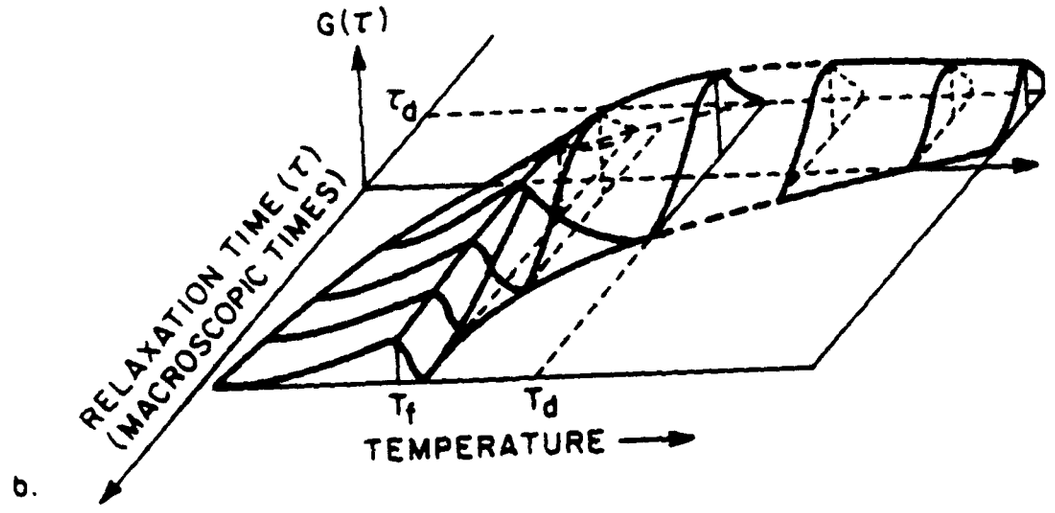
G(τ)
τd
RELAXATION TIME (τ)
(MACROSCOPIC TIMES)
Tf
Td
TEMPERATURE

b.

APPENDIX 29

Accpt. in J. Appl. Phys

INTERNAL STAIN RELAXATION DUE TO THE TILTING OF THE OXYGEN OCTAHEDRA AND THE GLASSY BEHAVIOR OF LA MODIFIED LEAD ZIRCONATE TITANATE RELAXORS

Dwight Viehland, S. J. Jang, L. Eric Cross*

Materials Research Laboratory, Pennsylvania State University

University Park, Pa. 16802

Manfred Wuttig

Dept. of Materials and Nuclear Engineering, University of Maryland

College Park, Md. 20742

ABSTRACT

Non-linear internal friction measurements have been carried out on La modified lead zirconate titanate relaxors with a Zr/Ti ratio of 65/35. Measurements have been made as a function of La content and DC bias. The elastic softening is believed to have a ferroelastic contribution due to the tilting of the oxygen octahedra, in addition to the expected electrostrictive effects. The temperatures of the maximum softening form a plausible extension to the rhombohedral rhombohedral phase boundary (1). A frequency dependence of the softening has also been found which was interpreted as the existence of fluctuations in the orientations of the tilts. These fluctuations are proposed to arise in an attempt to partially relieve an inhomogeneity in the electrostrictive strains associated with the polarization fluctuations. The results are discussed in context with previously reported transmission electron microscopy work (2). Dielectric measurements have also been done as a function of La content and bias, and the freezing temperature of the polarization fluctuations determined as a function of composition. A revised phase diagram has been proposed using this data base which shows different phase fields having various combinations of freezing mechanisms.

I. INTRODUCTION

Lanthanum modified lead zirconate titanate solid solutions (PLZT) with La contents between 5 and 14 atomic% and with a Zr/Ti ratio of 65/35 are relaxors. Relaxors are ferroelectrics which exhibit a classic dielectric relaxation, and have the inability to sustain a macroscopic polarization until temperatures significantly below the radio frequency permittivity maxima. Burns (3) has shown that an RMS (local) polarization exists in PLZT upto the transition temperature for pure PZT (623^{o}K). He subsequently proposed a glassy polarization mechanism. Cross has proposed that the orientations of the local moments are thermally reversible (4), analogous to superparamagnetism. He has recently shown (5) that interactions between superparaelectric moments control the kinetics of the polarization fluctuations, and the onset of a frozen state below a characteristic temperature (T_f). The implication is that the frustration is incipient from higher temperatures into the frozen state. Smolenski's original model of relaxors (6) was based on the concept of local variations of the transition temperature due to compositional heterogeneity. Randall more recently has shown using transmission electron microscopy (TEM) that in PLZT antiphase boundaries separate regions which have a doubling of the unit cell. He subsequently proposed that it was the scale of an inhomogeneity which predetermines the relaxor behavior (7).

Meitzler and O'Bryan (1) have investigated the elastic behavior of PLZT for La contents less than 6 atomic%. The temperature of the maximum elastic softening was found at significantly lower temperatures than the maximum in the dielectric permittivity. The temperatures of the maximum softening were instead found to form a plausible extension to the rhombohedral rhombohedral phase boundary of the PZT phase diagram. Yushin (8) has recently investigated the elastic stiffness of PLZT-9 (65/35). He found that the temperature of the maximum elastic softening nearly coincided with the temperature of the permittivity maximum for this

composition, similar to lead magnesium niobate (PMN) (9). Beige has also investigated the elastic properties of PLZT (10). The purpose of this work is to investigate the field and compositional dependence of the elastic response at various frequencies, and to determine if the elastic response is dependent on the amplitude of the applied stress. The intention is to determine the glassy behavior for the various La contents, and to compare this behavior to the PMN family of relaxors.

II. EXPERIMENTAL PROCEDURE

The samples used in this study were PLZT (65/35) with La contents of 6, 6.5, 7, 7.5, 8, 8.5, 9, 10, 12, and 14 atomic%. The samples were donated by Honeywell Inc. of Bloomington, Minnesota.

The elastic properties were studied using a non-linear internal friction technique developed by Wuttig and Suzuki (11). A diagram of the experimental apparatus is given in Figure 1. The technique uses a cantilever type sample which is driven through its natural resonance by Sm-Co magnets (placed on the free end of the cantilever) coupling to constant gradient Helmholtz coils. The cantilever was placed into sinusoidal flexural motion, and the displacement was measured capacitively using a technique developed by Tomboulian (12). The samples were driven into the non-linear regime which resulted in asymmetric resonance curves. The resonance curves were analyzed using a nonlinear least squares fitting to equation 1;

$$\omega = \omega_0 + \frac{3}{8}\left(\frac{\alpha a^2}{\omega_0}\right) \pm \frac{1}{2}\sqrt{\left(\frac{K}{\omega_0 a}\right)^2 - \delta^2} \qquad (1)$$

where ω_0 is the resonance frequency, α the effective non-linear elastic constant, δ the linear damping, K the external excitation, and a the RMS displacement of the reed. Resonance curves were measured as a function of temperature on heating between 250 and 420°K, with resonance frequencies between 10 and 400 Hz. Measurements were done as a function of DC bias, the bias levels used were 0, 1,

2, 3, 4, 5, 6 ,7, 8, 10, 12, 15 kV/cm. X-ray line broadening measurements were also carried out using a position sensitive detector. Measurements were made on the (200), (220), and (321) diffraction peaks.

The dielectric response was measured as a function of frequency and temperature at the same bias levels used for the elastic measurements. The frequencies used were 0.1, 0.2, 0.4, 1, 2, 4, 10, 20, 40, and 100 KHz. All measurements were made on cooling at a rate of 1°C/min. The measurements were made using a HP4275A LCR meter. Two large blocking capacitors were used to protect the dielectric bridge from possible breakdown of the sample. A 20 MΩ resistor was put in series with the DC power supply so as not to bypass the AC current from the capacitance bridge. The dielectric curve for each frequency was curve smoothed and interpolated to determine the temperature of the dielectric maximum as accurately as possible. The remanent polarization was also measured as a function of temperature for comparison using standard techniques.

III. RESULTS

Sample resonance curves are illustrated for PLZT-8 in Figures 2(a)-(d) at $T<T_f$, $T=T_f$, $T=T_{max}$, and $T>T_{max}$ respectively. Each figure contains data under DC bias levels of 0, 6, and 12 kV/cm. An electrical field increased the resonance frequency (stiffened the lattice), and decreased the linear damping at all temperatures. The maximum field dependence can be seen to occur near $T=T_f$. At lower temperatures the resonance curves characterized a linear oscillator. Near T_f the elastic response was soft to the amplitude of the applied stress, i.e. the resonance curves shift to lower frequencies with increasing displacement. At higher temperatures the elastic response was hard to the amplitude of stress, i.e. the resonance curves shifted to higher frequencies with increasing displacement. The DC bias decreased the magnitude of the nonlinearity at all temperatures.

The permittivity as a function of temperature at various frequencies is shown in Figures 3(a)-(d) for La contents of 6, 6.5, 7, and 8 atomic%. At lower La contents no dispersion in T_{max} was observed, the dispersion in T_{max} did not become obvious until near 8 atomic%. The magnitude of the permittivity was dispersive for all compositions investigated, although the dispersion increased with increasing La content. The permittivity as a function of temperature for PLZT under DC bias levels of 0 and 4 kV/cm are shown in Figures 4(a) and (b), respectively.

IV. DISCUSSION

The elastic stiffness of relaxor ferroelectrics is known to start to soften at the temperature of the onset of local polarization (13). The anelastic relaxation of PMN has recently been shown to reflect the kinetics of the polarization fluctuations by a coupling of the applied stress to the internal strain, via the electrostriction. Near T_f, the orientations of the local electrostrictive strain fields are believed to freeze into an orientational glassy state. The frustration in this frozen state is believed to have contributions from both dipolar and quadrupolar interactions between superparaelectric moments. The elastic stiffness and linear damping of PLZT-8 are shown in Figure 4(a), the polarization and permittivity are shown in Figure 4(b) for comparison. The maximum softening of the 100 Hz elastic response occurred near the temperature of the collapse in the remanent polarization, rather than at the temperature of the 100 Hz T_{max} in the dielectric response. The implication is that the anelastic relaxation may have contributions other than the electrostrictive, and that the frustration in the frozen state is different from that in PMN.

The compositional dependence of the 100 Hz elastic stiffness of PLZT is illustrated in Figures 5(a)-(d) for La contents of 7, 8, 9, and 10 atomic% respectively. The maximum softening occurred at a temperature significantly below T_f for PLZT-7, near T_f for PLZT-8, between T_f and T_{max} for PLZT-9, and near

T_{max} for PLZT-10. The degree of softening was found to decrease with increasing La. The temperatures of the maximum lattice softening form a plausible extension to the rhombohedral rhombohedral phase boundary found by Meitzler and O'Bryan (1). They determined this boundary from the temperature of the maximum elastic softening of poled samples driven into resonance piezoelectrically. The transition temperature was estimated as 75°C for PLZT-6, the temperature of the maximum softening determined here for PLZT-7 was approximately 70°C. In the low temperature rhombohedral phase the oxygen octahedron is tilted with respect to the high temperature phase. The tilting is an attempt to partially relieve the octahedral strain (14) and results in a doubling of the unit cell (15). At the rhombohedral rhombohedral phase boundary the octahedral strain is coupled to an applied stress through the rotostriction (16), consequently the lattice softening has a ferroelastic contribution in addition to the electrostrictive. The compositional dependence of the electroelastic coupling (β) is illustrated in Figures 7(a)-(d) for PLZT-7, 8, 9, and 10 respectively. β was calculated from the field dependence of the elastic response using an expansion in even powers of the field (13). The maximum coupling was found near T_f for each composition irrespective of the relative temperature of the maximum softening. The maximum softening may occur when an applied stress most effectively couples to the internal strain through the rotostriction, whereas the maximum in β may occur at T_f when an electric field most effectively couples to the internal strain through the electrostriction. The relative temperatures of the maximum softening and electroelastic coupling show that both rotostrictive and electrostrictive contributions to the total response are important.

The frequency dependence of the elastic stiffness is illustrated in Figure 8(a) for PLZT-7. This graph shows the elastic stiffness as a function of temperature at measurement frequencies of 25 and 150 Hz. The dispersion in the temperature of the maximum softening is obvious and occurred below T_f. Anelasticity is a

reflection of internal stress relaxations, and is required to occur in any elastically dispersive system. The tilting of the oxygen framework in the low temperature rhombohedral phase is known to reduce the strain in the octahedra, the anelastic response may then be a reflection of the kinetics of this ferroelastic switching. It is proposed that within a micropolar region the orientations of the tilts fluctuate above a characteristic anelastic freezing temperature (T_f'), and that the frustration in the frozen state is partially elastic. The kinetics of the anelastic relaxation may be determined in part as a response to the polarization fluctuations as an attempt to relieve its corresponding electrostrictive strain. The freezing of the polarization and electrostrictive strains are coupled, however the freezing of the stress relaxations due to the rotostriction is independent. Consequently the freezing temperatures of the dielectric and anelastic relaxations may vary. The nature of the glassy phase of PLZT may then different from that of PMN, because the strain inhomogeneity can be partially relieved below T_f by the oxygen tilting. The elastic stiffness of PLZT-10 is shown in Figure 8(b) for comparison. The dispersion in the response is significantly less than for PLZT-7, and the temperature of the maximum softening occurred near its respective maximum dielectric softening.

PLZT relaxors are known to have antiphase boundaries separating regions which have a F-type superstructure (doubling of the unit cell) as found by Randall using TEM (2). This is the same type of superstructure known to occur in the low temperature rhombohedral phase of PZT due to the tilting of the oxygen octahedra. A possible explanation is that the antiphase boundaries in PLZT separate polar clusters with opposing tilts. The size of the antiphase regions and the reflection intensity of the superstructure in PLZT-9 have been found to grow as the temperature is decreased below 0°C (T_f= 260°K) (2), unlike the scale of the "fossil" chemistry in PMN (17) which is known to be static with decreasing temperature. The rhombohedral rhombohedral boundary is close in temperature to

the onset of growth of the antiphase regions and superlattice intensity for this composition. The implication is that the coarsening of the antiphase domains occurs near and below the freezing temperature of the anelastic relaxations. The driving force of the coarsening may be the minimization of the local elastic strain energy by partially relieving the inhomogeneity in the electrostrictive strains due to the tilting of the oxygens. Strain fields between precipitates are well known to influence the phase separation process and coarsening in solid solutions (18). The tilting of the octahedra occurs due to a softening of a R-point Γ_{25} mode in the high temperature rhombohedral phase. It has been suggested that the softening of the Γ_{25} mode plays an essential role in the antiferroelectric phase transition near the $PbZrO_3$ side of the PZT phase diagram (19), consequently the possibility of antiferroelectricity in PLZT (65/35) as suggested by Randall should not be ignored as an alternative explanation.

Effective third order elastic constants for PLZT-8 and 10 are shown in Figures 9(a) and (b) respectively, under zero bias. The temperature of the maximum elastic softening under stress followed the rhombohedral rhombohedral boundary for all compositions investigated. The stress sensitivity of PLZT is well known (1,20) and arises due to a large planar coupling coefficient. The microscopic origins of the elastic softening and large coupling coefficient may be due to a stress driven ferroelastic switching of the octahedral tilt, partially relieving the internal strain. The natural elastic hardening is observed at higher temperatures, when the deformation process is much faster than the applied AC stress. The maximum nonlinearities can then be expected at temperatures near the rhombohedral rhombohedral phase boundary for compositions having the largest strain inhomogeneity. The room temperature (321) diffraction peaks for PLZT-7, 8, 9, and 10 at various bias levels are shown in Figures 10(a)-(d) respectively. The width of the peak decreased with increasing La content indicating that the inhomogeneity is maximum at lower La

contents. These results are in agreement with the compositional dependence of the elastic nonlinearities shown in Figure 8(c), which are taken at the respective T_{max} for each composition. The maximum softening can be seen to occur between 7 and 8 atomic%. At higher La contents the magnitude of the softening was significantly less which is in agreement with the strong decrease in the internal strain and planar coupling coefficient (1). The effective third order elastic constant under 10 kV/cm is also shown in Figures 9(a) and (b) for PLZT-8 and 10, respectively. The magnitude of the softening decreased with increasing bias. This can be understood as a decrease in the internal strain due to the alignment of moments. Consequently, the internal deformation process is less stress sensitive.

The stress driven ferroelastic switching may essentially involve a micro to macro domain transition. Stress induced macrodomain formation has been visually observed for compositions between 4 and 8 atomic% La (1), but not for La contents greater than 10 atomic%. This agrees with the compositional dependence of the elastic nonlinearities, internal strain, and coupling coefficient. The morphology of the antiphase domains in the absence of an ordering field, as observed by Randall (2), is suggestive of an elastically isotropic environment. The isotropy may be a reflection of the random freezing of the orientations of the local electrostrictive strains. Under prolonged illumination, the morphology was switched to finely aligned domains (2). The observed elastic nonlinearities may then relate to stress induced local elastic anisotropy and the establishment of long range elastic ordering of the strains. The glassy character of relaxors is then destroyed by an ordering stress which establishes a global equilibrium. In the composition range between 6 and 8 atomic% the crystal structure has been reported to depend on its orientation with respect to an applied electrical or mechanical field (1), the so-called polymorphism. This is the same composition range where the inhomogeneity in the internal strain was maximum (see Figures 10(a)-(d)). The polymorphism may be a

reflection of the local elastic isotropy of the unpoled state, and of a strong desire by the macroscopic system to relieve the frustration associated with the internal strain.

When La is added to PZT, charge neutrality is preserved by creating lead vacancies (21), one vacancy for every two La atoms. The role of La in the development of the relaxational character is probably to break the translational symmetry of the polarization within the domains, either by heterogeneities in the composition or the electric field associated with the defect structure. The net effect is that the polar behavior is localized on a scale where relaxational processes can contribute to the dielectric response. Between 4 and 7 atomic% La the magnitude of the response was dispersive, but there was no dispersion in T_{max} at radio frequencies until near 8 atomic% (see figure 3(a)-(d)). Figure 11(a) shows a plot of $1/T_{max}$ as a function of the $\ln(\omega)$ for PLZT-7 at DC bias levels of 0 and 4 kV/cm. $1/T_{max}$ approached a constant value at approximately 40 KHz under 0 kV/cm, but under 4 kV/cm the low frequency T_{max} was much more dispersive. The dispersion of T_{max} under 4 kV/cm was modelled using the Vogel-Fulcher relationship (5), shown as the solid line in the figure. An activation energy, freezing temperature, and pre-exponential factor of 0.086 eV, 380.5°K, and 10^{14} sec^{-1} were obtained respectively. The remanent polarization as a function of temperature is shown in figure 11(b). The extrapolation of the collapse in the polarization to zero yielded a temperature of approximately 105°C which is close to the freezing temperature. Analysis of the results under 0 kV/cm yielded erroneous values for the parameters, for example a pre-exponential factor of 10^5. It is proposed that at the lower La contents the inhomogeneity in the internal strain clamps the polarization fluctuations, and on application of a small bias the inhomogeneity is partially relieved and the kinetics of the fluctuations enhanced. The clamping may occur by local alignments of cluster moments, consequently slowing down the kinetics of the polarization fluctuations. Local equilibrium configurations of moments on the scale

of 100-200 A° have been proposed previously (22). On application of a field, these configurations must be overridden before a global equilibrium can be established. The broadening of the dielectric response at low La contents may also be caused by the strain inhomogeneity, and may not necessarily be related to a distribution of local Curie temperatures as predicted by the Smolenski model (6). The broadening of the response is significantly larger than for PMN.

Figures 12(a)-(d) show plots of $1/T_{max}$ as a function of the $\ln(\omega)$ for PLZT-7, 8, 9, and 10 respectively. Each figure contains data under various bias levels. With increasing La, the field dependence of the dispersion in T_{max} decreased. The dispersion under zero bias could not be effectively modelled for PLZT-7 and 8, but reasonable results were obtained at all bias levels for PLZT-9 and 10. This is probably a reflection of the compositional dependence of the strain inhomogeneity. The Vogel-Fulcher freezing temperature is tabulated in table 1, along side the corresponding La content. T_f was determined by the temperature of the collapse in the remanent polarization for PLZT-6 and 6.5. The compositional dependence of the second order nonlinear permittivity at T_{max} ($\chi_{nl}(T_{max})$) is shown as a function of composition in Figure 13 for comparison. χ_{nl} was calculated from the field dependence of the permittivity using an expansion in even powers of the field (22). The dielectric response was soft to small applied biases for La contents greater than 6.5 atomic%, and stiff for lower La content. The maximum softening was observed between 7 and 8 atomic%, near the maximum field dependence of the dispersion in T_{max}. At higher La contents, the response was nearly linear.

The deviation from the Vogel-Fulcher freezing of the polarization fluctuations may arise due to the frustration associated with the strain inhomogeneity. The inhomogeneity depends on the La content which is probably a reflection of the relative sizes of the cluster moments. The dipolar and quadrupolar interactions scale as $1/r^2$ and $1/r^3$, respectively. The maximum strain inhomogeneity will then be

found near a critical composition when the density of polar regions is relatively high, and the distances between them relatively small. This composition seemingly occurs between 6 and 8 atomic% when the temperature of the rhombohedral rhombohedral boundary approaches T_f. Even though the polarization fluctuations are coupled to the fluctuations of the electrostrictive strains, their freezing mechanism may vary as a function of La content reflecting a change in the dominant field between cluster moments. The freezing mechanism may also vary as a function of an ordering field, due to the removal of the strain inhomogeneity. The changes in the dielectric and anelastic responses with La content can then be understood as a reflection of the change in the nature of the glassy character. The frustration in PMN has also been shown to have contributions from both dipolar and quadrupolar interactions (13). The differences between the glassy behavior in PLZT and PMN may relate to differences in the magnitude of the inhomogeneity, and tilting of the oxygen octahedra.

A summary of the results are illustrated in a revised phase diagram for PLZT (65/35) shown in Figure 14. The rhombohedral rhombohedral phase boundary, as determined here, is extended to La contents upto 12 atomic%. The low and high temperature rhombohedral phases are shown as F.E. rhom. I and II, respectively. The relaxational character of the dielectric response of PLZT began to be noticeable between 4 and 5 atomic% La which is illustrated as a dashed line in the diagram. The temperature of the onset of local polarization, T_{Burns}, is shown in the phase diagram as a dashed line at 623°K. T_{Burns} is shown to exist for all La contents to illustrate that the effect of the heterogeneity is incipient from the addition of very small amounts of La. Although the equilibrium size of the relaxing units may be determined by the heterogeneity, T_{Burns} does not necessarily reflect the onset of the relaxational process and the nature of the relaxor ferroelectric. At T_{Burns}, local distortions start to occur in a stiff matrix. At lower temperatures a perculation limit

may be reached when the matrix can start to deform in response to the polarization fluctuations, consequently the orientation of the electrostrictive strain may fluctuate. An isothermal line, T_{perc}, is shown in the phase diagram to represent this temperature. Evidence of such behavior has been found by Darlington (23) who showed that an inhomogeneity in the volume deformation saturated when an inhomogeneity in the shear deformation started to develop at about 75°C below T_{Burns}. A dashed line is drawn in the diagram to represent the compositional dependence of the 100 Hz T_{max}, shown as T_{max}. A solid line is drawn in the diagram to represent the compositional dependence of the Vogel-Fulcher freezing temperature, shown as T_f. The freezing temperature is shown to approach 0 K near 14 atomic% La which is close to the composition at which the local structure is believed to be cubic (1). The rhombohedral rhombohedral phase boundary touches T_f at approximately 8 atomic% La, and touches T_{max} near 10 atomic%. This is the *compositional range* where the strain inhomogeneity decreased markedly. The phase region defined by T_{Burns} and T_{perc} is shown to have fluctuations in only the polarization. The region defined by the line T_{perc} and the compositional dependence of T_f is shown to have fluctuations in the polarization, local electrostrictive strain fields (orientation), and tilting of the oxygen octahedra (elastic). The region defined by the compositional dependence of T_f and the rhombohedral rhombohedral phase boundary for La contents greater than 4 atomic% is shown to have fluctuations in the tilting of the oxygen octahedra, but the polarization and electrostrictive strain are shown to be frozen. The region defined by T_f at La contents above 8 atomic% and the rhombohedral rhombohedral phase boundary for La contents between 4 and 8 atomic% is shown to have the polarization, electrostrictive strain, and tilting of the oxygen octahedra all frozen.

CONCLUSION

An extension to the rhombohedral rhombohedral phase boundary has been proposed for La contents between 7 and 14 atomic% based on the compositional dependence of the temperature of the maximum elastic softening. A frequency dispersion of the elastic softening has also been found below the freezing temperature of the polarization fluctuations (T_f), and interpreted as the kinetics of internal strain relaxations due to the tilting of the oxygen octahedra. The glassy phase in PLZT is believed to be different than PMN due to this additional ferroelastic response. T_f has also been determined as a function of La content. A revised phase diagram was then proposed which has different phase regions having various combinations of freezing mechanisms.

ACKNOWLEDGMENTS

This work has been supported in full by contracts administered through the Office of Naval Research. Thanks must be expressed to Dr. Clive Randall for explaining the TEM micrographs of PLZT to the authors, and for many stimulating discussions through many years.

* Also in the Electrical Engineering Department.

REFERENCES

1) A. Meitzler, H. O'Bryan, Proc. of IEEE **61**, 959 (1973).

2) C. Randall, PhD Dissertation, University of Essex (1987).

3) G. Burns, F. Dacol, Sol. State Commun. **48**, 853 (1983).

4) L. Cross, Ferroelectrics **76**, 241 (1987).

5) D. Viehland, S. Jang, M. Wuttig, L. Cross, To be published in J. Appl. Phys., Sept. 1990.

6) G. Smolenski, A. Agranovska, Sov. Phys. Sol. State **1**, 1429 (1960).

7) C. Randall, A. Bhalla, J. Mat. Sci. **29**, 5 (1990).

8) N. Yushin, L. Bazarova, G. Gulyamov, Ferroelectrics **90**, 57 (1989).

9) N. Yushin, Proc. of Ferroelektrizitat 1988, 102, Halle, GDR.

10) G. Schmidt, H. Beige, G. Borchhardt, J. Cieminski, R. Rossbach, Ferroelectrics **22**, 683 (1978).

11) A. Anning, T. Suzuki, M. Wuttig, J. Appl. Phys. **53**, 6797 (1982).

12) R. Tomboulian, IBM Research Report, RC-396 (1961).

13) D. Viehland, S. Jang, M. Wuttig, L. Cross, Submitted to Phil. Mag.

14) R. Clarke, M. Glazer, Ferroelectrics **12**, 207 (1976).

15) C. Michel, J. Moreau, G. Achenbach, R. Gerson, W. James, Sol. State Comm. **7**, 865 (1969).

16) M. Haun, PhD Dissertation, The Pennsylvania State University, 1988.

17) J. Chen, H. Chan, M. Harmer, J. Am. Cer. Soc. **72**, 593 (1989).

18) A. G. Khachaturyan, THEORY OF STRUCTURAL TRANSFORMATIONS IN SOLIDS, John Wiley and Sons, New York (1983).

19) M. Lines, A. Glass, PRINCIPLES AND APPLICATIONS OF FERROELECTRICS AND RELATED MATERIALS, Oxford University Press, Oxford (1977).

20) A. Meitzler, H. O'Bryan, Appl. Phys. Lett. **19**, 106 (1972).

21) K. Hardtl, D. Henings, J. Am. Cer. Soc. **55**, 230 (1970).

22) D. Viehland, S. Jang, M. Wuttig, L. Cross, Accepted for publication in J. Appl. Phys.

23) C. Darlington, Phys. Stat. Sol. (a) **113**, 63 (1989).

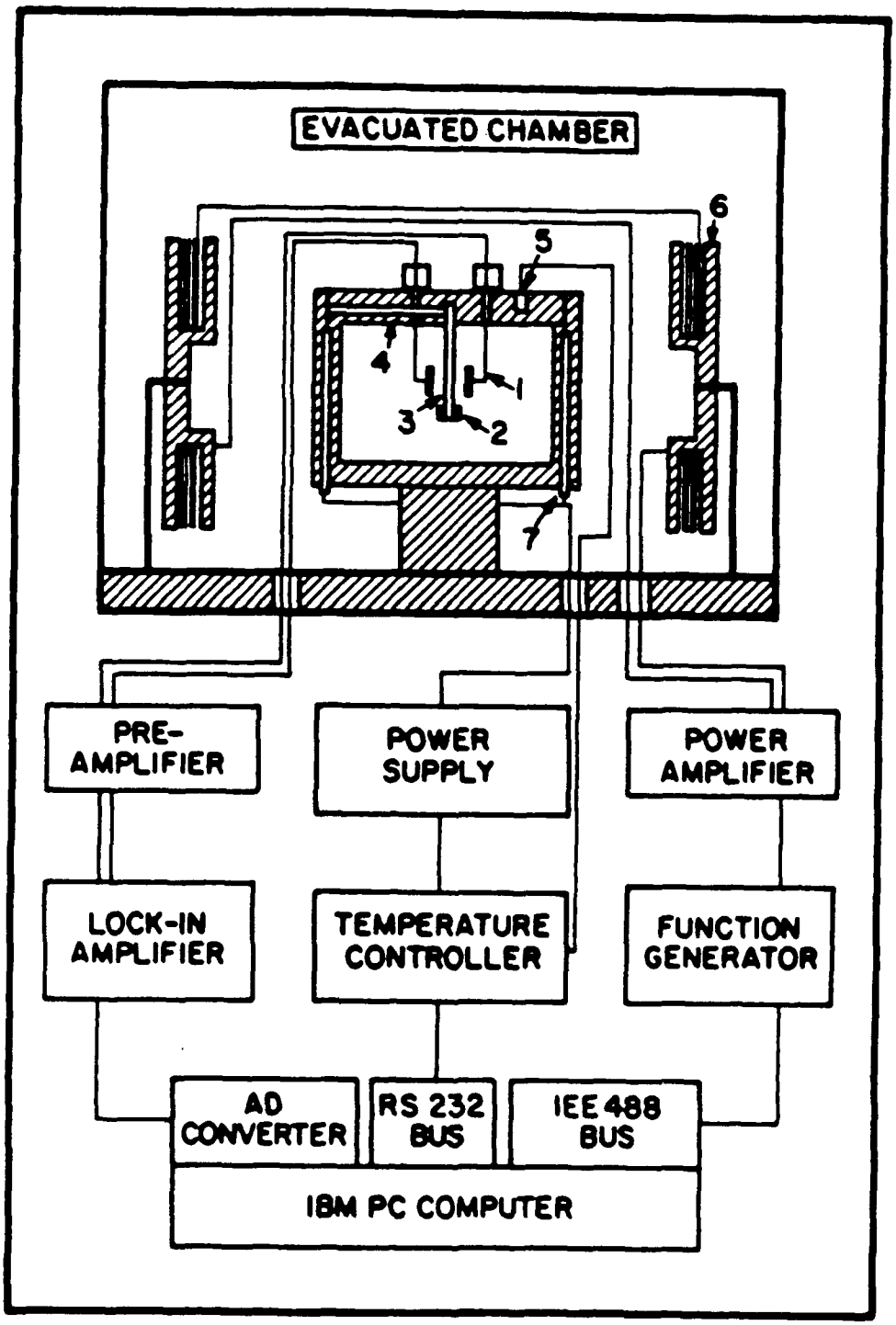
EVACUATED CHAMBER
6
5
4
1
3
2
7
PRE-
AMPLIFIER
POWER
SUPPLY
POWER
AMPLIFIER
LOCK-IN
AMPLIFIER
TEMPERATURE
CONTROLLER
FUNCTION
GENERATOR
AD
CONVERTER
RS 232
BUS
IEE 488
BUS
IBM PC COMPUTER

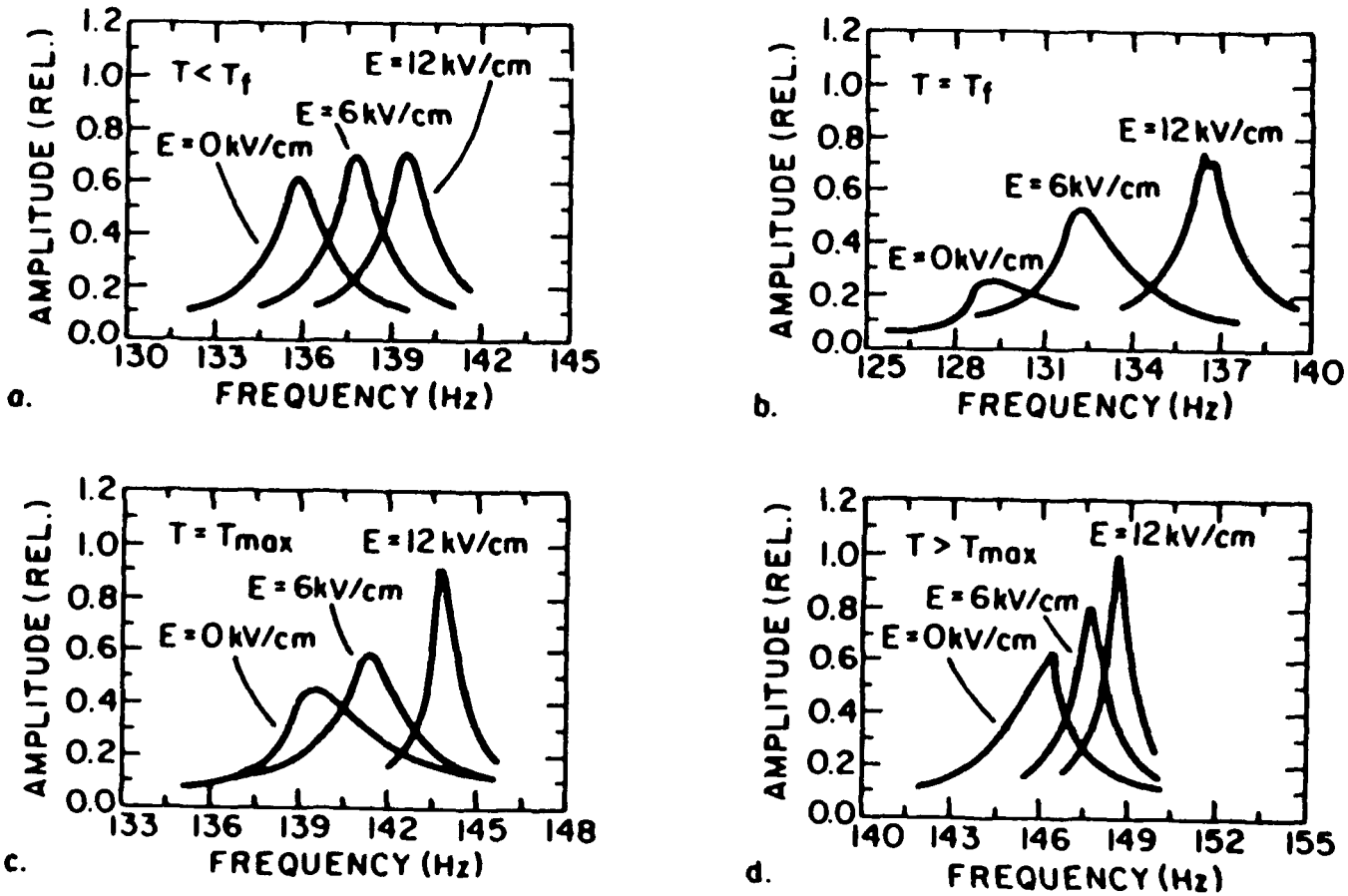
a.
T < Tf
E = 12 kV/cm
E = 6 kV/cm
E = 0 kV/cm
AMPLITUDE (REL.)
1.2
1.0
0.8
0.6
0.4
0.2
0.0
130 133 136 139 142 145
FREQUENCY (Hz)
b.
T = Tf
E = 12 kV/cm
E = 6 kV/cm
E = 0 kV/cm
AMPLITUDE (REL.)
125 128 131 134 137 140
FREQUENCY (Hz)
c.
T = Tmax
E = 12 kV/cm
E = 6 kV/cm
E = 0 kV/cm
AMPLITUDE (REL.)
133 136 139 142 145 148
FREQUENCY (Hz)
d.
T > Tmax
E = 12 kV/cm
E = 6 kV/cm
E = 0 kV/cm
AMPLITUDE (REL.)
140 143 146 149 152 155
FREQUENCY (Hz)

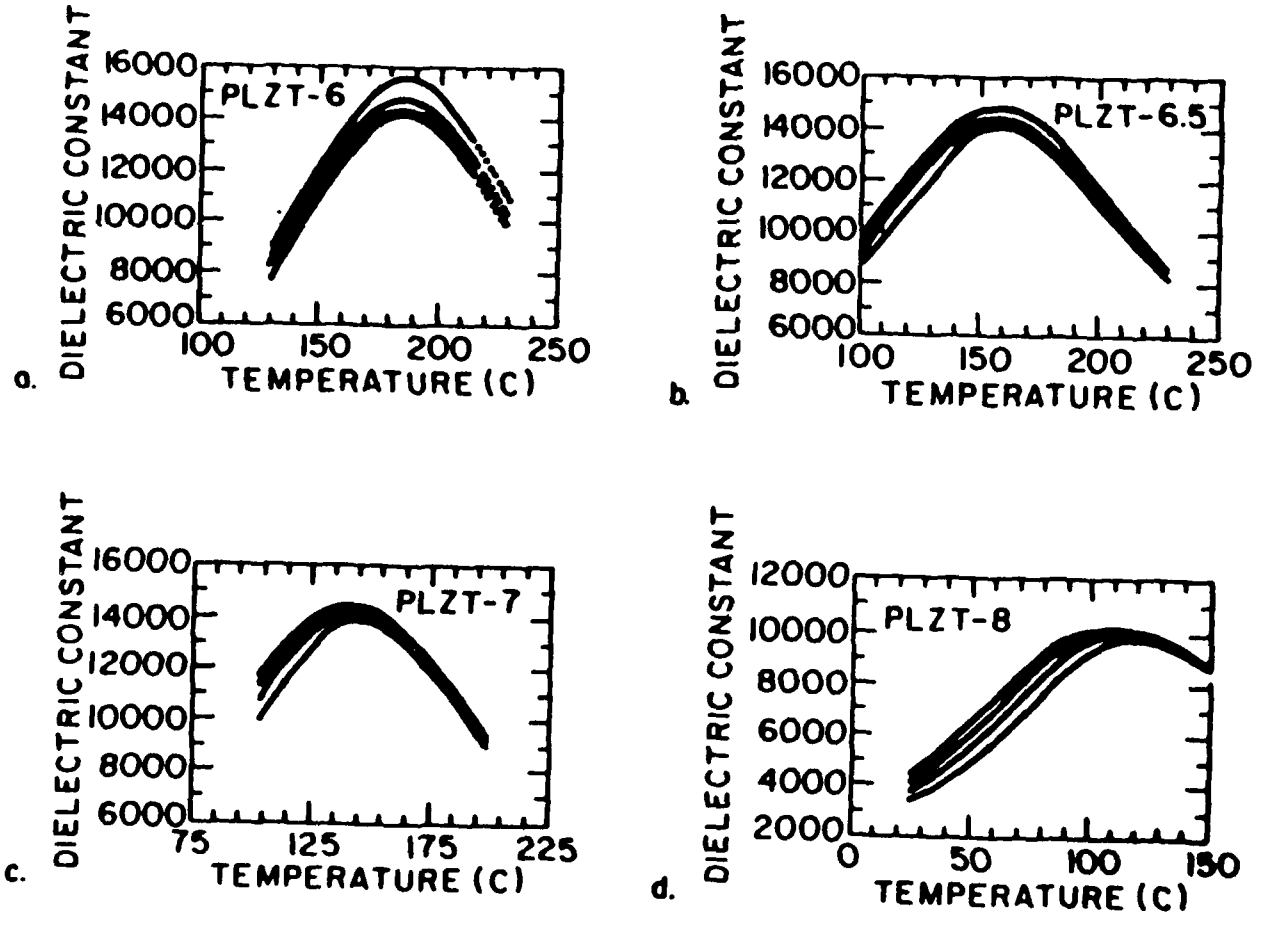
a.
DIELECTRIC CONSTANT
16000
14000
12000
10000
8000
6000
PLZT-6
100
150
200
250
TEMPERATURE (C)
b.
DIELECTRIC CONSTANT
16000
14000
12000
10000
8000
6000
PLZT-6.5
100
150
200
250
TEMPERATURE (C)
c.
DIELECTRIC CONSTANT
16000
14000
12000
10000
8000
6000
PLZT-7
75
125
175
225
TEMPERATURE (C)
d.
DIELECTRIC CONSTANT
12000
10000
8000
6000
4000
2000
PLZT-8
0
50
100
150
TEMPERATURE (C)

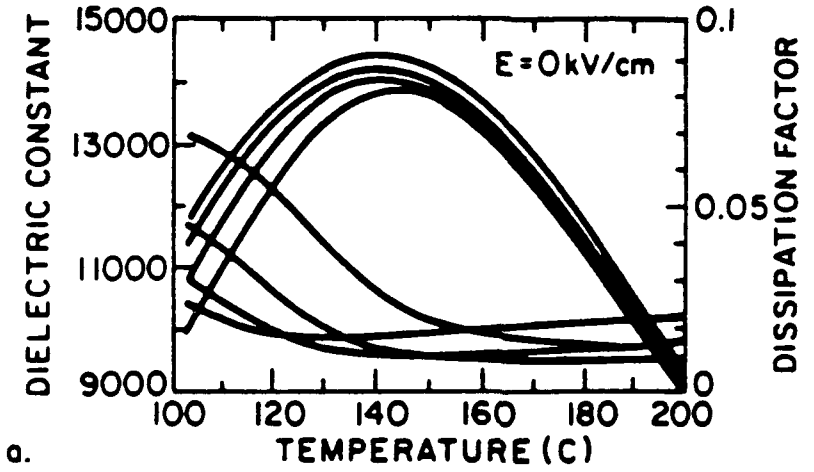
15000
13000
11000
9000
DIELECTRIC CONSTANT
E = 0 kV/cm
0.1
0.05
0
DISSIPATION FACTOR
100 120 140 160 180 200
TEMPERATURE (C)

a.

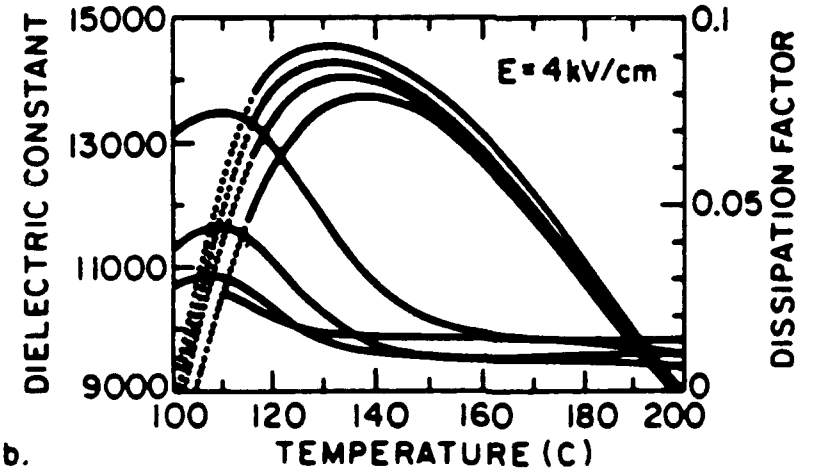
15000
13000
11000
9000
DIELECTRIC CONSTANT
E = 4 kV/cm
0.1
0.05
0
DISSIPATION FACTOR
100 120 140 160 180 200
TEMPERATURE (C)

b.

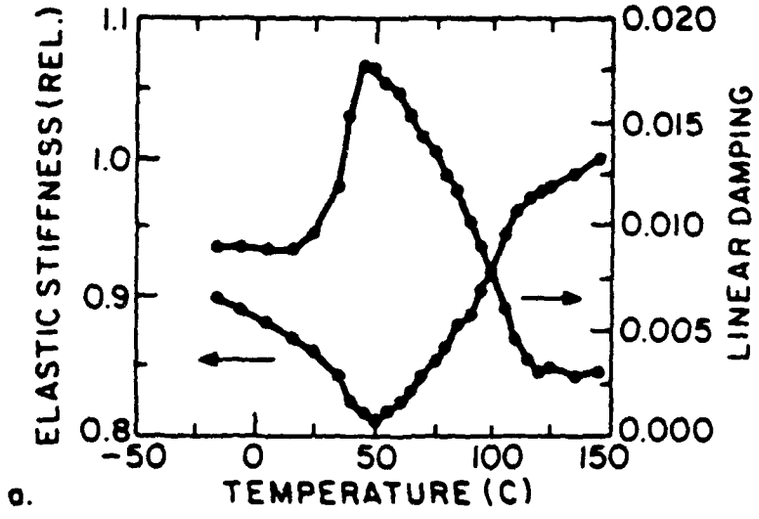
ELASTIC STIFFNESS (REL.)
1.1
1.0
0.9
0.8
0.020
0.015
0.010
0.005
0.000
LINEAR DAMPING
-50
0
50
100
150
TEMPERATURE (C)

a.

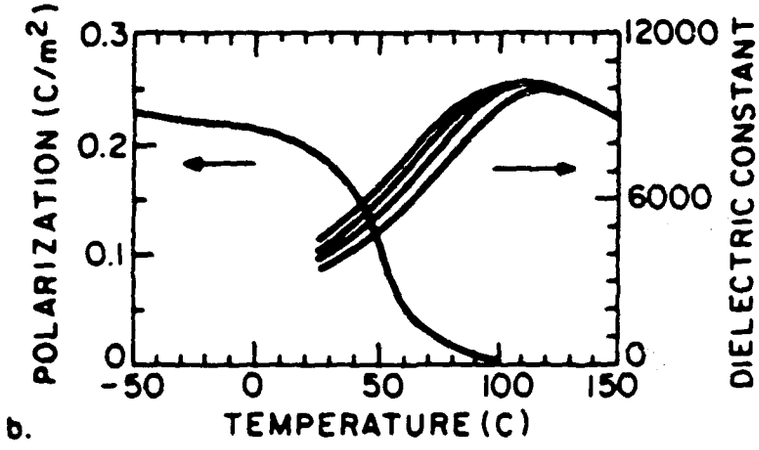
POLARIZATION (C/m²)
0.3
0.2
0.1
0
12000
6000
0
DIELECTRIC CONSTANT
-50
0
50
100
150
TEMPERATURE (C)

b.

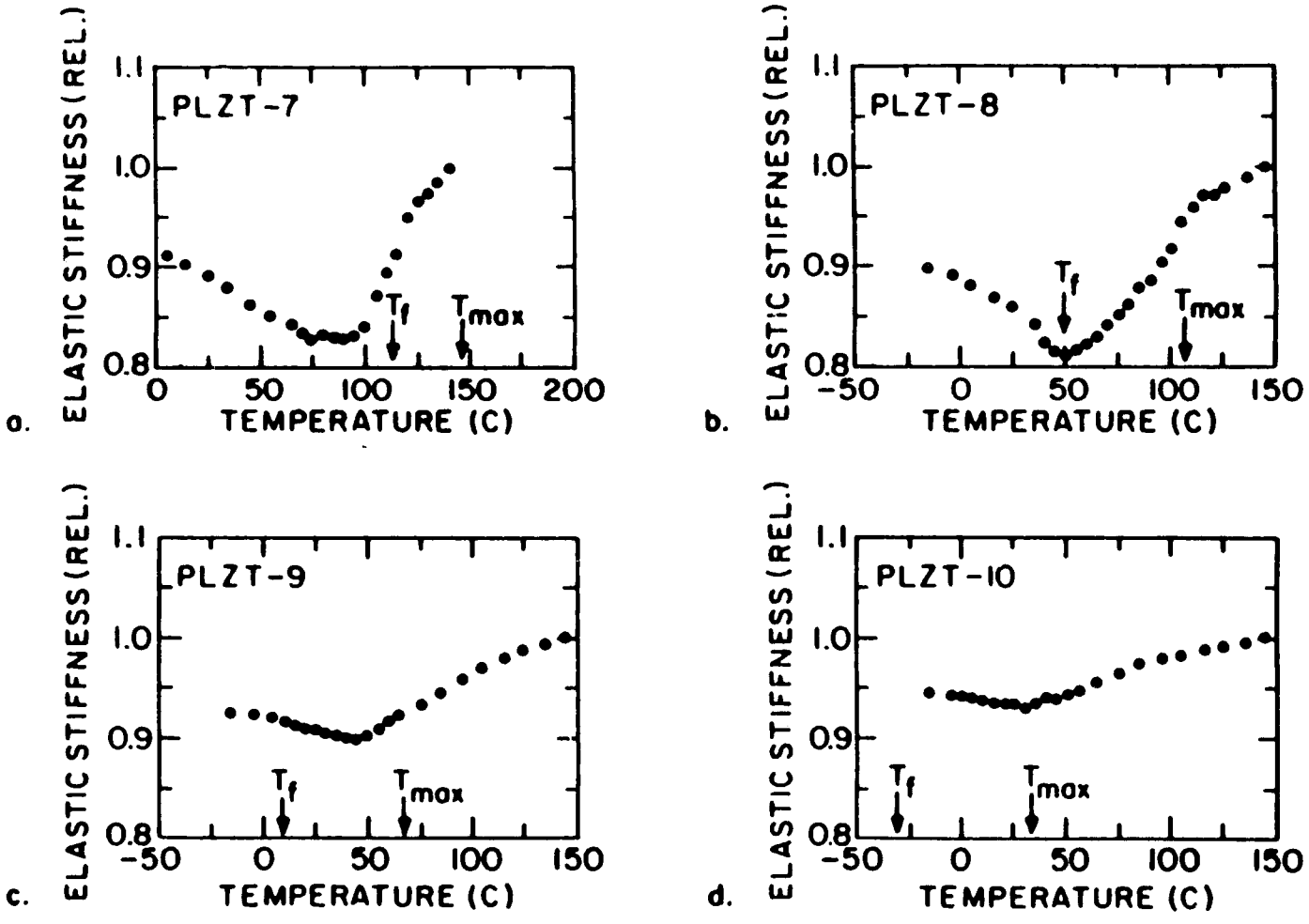
a.
ELASTIC STIFFNESS (REL.)
PLZT-7
1.1
1.0
0.9
0.8
T_f
T_{max}
0
50
100
150
200
TEMPERATURE (C)
b.
ELASTIC STIFFNESS (REL.)
PLZT-8
1.1
1.0
0.9
0.8
T_f
T_{max}
-50
0
50
100
150
TEMPERATURE (C)
c.
ELASTIC STIFFNESS (REL.)
PLZT-9
1.1
1.0
0.9
0.8
T_f
T_{max}
-50
0
50
100
150
TEMPERATURE (C)
d.
ELASTIC STIFFNESS (REL.)
PLZT-10
1.1
1.0
0.9
0.8
T_f
T_{max}
-50
0
50
100
150
TEMPERATURE (C)

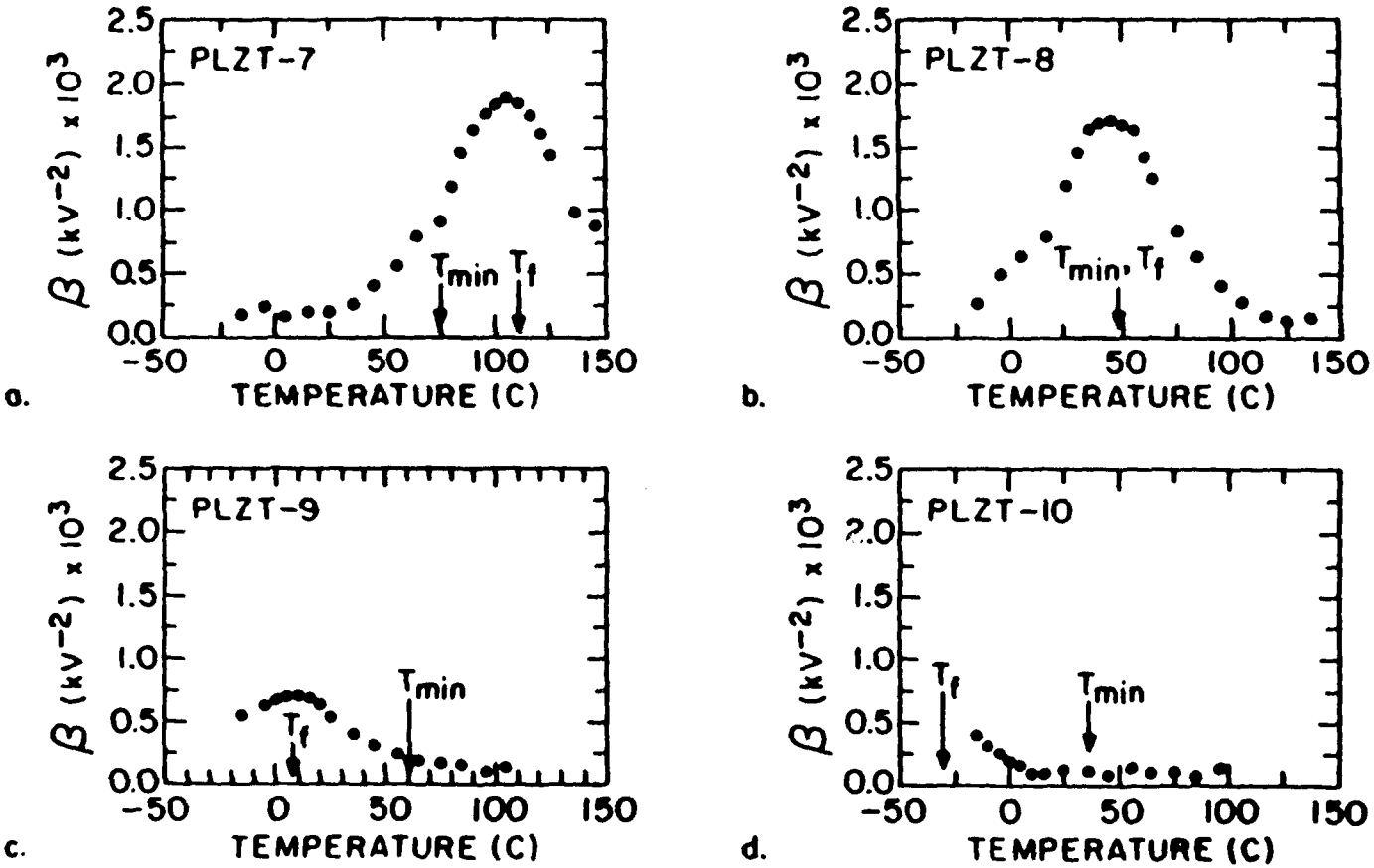
PLZT-7
PLZT-8
PLZT-9
PLZT-10
β (kV⁻²) x 10³
2.5
2.0
1.5
1.0
0.5
0.0
-50
0
50
100
150
TEMPERATURE (C)
Tmin
Tf
a.
b.
c.
d.

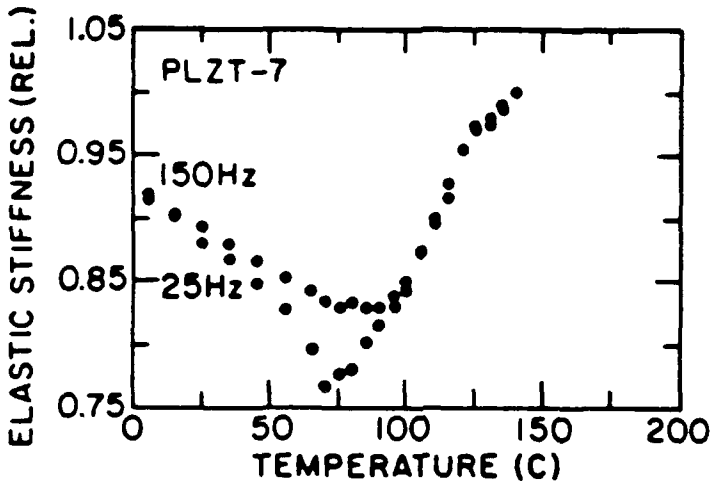
PLZT-7
150Hz
25Hz
ELASTIC STIFFNESS (REL.)
1.05
0.95
0.85
0.75
0
50
100
150
200
TEMPERATURE (C)

a.

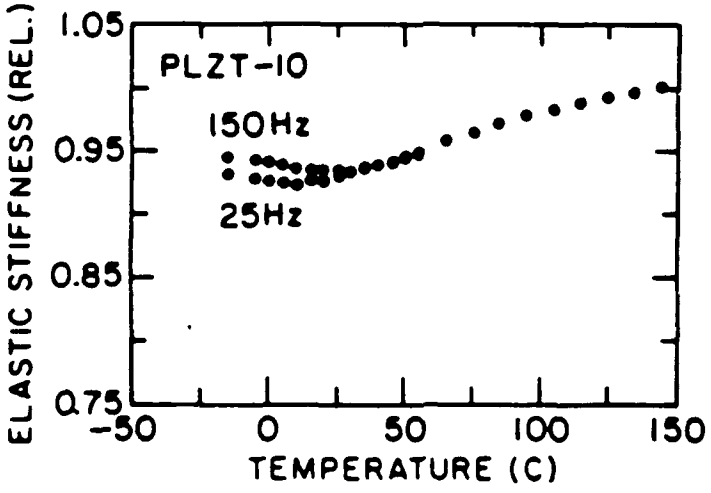
PLZT-10
150Hz
25Hz
ELASTIC STIFFNESS (REL.)
1.05
0.95
0.85
0.75
-50
0
50
100
150
TEMPERATURE (C)

b.

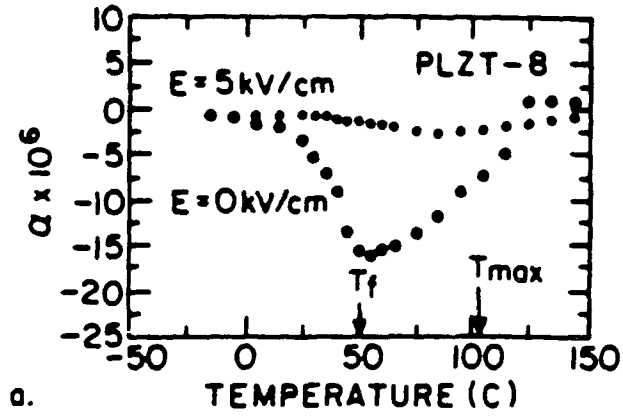
PLZT-8
E=5kV/cm
E=0kV/cm
Tf
Tmax
α x 10⁶
TEMPERATURE (C)

a.

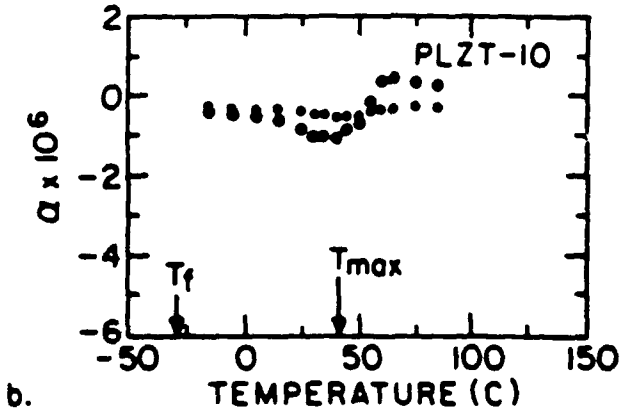
PLZT-10
Tf
Tmax
α x 10⁶
TEMPERATURE (C)

b.

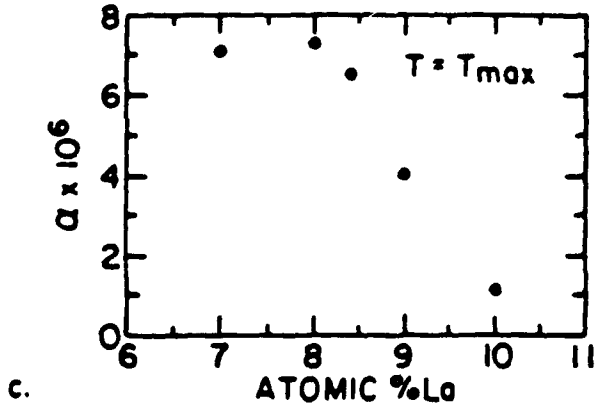
T = Tmax
α x 10⁶
ATOMIC %La

c.

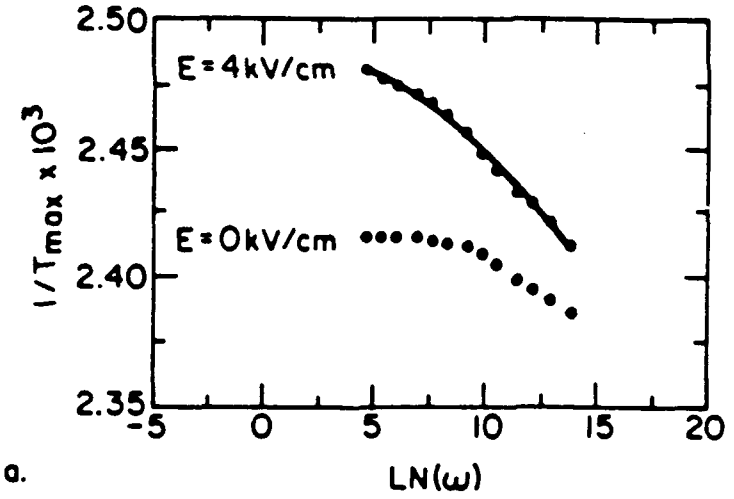
2.50
2.45
2.40
2.35
E=4kV/cm
E=0kV/cm
1/T_max x 10^3
-5
0
5
10
15
20
LN(ω)

a.

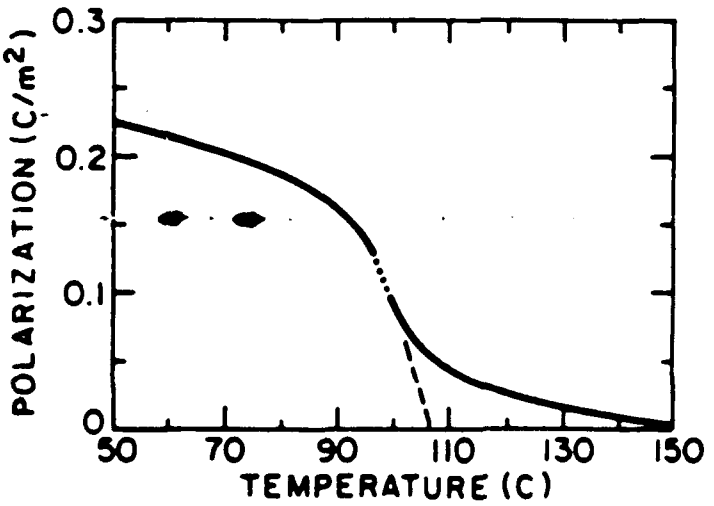
0.3
0.2
0.1
0
POLARIZATION (C/m^2)
50
70
90
110
130
150
TEMPERATURE (C)

b.

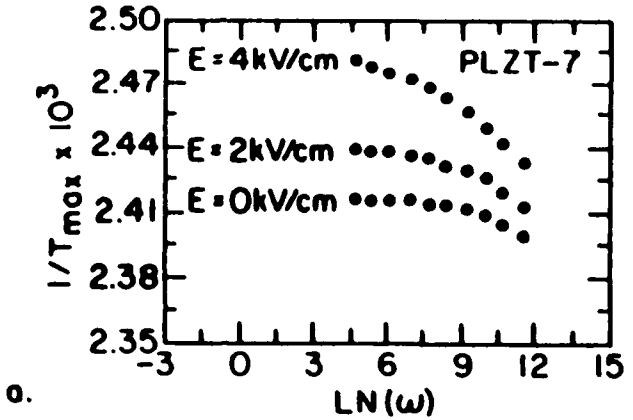
2.50
2.47
2.44
2.41
2.38
2.35
E = 4kV/cm
E = 2kV/cm
E = 0kV/cm
PLZT-7
1/T_max x 10^3
-3 0 3 6 9 12 15
LN(ω)

a.

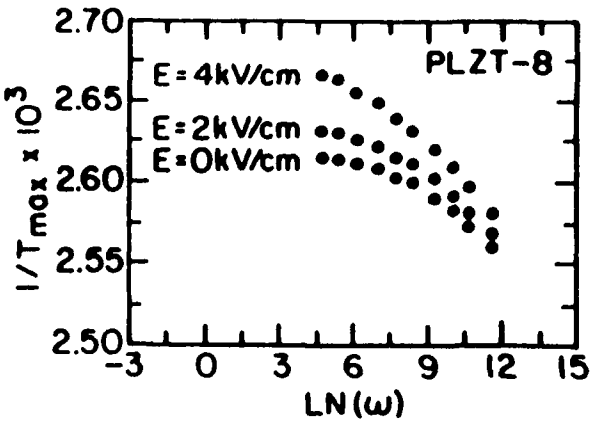
2.70
2.65
2.60
2.55
2.50
E = 4kV/cm
E = 2kV/cm
E = 0kV/cm
PLZT-8
1/T_max x 10^3
-3 0 3 6 9 12 15
LN(ω)

b.

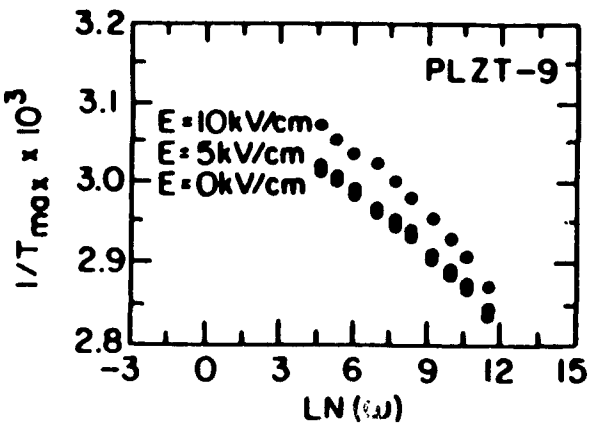
3.2
3.1
3.0
2.9
2.8
E = 10kV/cm
E = 5kV/cm
E = 0kV/cm
PLZT-9
1/T_max x 10^3
-3 0 3 6 9 12 15
LN(ω)

c.

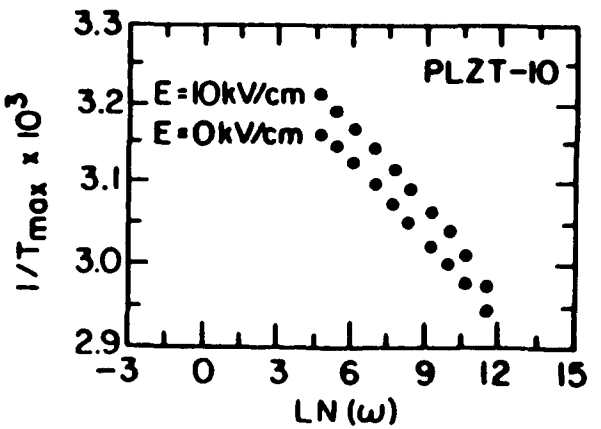
3.3
3.2
3.1
3.0
2.9
E = 10kV/cm
E = 0kV/cm
PLZT-10
1/T_max x 10^3
-3 0 3 6 9 12 15
LN(ω)

d.

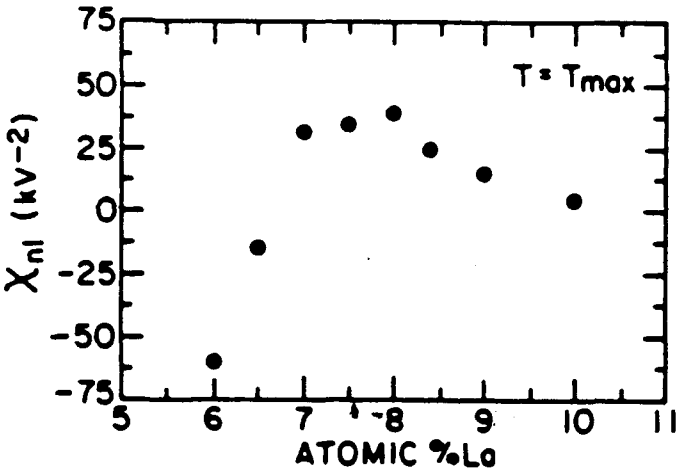
75
50
25
0
-25
-50
-75
5
6
7
8
9
10
11
T = Tmax
χ_{nl} (kV^{-2})
ATOMIC %La

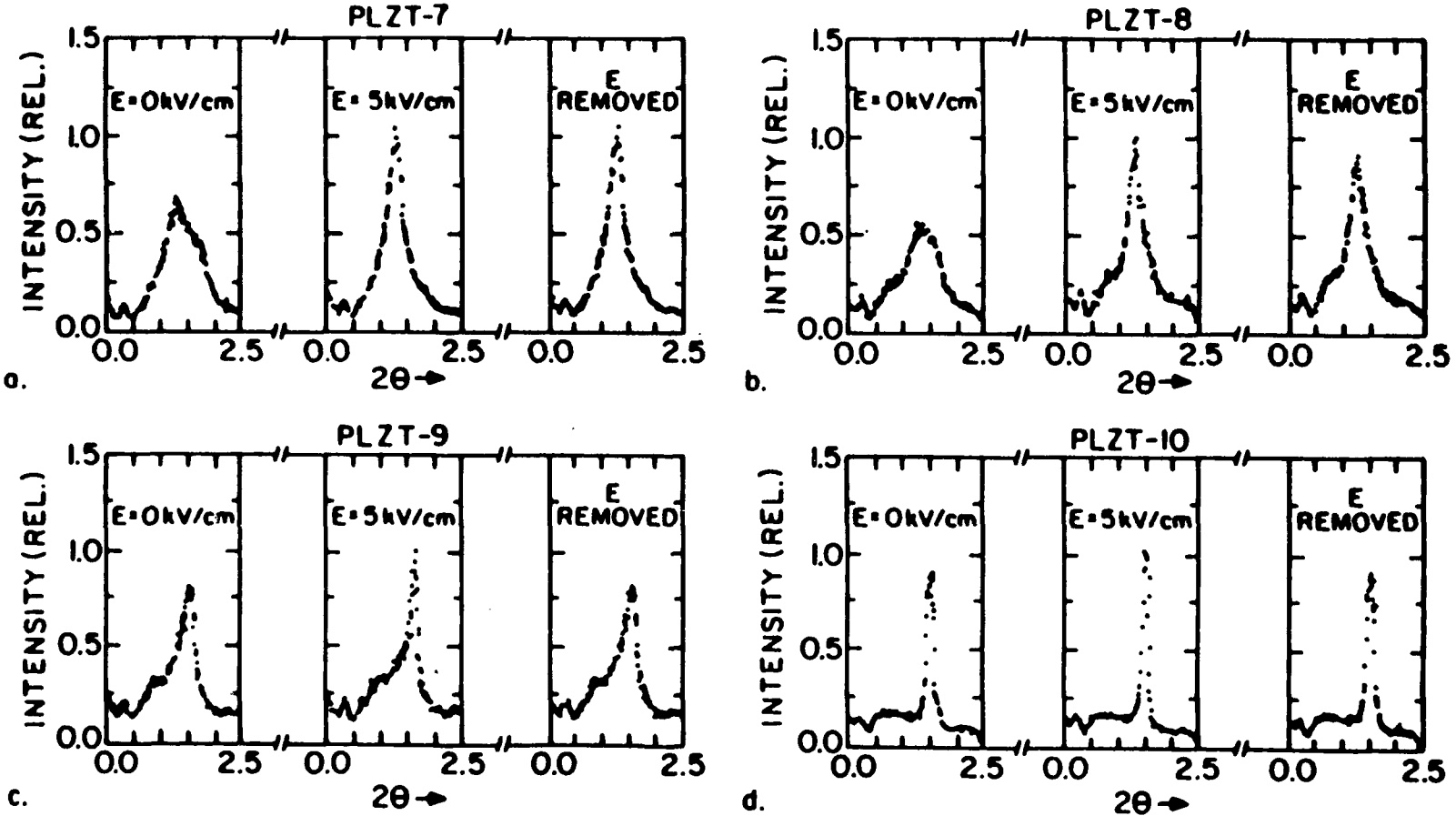
PLZT-7
PLZT-8
PLZT-9
PLZT-10
INTENSITY (REL.)
1.5
1.0
0.5
0.0
E = 0kV/cm
E = 5kV/cm
E REMOVED
0.0
2.5
2θ →
a.
b.
c.
d.

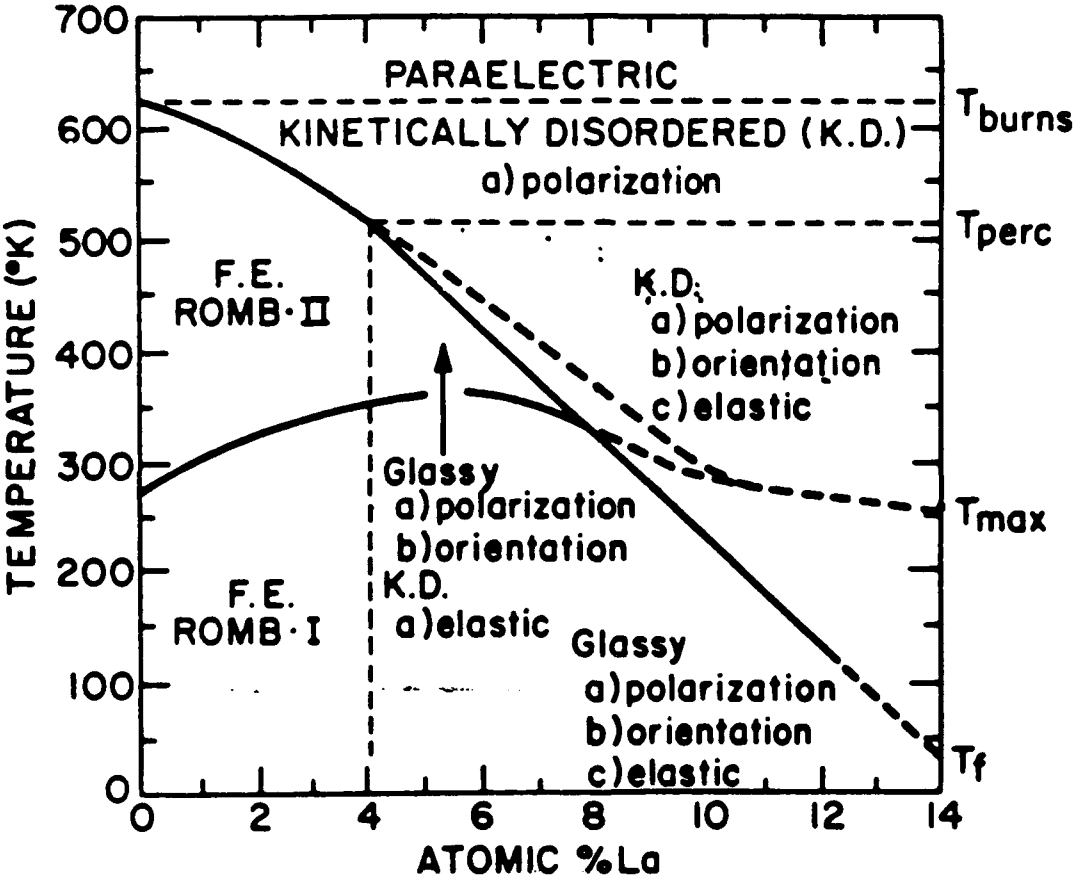
700
600
500
400
300
200
100
0
TEMPERATURE (°K)
0
2
4
6
8
10
12
14
ATOMIC %La
PARAELECTRIC
KINETICALLY DISORDERED (K.D.)
a) polarization
T burns
T perc
T max
T f
F.E.
ROMB·II
F.E.
ROMB·I
K.D.
a) polarization
b) orientation
c) elastic
Glassy
a) polarization
b) orientation
K.D.
a) elastic
Glassy
a) polarization
b) orientation
c) elastic

APPENDIX 30

THE DEPENDENCE OF THE GLASSY POLAR BEHAVIOR ON CHEMICAL ORDERING IN RELAXOR FERROELECTRICS

Dwight Viehland, S.J. Jang, and L.E. Cross

Materials Research Laboratory, The Pennsylvania State University

Manfred Wuttig

Department of Nuclear and Materials Engineering, The University of Maryland

ABSTRACT

The complex susceptibility of lead scandium tantalate relaxor ferroelectrics has been modelled for samples with varying degrees of long range chemical ordering. The development of correlations between polar moments occured relatively sharply near freezing in the highly ordered state, whereas the development of correlations in the partially ordered state occurred over a broadened temperature interval. The relaxation time distributions were also calculated. A sharp peak in the distribution was found on freezing in the highly ordered state, characteristic of a distinct condensation of moments. The distribution in the partially ordered state was diffuse near freezing, suggestive of a more dispersive condensation. It is proposed that in the highly ordered state. the polar moments freeze into configurations with correlation lengths approaching the macroscopic scale typical of a normal ferroelectric, whereas in the partially ordered state the moments freeze into a dipolar glass phase.

I. INTRODUCTION

A relaxor is a ferroelectric material which exhibits a dispersion of the complex susceptibility in the zero field cooled (ZFC) state, and which posesses a local polarization to temperatures much higher than the radio frequency permittivity maximum (T_{max}) (1). In the ZFC state, the scale of the polar behavior is known to remain smaller than the coherence length of x-rays (2) down to liquid nitrogen temperatures. But in the FC state, a remanent polarization can be sustained up to a characteristic temperature, and normal domains are observed.

Smolenski (3) originally proposed that underlying the relaxor behavior in $Pb(Mg_{1/3}Nb_{2/3})O_3$ (PMN) was a positional disorder on the B-site cation leading to compositional hetereogeneity and locally varying transition temperatures, which effectively "diffused" the macroscopic transition. Randall (6) and Harmer (7) have recently observed contrast on the nanometer scale in PMN using transmission electron microscopy (TEM). It is believed that the contrast signals compositional variation on the scale of approximately 50 A^o. Setter (5) found the development of a superlattice on annealing $Pb(Sc_{1/2}Ta_{1/2})O_3$ (PST) relaxors, a corresponding change in the relaxor behavior was also observed. In the annealed sample the relaxor character was suppressed, whereas in a quenched sample it was enhanced. Randall has also observed small scale contrast in quenched PST, but upon annealing the scale of the contrast coarsened (8). Such coarsening and corresponding change in the relaxor character upon heat treatment have not been observed in PMN.

Cross (9) has proposed that the scale of the chemically homogeneous regions in PMN is such that the orientation of the spontaneous polarization can be thermally agitated, analogous to superaparamagnetism (10). He has recently shown that the polarization fluctuations undergo a Vogel-Fulcher type freezing (11), analogous to spin and dipole glasses (12,13,14). It was suggested that correlations between

superparaelectric sized moments were responsible for freezing, leading to a broadening of the relaxation time distribution (15) and a deviation from Curie-Weiss behavior (16). It is the intent of this work to study the dependence of the glassy character on the degree of long range chemical ordering (LRO) in PST.

II. EXPERIMENTAL PROCEDURE

The data analyzed in this study was previously reported by Setter (5). Her samples were PST single crystals grown by a flux method, and were aligned along the (100) direction. The as grown single crystals had a high degree of long range positional order on the B-cation site, S=0.80 (where S is the % LRO). In order to introduce chemical disorder, crystals were soaked at 1400°C for 30 minutes and subsequently air quenched, resulting in S=0.35. The complex susceptibility was measured as a function of temperature between 120 and -70°C at a cooling rate of 2°C/min using a HP 4270A LCR meter. The measurement frequencies used were 1, 10, 10^2, and 10^3 KHz.

III. RESULTS AND DISCUSSION

The complex susceptibility, $\chi=\chi'+i\chi''$, of PST for S=0.35 and 0.8 are shown in Figures 1(a) and (b). A plot of Curie-Weiss behavior ($C/(T-\theta)$) is also shown in figure 1(a), C and θ were determined from high temperatures (*). The maxima of χ' and χ'' were supressed with decreasing LRO, and shifted to lower temperatures. Dispersion of T_{max} was observed in both samples, but the degree of dispersion increased with decreasing LRO. The dispersion of χ' was also enhanced below T_{max} with decreasing LRO. At temperatures above 75°C, the value of χ' for both the S=0.35 and 0.80 responses exhibited Curie-Weiss behavior. At lower temperatures deviation from Curie-Weiss behavior developed which increased with decreasing LRO. The width of the absorption peak also increased with decreasing LRO, and became less dispersive. The value of χ'' was essentially frequency independent below -40 and 5°C for S=0.35 and 0.80, respectively, reflecting a

freezing. Similar behavior has recently been observed in PMN (15). The implication is that the nature of the frozen state is strongly dependent on the degree of LRO, changing from spin glass like behavior for S=0.35 to normal ferroelectric behavior for S=0.80.

The dispersion of T_{max} was modelled using the Vogel-Fulcher relationship, $1/\tau=1/\tau_o exp(-E_a/k(T-T_f))$ where E_a is an activation energy and T_f a freezing temperature. Minimum variance was obtained for $1/\tau_o$ equal to 10^{12} sec^{-1}. E_a was found to be 0.03 and 0.015 eV for S=0.35 and 0.80, and T_f equaled 233 and 279°K respectively agreeing with the temperatures at which the stable remanent polarizations collapsed (5). The modelling of the data is shown in Figures 2(a) and (b). The deviation from Curie-Weiss behavior was also modelled using the Sherrington- Kirkpatrick relationship (16,17); $\chi'= C(1-q)/(T-\theta(1-q))$ where C is the Curie constant, θ the Curie-Weiss temperature, and q a local order parameter. The modelling was done using the 100 KHz permittivity data. The parameters C and θ were determined from high temperatures were Curie-Weiss behavior was observed, following a procedure previously described (16). The paramters C and θ were found to be independent of the degree of LRO, having values of $1.5x10^5$ and 310°K respectively. This suggests that the temperature of the onset of local polarization (T_{burns}) may also be independent of the degree of LRO. q as function of temperature for S=0.80 and 0.35 is shown in Figure 3. For S=0.35, q decreased nearly linearly between 200 and 300°K, and seemingly tailed to zero near 370°K. For S=0.80, q decreased slowly between 200 and 260°K, and decreased dramatically around T_f tailing to zero near 350°K. The tailing of q to zero occurred more sharply in the highly ordered state than in the partially ordered, indicating the development of characteristics of a normal ferroelectric transition.

The development of LRO has been shown to occur by the coarsening of B-site cation ordered regions (8). These regions were on the scale of 2-5 nm in the partially

ordered (quenched) state (similar size as in PMN), and the relaxor behavior is pronounced. In contrast in the highly ordered (annealed) state the scale of the regions was nearly 500 nm, and the relaxor character suppressed. These observations suggest that the relaxor behavior reflects the degree of LRO, and consequently the scale of the spontaneous polarization. The larger the scale of the chemical inhomogeneity, the larger the scale of the homogeneously polarized regions, consequently strong correlations can develop and the relaxor character is suppressed. The inhomogeneity may prevent the development of correlations by breaking the local translational symmetry of the polarization, "diffusing" the dielectric response in a manner which reflects the temperature dependence of the development of correlations. The sharp change in q near T_f for S=0.80 shows that correlations develop relatively rapidly over a small temperature interval, and suggests that the moments may freeze into ordered configurations with correlation lengths approaching the macroscopic scale similar to a normal ferroelectric. The evolution of the normal ferroelectric state may occur by the development of correlations sufficiently strong to override the chemical inhomogeneity which prevent long range polar ordering in the quenched state. The decrease in the tailing of q to zero above T_f with increasing LRO also indicates that the development of correlations between moments are occuring over a sharper temperature interval.

Freezing of the fluctuations may occur when q reaches a certain value. Assuming this value to be 0.3, it can be seen that the temperature interval (ΔT) from q=0 to 0.3 is larger for S=0.35 than 0.80. The Vogel-Fulcher relationship is believed to phenomelogically describe a temperature dependent correlation length between Debye relaxators (18,19). It is proposed that the decrease in E_a with increasing LRO is a reflection of the sharper temperature interval over which correlations develop. The smaller the temperature interval, the smaller the dispersion

in T_{max}, consequently the smaller E_a. At the limit of ΔT approaching zero, E_a is zero, and quite simply a normal ferroelectric transition occurs.

On zero field heating from the field cooled state to temperatures below T_f and subsequently recooling, it has been shown that the macroscopic polarization does not return to the initial value in the partially ordered state but rather remains at the value of the highest temperature reached (20). Whereas in the highly ordered state P_r tends to return to its initial value on recooling. These results show that the polarization mechanism of the disordered state is glassy, as discussed previously for PMN (21). The mechanism in the highly ordered state has characteristics of a normal ferroelectric, in which the temperature dependence of the spontaneous polarization is in part governed by Landau-Devonshire phenomenology.

The dielectric response of PMN has been modelled by assuming a distribution of relaxators (15), by analogy to spin and dipolar glasses (22). Following the previous procedure, χ'' can be approximated by ;

$$\chi''(T,\tau) = \chi'_o(T)\ G(T,\tau) \qquad (1)$$

where $G(T,\tau)$ is the distribution of relaxation times, $\chi'_o(T)$ the low frequency limit of $\chi'(T,\omega)$, and $\tau=\omega^{-1}$. The isotemporal cross sections, $G(\tau_o,T)$, as a function of temperature are shown in Figure 4(a) and (b) for S=0.35 and 0.80, respectively. For S=0.35 the relaxation time distribution increases distinctly near T_{max}, and then decreases slowly with decreasing temperature presumably approaching zero near 0^oK. With increasing frequency, the edge of the distribution moved to higher temperatures. For S=0.80 similar behavior was observed, but a sharp maximum in $G(\tau_o,T)$ was observed at T_f. Above T_f the edge of the distribution was not significantly dispersive in the frequency range investigated, and below T_f $G(\tau_o,T)$ was much smaller than for S=0.35. The sharp maximum in $G(\tau_o,T)$ near T_f for S=0.80 indicates that there is a distinct condensation of moments. This sharp

condensation is somewhat characteristic of a phase transition, rather than a freezing into a glassy state.

Temperature dependent relaxation time spectra for S=0.35 and 0.80 are proposed in Figures 5(a) and (b), respectively. Both figures show the isothermal width of the spectrum becoming very broad near T_f, approaching the macroscopic time regime. The shortest relaxation time (τ_{min}) is shown to approach macroscopic times only at temperatures far below T_f for both distributions. The shape of the distribution for S=0.80 is shown to be much less frequency dependent than for S=0.35, remaining relatively independent until microscopic times. The temperature of the maximum relaxation time (τ_{max}) is also shown to be much less dispersive than for the disordered state, again only becoming frequency dependent in the microscopic regime. In the microscopic regime the distribution for S=0.80 is shown to sharpen more rapidly with increasing temperature than for S=0.35. At higher temperatures, τ_{max} is shown to approach τ_{debye} near T_{burns} for both distributions illustrating the fact that the temperature of the onset of local polarization is not significantly dependent on the degree of LRO. In the limit of S=1 the distribution would continue sharpening around T_f, τ_{max} would be nondispersive until frequencies approaching τ_{debye}, and the distribution would be skewed more towards macroscopic times at T_f.

A summary of the results are illustrated in the phase diagram shown in Figure 6. The region bounded by θ and T_f is shown to have the polarization thermally fluctuating. The polarization fluctuations are shown to freeze into a glassy phase for low degrees of LRO. This glassy behavior has previously been shown to arise due to correlations between superparaelectric moments (11,15,16,21). The phase boundary is extrapolated to 0^oK at a finite degree of LRO. The extrapolation was done to illustrate the fact that below a certain chemical cluster size, superparaelectric effects will not be observed. The polarization fluctuations are shown to freeze into a

ferroelectric phase with rhombohedral symmetry for high degress of LRO. The boundary between the spin glass and ferroelectric phases is dashed in, but in reality there is probably a gradual transition from the glassy state to the ferroelectric state. The paramters θ and T_{burns} are shown to be essentially independent of the degree of LRO, indicating that they are solely determined by the macroscopic composition. The value of T_f is shown to approach θ as the %LRO approaches one, indicating the relaxor character is incipient from small degrees of disorder.

IV. CONCLUSIONS

The deviation from Curie-Weiss behavior has been modelled for PST samples with various degrees of long range chemical ordering. A distinct increase in correlations between moments was found near T_f in the highly ordered state. It was consequently proposed that the polarization fluctuations "freeze" into a ferroelectric state in the highly ordered samples, and into a dipolar glass state in the partially ordered. The relaxation time distributions were also calculated for both the highly and partially ordered states, and a phase diagram as a function of the percentage long range order proposed.

ACKNOWLEDGEMENTS

This work has been supported in full by contracts administered through the Office of Naval Research.

REFERENCES

1) G. Burns, F. Dacol, Sol. State Commun. **48**, 853 (1983).

2) V. Bokov, I. Myl'nikova, Sov. Phys. Sol. State **3**, 3 (1960).

3) G. Smolenski, A. Agranovskaya, Sov. Phys. Sol. State **1**, 1429 (1960).

4) Private Communication between L.E. Cross and G. Smolenski.

5) N. Setter, PhD Dissertation, The Pennsylvania State University (1980).

6) C. Randall, A. Bhalla, J. Mat. Sci. **29**, 5 (1990).

7) J. Chen, H. Chan, M. Harmer, J. Amer. Cer. Soc. **72**, 593 (1989).

8) C. Randall, D. Barber, R. Whatmore, P. Groves, J. Mat. Sci. **21**, 4456 (1986).

9) L.E. Cross, Ferroelectrics **76**, 241 (1987).

10) L. Neel, Compt. Rend. Acad. Sci. **228**, 664 (1949).

11) D. Viehland, S.J. Jang, M. Wuttig, L.E. Cross, J. Appl. Phys. **68**, 2916 (1990).

12) J. Tholence, J. Appl. Phys. **50**, 7369 (1979).

13) J. Tholence, Sol. State Com. **35**, 113 (1980).

14) E. Courtens, Phys. Rev. Lett. **52**, 69 (1984).

15) D. Viehland, S.J. Jang, M. Wuttig, L.E. Cross, unpublished.

16) D. Viehland, S.J. Jang, M. Wuttig, L.E. Cross, Submitted to Phys. Rev. B.

17) D. Sherrington, S. Kirkpatrik, Phys. Rev. Lett. **35**, 1972 (1975).

18) S. Shtrikman, E.P. Wohlfarth, Phys. Lett. **85A**, 467 (1981).

19) R. Chantrel, E.P. Wohlfarth, J. Magn. Magn. Mat. **40**, 1 (1983).

20) N. Setter, unpublished.

21) D. Viehland, S.J. Jang, M. Wuttig, L.E. Cross, Submitted to Phys. Rev. B.

22) L. Lundgren, P. Svedlinch, O. Beckman, J. Magn. Magn. Mat. **25**, 33 (1981).

LIST OF FIGURES

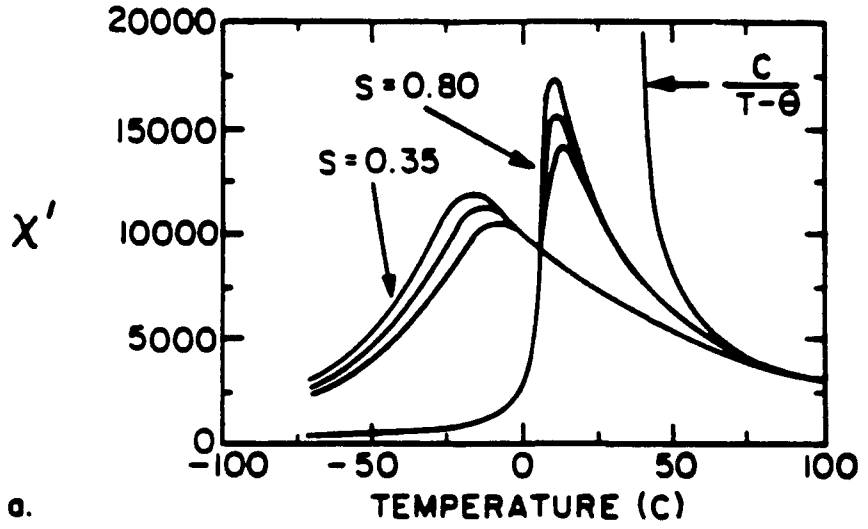
20000
15000
10000
5000
0
χ'
S = 0.80
S = 0.35
C
T-θ
-100
-50
0
50
100
TEMPERATURE (C)

a.

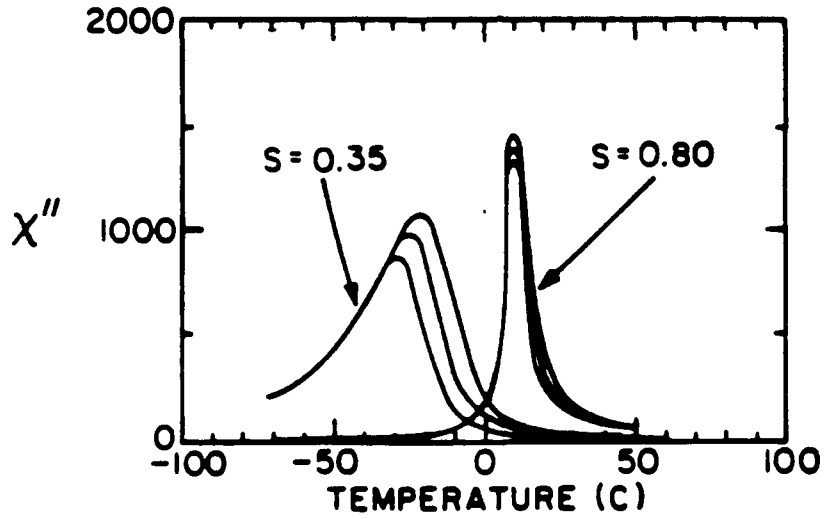
2000
1000
0
χ''
S = 0.35
S = 0.80
-100
-50
0
50
100
TEMPERATURE (C)

b.

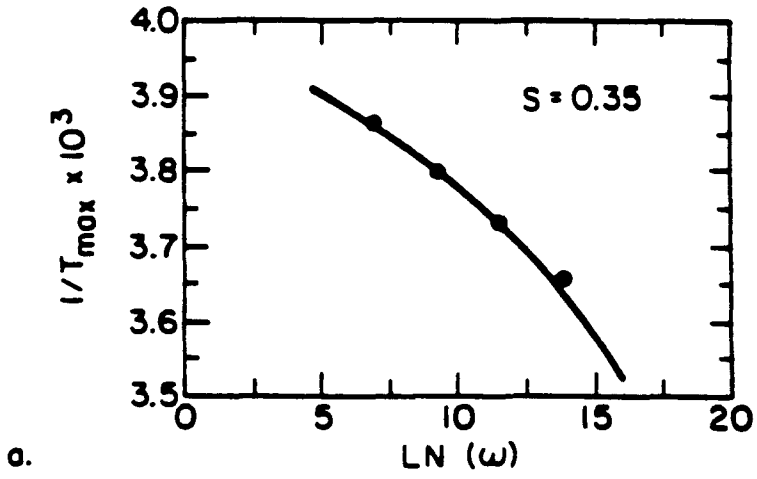
4.0
3.9
3.8
3.7
3.6
3.5
$1/T_{max} \times 10^3$
S = 0.35
0
5
10
15
20
LN (ω)

a.

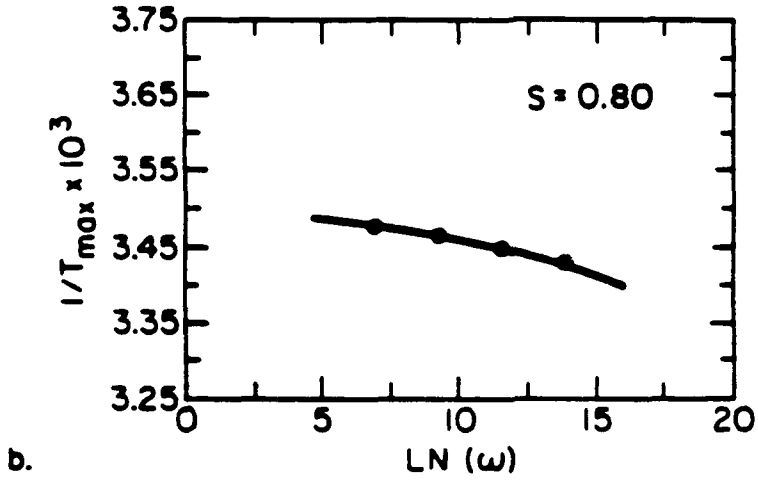
3.75
3.65
3.55
3.45
3.35
3.25
$1/T_{max} \times 10^3$
S = 0.80
0
5
10
15
20
LN (ω)

b.

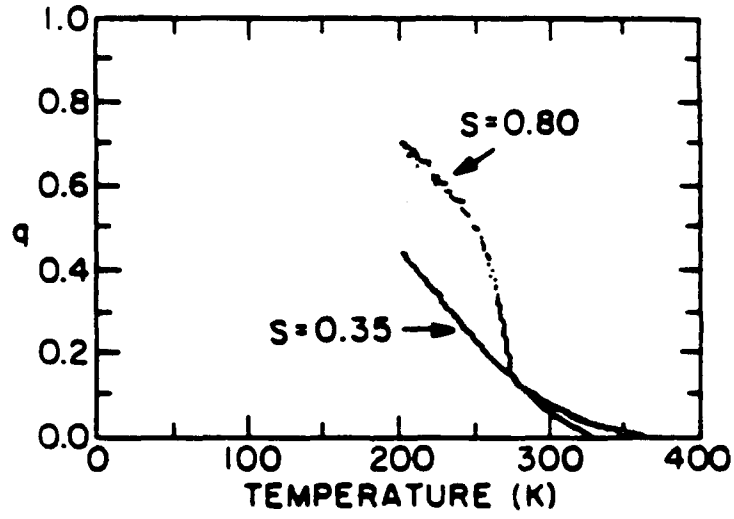
1.0
0.8
0.6
0.4
0.2
0.0
q
S=0.80
S=0.35
0
100
200
300
400
TEMPERATURE (K)

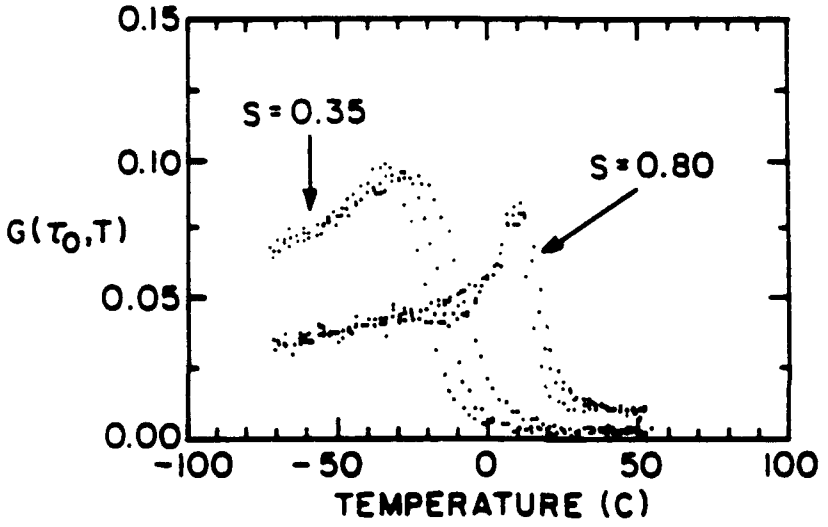
0.15
0.10
0.05
0.00
S = 0.35
S = 0.80
G(τ0,T)
-100
-50
0
50
100
TEMPERATURE (C)

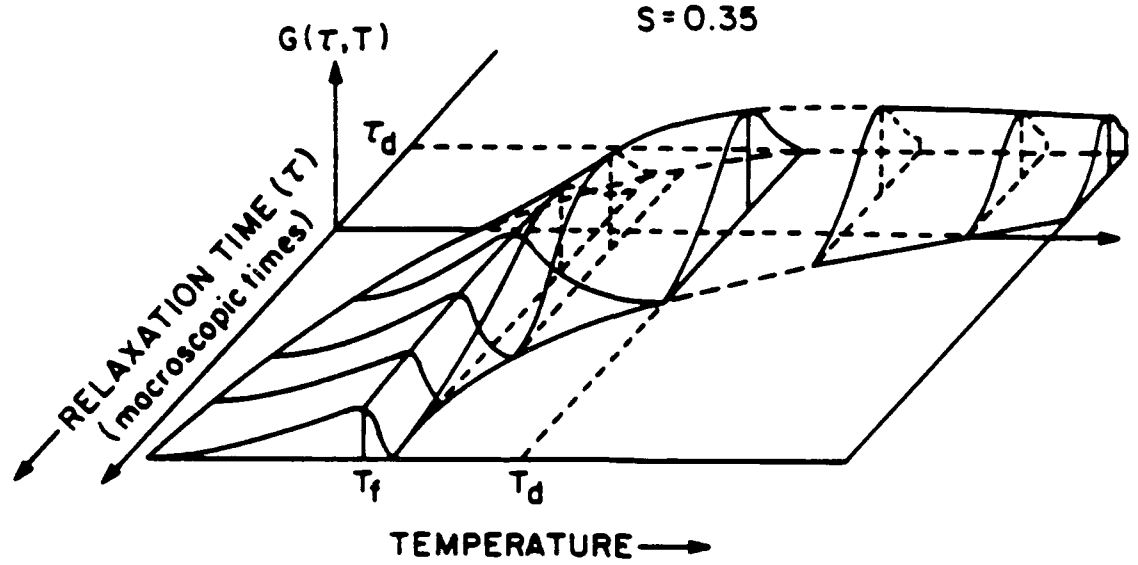
S = 0.35
G(τ,T)
τ_d
RELAXATION TIME (τ)
(macroscopic times)
T_f
T_d
TEMPERATURE

a.

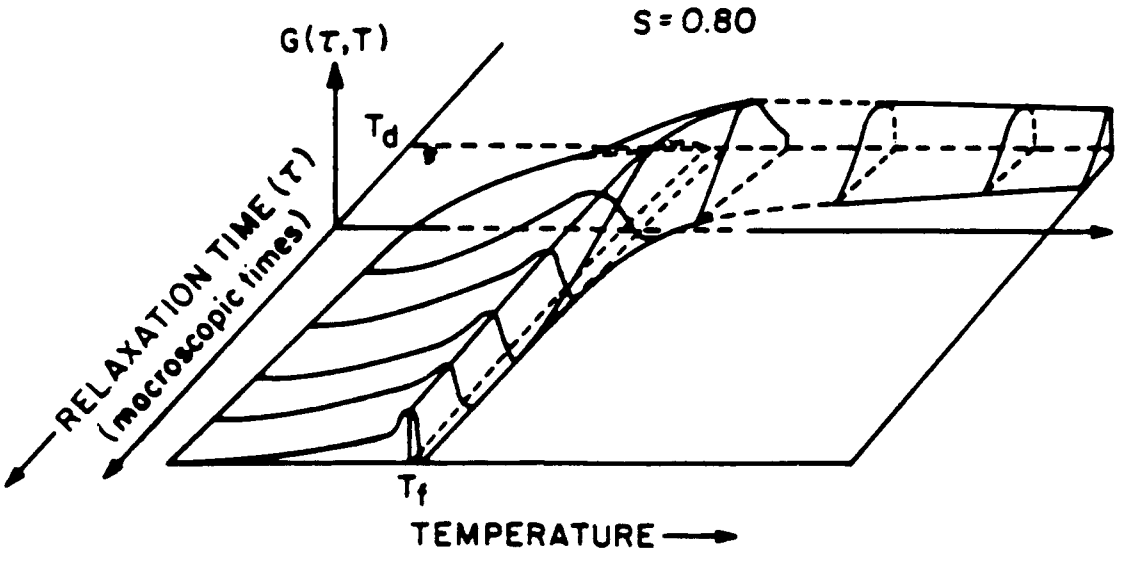
S = 0.80
G(τ,T)
T_d
RELAXATION TIME (τ)
(macroscopic times)
T_f
TEMPERATURE

b.

APPENDIX 31

Ferroelectrics Letters, 1990, Vol. 12, pp. 35-42
Reprints available directly from publisher
Photocopying permitted by license only

AN INVESTIGATION OF THE STRUCTURAL AND DIELECTRIC PROPERTIES OF THE SOLID SOLUTION SYSTEM (1-x) $Pb(Sc_{1/2}Ta_{1/2})O_3$ - (x) $PbTiO_3$†

J.R. GINIEWICZ, A.S. BHALLA , and L.E. CROSS
Materials Research Laboratory, The Pennsylvania State University, University Park, Pennsylvania - USA

(Received for Publication June 27, 1990)

Abstract The preliminary characterization of the structural and dielectric properties of compositions from the solid solution system (1-x) $Pb(Sc_{1/2}Ta_{1/2})O_3$ - (x) $PbTiO_3$ is presented. A morphotropic phase boundary between rhombohedral (pseudocubic) and tetragonal compositions is observed to exist between x = 0.4 and x = 0.45. A wide range of dielectric response is exhibited by the various compositions investigated ranging from the diffuse dispersive response characteristic of relaxor - type ferroelectrics to the sharp K(T) response associated with normal ferroelectrics. A high dielectric constant maximum is observed for all compositions with a peak K(max) of 33000 occurring for x=0.4.

INTRODUCTION

A relaxor ferroelectric is generally characterized by the following: (a) a diffuse and dispersive dielectric response as a function of temperature and frequency in the radio frequency range, (b) a quadratic dependence of the inverse permittivity on temperature, (c) a remanent polarization, P(r), which does not exhibit a sharp transition but rather gradually varies through a broad range of temperatures so that the maximum spontaneous polarization, P(s), occurs only at temperatures well below that of the dielectric maximum and, (d) a pseudocubic nature whereby there is observed virtually no optical anisotropy or x-ray diffraction line splitting when specimens are cooled to very low temperatures. Typical relaxor materials have either a perovskite or tungsten - bronze stucture.

Perovskite relaxor ferroelectrics of the form ABO_3 generally occur with the A and/or B-sites shared by two or more cations of the appropriate valence and ionic radii. The weak field dielectric permittivity and Tanδ as a function of temperature and frequency exhibit broad dispersive maxima characteristic of a diffuse ferroelectric transition This behavior has been described by the theory of "compositional fluctuations" in which local variations in composition lead to the formation of ferroelectric (polar) and paraelectric (non-polar) microregions on the order of 100 - 200 Å. [1] Each polar region will possess its own Curie temperature dependent on its local composition so that the material as a whole will proceed through the transition over a range of temperatures known as the Curie range. Polar regions with volumes on the order of 100 ($Å^3$) are unstable against thermal agitation and, hence, the distribution and relative density of the microregions are strongly temperature dependent. [2]

The material of interest in this study is $Pb(Sc_{1/2}Ta_{1/2})O_3$ [PST], a relatively simple system whose degree of ordering can be easily "adjusted" by the appropriate heat treatment and is readily characterized for its degree of order by x-ray diffraction. Previous investigations of this material were concerned chiefly with the unmodified compound and correlated the occurrence of relaxor behavior, as evidenced by the

†Communicated by Dr. George W. Taylor

dispersion of K(T) in the radio frequency range, with the degree of ordering.[3-5] This study extends this previous work by considering the solid solution system of (1-x) Pb(Sc1/2Ta1/2)O3 - (x) PbTiO for which a variety of order / disorder conditions exist as a function of composition. This system is unique in that, unlike other complex systems of its kind, it could conceivably cover the entire spectrum of ferroelectric behaviors specifically associated with the three main catagories of structural ordering[6] indicated in Table 1 for this family of materials. Based on the preliminary results of this study, it appears that the system (1-x)Pb(Sc1/2Ta1/2)O3 - (x)PbTiO3, being of variable structural order both by means of heat treatment and compositional variations, will exhibit the representative ferroelectric behavior of all three states of structural order shown in Table 1. This "all-in-one" system could thereby be of considerable importance in further elucidating the fundamental nature of relaxor ferroelectric materials as it correlates to structural (dis)order.

In this preliminary investigation of the solid solution we have sought to locate the morphotropic phase boundary region by means of x-ray diffraction and dielectric measurement. The effect of compositional variations on the nature of the ferroelectric behavior as evidenced in representative K(T) / D(T) curves was also examined.

TABLE 1. Classification scheme of the complex lead perovskites.[6]

ORDER TYPE	DISORDER	SRO	LRO
FERROELECTRIC BEHAVIOR	NORMAL FE /AFE	RELAXOR	NORMAL FE/AFE
MATERIALS	PMN : PMN - PT	PMN : PMN - PT	PIN
	PZN: PZN - PT	PZN: PZN - PT	PST
	PZT	PST / PSN	PSN
	(1-x)PST - (x)PT	(1-x)PST - (x)PT	(1-x)PST - (x)PT

SAMPLE PREPARATION

Ceramic samples of compositions (1-x)Pb(Sc1/2Ta1/2)O3 - (x)PbTiO3 [x: 0, 0.025, 0.05, 0.1, 0.2, 0.3, 0.4, 0.45, 0.5] were prepared by a conventional mixed oxide technique employing the wolframite precursor method[7] in order to reduce to the occurrence of undesirable pyrochlore phases. Starting oxides Sc2O3† and Ta2O5† were initially batched and double calcined at 1400°C for 4 hours to form the wolframite [8] [ScTaO4] precursor phase. The compositions of interest were then formulated from PbO†, TiO2†, and ScTaO4, ball milled with zirconia media for ~6 hrs and subjected to double calcination in closed crucibles at 900 °C for 4 hours and 1000 °C for 1 hour. Pellets [1.25 cm] in diameter were formed and sintered in

†PbO [Johnson Matthey - Materials Technology UK - Grade A1]; Sc2O3 [Boulder Scientific Co. - 99.99%]; Ta2O5 [Hermann C. Starck (Berlin) - Stand. Opt. Grade]; TiO2 [Aesar (Johnson Matthey Inc.) - 99.999%]

sealed crucibles at temperatures ranging from 1400-1560 °C and for times [0.5 - 1.5 hours] depending on the sample composition. Source powders of PST and $PbZrO_3$ were used to maintain a suitable Pb atmosphere within the crucibles. Total weight losses after sintering were typically $\leq 1\%$ for compositions [$x \geq 0.2$] and somewhat higher, 2 - 5%, for those with [$x < 0.2$] for which the higher sintering temperatures were required.

Samples prepared for the x-ray diffraction study described in the next section were all sintered at 1400 °C for 1 hour and ground to a powder for measurement. Specimens for dielectric testing were cut as blocks from the sintered disks typically [0.75 cm] on edge and [0.15 cm] in thickness. The sample surfaces were ground [12 μm Al_2O_3], cleaned, and sputtered with gold. Silver contact points were applied to the gold sputtered surfaces.

X-RAY DIFFRACTION

Structure type, lattice parameter, theoretical density, and the degree of long range structural ordering were determined for each composition by means of x-ray diffraction using a Philips APD3600 automated x-ray diffractometer and are recorded in Figure 1 and Table 2. Cu Ka radiation was employed. Scans were made on powder samples incorporating a Si [SRM 640] standard over a range of 42 - 52 ° (2O) at a rate of [0.25 ° / min] and the 200 and 210 reflections were used to determine lattice parameters and to identify the region of the morphotropic phase boundary. Compositions for which [$x \leq 0.4$] are pseudocubic with lattice parameter, a, that decreases with increasing $PbTiO_3$ content as shown in Figure 1. The density also decreases with increasing x [Table 2]. Compositions [$x \geq 0.45$] are tetragonal. The observations recorded in Figure 1 along with the associated values of Kmax(x), to be described further in the next section, indicate that the morphotropic phase boundary lies in the composition range between $x = 0.4$ and $x = 0.45$.

The degree of structural order was evaluated by means of the long range order parameter, S, which is defined in terms of the relative intensities of the superlattice and normal lattice reflections as:

$$S^2 = \left[\frac{I_{super}}{I_{norm}}\right]_{obs.} \left[\frac{I_{norm}}{I_{super}}\right]_{calc.} \qquad (1)$$

where the superlattice / normal reflection pairs generally employed are 111/200 and 311/222. [3-5] The long range order parameter, S, describes the average distribution of ions sharing the B-site; a completely ordered arrangement of ions has S=1 while a completely disordered arrangement is denoted by S=0. The calculated ratio in Equation (1) is determined for the completely ordered condition [S=1] and takes on values 1.33 and 0.59 for the 111/200 and 311/222 pairs respectively. [5]

The long range order parameter, S, was determined for samples in this series for which [x=0.025 - 0.1], all of which retained some degree of order as evidenced by the presence of superlattice lines at the sintering and / or calcination steps of the processing agenda. The 111/200 reflection pair was recorded at a scan rate of [1 °/min] and used to evaluate S in these cases. It is seen [Table 2] that some ordering may still be retained for the [x=0.025] and [x=0.05] specimens which were

TABLE 2. Volume, x-ray density, and S parameter for (1-x)Pb(Sc1/2Ta1/2)O3 - (x)PbTiO3.

x	Vol. (Å)	S	Density (xrd) (g/cc)	ref.
0	67.52	-	9.051	9
0.025	67.47	0.6	9.021	
0.05	67.32	0.5	9.002	
0.1	66.92	0.0	8.975	
0.2	66.58	-	8.855	
0.3	66.09	-	8.760	
0.4	65.50	-	8.674	
0.45	65.40	-	8.606	
0.5	64.92	-	8.585	

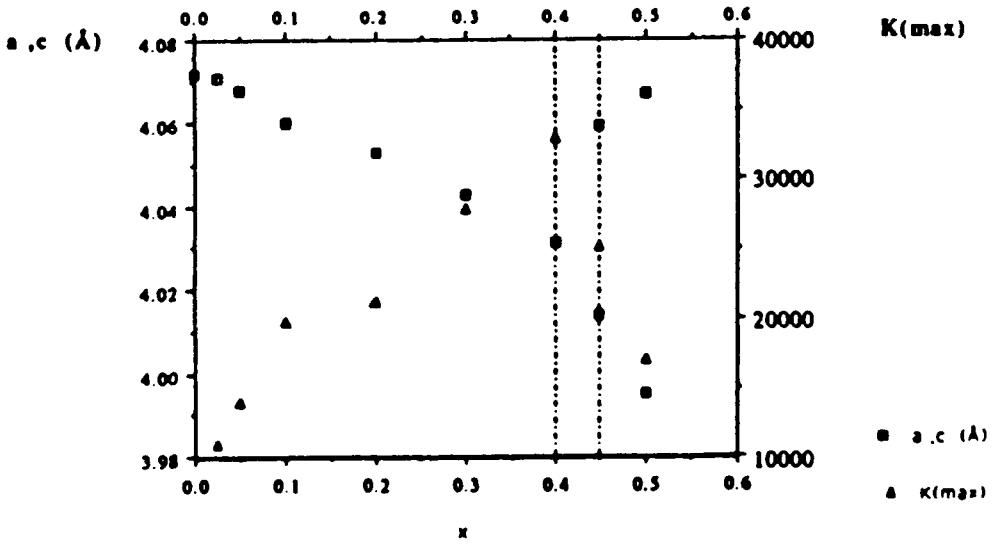

FIGURE 1 Lattice parameter and K(max) as a function of x.

sintered at a somewhat lower temperature than what was employed to produce the denser samples for dielectric measurement. Superlattice lines were also persistent in [x=0.1] calcined powders indicating a degree of order [S = 0.35] but were not observed in the sintered samples. Samples of all three compositions, x = 0.025, 0.05, 0.1, fired at temperatures ≥ 1500°C do not possess superlattice peaks. It has yet to be determined if the superstructure detected for the specimens prepared at lower temperatures reflects a true ordering of the solid solution phase or simply that associated with remnant $Pb(Sc_{1/2}Ta_{1/2})O_3$. A more thorough investigation of these compositions is currently underway to better establish both the degree of order that is retained with small concentrations of $PbTiO_3$ and the range of compositions for which some long range order persists. It is anticipated that for those compositions very near to pure PST there will still be present considerable structural ordering which, as for PST, may be affected by heat treatment. The optimum degree of ordering realized in these specimens will likely be limited by the concentration of Ti ions whose presence is expected to shorten the coherence length† of the ordering.

DIELECTRIC BEHAVIOR

The dielectric constant, K, and dissipation factor, D, were measured as a function of temperature and frequency using an automated system consisting of an oven (Model 2300, Delta Design Inc.), an LCR meter (Model 4274A, Hewlett Packard Inc.), and a digital multimeter interfaced with a desk top computer (Model 9816, Hewlett Packard Inc.). Dielectric runs were made over a temperature range of [-150 - +260 °C] and at frequencies of 100 Hz, 1 KHz, 10 KHz and 100KHz.

The data recorded in Table 3 and plotted in Figures 2 and 3 were taken on cooling at 1 KHz. A steady increase in K(max) is observed for compositions up to [x = 0.4] beyond which there is seen a decrease in the maximum value of the dielectric constant [Table 3 ; Figure 2]. The temperatures of K(max) and D(max) are both seen to increase markedly with increasing x. The extremely high value of K(max) obtained in the vicinity of the morphotropic phase boundary is worthy of note since it is indicative of strong piezoelectric, pyroelectric, and electrooptic responses.

The existence of relaxor nature for the various compositions is reflected in the values of the diffuseness coefficients ∂ and b(3/4) [Table 3], the difference [T(Kmax) - T(Dmax)] [Table 3 ; Figure 3], and in the degree of dispersion observed for K(T) / D(T) in the vicinity of the Curie range [Figure 4]. The diffuseness coefficient, ∂, is the most representative physically of the true relaxor nature of the material as it is derived directly from the quadratic dependence of [1/K] on temperature, characteristic of this class of ferroelectrics. This quadratic dependence has been described in conjuction with the "composition fluctuation" model.[10-12] A large ∂ value reflects a strong relaxor type response. The coefficient b(3/4) is the width of K(T) at values [3/4 K(max)]. It is a measure of diffuseness frequently employed by Stenger, et al. [5] to characterize the relaxor nature of PST and, hence, is presented here with the more conventional parameter, ∂, to facilitate comparison with earlier results on PST. A large value of b(3/4) indicates a strongly diffuse K(T) characteristic, but does not in itself completely reflect the relaxor nature of the material.

---

†The coherence length is defined in terms of the size of ordered domains as determined by TEM.[6]

TABLE 3. Dielectric data for (1-x)Pb(Sc1/2Ta1/2)O3 - (x)PbTiO3.

x	K(max)	T °C	D(max)	T °C	b(3/4) (K)	∂ (K)	% Density(xrd)
0 [S=0.5]	17500	7	0.07	-12	34	35	95
0.025	10900	9	0.08	-30	58	43	87
0.05	14000	26	0.07	-13	49	38	92
0.1	19800	39	0.06	18	38	34	92
0.2	21200	89	0.06	77	32	28	88
0.3	27800	134	0.04	117	33	26	93
0.4	33000	182	0.04	169	27	22	94
0.45	25100	204	0.04	201	23	-	94
0.5	17000	247	0.05	247	19	-	86

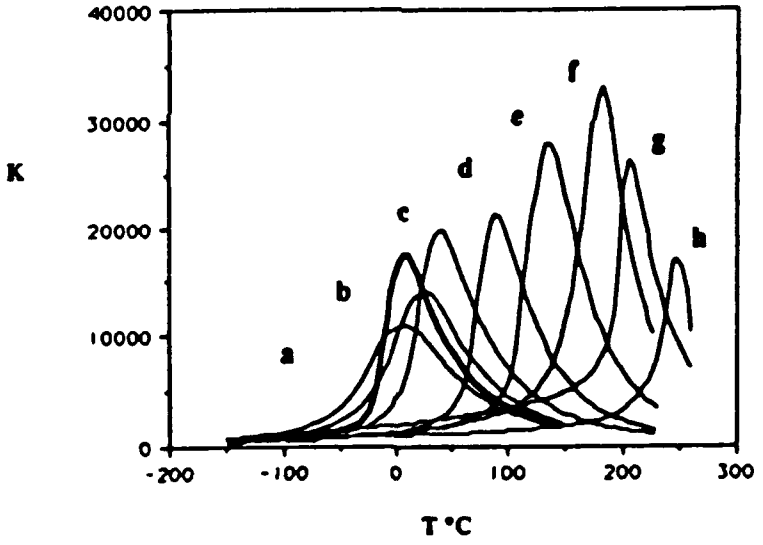

FIGURE 2 K(T) at 1KHz for (bold curve) PST, (a) x= 0.025, (b) x=0.05, (c) x=0.1, (d) x=0.2, (e) x=0.3, (f) x=0.4, (g) x=0.45, and (h) 0.5.

It is seen from the data appearing in Table 3 and Figure 3 that with increasing x the relaxor type response of the material is steadily decreasing as evidenced by the decrease in the coefficients ∂ and b(3/4) and the reduction in the difference between the temperatures of K(max) and D(max). The change in the shape of K(T) and the magnitude of K(max) with x at 1 KHz is shown in Figure 2 where there is observed a definite sharpening of the peak as x approaches the morphotropic phase boundary and the steady increase of K(max) up to x = 0.4 followed by a reduction in K(max) through the morphotropic phase boundary region. The dispersion of K(T) is also observed to become considerably less with increasing concentrations of PbTiO3 as shown in Figure 4 for compositions [x: 0.025, 0.3, 0.5] respectively. Hence, we see for this solid solution system a wide range of ferroelectric behaviors extending from full relaxor to normal ferroelectric responses which are dictated by both the variations in structural ordering, which develop with the addition of Ti ions to the B-site of the perovskite lattice, as well as to the transformation of the structure to that of the normal first order ferroelectric PbTiO3.

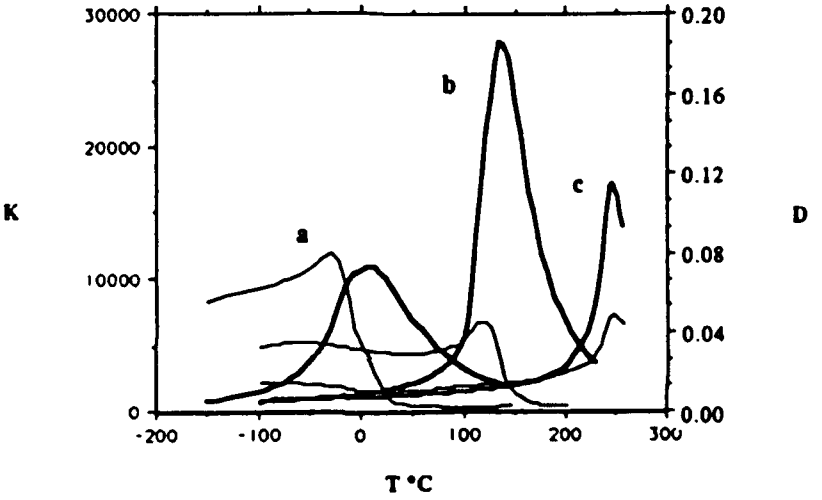

FIGURE 3. K(T) and D(T) at 1 KHz for (a) x=0.025, (b) x=0.3, and (c) x=0.5.

SUMMARY

Compositions from the solid solution system (1-x)Pb(Sc1/2Ta1/2)O3 - (x)PbTiO3 were prepared as ceramics through x = 0.5 in order to identify the region of the morphotropic phase boundary and to monitor the effect of increasing PbTiO3 content on the dielectric response. The morphotropic phase boundary was observed to lie in the composition range between x=0.4 and x=0.45. The dielectric constant, K, and dissipation factor, D, were measured as a function of temperature and frequency. The maximum dielectric constant was observed to increase steadily on approaching the morphotropic phase boundary with increasing x reaching a peak value of 33000 for the x=0.4 composition beyond which the dielectric constant maximum was observed to decrease. The dielectric response becomes less diffuse and dispersive with increasing PbTiO3 content reflecting a decrease in relaxor type behavior.

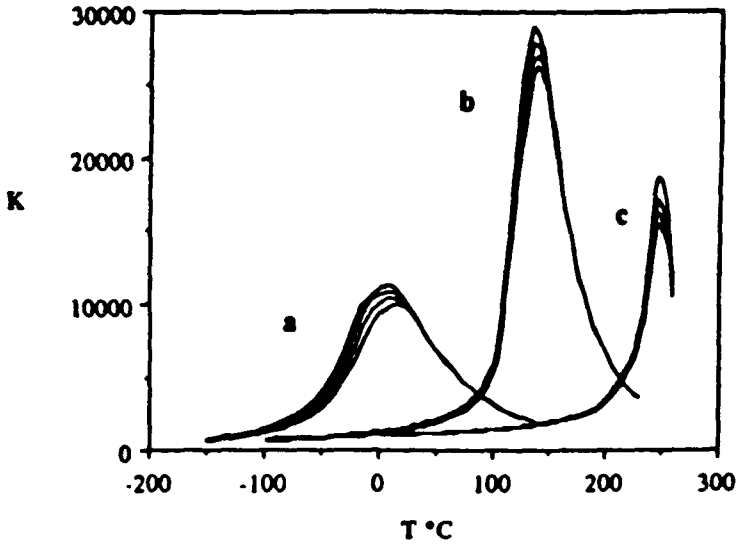

FIGURE 4. Dispersion of K(T) at 100 Hz, 1 KHz, 10 KHz, and 100 KHz for (a) x=0.025, (b) x=0.3, and (c) x=0.5.

ACKNOWLEDGEMENT

The authors would like to express their appreciation to Judy Marks for her assistance in collecting the x-ray data required for this investigation.

REFERENCES

1. G.A. Smolenskii and A.I. Agronovskaya, Sov. Phys.-Sol. State, 1, 1429 (1959).
2. L.E. Cross, Ferroelectrics, 76, 241 (1987).
3. N. Setter, Ph.D. Thesis, The Pennsylvania State University, (1980).
4. N. Setter and L.E. Cross, J. Appl. Phys., 54, 4356 (1980).
5. C.G.F. Stenger and A.J. Burggraaf, phys. stat. sol. (a), 61, 275 (1980).
6. C.A. Randall and A.S. Bhalla, Japan. J. Appl. Phys., 29(2), 327 (1990).
7. T.R. Shrout and A. Halliyal, Am. Ceram. Soc. Bull., 66(4), 704 (1987).
8. JCPDS #24-1017 - ScTaO4.
9. F.S. Galasso, Structure, Properties, and Preparation of Perovskite-Type Compounds (Pergamon Press, Inc., New York, 1969), p. 153.
10. V.A. Isupov, Sov. Phys.-Tech. Phys., 1, 1846 (1956).
11. V.A. Isupov, Sov. Phys.-Sol. State, 5, 136 (1963).
12. B.N. Rolov, Sov. Phys.-Sol. State, 6, 1676 (1965).

APPENDIX 32

Ferroelectrics Letters, 1990, Vol. 12, pp. 63-69
Reprints available directly from publisher
Photocopying permitted by license only

DIELECTRIC BEHAVIOR OF SINGLE CRYSTALS NEAR THE (1-x) $Pb(Mg_{1/3}Nb_{2/3})O_3$-(x) $PbTiO_3$ MORPHOTROPIC PHASE BOUNDARY†

THOMAS R. SHROUT, ZUNG P. CHANG, NAMCHUL KIM, and STEVEN MARKGRAF
Pennsylvania State University, Materials Research Laboratory, University Park, PA 16802

(Received for Publication August 22, 1990)

Abstract. Single crystals in the lead magnesium niobate-lead titanate-(1-x) $Pb(Mg_{1/3}Nb_{2/3})O_3$-(x) $PbTiO_3$ solid solution system were grown using a flux growth technique. Crystals over the compositional range of $0.3 \leq x \leq 0.4$ being near the rhombohedral (pseudo-cubic)-tetragonal morphotropic phase boundary were characterized. The dielectric behavior along the pseudo cubic [111] and [100] directions were measured as a function of temperature and frequency. The effect of poling was also examined.

INTRODUCTION

The complex perovskite lead magnesium niobate [$Pb(Mg_{1/3}Nb_{2/3})O_3$], hereafter designated PMN, exhibits a diffuse phase transition (Tc ~ 10°C) and strong frequency dispersion in the dielectric behavior characteristic of a relaxor ferroelectric.[1] In solid solution with the simple perovskite $PbTiO_3$ (PT), which exhibits a normal ferroelectric transition @ 490°C, the existence of a morphotropic phase boundary (MPB) has been reported.[2] The MPB separating the rhombohedral (pseudo cubic) and tetragonal phases was reported to occur at x = 0.4 PT, but with improved processing, (columbite precursor method)[3] occured at approximately x = 0.33 PT (see Fig. 1).[4] As found for other solid solution systems, both normal ($PbZrO_3$-$PbTiO_3$)[5] and relaxor type PZN $Pb(Zn_{1/3}Nb_{2/3})O_3$-PT,[6] compositions near the MPB exhibit anomalously high dielectric and piezoelectric properties making them candidates for a wide range of applications. To date, however, only polycrystalline PMN-PT materials have been examined.

It was the purpose of this work, to grow single crystals of PMN-PT near the MPB and to determine their dielectric and ferroelectric related properties.

This paper was originally presented at the Seventh International Meeting of Ferroelectricity, Saarbrucken, F.R. Germany, August 28 to September 1, 1989.

†Communicated by Dr. George W. Taylor

EXPERIMENTAL PROCEDURE

Single crystals in the (1-x) PMN-(x) PT solid solution system were grown from a PbO-B_2O_3 flux (mole ratio 2.65:0.35) similar to that previously reported.[7] The starting materials were completely reacted perovskite powder (reagent grade) with compositions x = 0.30, 0.35, and 0.40, all prepared using the columbite precursor method described by Swartz and Shrout.[3] The compound to flux ratio 1:3 was used. The reagents were mixed and charged in a platinum crucible (~ 100 ml) and heated to ~ 1150°C. Upon soaking for 10 hrs, the charge was slowly cooled at a rate of 3°C/hr to ~ 950°C and then to 800°C at 5°C/hr and finally to room temperature at 500°C/hr. The flux was removed by dissolving in a dilute nitric acid solution.

The crystals grown ranged from a few mm up to ~ 1 cm on a side, being light yellow, but dark brown with increasing size. The darkness of the crystals is believed to be the result of point defects as found for flux grown $PbTiO_3$ crystals,[8] thus the smaller crystals were mainly employed in this work. The crystals were generally in the form of simple cubes with (100) faces. X-ray powder diffraction of crushed crystals was used to confirm phase purity and to determine the structure and unit cell parameters.

In preparation for the dielectric measurements, samples in platelet form with the major face normal to the pseudo cubic {111} or {100} directions were prepared and electroded with sputtered on gold. Dielectric measurements (K and loss) were carried out as a function of temperature and frequency (0.1, 1, 10, and 100 kHz) for both unpoled and poled states. For ferroelectrics with diffuse phase transitions, the law, $1/K \sim (T - T_c)^2$, is found instead of the normal Curie-Weis law, from which the level of diffuseness (δ) was obtained. Poling was achieved by field cooling ($\equiv$ 10 Kv/cm) through T_c to room temperature. The piezoelectric constant d_{33} was measured on a Berlincourt d_{33}-meter.

RESULTS AND DISCUSSION

Physical and dielectric characteristics of the various crystals are reported in Table I. As presented, x-ray powder diffraction revealed them to be single phase possessing rhombohedral symmetry. Though it was anticipated that the 0.6 PMN-0.4 PT crystals be tetragonal, the observed rhombohedral (pseudo-cubic) symmetry was probably the result of compositional gradients.

The temperature dependence (on cooling) of the dielectric constant K for the various crystals, in general, increased with increasing PT content, as well as the sharpness (less diffuse) of the transition (see Fig. 2). The level of diffuseness for a relaxor ferroelectric, δ, as presented in Table I, also reflected the degree of order of the materials. However, as reported in Table I and shown in Fig. 1, a range of T_cs, (K_{max} @ 1 kHz) were observed for all starting compositions with the largest deviation found for 0.6 PMN-0.4 PT again indicating compositional variations. A

TABLE I. Physical and Dielectric Properties of PMN-PT MPB Crystals.

Growth Composition	Lattice Parameters Å	T_c (°C)	δ (°C)	+Piezo d_{33} (pC/N)
0.7 PMN-0.3 PT	a = 4.0196 α = 89°49'	120-155	31-24	1000-1500 (~ 300)
0.65 PMN-0.35 PT	a = 4.0165 α = 89°48'	150-170	23-22	900-1100 (~ 550)
0.6 PMN-0.4 PT	a = 4.017 α = 89°44'	160-203	20-18	1000-1500 (~ 350)

+Piezo d_{33} for pseudo-cubic [100] and value in parenthesis for [111].

range of K_{max} was also observed (20,000-60,000) with no clear correlation of optimum dielectric properties corresponding to a MPB being determined. The dielectric loss behavior was found to be typical for PMN-PT and thus was not shown. Variations in T_c for relaxor type MPB materials was not surprising. Not only do you have the coexistence of two ferroelectric states (rhombohedral and tetragonal), being relaxors (rhombo side) you also have the presence of micro-regions possessing a statistical distribution of T_cs. In addition, the coexistence of a tetragonal phase may influence the relaxor type behavior.

As presented in Fig. 1, the MPB for PMN-PT is curved indicating successive phase transitions from rhombohedral T_{R-T} tetragonal T_{T-C} cubic upon heating. This behavior is marked by anomalies in K vs. T curves as shown in Fig. 3a, whereby the highly diffuse T_{R-T} transition is evident by a change in slope. Such anomalies were observed in both [100] and [111] plates, being pronounced for those which possessed T_cs near the reported MPB boundary. Upon poling, the multiple transitions were enhanced with the T_{R-T} transitions shifting down for [100] and up for [111], but other influences existed. What were believed to be T_{R-T} transitions (see Fig. 3b) are actually macro —> micro domain transitions near T_{R-C} similar to that observed in PLZT.[11] Poling also influenced the level of K_{max} being increased for the more rhombohedral compositions (0.7 PMN-0.3 PT) and decreasing for the higher T_c and hence more tetragonal materials. This behavior is exemplified in Fig. 4, where upon poling, the R-T region and associated permittivity increased while the T-C region showed normal ferroelectric behavior, that is, less diffuse with little frequency dispersion due to macro-domain pinning. The piezoelectric properties of the various crystals are reported in Table I, again

showing variations. The piezoelectric d33 [100] values found to be very high > 1000 pC/N, whereas, the d_{33} values in [111] plates were much lower, approximately one third to one half. The fact that the piezoelectric constants are larger n the non-polar axis was also found in the PZT-PT system.[9]

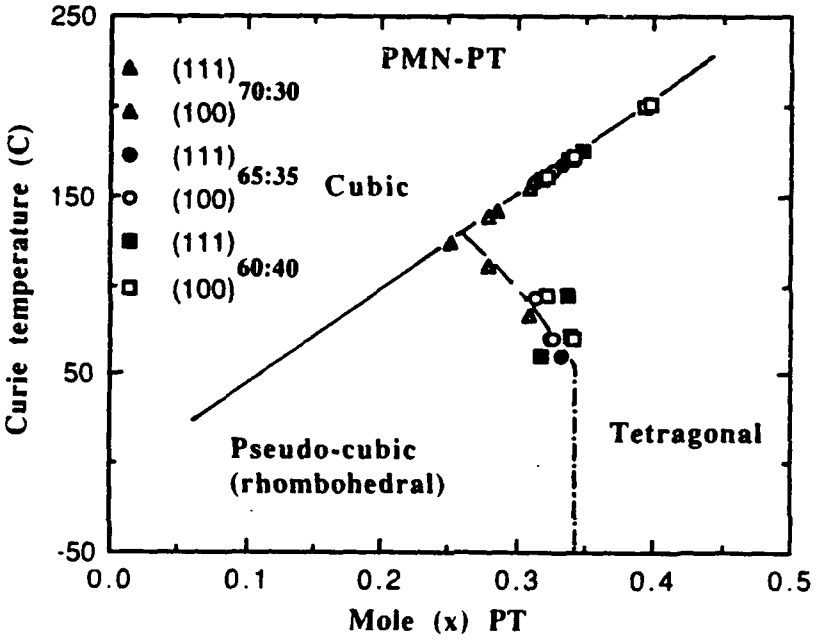

FIGURE 1. The PMN-PT Phase System Showing the Reported[4] MPB. Data Shown is for Single Crystals Grown in this Work.

SUMMARY

(1) Single crystals in the lead magnesium niobate-lead titanate (1-x) $Pb(Mg_{1/3}Nb_{2/3})O_3$-(x) $PbTiO_3$ solid solution (x = 0.3, 0.35, and 0.4) were grown using a PbO-B_2O_3 flux growth technique.

(2) Variations in composition associated with growth parameters or the complex nature of relaxor ferroelectrics near a MPB, were reflected in the range of T_cs, for a given starting composition.

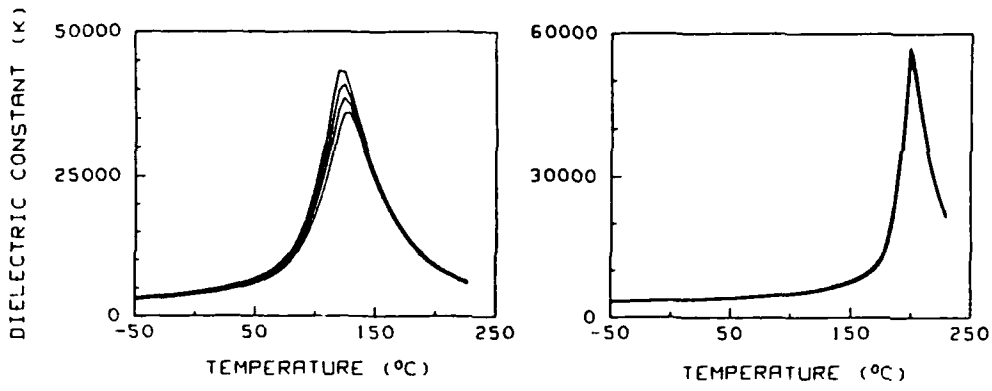

FIGURES 2a,b. The Dielectric Constant K Versus Temperature on Cooling for (a) 0.7 PMN-0.3 PT [111] (Left) and (b) 0.6 PMN-0.4 PT [100] (Right).

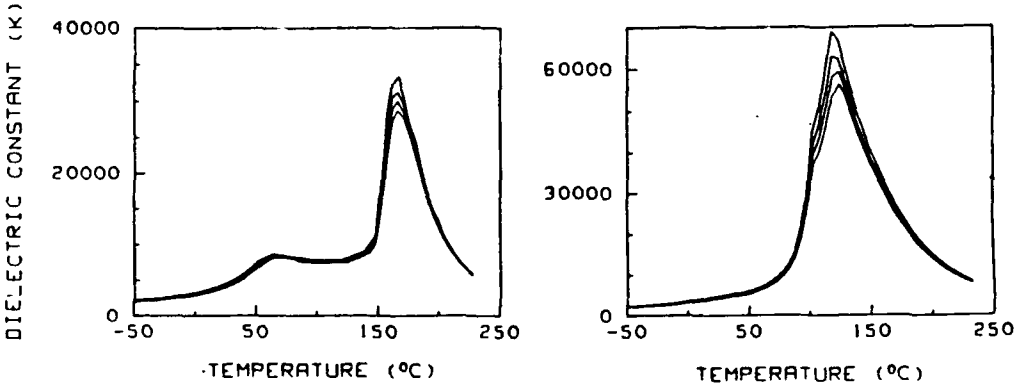

FIGURES 3a,b. The Dielectric Constant K Versus Temperature for (a) Unpoled and Poled 0.65 PMN-0.35 PT [100] (Left) and (b) Unpoled and Poled 0.7 PMN-0.3 PT [111] (Right).

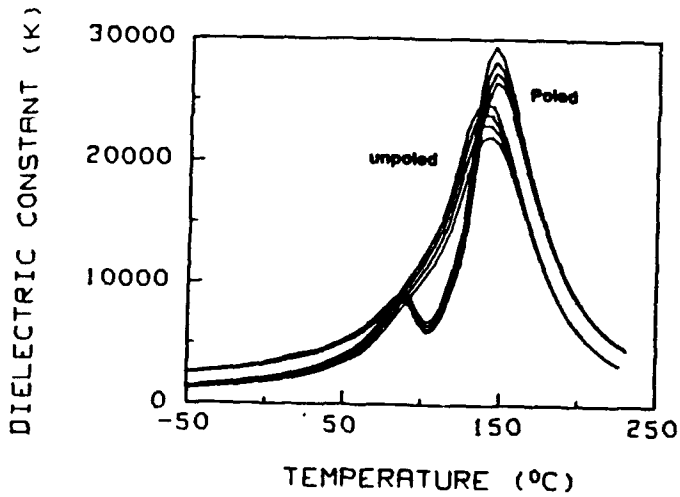

FIGURE 4. The Dielectric Constant K Versus Temperature for Both Poled and Unpoled 0.7 PMN-0.3 PT [100] Crystal.

(3) Though x-ray diffraction revealed rhombohedral symmetry for all compositions, the dielectric temperature behavior revealed the successive transitions from rhombohedral —> tetragonal —> cubic as indicated by the MPB being curved.

(4) Upon poling, a macro-micro domain anomaly was observed in compositions exhibiting a T_{R-C} transition. Poling also influenced the T_{R-T} and T_{T-C} transitions, by enhancing the dielectric anomaly of T_R through macro domain pinning of the tetragonal component, thereby greatly reducing relaxor type behavior.

(5) The piezoelectric coefficient d_{33} [100] was found to be ≡ 1050-1500 pC/N, similar to that observed in PZT-PT MPB compositions.

REFERENCES

1. G.A. Smolenskii, V.A. Isupov, A.I. Agranovskaya, and S.N. Popov, Sov. Phys.-Solid State, 2, 2584 (1961).
2. H. Ouchi, J. Am. Ceram. Soc., 51, 169 (1968).
3. S.L. Swartz and T.R. Shrout, Mat. Res. Bull., 17, 1245 (1982).
4. S.W. Choi, T.R. Shrout, S.J. Jang, and A.S. Bhalla, to be published in Ferroelectrics.
5. B. Jaffe, W.R. Cook, and H. Jaffe, Piezoelectric Ceramics, Acad. Press, New York (1971).
6. S. Nomura, T. Takahashi, and Y. Yokomizo, J. Phys. Soc. Jap., 27, 262 (1969).
7. W.A. Bonner and L.G. Van Uitret, Mat. Res. Bull., 2, 131 (1967).
8. K. Wojcik, Ferroelectrics, 82, 25 (1988).
9. J. Kuwata, K. Uchino, and S. Nomura, Ferroelectrics, 37, 579 (1981).
10. Z.P. Chang, A.S. Bhalla, and L.E. Cross, Proceedings of the 6th International Symposium on Applications of Ferroelectrics, 482 (1986).
11. Y. Xi, Z.L. Chen, and L.E. Cross, Ferroelectrics, 163 (1984).

APPENDIX 33

Ferroelectrics, 1990, Vol. 109, pp. 167–172
Reprints available directly from the publisher
Photocopying permitted by license only

CHARACTERIZATION OF (1-x)Pb(Mg1/3Nb2/3)O3 - (x)PbTiO3 AND Pb(Sc1/2Ta1/2)O3 TRANSPARENT CERAMICS PREPARED BY UNIAXIAL HOT-PRESSING

J.R. GINIEWICZ, D.A. MCHENRY, T.R. SHROUT, S.-J. JANG and A.S. BHALLA

Materials Research Laboratory, The Pennsylvania State University, University Park, PA U.S.A.

F. W. AINGER, Plessey Research (Caswell) Limited, Caswell Towcester, U.K.

Abstract Transparent relaxor ferroelectric ceramics of (1-x)Pb(Mg1/3Nb2/3)O3-(x)PbTiO3 and Pb(Sc1/2Ta1/2)O3 have been prepared by low temperature uniaxial hot-pressing. The ceramics are highly dense (> 99.5 % theor.) and transmit throughout the visible. The addition of excess PbO and La2O3 and post-pressing heat treatment are found to enhance transparency. The ceramics have been characterized for phase purity, development of microstructure, dielectric behavior and optical transmission in order to determine optimum conditions.

INTRODUCTION

Considerable interest is currently focused on the optical and electro-optical character of relaxor ferroelectric materials. The excellent electro-optic response, switching time, and half-wave voltages, $V\pi$, distinguish these materials as promising candidates for a variety of electro-optic device applications.[1] Further, optical / electro-optical property measurements on transparent relaxor compositions provide important new data useful for a more thorough understanding of the material's diffuse nature.[2,3] Transparent relaxor ferroelectric ceramics have been prepared for this investigation by hot uniaxial pressing (HUP). The ceramics have been characterized for phase purity, microstructure, dielectric behavior, and optical transmission.

SAMPLE PREPARATION AND EXPERIMENTAL PROCEDURE

Polycrystalline specimens transparent enough for optical / electro-optical measurements possessing desirable characteristics such as uniform microstructure, high density, and phase purity are not easily produced by conventional sintering methods. The samples examined in this investigation were prepared by means of hot uniaxial pressing. The powders of Pb(Mg1/3Nb2/3)O3, [PMN], (1-x)Pb(Mg1/3Nb2/3)O3 - (x)PbTiO3, [PMN-PT], (x = 0.7) and Pb(Sc1/2Ta1/2)O3, [PST] were prepared from reagent grade and optically pure starting oxides by the columbite / wolframite [4] precursor method [5] in order to produce phase - pure compositions. The compositions of interest were prepared stoichiometrically and with excess PbO and / or La2O3 as indicated in Table I so as to allow for a range of hot-press conditions and to enhance transparency.

The samples were prepared for hot-pressing in the form of disks 38 mm or 64 mm in diameter. The disks were pressed at a pressure of ≈38 MPa for 6 hours at a temperature in the range 900 °C to 1200 °C. Flowing O2 was used during the heating cycle. The specific

conditions for each sample investigated are given in Table I. The samples were embedded in coarse alumina sand to prevent reaction with the silicon nitride rams.

The uniaxially hot-pressed samples were initially characterized for phase-purity, density, and average grain size. It was determined by x-ray diffraction that all specimens were phase pure. The order parameters, Ω, of the PST specimens were also evaluated as described in the next section by means of x-ray diffraction. Sample densities as determined by the Archimedes technique and average grain size as evaluated by means of the line intercept method on scanning electron micrographs of fractured surfaces are recorded in Table I.

The samples were sliced into Top, Bottom, and Parallel sections, as shown in Figure 1, and the sections annealed in air at 900 °C for 8 hours in order to eliminate excess PbO. The sample surfaces were then ground with Al_2O_3 grinding media and coated with a sputtered gold electrode for dielectric measurement.

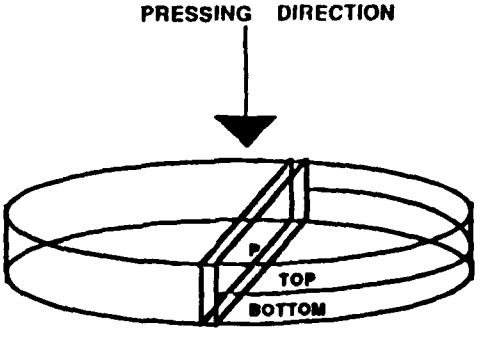

FIGURE 1 Test plates sliced from the hot uniaxially pressed ceramic.

Samples prepared for optical transmission measurement were taken as adjacent slices (arbitrary direction) from the original hot-pressed disk. One of the slices was annealed in air at 900 °C for 8 hours before it was optically polished, while the other slice was polished with no post-pressing heat-treatment. Optical transmission measurements were made on a Cary 2300 spectrophotometer.

RESULTS AND DISCUSSION

All the samples under investigation are of high density with most higher than 99.5 % theoretical density as indicated in Table I. The average grain size, as determined by the line intercept method on scanning electron micrographs of fracture surfaces, appears to depend upon the processing conditions and compositional modifications (Table I); it is observed that both excess PbO and higher hot-press temperatures encourage grain growth. In all cases, no variation in average grain size is observed with position (i.e.-- top or bottom sections) within the sample. In general, the microstructures are found to be uniform with well-formed, equiaxed grains.

TABLE I Processing conditions and physical properties of test samples.

SAMPLE	PbO	La2O3	T (°C)	∂ (%theor.)	Ave Grn Size (μm)
PMN					
PMN	- -	- -	1100	99.7	2
PMN-PT					
PMNTA	- -	- -	900	99.8	2
PMNTB	- -	- -	1050	99.7	10
PMNTC	2 wt%	- -	1100	99.8	20
PMNTD	2 wt%	1 mol%	900	99.1	5
PMNTE	2 wt%	1 mol%	1100	99.6	15
PST					
PSTA	10 wt%	- -	1050	99.8	5
PSTB	2 wt%	- -	1200	98.9	5
PSTC	2 wt%	- -	1250	99.8	5

TABLE II Dielectric properties [10 KHz].

SAMPLE	SECTION	K	T (°C)	Ω	b 3/4 (°C)
PMN	T	10600	-14		62
	B	10200	-15		62
	P	11200	-16		62
PMNTA	T	14300	37		65
	B	11400	37		65
	P	15700	36		60
PMNTB	T	25000	35		35
	B	24000	34		35
	P	19100	15		57
PMNTC	T	20600	31		40
	B	21600	36		40
	P	30800	34		40
PMNTD	T	20800	13		52
	B	13900	12		58
	P	17600	15		52
PMNTE	T	17300	14		50
	B	21600	13		50
	P	25100	13		38
PSTA					
	N	6077	25	0.9	25
	P	7342	23	0.9	20
PSTB					
	N	7862	21	0.9	26
	P	7093	22	0.9	20
PSTC					
	N	6575	21	0.9	26
	P	8061	22	0.9	20

TABLE III Optical transmission.

SAMPLE		t (mm)	% Transmission 470 (nm) (blue)	550 (nm) (green)	750 (nm) (red)
	*(Anneal)				
PMN	Before	0.8	<1	<1	<1
	After	0.8	<1	<1	<1
	After	0.5	<1	<1	2
PMNTA	Before	0.8	<1	<1	<1
	After	0.8	<1	<1	<1
PMNTB	Before	0.9	<1	<1	<1
	After	0.9	<1	<1	<1
PMNTC	Before	0.7	2	2	3
	After	0.7	2	2	3
PMNTD	Before	0.8	<1	<1	5.6
	After	0.8	12	19	28
	After	0.5	18	35	45
PMNTE	Before	1.3	7	10	13
	After	0.8	12	17	22
	After	0.4	35	42	45
PSTA	Before	0.6	<1	2	20
	After	0.4	30	45	90
PSTB	Before	0.9	<1	<1	<1
	After	0.9	<1	<1	<1
PSTC	Before	- -	- -	- -	- -
	After	0.4	20	22	22

The dielectric response of the various samples, which have undergone post-pressing heat-treatment, at a frequency of 10 KHz is recorded in Table II. The particular slice of the sample as indicated in Figure 1 is designated by the labels T, B, and P for each specimen. The quantity (b 3/4) is a measure of the diffuseness of the permittivity as a function of temperature,[6] representing the width of K(T) at 3/4 the value of K(max). The order parameter, Ω, is relevant to the PST samples only which exhibit order / disorder variations as a function of temperature and thermal history.[6,7] It is defined by the ratio of the x-ray diffraction intensities of peaks corresponding to the normal and superstructure lattices. A completely ordered material has a value $\Omega = 1$.[7]

The dielectric response K(T) at various frequencies within the range 100 to 100,00 Hz was measured over a temperature range of -60 to 200 °C for each sample. The dielectric constant as a function of temperature is diffuse and strongly frequency-dependent for both PMN and PMN-PT specimens, characteristic of the relaxor ferroelectrics. The K(T) for PST is sharp and only slightly diffuse at the transition, indicative of the high degree of structural order.

The general effect of varying hot-press temperatures and of the various chemical modifications on the dielectric response is outlined in Table II. Based on the data presented, some basic tendencies can be deduced. It is seen that the largest K(max) values at 10 KHz are observed for samples prepared at higher pressing temperatures with the highest K(max), in the PMN-PT series, occurring for samples that were batched with excess PbO and 1 mol% La_2O_3. There is some correlation between the average grain size and the higher dielectric constants with specimens of larger average grain sizes exhibiting the higher magnitudes of K consistent with the previously reported grain-size dependence of the dielectric response of PMN.[8] Addition of 1 mol% La_2O_3 is seen to effectively reduce the temperature of the maximum dielectric constant by more than 20 °C again in agreement with prior investigation on PMN transparent ceramics.[9] The variation of the diffuseness of the K(T) as indicated by (b 3/4) in Table II for the various pressing temperatures and chemical modifications is also largely a function of grain size. The diffuseness (b 3/4) of the PST samples is not at all affected by the pressing temperature variations implemented in this investigation. This is further reflected in the constant value of the order parameter, $\Omega = 0.9$, for all the PST specimens. It should be noted that the high degree of ordering obtained for these samples is generally not easily achievable by the conventional means of preparing ordered PST ceramics [10] which generally requires an additional long, high temperature annealing under controlled atmosphere to induce structural ordering. Since the HUP temperatures employed to produce these dense PST ceramics are well below the order/disorder transition temperature (≈1475 °C) [10], highly ordered ceramics may be produced. Further, the degree of order is not affected by the low temperature post-pressing anneal conducted here since the annealing temperature in this case is well below the temperature at which a disordered PST ceramic becomes ordered (≈1050 °C). [10]

There is observed for all samples some anisotropy of the dielectric response with respect to the pressing direction as well as a gradient of the response between top and bottom portions of the ceramic. The PMN sample exhibits the least variation with direction and location within the ceramic of all the speicmens examined. The anisotropy observed in the PST samples appears to become slightly less for higher pressing temperatures. The large anisotropy of PSTA may also be related in part to the rather high PbO content of this specimen. The anisotropy with respect to pressing direction for all the PMN-PT samples except PMNTD is considerable. There is no clear correlation between the "polarity" of the anisotropy (i.e. - the direction of the higher magnitude) and the compositional and pressing temperature variations. Further, all PMN-PT specimens exhibit a significant difference in K between the top and bottom sections, again with no definite correlation with the compositional and pressing temperature variations.

Since in most cases, no clear correlation can be made between the dielectric anisotropy and the modifications made, it seems likely that the source of the variations of K(Max) throughout the sample arises in the initial, pre-pressing stages of sample preparation (e.g.-- mixing, forming, etc.) and that the resulting anisotropy and gradients between top and bottom are enhanced by the final HUP process. It is suggested that the macroscale inhomogeneities introduced in the early stages of sample preparation lead to a non-uniform distribution of PbO thereby making conditions favorable for the formation of Pb-rich phases, in particular at the grain boundaries, during the uniaxial hot-pressing procedure. The formation of such intergranular phases in relaxor ferroelectric ceramics produced by various methods has been extensively reported.[11,12,13] Although no second phases were detected by means of XRD or by routine SEM investigation of the microstructure in this investigation, a very thin intergranular phase may be present in these materials which, as previous research has demonstrated,[13] can significantly affect the dielectric response of the material. The largely intergranular fracture of the ceramics as observed in SEM micrographs suggests the existence of such a grain boundary layer. Further, a considerable amount of aging was observed for PMN-PT samples prepared both stoichiometrically and with excess PbO and La2O3. Although it is beyond the scope of the present work and will not be presented here, this aging is worthy of note since the aging phenomenon in PMN has been found to be very closely related to variations in stoichiometry due to an excess or deficiency of PbO in the material.[14] The results obtained in this study suggest that such a variation in stoichiometry may occur non-uniformly throughout the specimen as a result of the processing procedure. A more thorough investigation of possible grain boundary phases and local variations in stoichiometry is required.

The percent transmission at various wavelengths across the visible spectrum are recorded in Table III for samples before and after post-pressing annealing and for selected specimens at two sample thicknesses. Reflection losses, as calculated by means of the Fresnel formula, are about 30% assuming an average refractive index of 2.5 at room temperature for the samples

under consideration. In general, it appears that higher temperatures and, in the case of the PMN-PT series, additions of both excess PbO and 1 mol% La_2O_3 significantly enhance the transparency of the ceramics, conditions which were shown to also encourage grain growth and high dielectric response. Post-pressing annealing is also seen to further enhance transmission across the entire visible spectrum due likely to the liberation of excess PbO.

SUMMARY

Hot uniaxial pressing of chemically modified relaxor ferroelectric compositions is an effective means of producing dense, transparent ceramics with a high dielectric response. Transparent PST ceramics may be produced with an extremely high degree of ordering due to the low hot-pressing temperatures employed. Some variations in dielectric response and the appearance of dielectric aging suggest the formation of intergranular Pb-rich phases and/or local variations in stoichiometry induced by the HUP process. Further investigation into the nature of these irregularities and the mechanism of their formation is required to optimize samples prepared by this procedure.

ACKNOWLEDGEMENTS

The authors are grateful to Mick Latimer and Dave Roberts of Plessey Research, U.K. for their help in the preparation of the samples. The authors also wish to ackowledge the research funding provided by the Office of Naval Research.

REFERENCES

1. D.A. McHenry, J. Giniewicz, S.-J. Jang, A. Bhalla and T.R. Shrout, Ferroelectrics, 93, 351 (1989).
2. G. Burns and F. Dacol, Phase Transitions, 5, 261 (1983).
3. L.E. Cross, Ferroelectrics, 76, 241 (1987).
4. JCPDS #24-1017 $ScTaO_4$.
5. S.L. Swartz and T.R. Shrout, Materials Research Bulletin, 18, 663 (1983).
6. C.G.F. Stenger, F.L. Scholten, and A.J. Burggraaf, Solid State Communications, 32, 989 (1979).
7. N. Setter, Ph.D. Thesis, Pennsylvania State University, (1980).
8. T.R. Shrout, U. Kumar, M. Megherhi, N. Yang and S.-J. Jang, Ferroelectrics, 76, 479 (1987).
9. N. Kim, W. Huebner, S.-J. Jang and T.R. Shrout, Ferroelectrics, 93, 341 (1989).
10. C.G.F. Stenger and A.J. Burggraaf, physica status solidi (a), 61, 275 (1980).
11. E. Goo, T. Yamamoto, K. Okazaki, Journal of the American Ceramic Society, 69 [8], C-188 (1986).
12. J. Guha, D.J. Hong and H.U. Anderson, Journal of the American Ceramic Society, 71 [3], C-152 (1988).
13. K.Z. Baba-Kishi and D.J. Barber, Ferroelectrics, 93, 321 (1989).
14. T.R. Shrout, W. Huebner, C.A. Randall and A.D. Hilton, Ferroelectrics, 93, 361 (1989).

APPENDIX 34

Ferroelectrics, 1990, Vol. 102, pp. 161–171
Reprints available directly from the publisher
Photocopying permitted by license only

ELECTRICAL AND OPTICAL PROPERTIES OF RELAXOR FERROELECTRICS

D. A. MCHENRY, J. R. GINIEWICZ, T. R. SHROUT, S. J. JANG and A. S. BHALLA

Materials Research Laboratory, The Pennsylvania State University, University Park, Pennsylvania 16802 USA

(Received May 1, 1989)

The dielectric and optic/electro-optic properties of hot-pressed ceramics of composition $(1-x)(Pb_{1-y}La_y)(Mg_{1/3}Nb_{2/3})O_3 - xPbTiO_3$ ($y = 0.01$) have been investigated. The materials exhibit high peak dielectric constants (>20000) with typical relaxor ferroelectric behavior. The ceramics are adequately transparent for optical and electro-optical evaluation with transmission better than 50% at 600 nm. High refractive indices are observed (>2.5 at 632.8 nm) and the dispersion of the refractive index is well described by a single-term Sellmeier equation. The temperature dependence of the refractive index exhibits a linear region above 390°C and a polarization induced decrease of the index via the electro-optic effect below this temperature. The transverse quadratic electro-optic coefficients, $(R_{11}-R_{12})$ and $(g_{11}-g_{12})$, were evaluated both as a function of temperature and frequency. Electro-optic switching experiments indicate rapid response of less than 1 μsec, suitable for transverse shutter mode operation.

1. INTRODUCTION

Relaxor ferroelectrics such as $Pb(Mg_{1/3}Nb_{2/3})O_3$ and its solid solution with $PbTiO_3$ are of particular interest for applications as multilayer capacitors,[1] electrostrictive actuators,[2,3] and piezoelectric transducers.[4] These applications are based on the exceptional dielectric and electrostrictive properties as well as the low thermal expansion exhibited by these materials.[6,7] Recently, relaxor ferroelectrics have been investigated for a variety of electro-optic properties; good electro-optic switching times and modest half-wave voltages, V_π, could make these materials viable alternatives to the $(Pb,La)(Zr,Ti)O_3$(PLZT) compositions conventionally used in electro-optic devices.[8] In addition to evaluating their device potential, optical property measurements on relaxors can substantiate previous studies in determining the onset and magnitude of the polarization for diffuse phase transitions of relaxor ferroelectrics.[9,10]

Typical perovskite relaxor ferroelectrics of the form ABO_3 generally occur with the *A* and/or *B* sites shared by two or more cations whose valence and ionic radii are suitable for maintaining a stable atomic configuration. Both sites may be occupied by more than one kind of cation as in the $(Pb,La)(Zr,Ti)O_3$(PLZT) series of compounds where oxygen vacancies further compensate for the charge imbalances arising from the substitution of La^{3+} for Pb^{2+} on the *A*-site.[11] Compounds and complex compositions which involve the occupation of the *B*-site only by two or more cations are exemplified by $Pb(Mg_{1/3}Nb_{2/3})O_3$ (PMN) and $Pb(Zn_{1/3}Nb_{2/3})O_3$ (PZN) and their solid solutions with $PbTiO_3$.

$Pb(Sc_{1/2}Ta_{1/2})O_3$ and $Pb(Sc_{1/2}Nb_{1/2})O_3$ are compounds for which the ionic valence and size as well as the relative distribution of their *B'* and *B''* cations on the *B*-site

allow for 1:1 ordering when the material is in a ferroelectric state, a condition detectable by means of x-ray diffraction, electron diffraction, and Raman scattering.[12] A model has been proposed for PMN in which regions of ordered (Mg-rich) and disordered (Nb-rich) regions coexist between which space charges are generated which effectively charge compensate thereby limiting the degree of order possible in the system.[13] This state of disorder is believed to lead to the "glassy" polarization behavior observable in the temperature dependences of both the electrostrictive strain and the refractive index exhibited by materials from these systems. Based on the values of these quantities as a function of temperature, a "glassy" polarization, P_d, which bears a quadratic relationship to the induced strain and the induced birefringence through the electrostriction and the quadratic electro-optic effect (Kerr Effect) is found to persist for a broad range of temperatures above T_c in contrast to the more abrupt disappearance of the reversible polarization, P_r, generally observed in normal ferroelectrics.[9,10]

The weak field dielectric permittivity and tanδ as a function of temperature exhibit broad frequency dependent (i.e.-dispersive) maxima as shown in Figure 1 characteristic of a diffuse ferroelectric phase transition for materials with no long-range structural order such as the $Pb(B'_{1/3}B''_{2/3})O_3$ compounds and solid solutions. This behavior has been described by the theory of "compositional fluctuations" in which local variations in composition lead to the formation of ferroelectric (polar) and paraelectric (non-polar) microregions on the order of 100–200 Å.[14] Each polar region will possess its own Curie temperature dependent on its local composition so that the material as a whole will proceed through the transition over a range of temperatures known as the Curie range. Polar regions with volumes on the order of 10^2 Å are unstable against thermal agitation and, hence, the distribution and relative density of the microregions are strongly temperature dependent.[10] The dielectric response measured as a function of temperature and degree of long-range order for systems such as $Pb(Sc_{1/2}Ta_{1/2})O_3$, whose degree of structural (dis)order may be varied by controlled heat treatment, demonstrates a direct correlation between the degree of ordering of *B*-site cations and the diffuseness of the dielectric response, where a decrease in structural order leads to increased "smearing" of the permittivity maximum.[15,16] The observed relationship between structural order and the diffuseness of the phase transition has been cited as evidence in sup-

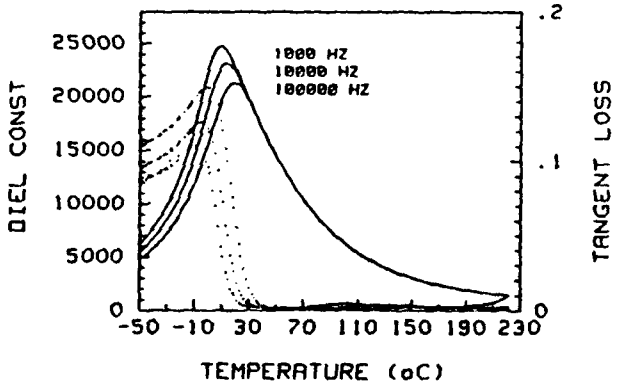

FIGURE 1 K(T) and Tanδ(T) for $(0.93)(Pb_{0.99}La_{0.01})(Mg_{1/3}Nb_{2/3})O_3 - (0.07)PbTiO_3$

port of the "composition fluctuation" model.[10] Recent studies on $(1\text{-}x)Pb(Mg_{1/3}Nb_{2/3})O_3 - (x)PbTiO_3$, ($x$ = 0.07 and 0.1) and La-substituted compositions prepared by hot-uniaxial pressing as transparent ceramics have generated new data which suggests promising application potential and supports models previously proposed concerning the "glassy" polarization behavior[9] of this family of materials. The compositions investigated demonstrate the classic diffuse phase transition behavior (Figure 1) of PMN with a distinct enhancement of the electromechanical and capacitive properties. The optical and electro-optical character of these materials are also of interest in the development of relaxor-based optical devices and for further advances in the understanding of the fundamental mechanisms contributing to the diffuse phase transition. The results of this investigation are presented with particular regard to fundamental concepts and application considerations.

2. SAMPLE PREPARATION

In order to produce polycrystalline specimens transparent enough for optical/electro-optical property measurements, desirable characteristics including uniform grain-growth, high density, and the elimination or reduction of second phases are requirements not easily achievable by conventional sintering methods. The specimens used in this investigation were prepared by means of hot-uniaxial pressing with additions of excess PbO and La_2O_3 to aid in densification and to promote transparency. Powders of $(1\text{-}x)$PMN-(x)PT, (x = 0.07 and 0.1) were prepared by the columbite precursor method[1] in order to produce phase-pure compositions. Both excess PbO (~2–5 mol%) and/or La_2O_3 (0.5 mol%) compositional modifications were made to allow for a range of hot-pressing conditions and to enhance transparency. In general, ceramics with densities greater than 99.7% and optical transparency were achieved.[5]

3. EXPERIMENTAL RESULTS AND DISCUSSION

Transparent ferroelectric ceramics as exemplified by PLZT have demonstrated considerable usefulness as electro-optic materials. Practical applications for these ceramics include use in such devices as optical shutters, modulators, displays, and gate arrays for optical data processing.[17] Recent measurements of $(1\text{-}x)(Pb_{1-y}La_y)(Mg_{1/3}Nb_{2/3})O_3 - xPbTiO_3$(PLMN-PT) relaxor ferroelectric ceramics indicate that this and similar compositions can be made with reasonable transparency and large electro-optic coefficients comparable to those of the PLZT compositions currently in use.[8]

The range of transparency for the ceramics under investigation extends through the visible and into the near IR with transmission in excess of 50% at wavelengths longer than 550 nm for samples 1.0 mm thick. The fundamental UV optical absorption wavelength of about 375 nm is in agreement with the wavelength reported for other corner-shared oxygen-octahedra materials.[18] Improvements in optical transmission characteristics for PLMN-PT ceramics could be anticipated with the use of ultra-high purity powders and improved processing conditions.

The dispersion of the refractive index was measured by means of the method of minimum deviation.[8,9] The dispersion data were fitted to a single-term Sellmeier oscillator equation of the form,

$$n^2 - 1 = S_0 \lambda_0^2/(1 - \lambda_0^2/\lambda^2) = E_d E_0/(E_o^2 - E^2) \quad (1)$$

where E and E_0 are the energy of the incident light and the average oscillator energy, respectively, λ and λ_0 are the wavelength of the incident light and the average oscillator position respectively, and E_d is the dispersion energy.[18] The Sellmeier parameters are derived from a straight-line least squares fit of $(n^2 - 1)^{-1}$ vs. $(1/\lambda^2)$. The room temperature Sellmeier parameters for various $(1\text{-}x)$-$(Pb_{1-y}La_y)(Mg_{1/3}Nb_{2/3})O_3 - xPbTiO_3$ compositions and the end-members PMN and $PbTiO_3$ of the system appear in Table I. The temperature dependence of the Sellmeier parameters E_0 and E_d are shown, respectively, in Figures 2a and 2b as determined from measuring the refractive index to high temperature for .93 PLMN − .07 PT. The slope, dE_0/dT, is related to the shift of the absorption spectra as a function of temperature. This change is apparently linear in the temperature range measured with a value of approximately -6.48×10^{-4} eV/°C.

Refractive index measured as a function of temperature can also be a sensitive indicator of polarization fluctuations in the precursor region in the vicinity of the paraelectric-ferroelectric transition. The temperature dependence of (0.93)-$(Pb_{0.99}La_{0.01})(Mg_{1/3}Nb_{2/3})O_3 - (0.07)PbTiO_3$ at four different wavelengths is shown in Figure 3. An essentially linear region is observed at high temperatures. A departure from linearity occurs at a temperature of about 390°C at all four wavelengths. The behavior of the refractive index below this temperature (referred to as T_d)[9,19] is believed to be significantly affected by locally ordered yet randomly oriented polarization, P_d, which may occur well above the Curie temperature in relaxor ferroelectrics. Hence, for perovskite ferroelectric ceramics the refractive index departure from linear behavior Δn can be given by the expression for the quadratic electro-optic effect with respect to the polarization,

$$\Delta n = (\Delta n_\parallel + 2\Delta n_\perp)/3 = -(n_0^3)/2\,[(g_{33} + 2g_{13})/3]P_d^2 \quad (2)$$

where Δn is expressed as an average of the Δn's both parallel and perpendicular to the polar [111] directions, and n_0 is the refractive index of the undistorted indicatrix, P_d is the local polarization, and the g coefficients are the appropriate

TABLE I

Refractive Index Parameters for the PMN-PT System

	PMN[5]	$(0.93)(Pb_{0.99}La_{0.01})(Mg_{1/3}Nb_{2/3})O_3 - (0.07)PbTiO_3$	0.90 PMN–0.10 PT	$PbTiO_3$[20]
n @ 632.8 nm	2.5219	2.5399	2.5455	2.688
λ_0 (μm)	0.216	0.218	0.220	0.222
S_0 ($x10^{14}$ m^{-2})	1.013	1.012	1.00	1.09
E_0 (eV)	5.73	5.69	5.64	5.59
E_d (eV)	27.2	27.40	27.31	30.3
f (eV)^2	156	155.9	154	168
E_0/S_0 ($x10^{-14}$ eVm^2)	5.66	5.62	5.64	5.13

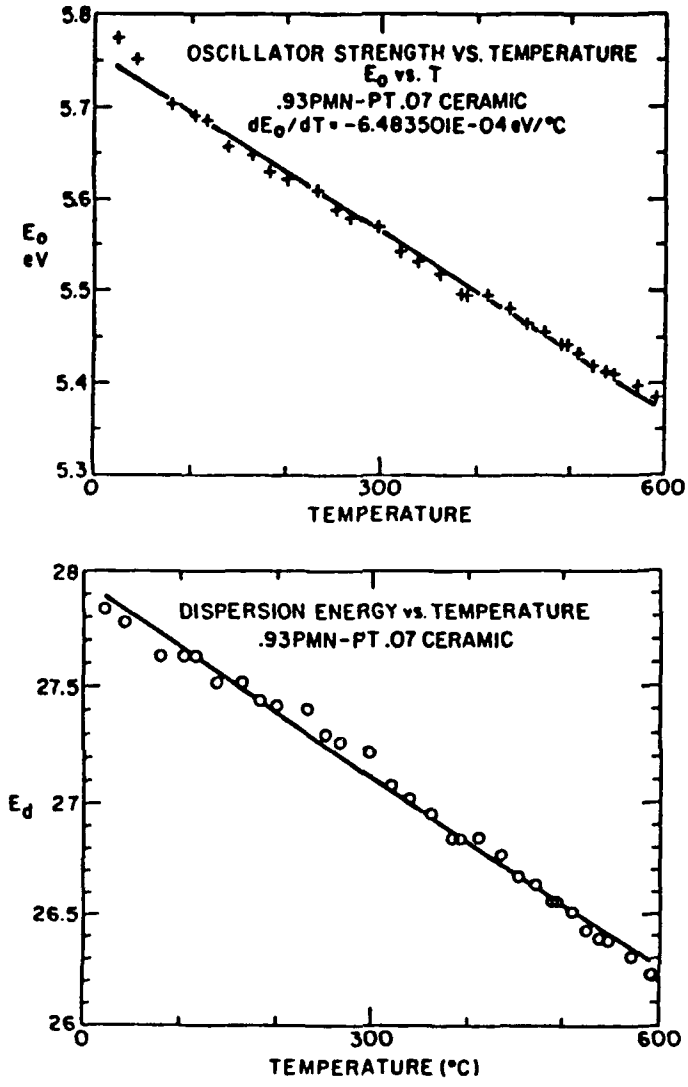

FIGURE 2 (a) E_0 vs. temperature and (b) E_d vs. temperature for $(0.93)(Pb_{0.99}La_{0.01})(Mg_{1/3}Nb_{2/3})O_3 - (0.07)PbTiO_3$

coefficients for this symmetry.[19] The magnitude of the average random local polarization, P_d, is evaluated by means of equation (2) using the measured values of n_0, Δn, and the electo-optic g coefficients.[8] Values of P_d calculated in this way for $(0.93)(Pb_{0.99}La_{0.01})(Mg_{1/3}Nb_{2/3})O_3 - (0.07)PbTiO_3$ appear in Figure 4.

The PLMN-PT ceramics investigated at room temperature exhibit "slim loop" ferroelectric hysteresis (Figure 5) P vs. E. The material has pseudocubic symmetry in its undistorted state; with the application of an electric field a uniaxial birefringent (presumably rhombohedral) ferroelectric phase may be induced.

The electro-optic effect for active optical ceramics operated in a transverse shutter mode can be described in terms of the expression for the quadratic electro-optic

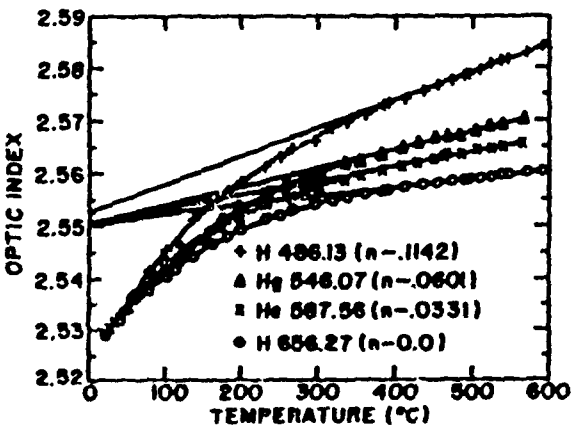

FIGURE 3 Refractive Index vs. temperature for $(0.93)(Pb_{0.99}La_{0.01})(Mg_{1/3}Nb_{2/3})O_3 - (0.07)PbTiO_3$

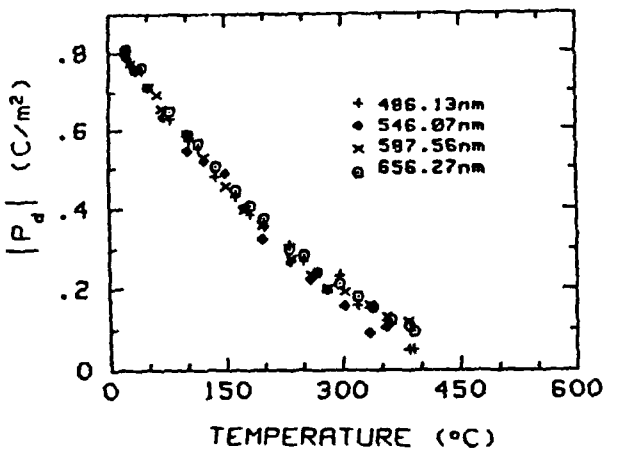

FIGURE 4 Polarization, P_d, as a function of temperature calculated from refractive index measurements using equation (2).

effect which relates to the applied electric field as follows:

$$\Delta n = -(\tfrac{1}{2})\, n_0^3\, (R_{11}-R_{12})\, E_1^2 \qquad (3)$$

where Δn is the induced birefringence, n_0 is the refractive index of the undistorted indicatrix, $R_{12}-R_{12}$ is the effective averaged unclamped (low frequency) quadratic electro-optic coefficient, and E_1 is the applied field. The transverse electro-optic response represented by $R_{11}-R_{12}$ is typically the largest induced in a perovskite ferroelectric ceramic.

The quadratic electro-optic coefficients were determined by means of the AC Senarmont compensator setup illustrated in Figure 6. The induced birefringence at room temperature is plotted against the square of the electric field in Figure 7. It can be seen that the electro-optic response is well described by the quadratic electro-optic effect where the proportionality constant relating Δn and E^2 yields $R_{11}-R_{12} = 2.1 \times 10^{-16}$ (m^2/V^2) at room temperature. The temperature depend-

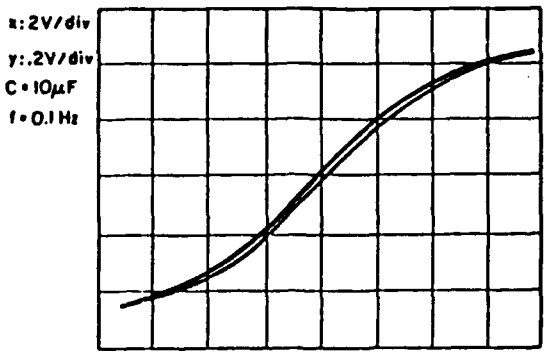

FIGURE 5 Ferroelectric hysteresis loop for $(0.93)(Pb_{0.99}La_{0.01})(Mg_{1/3}Nb_{2/3})O_3 - (0.07)PbTiO_3$ at T = 20°C

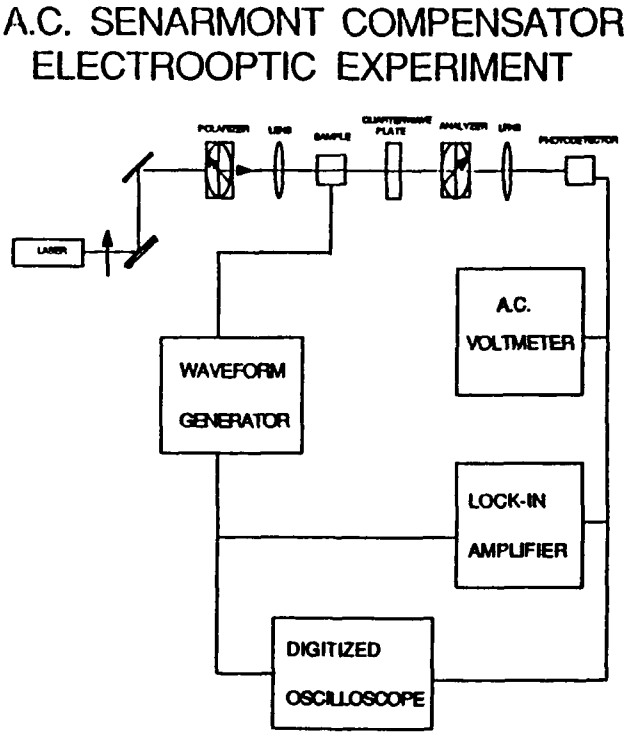

FIGURE 6 Schematic of the Senarmont Compensator $\Delta n(E)$ measurement system

ence of $R_{11}-R_{12}$ is shown in Figure 8 (curve-1). The electric field-related quadratic electro-optic coefficients are clearly temperature dependent. This is generally true for ferroelectrics operated near a phase transition where the values of the dielectric permittivity also change considerably with temperature. The maximum dielectric constant for small-field and low-frequency (1 KHz) conditions occurs at $T \sim 9°C$ for (0.93)PLMN – (0.07)PT and decreases markedly at higher temperatures above the Curie range, a trend reflected in the temperature dependence of the R-coefficients.

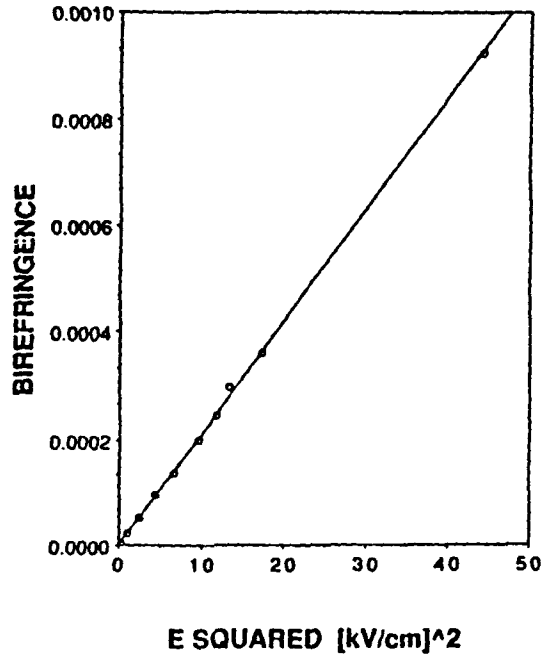

FIGURE 7 Induced birefringence Δn vs. E^2 for $(0.93)(Pb_{0.99}La_{0.01})(Mg_{1/3}Nb_{2/3})O_3 - (0.07)PbTiO_3$ at T = 20°C

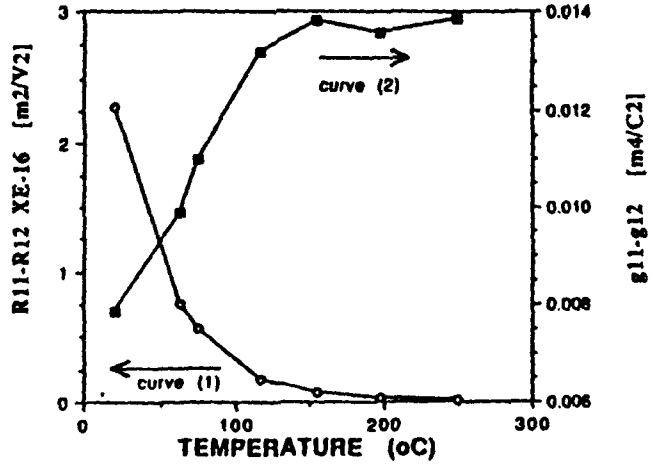

FIGURE 8 *1.*) $(R_{11}-R_{12})$ vs. temperature for $(0.93)(Pb_{0.99}La_{0.01})(Mg_{1/3}Nb_{2/3})O_3 - (0.07)PbTiO_3$; *2.*) $(g_{11}-g_{12})$ vs. temperature for $(0.93)(Pb_{0.99}La_{0.01})(Mg_{1/3}Nb_{2/3})O_3 - (0.07)PbTiO_3$

Alternatively, the electro-optic effect may be expressed in terms of the polarization as,

$$\Delta n = -(1/2)\, n_0^3\, (g_{11}-g_{12})\, P_1^2 \qquad (4)$$

This formulation is generally preferable when dealing with ferroelectric materials

since the response in terms of the polarization relates more directly to the fundamental polarization-related phenomena that accompany ferroelectric transitions. The two types of quadratic electro-optic coefficients are related through the dielectric permittivity as,

$$(g_{11}-g_{12}) = (R_{11}-R_{12})/(\varepsilon\ \varepsilon_0)^2 \qquad (5)$$

where ε is the dielectric permittivity and ε_0 is the permittivity of free space.

The temperature dependence of $g_{11}-g_{12}$ is shown in Figure 8 (curve-2). The polarization electro-optic coefficients, g_{ij}, are usually much less temperature dependent than the electric field-related coefficients, R_{ij}. For the polarization optic coefficients there is a gradual increase with temperature with a leveling off to $g_{11}-g_{12} = 0.014$ (C^2/m^4) at about 200°C. The temperature dependence of the g-coefficients has been reported as confirming the presence of polar phase regions for relaxors in the same temperature range where the quadratic dependence of the birefringence on applied electric field holds true.[25]

It has been previously observed that the polarization-optical coefficients are nearly the same for all oxygen octahedra materials ($g_{11}-g_{12} = 0.11 \pm 0.02\ m^4/C^2$). It has also been noted, however, that Pb-based perovskites (including the ferroelectric relaxors) are exceptions to this, exhibiting g-coefficients that are an order of magnitude smaller than the value common to the other oxygen-octahedra materials. This lowering of the g-coefficient in Pb-based systems has been attributed to a polarization induced shift of the electronic band gap due to the displacement of the Pb^{2+} sublattice which is generally not accounted for in the formulation of the g-coefficients.[20]

The frequency dependence of $(g_{11}-g_{12})$ has been measured and the response is observed to be nondispersive at low frequencies (<100 KHz) in agreement with the frequency dependence of the dielectric permittivity in this same frequency regime. This is expected for the composition under investigation since the Curie range over which the diffuse dielectric and electro-optic behavior occurs is below

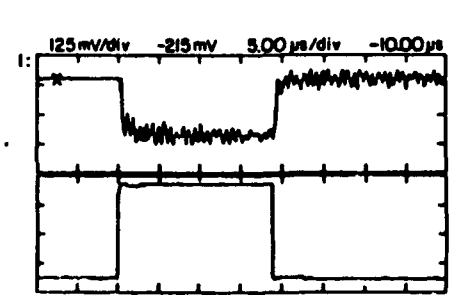

FIGURE 9 Signal Response as a function of time for $(0.93)(Pb_{0.99}La_{0.01})(Mg_{1/3}Nb_{2/3})O_3 - (0.07)PbTiO_3$

room temperature. This is a possible advantage in terms of device application over the PLZT compositions generally employed which exhibit dispersive dielectric behavior at room temperature that translates to the electro-optic frequency response as well.[21]

Response times for electro-optic switching have been examined by applying square wave pulses of different voltages and pulse widths. As compared with the switching times reported for bulk PLZT of 1–10 μsec[22–25] the response time for these PLMN-PT ceramic electro-optic switches is rapid; less than 1 μsec. The response of a $(0.93)(Pb_{0.99}La_{0.01})(Mg_{1/3}Nb_{2/3})O_3 - (0.07)PbTiO_3$ sample to a 157 V square pulse of about 18 μsec duration is shown in Figure 9. It was observed that the rise time consistently was <1 μsec and that the fall time is generally faster than the rise time. The post-switching oscillations are due to elecrostrictive vibrations in the unclamped ceramic. This electrostrictive response to the applied voltage contributes via the strain-optic effect to the amplitude of the transmitted signal.

4. CONCLUSIONS

(1) The various descriptions of the diffuse behavior associated with relaxor ferroelectric compounds as expressed in terms of the theory of compositional fluctuations[14] and in particular, the model concerning "glassy" polarization behavior[9,19] is consistent with the data for $(0.93)(Pb_{0.99}La_{0.01})(Mg_{1/3}Nb_{2/3})O_3 - (0.07)PbTiO_3$ ceramic specimens investigated. The weak field dielectric permittivity and tanδ as a function of temperature exhibit the broad frequency dependent maxima characteristic of the diffuse ferroelectric phase transition of materials with no long-range structural order. Evaluation of the refractive index as a function of frequency and temperature evidence a persistence of a non-reversible average local polarization to temperatures (with a T_d of approximately 390°C) very much higher than the temperature of the dielectric maximum. This trend follows that observed for other PMN and PZN relaxors and is well described by the relationships derived to describe "glassy" polarization behavior in these systems.

(2) The La-modified $(0.93)Pb(Mg_{1/3}Nb_{2/3})O_3 - (0.7)PbTiO_3$ compositions investigated exhibit good electro-optic response, rapid switching time and a moderate half-wave voltage as compared to PLZT indicating future possibilities for electro-optic device applications. The low transition temperature of this composition allows for efficient room temperature operation of such devices, a possible advantage over the PLZT compositions generally employed which exhibit dispersive dielectric behavior at room temperature thereby limiting, to a certain extent, the electro-optic frequency response of the device.[21]

ACKNOWLEDGEMENT

The authors wish to thank Dr. K. Vedam for the use of his optical equipment and to Dr. Qiming Zhang, Dr. Wuyi Pan, and Roy Austin, Jr. for their assistance in this investigation. The contributions of Frank Ainger of Plessey Co. in the preparation of the specimens and the support of the DARPA Nanocomposite Project are also gratefully acnowledged.

REFERENCES

1. T. R. Shrout and A. Halliyal, *American Ceramic Society Bulletin*, **66(4)**, 704 (1987).
2. K. Uchino, *American Ceramic Society Bulletin*, **65(4)**, 647 (1986).
3. K. Uchino, S. Nomura, S. J. Jang, L. E. Cross and R. E. Newnham, *Journ. Appl. Phys.*, **51(2)**, 1142 (1980).
4. S. Takahashi, A. Ochi, M. Yonezawa, T. Yano, T. Hamatsuki and I. Fukui, *Ferroelectrics*, **50**, 181 (1983).
5. N. Kim, W. Huebner, S.-J. Jang and T. R. Shrout, *Ferroelectrics*, **93**, 341 (1989).
6. S. J. Jang, Ph.D. Thesis, The Pennsylvania State University (1979).
7. K. Uchino, S. Nomura, L. E. Cross, R. E. Newnham and S. J. Jang, *Journ. Material Science*, **16**, 569 (1981).
8. D. McHenry, J. R. Giniewicz, S. J. Jang, A. Bhalla and T. R. Shrout, *Ferroelectrics*, **93**, 351 (1989).
9. G. Burns and F. Dacol, *Phase Transitions*, **5**, 261 (1983).
10. L. E. Cross, *Ferroelectrics*, **76**, 241 (1987).
11. K. Okasaki, M. Masuda, S. Tashiro, and S. Ishibashi, *Ferroelectrics*, **22**, 681 (1978).
12. N. Setter, Ph.D. Thesis, The Pennsylvania State University, (1980).
13. A. D. Hilton, C. A. Randall, D. J. Barber and T. R. Shrout, (to be published).
14. G. A. Smolenskii, A. I. Agranovskaya, *Sov. Phys. Solid State*, **1**, 1429 (1959).
15. C. G. F. Stenger and A. J. Burggraaf, *physica status solidi (a)*, **61**, 275 (1980).
16. N. Setter and L. E. Cross, *Journ. Appl. Phys.*, **54**, 4356 (1980).
17. G. H. Haertling and C. E. Land, *Journ. of the Am. Ceram. Society*, **54**, 1 (1971).
18. M. DiDomenico, Jr. and S. H. Wemple, *Journ. of Appl. Phys.*, **40(2)**, 720 (1968).
19. G. Burns and F. H. Dacol, *Physical Review B*, **28(5)**, 2527 (1983).
20. P. D. Thatcher, *Applied Optics*, **16**, 3210 (1977).
21. F. S. Chen, *Optics Communication*, **6**, 279 (1972).
22. J. R. Maldanado and A. H. Meitzler, *IEEE Transactions of Electronic Devices*, **148** (1970).
23. G. Wolfram, *Ferroelectrics*, **10**, 39 (1971).
24. C. J. Kirkby, *Ferroelectrics*, **37**, 567 (1981).
25. M. Ozolinsh, *Mat. Res. Bull.*, **17**, 741 (1982).

APPENDIX 35

Large Hydrostatic Piezoelectric Coefficient in Lead Magnesium Niobate: Lead Titanate Ceramics

D. J. Taylor, D. Damjanovic, A.S. Bhalla, and L.E. Cross
Materials Research Laboratory,
The Pennsylvania State University,
University Park, Pennsylvania, 16802
U.S.A.

Lead magnesium niobate ($PbMg_{1/3}Nb_{2/3}O_3$ - PMN) and its solid solution with lead titanate ($PbTiO_3$-PT), which exhibit relaxor ferroelectric characteristics, have recently been studied extensively for possible use in actuators and transducers [1,2]. The temperature range in which the dielectric permittivity is a maximum is of special interest for these applications, even though, in this relatively large temperature region the remnant polarization is absent. However, it has been demonstrated [3,4] that a very strong piezoelectric effect may be induced in the material by application of an external electric bias field. The possibility of controlling the amplitude and the phase of the piezoelectric response of a material by an external field is of considerable interest in applications for transducers operating at high frequencies (such as in ultrasonic tomography) and also at lower frequencies, for example, under conditions of hydrostatic pressure. Clearly in the latter, materials with high hydrostatic piezoelectric coefficients d_h and g_h are essential. In this paper we have evaluated the hydrostatic piezoelectric coefficient, d_h, in 0.9PMN:0.1PT ceramics, using the values of the transverse, d_{31}, and longitudinal, d_{33}, piezoelectric coefficients which were determined experimentally using an ultradilatometer [5]. This composition with its maximum in dielectric permittivity around 40°C at 100 Hz is particularly interesting for switchable transducers that operate near room temperature.

The 0.9PMN-0.1PT composition was prepared using the Columbite precursor method [6]. Sintering was carried out at 1250°C for four hours. After sintering, the samples were annealed in oxygen at 900°C for four hours. The annealing step was necessary so as to make the samples free of any ageing effects [7]. Fig. 1 shows, for a typical sample, the dielectric constant as a function of temperature for selected frequencies. These measurements were performed during a heating cycle after the sample was held at room temperature for several days. No dielectric ageing behavior was observed.

In previous works, the standard resonance technique [3] as well as a modified resonance technique [8] were successfully employed in studies concerning the field induced piezoelectric effect in relaxor ferroelectric ceramics. Advantages of the resonance methods include, first, the possibility of finding values of not only the piezoelectric coefficients but also the elastic and dielectric coefficients of the material and second, in a more sophisticated technique [8], the ability to obtain phase information for each of the above listed coefficients.

Recently, Pan et al. [4] have shown that the piezoelectric coefficients in relaxor ferroelectric ceramics depend strongly on frequency, particularly in the temperature range where the dielectric permittivity is also dispersive. This requires that all the piezoelectric coefficients be measured at the same frequency. For the resonance techniques this means that the lengths of the transverse (d_{31}) and the longitudinal (d_{33}) resonators should be approximately the same. The resonance techniques are then unsuitable for the longitudinal mode of the relaxor ferroelectric resonators as the D.C. electric bias field necessary to induce piezoelectricity may become impractically large. In addition, our experience shows that resonance of the longitudinal mode tends to be distorted under large electric bias fields, possibly because along the length of the resonator the field is no longer homogeneous.

For the above reasons we have measured d_{31} and d_{33} as a function of the electric bias field using a laser interferometer [5]. The interferometer allows for measurements of ultra low displacements (below 1 A) over a wide frequency range and the measurements of both coefficients may be made on the same sample. The details of the experimental approach to measure d_{33} are described in [5] while details for measuring d_{31} are described below and represented schematically in Fig. 2. First, a thin sample was prepared in the shape of a rectangle. Using five minute epoxy one of its sides was then mounted across the width to the sample mount and a mirror, made from glass which was gold sputtered, was attached to the other side (parallel to the sample mount) with five minute epoxy. Care was taken in mounting the mirror parallel to the mount. Silver conducting wires were attached across the thickness of the sample to which a DC bias and ~1 Volt rms ac electric field at 500 Hz was applied. The shape changes were measured in the length of the sample. An effect of the mirror on the measurements of d_{31} is discussed by Pan et. al. [9]. The dielectric properties were measured with an HP 4275A LCR bridge. The polarization, P, was determined at ~500Hz, with a Sawyer-Tower circuit. All measurements were made at room temperature.

The piezoelectric coefficients d_{33} and d_{31}, measured using the laser interferometer, are shown in Fig. 3 as a function of the electric bias field. Also shown is the hydrostatic charge coefficient, d_h, determined from the relationship

$$d_h = d_{33} + 2d_{31} \qquad (1)$$

d_h was calculated from the corresponding points in the two curves fitted through the experimental data. The maximum values for d_{33} (~1000 pC/N), d_{31} (~400 pC/N) and d_h (~300 pC/N) are remarkably high. Previously reported values of d_{33} in the same composition by Pan et al. are somewhat lower. This discrepancy could be due to i) the properties of 0.9PMN-0.1PT are very sensitive to preparation conditions, and ii) the ambient temperature ("room temperature") in Pan et al's work might not have been the same as in our measurements. In a related study we have found a strong temperature dependence of the piezoelectric coefficients in the 0.9PMN-0.1PT material. The most important result of our study is that d_h saturates at approximately 3.5 kV/cm reaching the value of ~ 300 pC/N (about an order of magnitude higher than that of a soft

PZT material). This large value of d_h suggests that 0.9PMN-0.1PT could be an interesting material for a transducer operating under conditions of hydrostatic pressure.

Unfortunately, the high dielectric constant, k, shown in Fig. 4, results in the low values of the voltage coefficient, $g_h = d_h/\varepsilon$, given in Fig. 5 together with the sensitivity of the transducer, $d_h g_h$. ε is the dielectric permittivity, and $\varepsilon = \varepsilon_o k$, where ε_o is the permittivity of free space. However, g_h is still comparable to that in PZT ceramics and the $d_h g_h$ product is almost an order of magnitude higher. In fact, in this study the dielectric constant was measured at 400 Hz so that the values of g_h given are slightly lower than what the actual values would be at 500 Hz (the frequency used for measuring d coefficients.

Earlier experiments suggest that the orgin of the major component of the total piezoelectric effect in relaxor ferroelectrics is polarization biased electrostriction [4]. The large values of the piezoelectric coefficients are due to the large dielectric permittivity and consequently the large induced polarization while electrostrictive coefficients, Q, are slightly smaller than those in conventional ceramics, such as $BaTiO_3$ [10].

In the dispersive region of the 0.9PMN-0.1PT composition, the thermodynamic phenomenological relationship [11]

$$d_{ij} = 2\varepsilon_i Q_{ji} P_i \tag{2}$$

was found to be only an approximation. However, the d coefficients calculated as a function of electric bias field do qualitatively follow the measured d values [4].

A question in our study arises as to whether or not the phenomenological description [11] of the hydrostatic piezoelectric response as a function of field agrees at least qualitatively with the data obtained experimentally. It follows from equations (1) and (2) that

$$d_h = 2\,\varepsilon_3 P_3 Q_h \tag{3}$$

where $Q_h = Q_{33} + 2Q_{31}$ and is defined as the hydrostatic electrostrictive coefficient. If Q_{33} and Q_{31} are assumed to be independent of the electric field [4] then d_h should have the same dependence on electric field as d_{33} and d_{31}. However, such behavior of d_h is not supported by experimental data. Fig. 6 shows the value of d_{33}, d_{31}, and d_h obtained from Equation (2) and (3). Electrostrictive constants are taken from reference [12] and the values used are $Q_{33} = 1.9 \times 10^{-4}$ m^4/V^2 and $Q_{31} = 0.8 \times 10^{-4}$ m^4/V^2. Polarization as a function of D.C. bias field was obtained from Fig. 7, averaging the values of P for each E. The reason for the observed discrepancy between the measured (Fig. 3) and calculated d_h may be, as shown by Pan et al, that d_{33} and d_{31} deviate at large fields and in the dispersive region from the behaviour expected from equation (2). As a result, the field dependence of the sum $d_{33} + 2d_{31}$ obtained from the experimental values of d_{33} and d_{31} (Fig. 3) does not even qualitatively agree, under our experimental conditions, with the ones predicted by equation (3), shown in Fig. 6.

Our study thus confirms earlier reports [4] that in addition to the polarization biased electrostriction, the induced piezoelectricity in the studied composition has additional components which become important at large electric bias fields. Clearly, it would be most interesting, from both the practical and fundamental point of view to identify all the contributions to piezoelectricity of 0.9PMN-0.1PT.

The hydrostatic piezoelectric coefficient, d_h, in the 0.9PMN-0.1PT ferroelectric relaxor composition was studied as a function of the electric bias field at 500 Hz using a laser interferometer. We found d_h approaching a very large value of ~300 pC/N and then saturating at an electric bias field of ~3.5 kV/cm. The voltage coefficient, g_h, and the sensitivity, $d_h g_h$, are also found to be comparable and larger, respectively, than those in PZT ceramics despite a high dielectric constant in the relaxor material. As contrary to the d_{33} and d_{31} piezoelectric coefficients, d_h does not, under our experimental conditions, depend on electric bias field in a manner predicted by the thermodynamic phenomenological theory.

Acknowledgements

The authors gratefully acknowledge the support of the Office of Naval Research for this research work and Joseph Fielding for preparing the 90PMN:10PT samples.

References

[1] K. Uchino, *Am. Ceram. Soc. Bull.*, 65 (1986) 647.
[2] L.E. Cross, in "Adaptive Structures", edited by B.K. Wada, (ASME vol. AD-15, New York, N.Y., 1989) 9.
[3] Y. Tsuchiya, K. Uchino and S. Nomura, *Jap. J. Appl. Phys.*, 20 (1981) 1841.
[4] W.Y. Pan, W.Y. Gu, D.J. Taylor and L.E. Cross, *Jap. J. Appl. Phys.*, 28 (1989) 653.
[5] W.Y. Pan and L.E. Cross, *Rev. Sci. Instrum.*, 60 (1989) 2701.
[6] S.L. Swartz and T.R. Shrout, *Mater. Res. Bull.*, 17 (1982) 1250.
[7] W.Pan, E. Furman, G.O. Dayton, and L.E. Cross, *J. Mat. Sci. Lett.*, 5 (1986) 647.
[8] D.J. Taylor, D. Damjanovic, A.S. Bhalla and L.E. Cross, *Ferroelectric Lett.*, 11 (1990) 1.
[9] W.Y. Pan, H. Wong and L.E. Cross, *Jap. J. Appl. Phys.*, 29 (1990) 1570.
[10] L.E. Cross, S.J. Jang and R.E. Newnham, *Ferroelectrics*, 23 (1980) 187.
[11] A.I. Devonshire, *Phil. Mag.*, 42 (1951) 1065.
[12] Q.M. Zhang, W. Pan, A. Bhalla and L.E. Cross, *J. Am. Ceram. Soc.*, 72 (1989) 599.

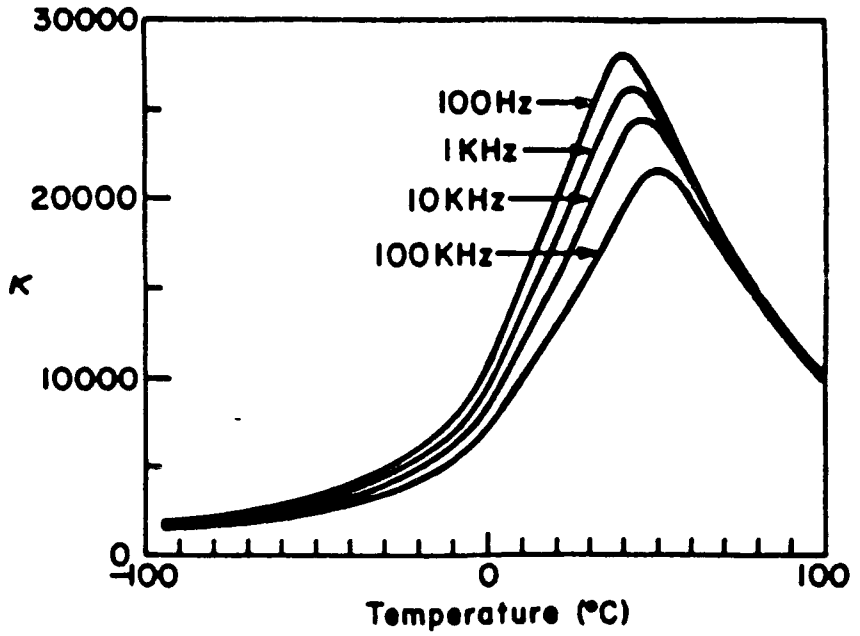

Figure 1. Dielectric constant of 0.9PMN-0.1PT as a function of temperature for selected frequencies.

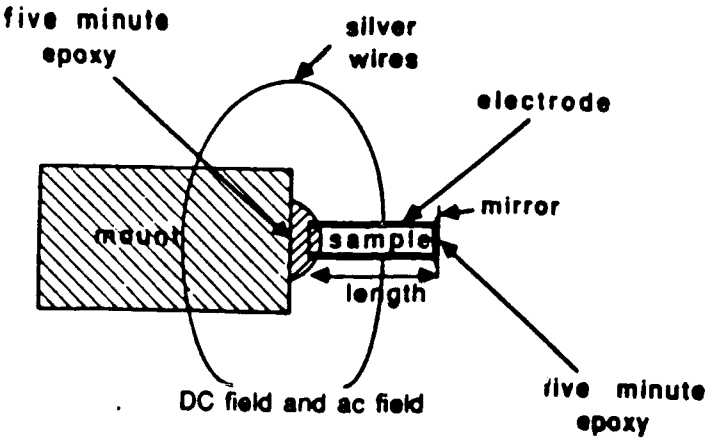

Figure 2. Experimental set-up used to measure d_{31}.

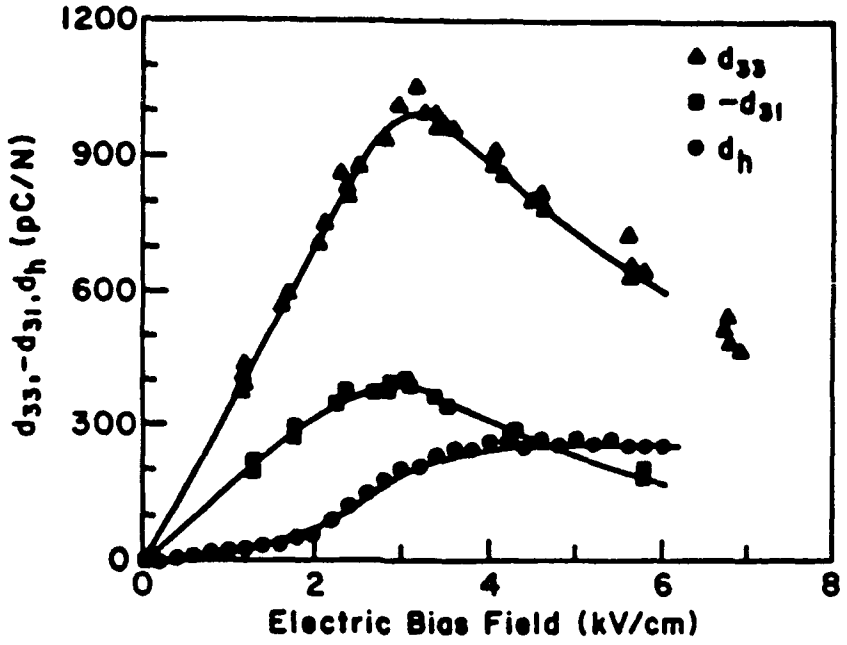

Figure 3. Piezoelectric coefficients d_{33}, d_{31}, and d_h of 0.9PMN-0.1PT measured at ~500 Hz using the laser interferometer (room temperature measurements).

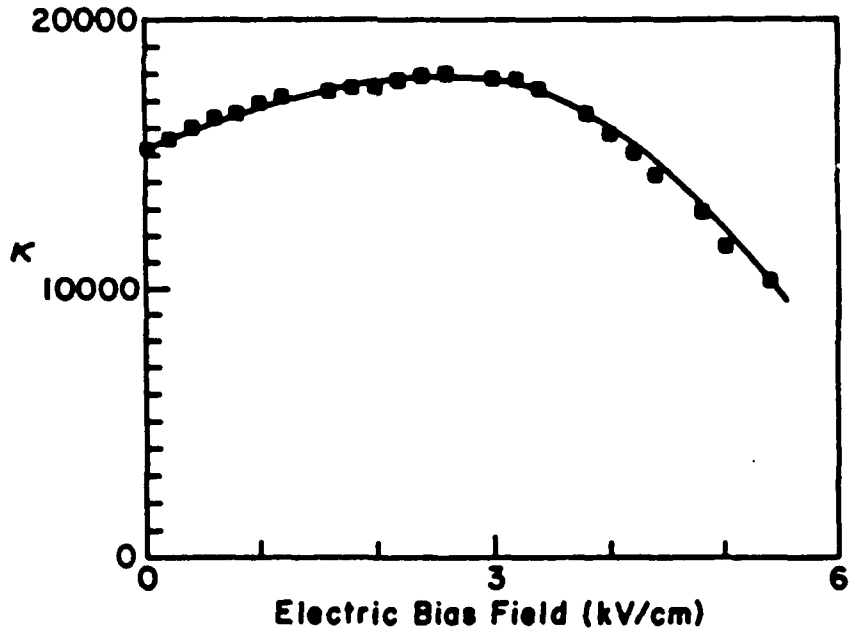

Figure 4. D.C. field dependence of the dielectric constant (~25°C) at 400 Hz for 0.9PMN-0.1PT.

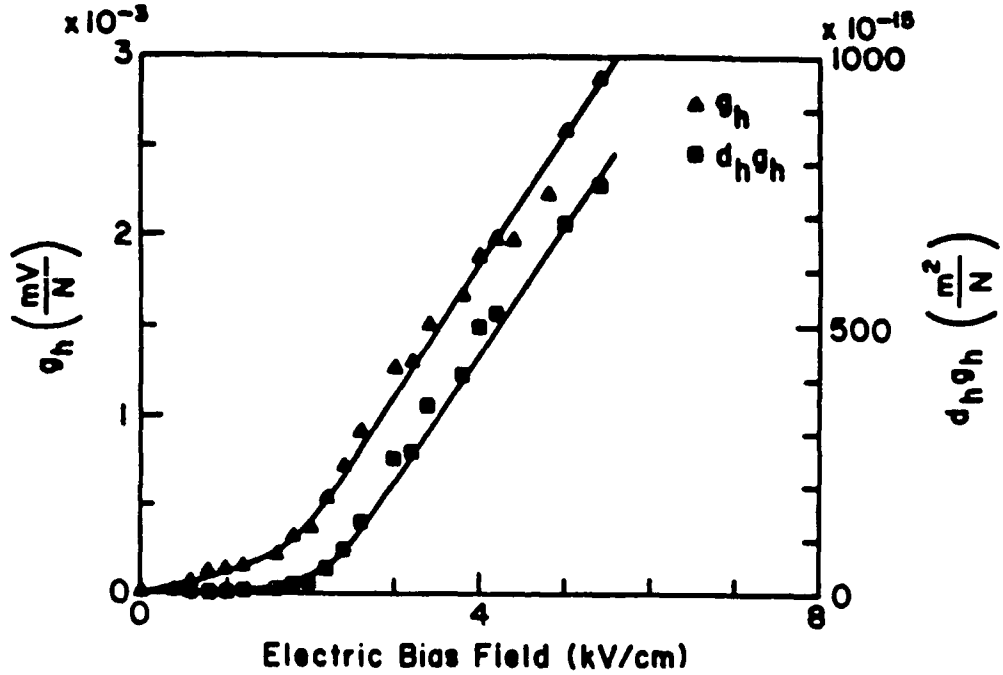

Figure 5. Plot of the voltage coefficient, g_h, and the sensitivity of the transducer, $d_h g_h$, versus D.C. bias.

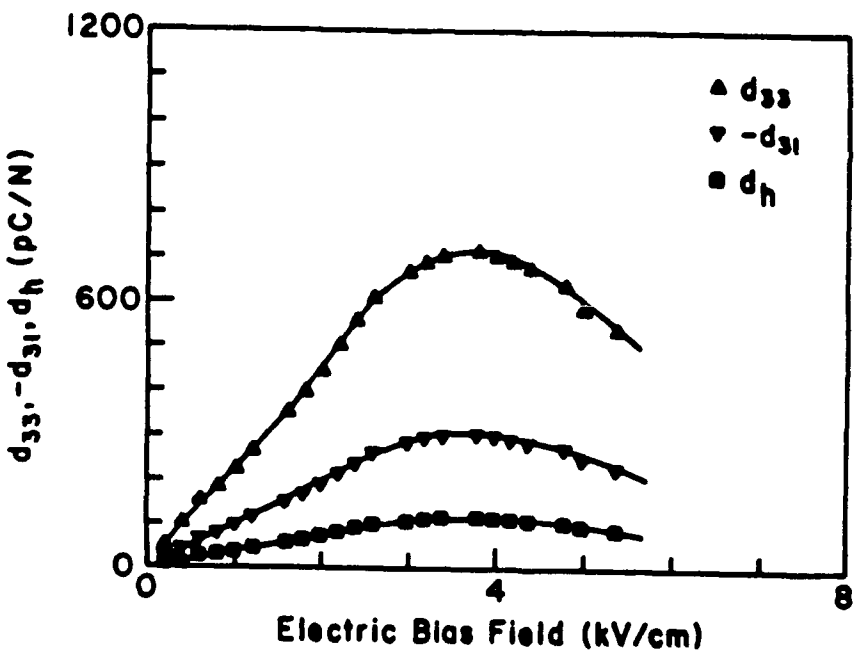

Figure 6. Piezoelectric coefficients d_{33}, d_{31} and d_h calculated from equations (2) and (3).

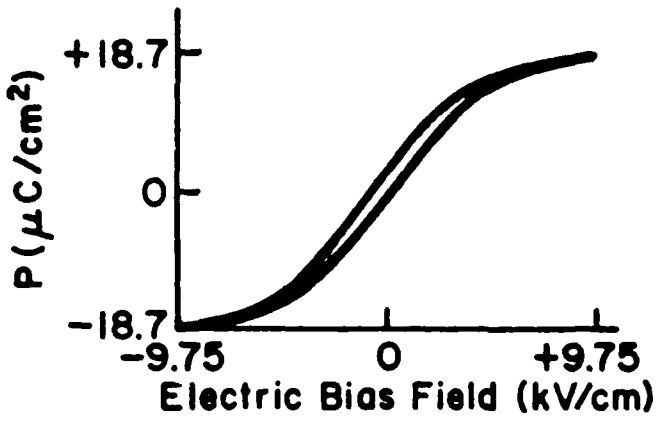

Figure 7. Polarization as measured by the Sawyer-Tower circuit at ~500 Hz (~25°C).

OPTICAL STUDIES

APPENDIX 36

Ferroelectrics, 1990, Vol. 107, pp. 45–46
Reprints available directly from the publisher
Photocopying permitted by license only

OPTICAL AND ELECTRO-OPTICAL PROPERTIES OF LEAD MAGNESIUM NIOBATE-LEAD TITANATE

D.A. MCHENRY, J.R. GINIEWICZ, S.J. JANG, T.R. SHROUT, and A.S. BHALLA
Materials Research Laboratory, The Pennsylvania State University, University Park, PA 16802

Earlier efforts to investigate the material properties of ceramic (1-x) $Pb(Mg_{1/3}Nb_{2/3})O_3$-$xPbTiO_3$ (PMN-PT) have primarily been concentrated upon exploring the utility of PMN-PT in applications where the high dielectric constant, low thermal expansion, and large, reproducible electrostrictive strains present in the compositional system could be exploited.[1] For the present work, relaxor ferroelectric ceramics of optical quality with the compositions .90 $Pb(Mg_{1/3}Nb_{2/3})O_3$-.10 $PbTiO_3$ [.90 PMN-.10 PT] and .93 $(Pb_{0.99}La_{0.01})(Mg_{1/3}Nb_{2/3})O_3$-.07 $PbTiO_3$ [.93 PLMN-.07 PT] have been investigated for usage in electro-optical devices. The ceramic samples were hot-pressed to an optical transparency of greater than 50% at 633 nm and have large refractive indices ($\tilde{}$ 2.54).[2]

The ceramic compositions are located within the "pseudocubic" phase region and evidence primarily a quadratic electro-optic response upon application of electrical voltages. In order to determine the quadratic electro-optical coefficients, the transmitted intensity as a function of voltage applied to the ceramic sample placed between crossed polarizers was measured. The measured birefringence vs E-field curves determined by this method are shown in the figure.

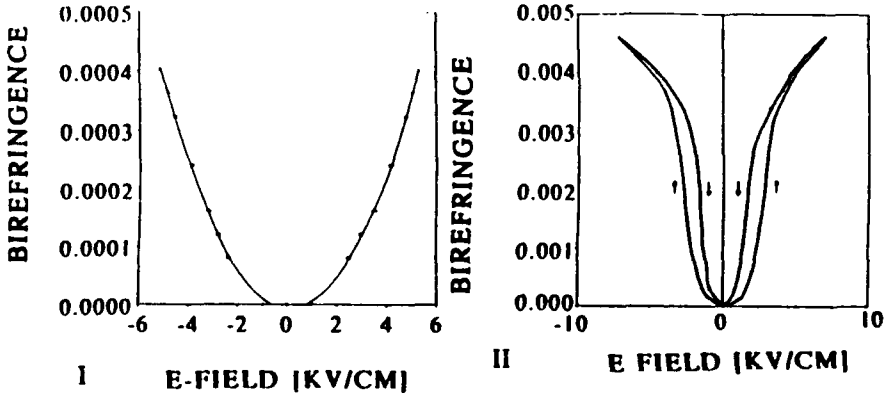

Birefringence vs E field curves at T = 24°C (and λ = 633 mm) for I .93 PLMN-.07 $PbTiO_3$ and II .90 PMN-.10 PT.

The effective quadratic coefficient, R, for the transverse geometry were obtained from the equation

$$R = -\frac{2\Delta n}{n_o^3 E^2}, \tag{1}$$

where Δn is the field-induced birefringence, n_0 the refractive index, and E is the applied electric field, by using the first half-wave retardation for increasing applied voltage.[3] The measured R coefficients for .93 PLMN-.07 PT and .90 PMN-.10 PT along with their polarization-optical g coefficients as defined by

$$\bar{g} = -\frac{2\Delta n}{n_o^3 P^2}, \tag{2}$$

(where the polarization P was obtained from hysteresis loops) are given in Table I.

Table I.

Composition	R[x 10^{-16} m^2/V^2] @ 633 nm T = 24°C	g[m^4/C^2]
.93 PLMN-.07 PT	2.1	.0056
.90 PMN-.10 PT	14.5	.0065

These compositions with no initial birefringence and large values of electro-optic coefficients may have possible use in optical modulators, shutters, or other electro-optic devices.

REFERENCES

1. S.J. Jang, K. Uchino, S. Nomura, and L.E. Cross, Ferroelectrics, 27, 31-34 (1980).
2. D.A. McHenry, J.G. Giniewicz, S.J. Jang, A.S. Bhalla, and T.R. Shrout, Ferroelectrics, 93, 351-359 (1989).
3. G.H. Haertling, "Electronic Ceramics: Properties, Devices, and Applications," ed., L.M. Levinson, Marcel Dekker (1987).

APPENDIX 37

Ferroelectrics, 1989, Vol. 93, pp. 351–359
Reprints available directly from the publisher
Photocopying permitted by license only

OPTICAL PROPERTIES OF HOT PRESSED RELAXOR FERROELECTRICS

D. A. MCHENRY, J. GINIEWICZ, S. J. JANG, A. BHALLA and T. R. SHROUT

Materials Research Laboratory, The Pennsylvania State University, University Park, PA 16802 USA

(Received August 29, 1988)

The optical properties of hot pressed transparent ceramics based on the relaxor ferroelectric (1-x)Pb($Mg_{1/3}$,$Nb_{2/3}$)O_3-xPbTiO$_3$ (known as PMN-PT) solid solution system have been examined in the visible region. We report transmission as a function of wavelength, refractive indices as a function of temperature and wavelength, and quadratic electro-optic coefficient data for the 632.8 nm HeNe laser wavelength. For our particular ceramic compositions, .93($Pb_{0.99}La_{0.01}$)($Mg_{1/3}$,$Nb_{2/3}$)O_3-.07PbTiO$_3$ and .90 PMN-.10 PT, the refractive index dispersion is well described by a single term Sellmeier equation. The observed temperature dependence of the refractive indices $n(T)$ can be discussed in terms of polar microregions which alter the refractive indices in these ceramics via the quadratic electro-optic effect. Transverse quadratic electro-optic coefficients measured were in accord with those reported for other Pb containing perovskite oxides.

INTRODUCTION

A study of the optical properties of transparent (1-x) Pb($Mg_{1/3}$,$Nb_{2/3}$)O_3-xPbTiO$_3$ (hereafter PMN-PT) ceramics is of interest both for possible insight into the physical nature of relaxor ferroelectrics as well as for making practical extension of its several present applications to include usage in electro-optic devices. Present applications take advantage of (1-x) PMN-xPTs singularly excellent dielectric, low thermal expansion, and electrostrictive properties.[1,2] Ceramics with the composition .90 PMN-.10 PT have been used in surface deformable mirror technology and unlike $Pb_{1-x}La_x(Zr_yTi_{1-y})O_3$ (PLZT $x/y/1-y$) can be prepared as a stoichiometric "fully-stuffed" compound without aliovalent defects and concomitant dielectric aging effects.[3]

PMN is the classic example of a relaxor ferroelectric. It has the perovskite structure with Pb^{2+} ions on the cation A-site and Mg^{2+} and Nb^{5+} ions in a disordered setting for the cation B-site. This disorder is believed to lead to "glassy" polarization behavior observable in the temperature dependence of the refractive index.[4] The weak field dielectric permittivity as a function of temperature exhibits a broad frequency dependent (i.e., dispersive) maximum characteristic of a diffuse phase transition. Studies of the optical birefringence have revealed that PMN samples when cooled to low temperatures evidence no optical anisotropy which would be indicative of a macro-volume change to a polar phase.[5] The quadratic polarization-optic coefficients which have been reported ($g_{11} - g_{12}$ = .015 m^4/C^2 and g_{44} = .008 m^4/C^2) are not very temperature dependent and are about an order of magnitude smaller than those of non-Pb-containing oxygen-octahedra ferroelectrics.[6] It is believed that Pb^{2+} ions on the A-site cause high refractive indices

and lowered g coefficients. The refractive index dispersion and its temperature dependence have also been reported.[7,8]

$PbTiO_3$ is also a perovskite ferroelectric but in contrast to PMN it undergoes a displacive first order phase transition at about 492°C. Optically, $PbTiO_3$ is uniaxial negative, has high refractive indices, and possesses an anomalous birefringence increase which disappears prior to the ferroelectric–paraelectric phase transition. $PbTiO_3$ is a good non-linear optical material with a large reversible polarization. $PbTiO_3$ has a value of only $g_{11} - g_{12} = +.003\ m^4/C^2$ at room temperature and is unusual in this regard even among Pb perovskites.[6]

It is the purpose of this paper to report on the optical properties of two relaxor ferroelectric compositions, $.93(Pb_{0.99}La_{0.01})(Mg_{1/3}Nb_{2/3})O_3$-$.07PbTiO_3$ and .90 PMN-.10 PT. Sample preparation for these hot pressed ceramics are detailed in Reference 9 along with other physical and dielectric measurements. Lanthanum addition to PMN or PZT enhances densification and thus improves transparency. The effect of La^{3+} addition on the dielectric properties of PMN is reported in Reference 10. It will be of interest to see what effect adding small amounts of La_2O_3 and $PbTiO_3$, a normal displacive ferroelectric, to form a solid solution with a relaxor ferroelectric like PMN will have on the optical properties.

TRANSMISSION

Ferroelectric hot pressed samples to be employed in optical and electro-optical devices must be made sufficiently transparent in the visible and near IR region. Optical transmission measurements were made as a function of wavelength using a Cary 2300 spectrophotometer upon electrically unpoled optically polished plates. Figure 1(a,b) shows the measured percent transmission as a function of wavelength (300 nm–800 nm). For both of these materials the percentage of transmitted light begins to rise abruptly at just below 380 nm and then increases only gradually with wavelength above 450 nm. This gradual increase in transmittance continues into the near IR at least through 1500 nm without any noticeable absorption bands being observed. The reflection loss line is drawn in from the calculated reflection $R = (n - 1)^2/(n + 1)^2$ values using the measured refractive indices from the next section.

The .90 PMN-.10 PT hot pressed sample is especially transparent (31.7%T @ 450 nm and 57.1%T @ 680 nm). The maximum value for the dielectric permittivity in this material is $Tc \cong 45$°C at 1 KHz. Ferroelectric regions are of pseudocubic symmetry for the PMN-rich compositions in this solid solution. The $.93(Pb_{0.99}La_{0.01})(Mg_{1/3}Nb_{2/3})O_3$-$.07PbTiO_3$ composition is well into the paraelectric region at room temperature ($T_c \sim 9$°C at 1 KHz). In PLZT it has been shown that the pseudocubic 9/65/35 composition is considerably more transparent than either the rhombohedral 7/65/35 or tetragonal 12/40/60 ferroelectric compositions, especially for shorter visible wavelengths where absorption and light scattering dominate.[11] Light scattering from domain walls and grain boundary scattering will occur in La-doped PMN-PT ceramics as well and lower the optical transparency. The addition of $PbTiO_3$ to PMN seems to cause the thermal stabilization of polar

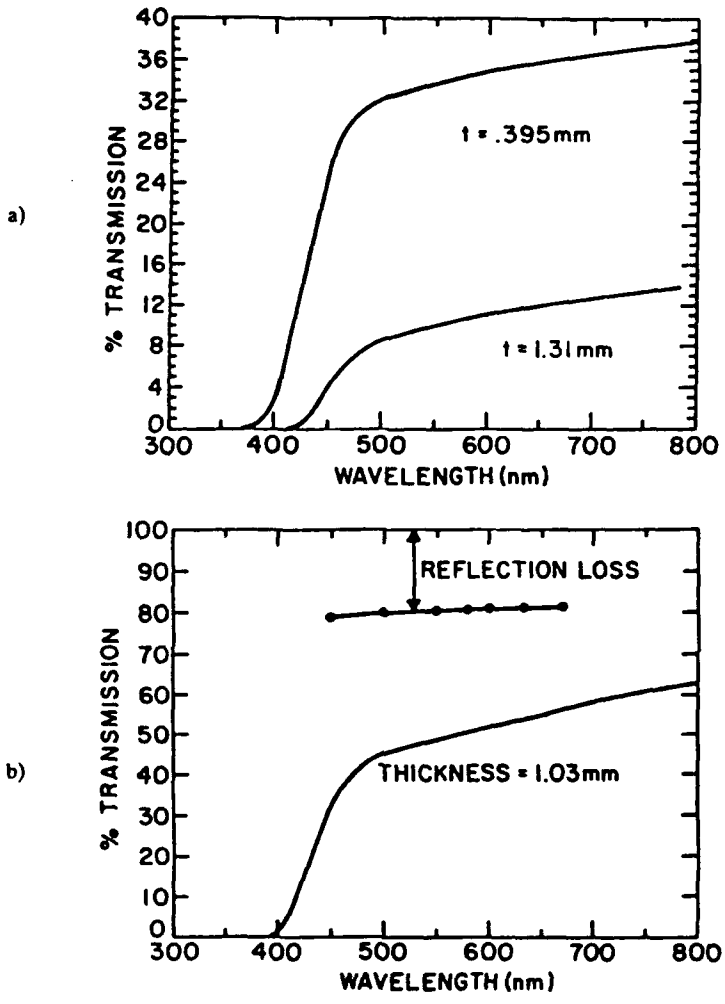

FIGURE 1 Percent transmission as a function of wavelength for hot pressed optically polished plates for ceramic compositions. a) .93($Pb_{0.99}La_{0.01}$)($Mg_{1/3}Nb_{2/3}$)O_3-.07$PbTiO_3$ excess; b) .90 PMN-.10 PT.

microferroelectric regions in these ceramics. Further improvements in transparency for these ceramics may be achieved by optimizing the processing and sintering conditions.

REFRACTIVE INDEX DISPERSION

The refractive indices for several visible wavelengths were measured by the method of minimum deviation. Prisms with apex angles of between 20°–30° were cut and polished from the bulk ceramics. The prisms were then annealed for 30 min at

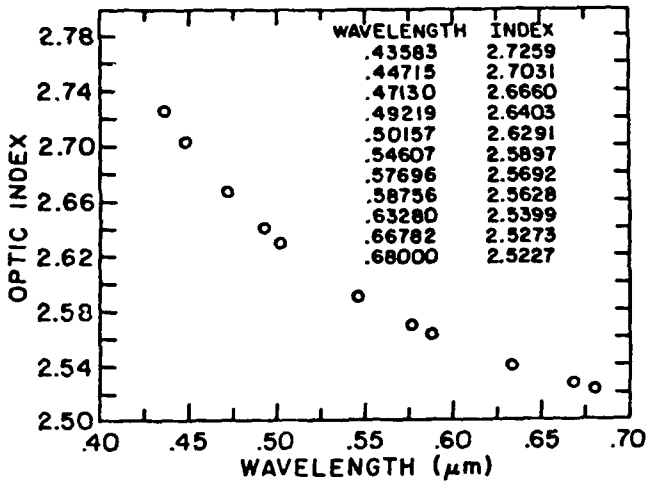

FIGURE 2 Refractive index dispersion for $.93(Pb_{0.99}La_{0.01})(Mg_{1/3},Nb_{2/3})O_3$-$.07PbTiO_3$ in the visible region.

525°C in order to relieve polishing strains. The prism apex angles and minimum deviation angles were determined using a Gaertner optical spectrometer with a smallest vernier reading of 20". Reproducibility and calibration of the spectrometer readings lead us to estimate that errors for the reported index values are within $\pm 3 \times 10^{-4}$.

A representative dispersion curve for prisms with composition $.93(Pb_{0.99}La_{0.01})(Mg_{1/3},Nb_{2/3})O_3$-$.07PbTiO_3$ is shown in Figure 2. These polycrystalline materials clearly have a very high refractive index (>2.7 for $\lambda < 450$ nm) which is mainly attributable to their having a high density of polarizable ions such as Pb^{2+}, Ti^{4+}, and Nb^{5+}. Also, the refractive index is quite dispersive in the visible region, characteristic of the optical spectrum on the long wavelength side of UV absorption peaks. Wemple and Didomenico have shown that the dispersion of the index is frequently well described by a single-term Sellmeier dispersion formula of the form[12]

$$n^2 - 1 = \frac{S_o\lambda_o^2}{\left(1 - \frac{\lambda_o^2}{\lambda^2}\right)} = \frac{E_dE_o}{E_o^2 - E^2} = \frac{f}{E_o^2 - E^2} \qquad (1)$$

where λ, E = wavelength and energy of the incident light, respectively
λ_o, E_o = average oscillatory position and energy, respectively
S_o, $f = E_oE_d$ = average oscillator strength
E_d = dispersion energy.

The Sellmeier constants in Equation (1) are determined by plotting $n^2 - 1$ vs. λ^{-2} to a straight line least squares fit. Figure 3 shows this type of plot for

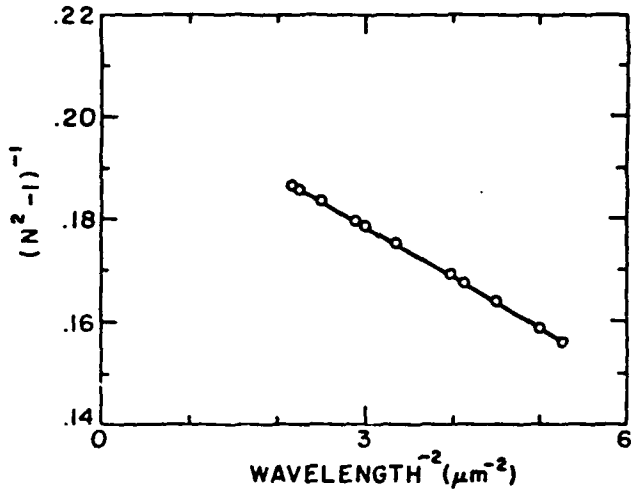

FIGURE 3 Plot of $1/n^2$-1 vs. $1/\lambda^2$ for .93($Pb_{0.99}La_{0.01}$)($Mg_{1/3}$,$Nb_{2/3}$)O_3-.07$PbTiO_3$ in order to determine Sellmeier parameters.

.93($Pb_{0.99}La_{0.01}$)($Mg_{1/3}Nb_{2/3}$)O_3-.07$PbTiO_3$. The tabulated Sellmeier parameters for our measurements as well as for the system end members PMN and $PbTiO_3$ are given in Table I.

Addition of $PbTiO_3$ appears to 1) raise the refractive index; 2) raise the dispersion energy E_d; and 3) lower E_o (a quantity related to the energy band gap) as compared to pure single crystal PMN. The addition of small amounts of La^{3+} and associated A-site vacancies in place of the Pb^{2+} ions would be expected to lower the refractive index values. The values for $PbTiO_3$ in the table are single crystal values averaged for a ceramic index.[13]

TABLE I

Refractive index parameters for the PMN-PT system

	PMN[6]	.93($Pb_{0.99}La_{0.01}$)($Mg_{1/3}$,$Nb_{2/3}$)O_3-.07$PbTiO_3$	.90 PMN-.10 PT	$PbTiO_3$[10]
n @ 632.8 nm	2.5219	2.5399	2.5455	2.688
λ_o (μm)	0.216	0.218	0.220	0.222
S_o($\times 10^{-14} m^{-2}$)	1.013	1.012	1.00	1.09
E_o (eV)	5.73	5.69	5.64	5.59
E_d (eV)	27.2	27.40	27.31	30.0
f (eV)^2	156	155.9	154	168
E_o/S_o ($\times 10^{-14}$ eV m^2)	5.66	5.62	5.64	5.13

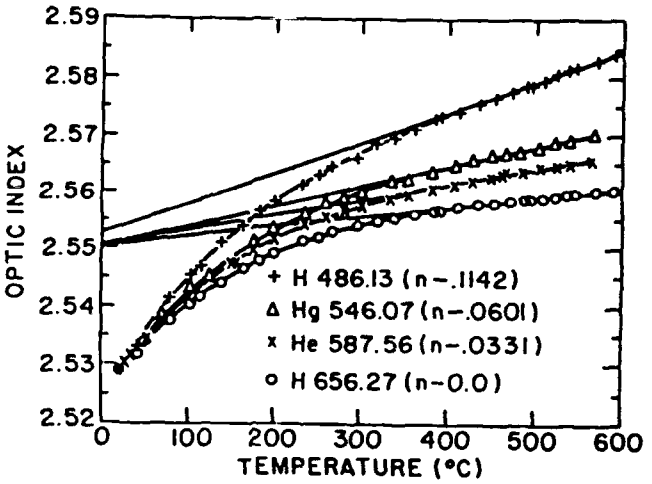

FIGURE 4 Temperature dependence of the refractive index for $.93(Pb_{0.99}La_{0.01})(Mg_{1/3},Nb_{2/3})O_3$-$.07PbTiO_3$ at four spectral wavelengths in the visible from 20°C–600°C.

REFRACTIVE INDEX TEMPERATURE DEPENDENCE

A small oven was constructed and mounted on the spectrometer to enable us to measure refractive indices in the range 20°C–600°C. Temperatures were measured using a pair of thermocouples located above and below the prisms. Control of the temperature was maintained within ±2°C for the indicated temperature readings.

The temperature dependence of the refractive index was measured at four common spectral wavelengths (H 486.13 nm, Hg 546.07 nm, He 587.56 nm, and H

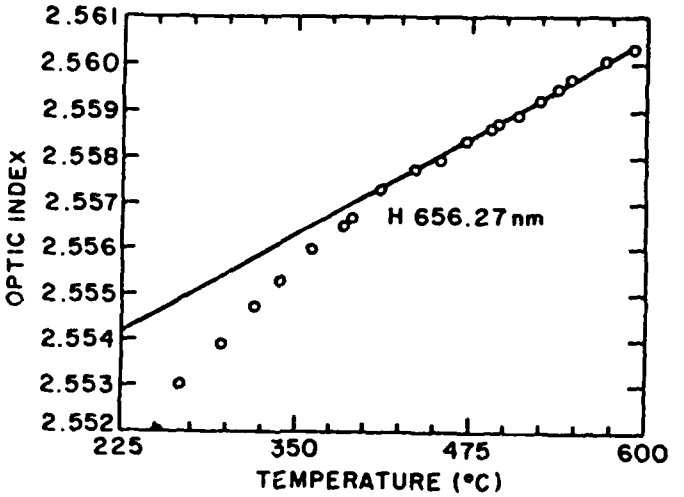

FIGURE 5 Expanded view of $n(T)$ for composition $.93(Pb_{0.99}La_{0.01})(Mg_{1/3},Nb_{2/3})O_3$-$.07PbTiO_3$ @ H 656.27 nm in order to ascertain T_c value.

656.27 nm). Figure 4 shows the measured $n(T)$ curves at the listed wavelengths for $.93(Pb_{0.99}La_{0.01})(Mg_{1/3},Nb_{2/3})O_3$-$.07PbTiO_3$. It should be noted that subtractions have been made as marked on the top three graphs in order to show all four curves on the same high resolution scale. A few features of these $n(T)$ curves should be pointed out. First, the high temperature region of the curves is given approximately by a straight line fit to the data in this region. The dn/dt values determined by the slopes of these lines increase for shorter wavelengths nearer to the energy band gap and range from 5.36×10^{-5}/°C for H 486.13 nm down to 1.69×10^{-5}/°C for H 656.27 nm. Secondly, the departure from linearity occurs at a point often called T_d[4] which is several hundred degrees above the regular Curie temperature ($Tc \cong$ 9°C). No major change in the refractive indices would then be expected to occur at T_c.

Figure 5 shows an expanded view of the H 656.27 nm curve in order to show more clearly this departure from linearity. The value of T_d was determined as being approximately 390°C for each of the four wavelengths. T_d is therefore seemingly independent of wavelength.

QUADRATIC ELECTRO-OPTIC COEFFICIENTS

The transverse quadratic electro-optic coefficients were measured using an AC Senarmont compensator method using phase sensitive lock-in amplifier detection. A HeNe laser with a 632.8 nm output was used as a light source. The values for the electro-optic coefficients as a function of temperature (20°C–250°C) were determined under low frequency (<50 KHz) unclamped conditions. At room temperature, the quadratic electro-optic coefficients in terms of polarization (polarization-optic) were, $g_{11} - g_{12} = 0.08 \pm 10\%$ m^4/C^2 and in terms of electric field $R_{11} - R_{12} = 2.25 \times 10^{-16}$ m^2/V^2 $\pm$ 10% for $.93(Pb_{0.99}La_{0.01})(Mg_{1/3},Nb_{2/3})O_3$-$.07PbTiO_3$. The electro-optic g coefficients increase weakly with temperature and level off so that an average value of $g_{11} - g_{12} \cong .012$ m^4/C^2 is found for the 20°C–250°C temperature range.[14]

DISCUSSION

The $n(T)$ behavior in relaxor ferroelectrics (as found in our samples Figures 4 and 5) is often explained as follows. At temperatures higher than T_d the refractive index is primarily controlled by thermal expansion and thus changes linearly with temperature. Below T_d, the departure from linear behavior occurs due to the presence of microregions of local polarization which causes a change Δn in the refractive index proportional to the square of the polarization by the quadratic electro-optic effect.[4,15]

For randomly oriented crystallites as found in our unpoled ceramics, the appropriate observed change in refractive index is given by[16]

$$\Delta n = \frac{\Delta n_{\parallel} + 2\Delta n_{\perp}}{3} = \frac{-(n^o)^3}{2}\left[\frac{g_{33} + 2g_{13}}{3}\right]P_d^2 \qquad (2)$$

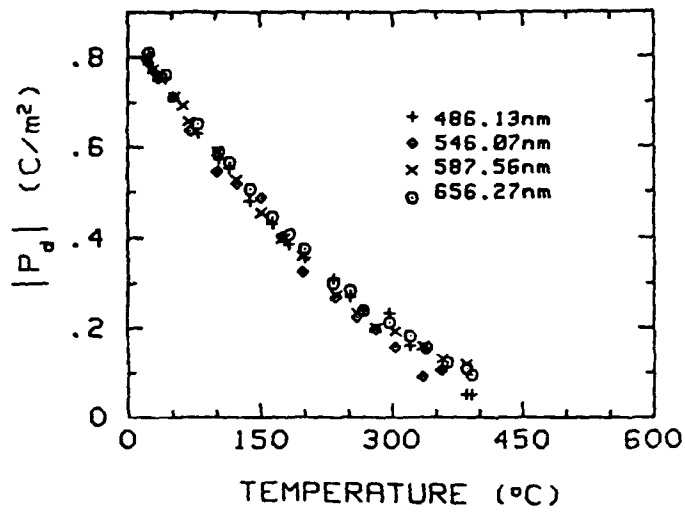

FIGURE 6 $|P_d|$ as a function of temperature for $.93(Pb_{0.99}La_{0.01})(Mg_{1/3}Nb_{2/3})O_3$-$.07PbTiO_3$ calculated from $n(T)$ data.

where n^o is the undeviated refractive index as given by the straight line, the g's are the appropriate combination of electro-optic coefficients, and P_d is the local polarization present. Since we know Δn, n^o, and can approximate the electro-optic coefficients by our measured value ($g_{11} - g_{12} \cong .012\ m^4/C^2$), we can invert Equation (2) to find the magnitude of local polarization, $|P_d|$. This is shown in Figure 6 for the four wavelengths at which $n(T)$ was measured.

Temperature dependent Sellmeier parameters have also been calculated based upon the four frequency measurements of $n(T)$. From a primarily linear graph of E_o vs. T we have determined $dE_o/dT = -6.48 \times 10^{-4}$ eV/°C. This quantity represents a change in the energy of the effective oscillator which can be correlated to the temperature variation of the band gap (quite close to $dE_{gap}/dT \cong -6.7 \times 10^{-4}$ eV/°C for indirect bandgaps).[7] P_d exists to much higher temperatures and is a great deal larger than the measured reversible polarization. The comparatively large values for P_d may be due to grain boundaries in the ceramic inhibiting polarization reversal.

The value of $T_d \sim 390$°C (as shown in Figures 4 and 5) is larger than has been measured for PMN single crystals[7] with $T_d \sim 344$°C. This increased value may have been caused by the addition of $PbTiO_3$. Further studies are underway to establish the cause of such an enhancement of T_d in these ceramics compared with single crystal PMN.

SUMMARY

We have prepared hot pressed optically transparent relaxor ferroelectric samples and have measured some of the important linear optical properties. Transmission measurements verify that PMN-PT based ceramics can be made optically trans-

parent in the visible range. Refractive index dispersion has been successfully modeled by a single term Sellmeier equation. Quadratic electro-optic coefficients were measured and used to interpret the $n(T)$ behavior of these ceramic samples according to a theory of micropolar regions applicable to relaxor ferroelectrics.

Future work to follow up this investigation will include examining a further series of La^{3+} modified PMN-PT and PST hot pressed transparent ceramics for electro-optic related properties.

ACKNOWLEDGEMENTS

The authors gratefully acknowledge Frank Ainger of Plessey Co. for his guidance during the hot pressing and DARPA for their support of the Nanocomposite Project.

REFERENCES

1. S. J. Jang, Ph.D. Thesis, The Pennsylvania State University (1979).
2. S. J. Jang, K. Uchino, S. Nomura and L. E. Cross, *Ferroelectrics*, **27**, 31 (1980).
3. W. Pan, E. Furman and L. E. Cross, *Journ. Mater. Sci. Lett.*, **5**, 647 (1986).
4. G. Burns and F. Dacol, *Phase Transitions*, **5**, 261 (1985).
5. L. E. Cross, *Ferroelectrics*, **76**, 241 (1987).
6. P. D. Thatcher, *Journ. Appl. Phys.*, **41**, 4790 (1970).
7. O. Yu Korshunov, P. A. Markovin and R. V. Pisarev, *Sov. Phys. Solid State*, **25** (7), 243 (1983).
8. G. Burns and F. H. Dacol, *Solid State Commun.*, **48** (10), 853 (1983).
9. J. Giniewicz, D. A. McHenry, S. J. Jang and T. R. Shrout, ECAPD-1, ISAF '88, Paper U12, Zurich, Switzerland (1988)
10. N. Kim, S. J. Jang and T. R. Shrout, ECAPD-1, ISAF '88, Paper U9, Zurich, Switzerland (1988).
11. G. Haertling, "Electronic Ceramics: Properties, Devices, Applications," ed., L. M. Levinson, Marcel Dekker, pp. 371–492 (1987).
12. M. DiDomenico, Jr. and S. H. Wemple, *Journ. Appl. Phys.*, **40** (2), 720 (1968).
13. P. D. Thatcher, *Applied Optics*, **16**, 3210 (1977).
14. D. A. McHenry, W. Pan, Q. M. Zhang, S. J. Jang and A. S. Bhalla, Unpublished work.
15. A. S. Bhalla, R. Guo, L. E. Cross, G. Burns, F. Dacol and R. R. Neurgaonkar, *Phys. Rev. B*, **36** (4), 2030 (1987).
16. G. Burns and F. H. Dacol, *Phys. Rev. B*, **28** (5), 2527 (1983).

APPENDIX 38

THERMAL HYSTERESIS OF OPTICAL SECOND HARMONIC IN PARAELECTRIC $BaTiO_3$

G.R. FOX, J.K. YAMAMOTO, D.V. MILLER, L.E. CROSS and S.K. KURTZ
Materials Research Laboratory, The Pennsylvania State University, University Park, PA 16802, USA

Received 5 February 1990

The SHG signal between 25 and 250°C was measured for a flux-grown single crystal, high-purity single-crystal fibers, and powder (0.5 μm average particle size) of $BaTiO_3$. All three $BaTiO_3$ sources showed a distinct symmetry-forbidden SHG signal with thermal hysteresis in the paraelectric phase. In the flux-grown crystal, annealing at temperatures above 140°C for 15 h causes the SHG signal in the paraelectric phase to disappear below the background noise level of the second-harmonic analyser. In the single-crystal fibers and powder the SHG signal is still observable at 250°C.

1. Introduction

Second-harmonic generation (SHG) is an extremely sensitive method for measuring the acentric nature of crystallographic structures. It is thus quite useful in the study of ferroelectric–paraelectric phase transitions [1,2]. $BaTiO_3$ has been investigated by several workers and its non-linear optical coefficients have been well characterized for each of the three acentric crystallographic structures [3–5]. SHG has also been observed in the paraelectric cubic phase of $BaTiO_3$ even though the paraelectric space group, Pm3m, contains a center of symmetry. It has been suggested that the symmetry-forbidden SHG in the paraelectric phase is due to the formation of polar regions about lattice defects [6] or due to the occurrence of dynamic micropolar regions which tetragonally modify the structure in localized regions [4,5]. The results presented in this paper for SHG experiments on flux-grown crystals, single-crystal fibers, and a powder of $BaTiO_3$ provide new information about the possible origin of the forbidden SHG in the paraelectric phase.

2. Procedure

The SHG signal of three different samples of $BaTiO_3$ was measured using a dual-beam second-harmonic analyzer (SHA) as described by Dougherty and Kurtz [4,7]. A Nd:glass laser with 1 J output intensity, 1.06 μm wavelength, and 300 μs pulse length was used in the analyzer. Photomultiplier signals from the second harmonic and reference channels were compared using a Hewlett-Packard 54111D digitizing oscilloscope. SHG signals were measured at discrete temperatures, point by point, on heating and cooling between 25 and 250°C. The temperature was allowed to stabilize for approximately 15 min at each temperature and the points reported are averages of three peak SHG intensities recorded at 1 min intervals.

The first sample investigated was a multidomain $BaTiO_3$ single-crystal platelet grown from a KF flux by the Remeika method. The faces of the platelet were oriented parallel to the pseudocubic 100 faces and from capacitance versus temperature measurements the ferroelectric–paraelectric transition temperature (T_c) was determined to be 118°C. The SHG signal was measured with the incident beam perpendicular to the plane of the crystal.

Cross sections of multidomain single-crystal fibers, grown from a ceramic feedstock (made from commercially available $BaTiO_3$ powder [#1]) by the laser-heated pedestal technique [8] were also analyzed. T_c for the fibers occurred at 133°C as determined from capacitance versus temperature mea-

[#1] TAM HPB, TAM Ceramics, Inc., Niagra Falls, NY 14805, USA.

surements. Fibers initially grown with c-axis orientation were annealed at 900°C and sliced to form disks 0.1 mm in thickness. Several slices were placed on a glass cover slide in the path of the incident beam, such that the beam propagated along the length of the fiber.

High-purity $BaTiO_3$ powder samples were prepared by placing less than 200 mg of powder between two glass cover slides so as to form a sandwich. The powder had an average particle size of 0.5 μm.

3. Results and discussion

3.1. $BaTiO_3$ flux-grown single crystal

Fig. 1 shows the heating and cooling curve for the flux-grown $BaTiO_3$ platelet. The sharp decrease in the SHG intensity between 115 and 120°C is indicative of the ferroelectric–paraelectric phase transition, in good agreement with the T_c determined by capacitance measurements. Above T_c a weak but distinct SHG signal is still observed which decreases steadily with increasing temperature. Above 220°C the SHG intensity can no longer be distinguished from the background (background equals 0.2 in relative units) and is assumed to be zero.

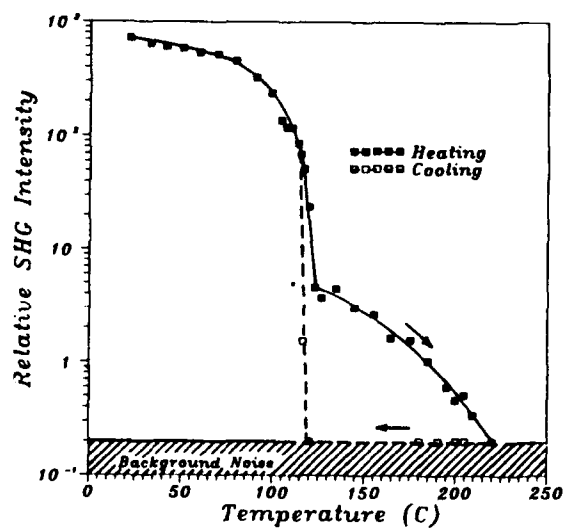

Fig. 1. Relative SHG intensity as a function of temperature for a multidomain flux-grown $BaTiO_3$ single crystal.

After holding the crystal at 220°C for 30 min, the crystal was cooled; no measurable SHG signal was observed on cooling until 117°C where the transition to the ferroelectric phase occurs. In two separate trials the crystal was heated from room temperature to 220°C and then cooled to 175°C and 145°C, respectively, where the crystal was held for 15 h. Soaking the crystal at 175°C or 145°C for 15 h produced no change in the zero SHG intensity on cooling.

Two other heating and cooling schedules are shown in fig. 2. In the first run, the sample was heated to 170°C, cooled to just below the transition, and then heated again to 220°C. During the initial heating (curve 1), the intensities follow a curve similar to fig. 1. On cooling from 170°C (curve 2) the SHG signal was constant until passing through the ferroelectric transition. During the second heating above T_c (curve 3), the SHG signal exhibits the same constant intensity as that observed during cooling. When the crystal was heated above 170°C (curve 4) the intensity decreases in a regular fashion. For the second run shown in fig. 2, the crystal was heated to

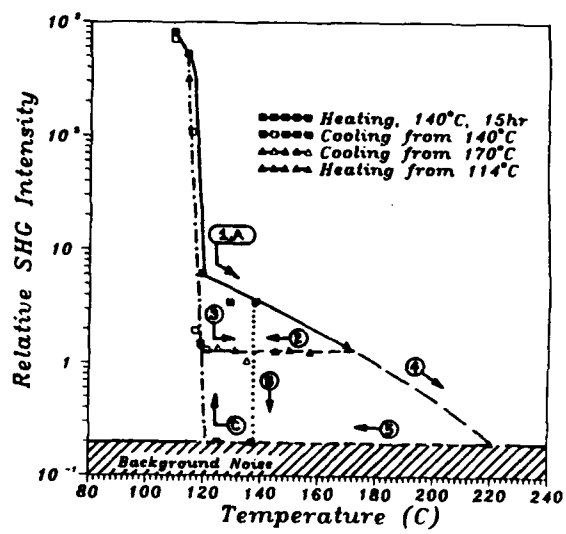

Fig. 2. SHG in the paraelectric phase for two different heating schedules, 1–5 and A–C. In the first heat schedule the crystal is (1) heated from room temperature to 170°C, (2) cooled to 114°C, (3) and (4) heated to 220°C, and (5) cooled to 110°C. In the second schedule the crystal is (A) heated from room temperature to 140°C, (B) soaked at 140°C for 15 h, and (C) cooled to 110°C.

145°C (curve A) and was then held for 15 h (curve B). During this hold time, the SHG signal decreased to zero, and did not reappear until the crystal was cooled below T_c (curve C).

The occurrence of an SHG signal above T_c indicates that the paraelectric phase contains some degree of acentricity, but the decrease of the SHG intensity above T_c indicates a decrease in the acentric nature of the structure with increasing temperature. The fact that the thermal hysteresis of the SHG intensity above T_c is both time and temperature dependent, suggests that the acentricity in the paraelectric phase is metastable. This metastable acentric structure slowly changes to a more thermodynamically stable centrosymmetric structure by annealing at temperatures above 140°C.

3.2. $BaTiO_3$ single-crystal fibers

Similar heating and cooling experiments were completed on $BaTiO_3$ single-crystal fibers and these are shown in fig. 3. The fibers were first heated to 150°C. At $T_c = 135$°C a sharp drop in the SHG intensity occurs and then the intensity decreases steadily but more slowly with increasing temperature. No change in the SHG intensity was observed after holding the fibers at 150°C for 15 h during heating.

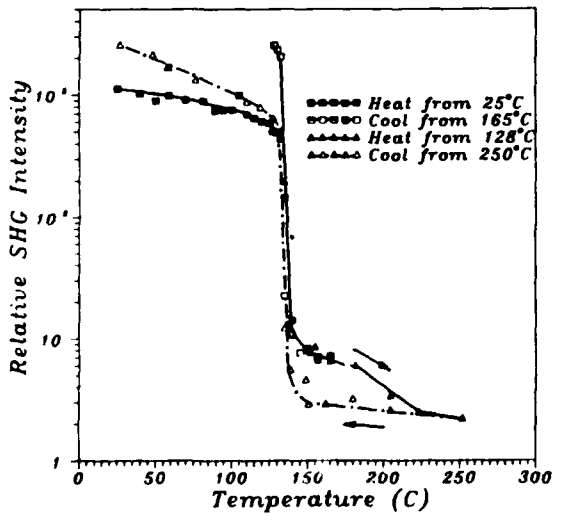

Fig. 3. Relative SHG intensity versus temperature for a multidomain single-crystal fiber of $BaTiO_3$.

The fibers were then further heated to 165°C and subsequently cooled below T_c to 128°C where the SHG signal showed an increase over that which was measured on heating; this difference in the SHG signal below T_c, upon cycling, may be due to changes in the multidomain structure of the crystal. Little or no hysteresis in the SHG intensity was observed between the first heating and the cooling run. On heating from 128 to 250°C, the SHG intensity above T_c decreased slowly but was always distinctly larger than the background noise. On cooling from 250°C the intensity remained constant until below 150°C where a slow increase is observed to the transition at 133°C. A 15 h hold at 150°C on cooling showed no decrease in the intensity.

A temperature hysteresis of the SHG intensity is clearly observed in the fibers but the temperature at which the SHG signal becomes zero could not be determined since the hot stage on the analyzer could only reach 250°C. Extrapolation shows that if the SHG intensity continues to decrease at the same rate, the SHG signal would not dissipate until the temperature is above 400°C. The temperature hysteresis above T_c in fig. 3 is analogous to the first heating–cooling curve in fig. 2 for the flux-grown platelet. A wider temperature range is needed to observe the complete hysteresis effect in the higher-purity crystal fibers.

3.3. $BaTiO_3$ powder

Heating and cooling curves for $BaTiO_3$ powder are shown in fig. 4. The decrease in the SHG signal at the transition is not nearly as sharp as that observed in the single-crystal platelet and fibers. It is interesting to note that even though the SHG intensity for the powder at room temperature is equal to the intensity for the flux-grown crystal and smaller than the intensity for the single-crystal fibers, the SHG intensity for the powder is comparatively larger above $T_c = 130$°C. The intensity above T_c also decreases more rapidly but is still as large as that measured for the single-crystal fibers at 250°C. From the change in the SHG signal with temperature, it appears that temperatures in excess of 350°C would be needed to obtain a zero SHG intensity. A hysteresis occurs above T_c but the SHG signal does increase with decreasing temperature.

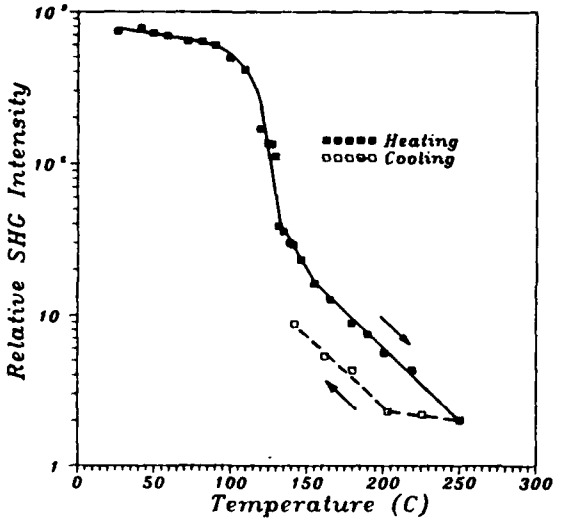

Fig. 4. Relative SHG intensity as a function of temperature for high-purity $BaTiO_3$ powder with an average particle size of 0.5 μm.

All three sources of $BaTiO_3$ exhibit a hysteresis in the SHG signal above T_c indicating that there is residual metastable acentricity which is both temperature and time dependent. The time and temperature dependence of the SHG signal appears to be highly dependent upon the purity of the $BaTiO_3$ since the high-purity single-crystal fibers and powder exhibited significant SHG signals at 250°C and because the SHG intensity for the single-crystal fibers did not decrease after annealing at 150°C.

There may also be a crystal (i.e. particle) size dependency of the SHG signal above T_c since the powder exhibited significantly higher SHG intensities than the single crystals. Such a size dependence may also be manifested in the difference between the hysteresis behavior of the powder, which showed partial recovery of the SHG intensity on cooling, and that of the single crystals, which showed no recovery on cooling. A sharper decline in the SHG intensity at T_c for the single crystals also seems to suggest that particle size, or boundary conditions in general, may affect the SHG intensity above T_c.

4. Conclusions

Any theory that attempts to explain the occurrence of SHG above T_c in $BaTiO_3$ must be able to answer several questions. How can an acentric structure that produces an SHG signal occur in a paraelectric globally non-centrosymmetric phase? Also, why is there a thermal hysteresis in the SHG signal? Such a theory must also explain why the source for acentricity is influenced by the presence of substitutional defects (impurities), since the lower-purity flux-grown crystal exhibited an additional time dependence of the SHG intensity above T_c. The influence of substitutional defects is also reflected in the temperature at which the SHG signal disappeared – 220°C for the flux-grown crystal, greater than 400°C for the high-purity single-crystal fibers, and greater than 350°C for the powder. Since the SHG hysteresis in the powder differs qualitatively from the SHG hysteresis observed in the single crystals, the source of acentricity must also be affected either through an intrinsic particle-size effect or by the nature of the crystallite surfaces of the powders. It is not yet possible to say which powder characteristic influences the SHG signal.

A theory based upon the occurrence of intrinsic dynamic micropolar regions can account for an acentric structure which produces an SHG signal above T_c, but in this theory the reason for the occurrence of thermal hysteresis in the SHG intensity above T_c is not immediately evident. All the observations in this work can be explained with a lattice-defect model in which residual polar regions above T_c occur due to defects with dipolar character or inhomogeneities of the lattice-defect structure. But in order to confirm this type of defect model, further evidence must be found to substantiate the occurrence of defect-induced polar regions above T_c.

Acknowledgement

The authors are grateful to Philips Laboratories for lending us the SHG analyser needed to complete this work. We also would like to thank Hewlett-Packard Corporation for providing the 54111D digitizing oscilloscope and Dr. Robert E. Newnham who lent us the $BaTiO_3$ flux-grown crystal. Dr. Clive Randall and Dr. Joe Dougherty also provided much helpful discussion.

References

[1] W. Vogt, Appl. Phys. 5 (1974) 85.
[2] S.K. Kurtz and T.T. Perry, J. Appl. Phys. 39 (1968) 3798.
[3] R.C. Miller, Phys. Rev. A 134 (1964) 1313.
[4] J.P. Dougherty and S.K. Kurtz, J. Appl. Cryst. 9 (1976) 145.
[5] V.S. Gorelik, O.P. Maksimov, G.G. Mitin and M.M. Sushchinskii, Soviet Phys. Solid State 15 (1973) 1133.
[6] G.V. Liberts and V.Ya. Fritsberg, Phys. Stat. Sol. a 67 (1981) K81.
[7] S.K. Kurtz and J.P. Dougherty, in: Systematic materials analysis, eds. J.H Richardson and R.V. Peterson (Academic Press, New York, 1978).
[8] M.A. Saifi, B. Duboid, E.M. Vogel and F.A. Thiel, J. Mater. Res. 1 (1986) 452.

PREPARATIVE STUDIES

APPENDIX 39

THE INFLUENCE OF PROCESSING ON DIELECTRIC PROPERTIES OF PMN:PT BASED CERAMICS

A.D. Hilton,[+] C.A. Randall,[*] D.J. Barber,[+] and T.R. Shrout[*]

[+]Department of Physics, University of Essex, Colchester, U.K.
[*]Materials Research Laboratory, Pennsylvania State University, University Park, PA 16802, USA

Key Words: Processing, Ferroelectric, Relaxor, TEM, PMN, Dielectric.

ABSTRACT

This paper addresses many of the variables which can occur in processing relaxor ferroelectric $Pb(Mg_{1/3}Nb_{2/3})O_3$-based ceramics. Processing variables of powder purity, batching composition, annealing, and average ceramic grain size were examined for to the solid solution $0.93\ Pb(Mg_{1/3}Nb_{2/3})O_3{:}0.07Pb(Ti)O_3$ and a detailed characterization of dielectric and micro/nanostructure properties is desired. The effect of each variables was discussed using traditional dielectric mixing laws (extrinsic effects) and by the recent underlying of the relaxor mechanism (intrinsic effects). This paper was intended to clarify the particular interactions between the intrinsic and extrinsic contributions to the dielectric behavior of a PMN ceramic. A modified brick wall model for dielectric mixing in ceramics is used to extrapolate information such as the single crystal values of dielectric maximum, K_{max}, the diffuseness coefficient δ and the average intergranular phase thickness ~ 1.8 nm. This calculated intergranular thickness agrees well with TEM observations.

INTRODUCTION

Complex lead based perovskites, with general formula $Pb(B_1B_2)O_3$, exhibiting diffuse frequency dependent dielectric transitions are commonly referred to as relaxor ferroelectrics. A typical example of the complex lead perovskite family is the $Pb(Mg_{1/3}Nb_{2/3})O_3$ compound. The underlying (size of the) mechanism(s) associated with relaxor dielectric behavior have been predicted to be on a scale of ~ 100 Å well below the size of polycrystalline ceramic microstructure but despite this there is evidence for microstructural variations in properties.[1,2,3]

Relaxor compositions in the (1-x) $Pb(Mg_{1/3}Nb_{2/3})O_3$-x$PbTiO_3$ (PMN:PT) solid solution system with x ~ 0.07 exhibit high dielectric constants over a broad range near room temperature making them attractive for applications such as MLC's (multilayer capacitors) and electrostrictive strain actuators.[4,5] The introduction of PMN-based ceramics for such commercial applications, however, has been a slow process owing to the poor reproducibility during fabrication and subsequent variations in their dielectric behavior. The aim of this paper is to relate to the readers some of the complexities of these PMN-based materials and to point out dielectric-structure inter-relationships with processing variables.

Background on Processing Variables in the PMN-Based Ceramics

The formation of perovskite PMN is a complex process, and as such leads to variations n subsequent properties in dielectric constant, dielectric aging, etc. PMN polycrystalline ceramics prepared by conventional mixed oxide routes typically result in large volume fractions (up to 30%) of a parasitic lead niobate pyrochlore phase ($Pb_3Nb_4O_{13}$). The generalized reaction sequence for conventionally processed PMN is summarized in equation (1).

$$3PbO + 2Nb_2O_5 \xrightarrow{530\text{ - }600\ ^\circ C} Pb_3Nb_4O_9 \qquad \text{(1a)}$$

exo (anion deficient cubic pyrochlore)

$$Pb_3Nb_4O_9 + PbO \xrightarrow{600\text{ - }700\ ^\circ C} 2\,Pb_2Nb_2O_7 \qquad \text{(1b)}$$

exo (rhombohedral pyrochlore)

$$Pb_2Nb_2O_7 + \frac{1}{3}MgO \xrightarrow{700\text{ - }800\ ^\circ C} Pb\left(Mg_{\frac{1}{3}}Nb_{\frac{2}{3}}\right)O_3 + \frac{1}{3}Pb_3Nb_4O_{13} \qquad \text{(1c)}$$

endo (perovskite)

These equations as first suggested by Inada demonstrated the conventional processing with mixed oxides formed intermediate pyrochlore phases before perovskite PMN was formed.[6] The first reaction (1a) is between PbO and Nb_2O_5 and forms cubic pyrochlore $Pb_3Nb_4O_{13}$. This cubic pyrochlore reacts with lead oxide to form a rhombohedral pyrochlore. This rhombohedral pyrochlore final reacts with MgO to form perovskite PMN and cubic pyrochlore as shown in equation (1c). Inada concluded higher yields of PMN could be obtained by controlling the PbO loss.

LeJeune and Boilot report three types of intermediate pyrochlore phase $Pb_3Nb_4O_{13}$, $Pb_2Nb_2O_7$, and also $Pb_3Nb_2O_8$.[7] This third pyrochlore is included to reaction sequence such that

$$\underset{\text{(pyrochlore)}}{Pb_2Nb_2O_7} + PbO \rightarrow \underset{\text{(pyrochlore)}}{Pb_3Nb_2O_8} + \underset{\text{(cubic pyrochlore)}}{Pb_3Nb_4O_{13}} \qquad (2)$$

$$Pb_3Nb_2O_8 \xrightarrow{830\ ^\circ C} liquid + MgO \rightarrow PMN + Pb_3Nb_4O_{13}.$$

The cubic pyrochlore is the stable form. Swartz and Shrout found only the cubic pyrochlore to be present in the study of the PMN formation.[8] This cubic pyrochlore had Mg substituted into the structure to give an approximate formulation $Pb_{1.83}Nb_{1.71}Mg_{0.29}O_{6.39}$. They found that this cubic pyrochlore reacted with PbO and MgO to form PMN as expressed in equation (3).

$$MgO + Pb_3Nb_4O_{13} + PbO \rightarrow PMN + Pb_3Nb_4O_{13} \qquad (3)$$

The presence of non-ferroelectric phases of $Pb_3Nb_4O_{13}$, MgO, PbO, and Nb_2O_5 result in large variations in the dielectric properties of the PMN ceramics. These variations in dielectric constant have been rationalized by on dielectric mixing. The relative amounts of phase(s) are determined semi-quantitatively by x-ray powder diffraction.

It was found that the pyrochlore formation could be somewhat suppressed with compositional modifications of excess PbO and MgO however, large variations in reported dielectric behavior still were observed.[9,10,11]

The introduction of the B-site precursor method overcame much of the reproducibility problems. Phase pure perovskite PMN ceramics were produced with corresponding dielectric properties close to those of single crystals. The precursor method pre-reacts the refractory B-site

components MgO and Nb_2O_5 to form $MgNb_2O_6$ columbite as shown as shown in equation (4a). Then a second reaction is made between the columbite and the PbO as shown in (4b).

$$MgO + Nb_2O_5 \rightarrow \underset{\text{(columbite)}}{MgNb_2O_6} \qquad (4a)$$

$$3PbO + MgNb_2O_6 \rightarrow 3Pb\left(Mg_{\frac{1}{3}}Nb_{\frac{2}{3}}\right)O_3 + \text{small amounts of pyrochlore} \qquad (4b)$$

(perovskite)

The success of this precursor method is mainly associated with an atomic dispersion of the MgO and Nb_2O_5 components. Minor additions of PbO and MgO in the batching further reduced the pyrochlore formation and enhanced densification. However, these additions of excess PbO and MgO, however, imbalances the stoichiometry of the whole PMN ceramic. This in turn leads to changes of dielectric properties from that of stoichiometric PMN.

With the production of phase pure perovskite PMN ceramics it became a natural extension to study microstructure affects on the dielectric properties. Transmission electron microscopy (TEM) work of Goo et al. reported small pyrochlore grains in boundary regions outside the detection limit of x-ray diffraction (< 2%).[12] Gorton et al. also inferred the importance of glassy grain boundary phase effects on the dielectric properties.[13] It was suggested that isolated pyrochlore phases would not significantly dilute the magnitude of the dielectric constant—hence other mechanisms must account for differences in dielectric properties.

Through a better understanding of the surface chemistry and dissolution of the component powders, and the use of high energy mixing/milling, stoichiometric phase pure (as determined by x-ray powder diffraction) perovskite PMN powder could be produced as low as 650°C.[14] Although phase pure powders are PMN are readily formed, densification of powder compacts requires atmosphere control to compensate for PbO volatility and to ensure densification.[15] This is generally accomplished through the additions of excess PbO to the calcined powders or by using a PbO source powder, e.g., $PbZrO_3$. Excess PbO has two major effects on the dielectric properties of the PMN ceramics. First is the lowering of the dielectric constant as the volume fraction of low dielectric constant material is increased. Second, is the dielectric constant varies with time, a process known as aging.

In summary, although optimum processing is performed on PMN:PT ceramics microstructural dependences are still observed. Scanning electron microscopy (SEM) and x-ray cannot explain these intrinsic and extrinsic effects. The purpose of this work was to characterize

features on the scale associated with relaxor behavior itself, i.e., on the nanometer scale with conventional TEM techniques.

Background on the Relaxor Ferroelectric

Since the early 1950's, work has been going on trying to understand the polarization mechanisms in relaxor materials. Smolenskii stated a model based on chemical inhomogeneities giving rise to a distribution of paraelectric to ferroelectric phase transitions thus resulting in diffuse phase transitions.(1) Later work by Cross(2) laid the ground work of a new understanding, he suggested the possibility of a system made up of an ensemble of superparaelectric polar regions and the relaxor nature was the result of thermal agitations upon these regions. Recently, a link was found between the nanostructural chemical B-site ordering and relaxor behavior in complex lead perovskites. It was hypothesized that the ordered domains localized the superparaelectric regions.(3) Work by Viehland et al., has found theoretical fits with a dipolar-glass models; inferring that interaction between the superparaelectric regions enhances the dielectric constant and also accounts for its broad dispersive response.(16)

This brief background gives the reader an up-to-date list of references which are the modern basis for understanding the relaxor behavior. The relevant parts of the theories used to explain processing effects on properties are discussed in more detail in the text below.

EXPERIMENTAL PROCEDURE

Polycrystalline ceramic disks with the relaxor composition 0.93 PMN-0.07 PT were prepared via the B-site precursor method. In processing the columbite precursor, the poor dispersion characteristics associated with MgO powders was addressed using both steric hinderance (polyelectrolyte dispersant)+ and electrostatic repulsion (pH adjustment by ammonia) in conjunction with high energy milling.++ Upon calcination the appropriate amount of PbO was added followed by a mixing in a dispersant adjusted to obtain minimum lead dissolution. A perovskite calcination is made at 700°C for 4 hrs. Both the columbite $Mg_{.93}Nb_{1.86}Ti_{.21}O_6$ and perovskite 0.93 PMN-.07 PT calcined powders were examined by x-ray powder diffraction to insure phase purity. Uniformity and reactivity of the PMN-PT powder was further enhanced by milling as above. Additional details of the processing methods used are reported elsewhere.(15)

Samples prepared for this study were engineered with variations in powder purity, powder composition (excess PbO), grain size, and annealing conditions. In terms of purity, both reagent grade (~ 99%) and high purity (≥ 99.99%) component powders were used to prepare samples.

+Tamol-901, Rohm and Haas (note: no impurities).

++Vibratory Mill.

The utmost care was taken to prevent contamination during processing of the high purity material, consequently, high energy milling was not performed. The lower reactive powder did not permit densification at temperatures ~ 1200°C resulting in a large grain size microstructure. Grain size variations in the reagent grade material were achieved by firing samples at different temperatures as reported in the reference.[15] Significant grain growth through longer firing times was found not to be effective. Previously reported grain growth behavior with firing time was probably associated with inadequately processed materials (phase impure) and/or materials containing additions of excess PbO and MgO powder along with excessive PbO atmosphere control during sintering. PbO additions used in this study for both reagent and high purity samples were to engineer grain boundary regions and promote dielectric aging.[17]

Along with grain boundary modifications using excess PbO, samples were annealed up to 7 days at a temperature ~ 950°C well below the firing temperature to disallow grain growth. PbO volatility during annealing and sintering was controlled using a coarse sand of the same composition in which the samples were buried. A non-PbO atmospheric source zirconate based sand ($BaZrO_3$) was also used for low temperature firings (< 1100°C) to attempt to modify PbO weight loss in the grain boundaries. Atmosphere control for the high purity samples was achieved using $PbZrO_3$ powder placed in platinum boats around the samples. All firings were performed in closed high density alumina crucibles.

Fired samples were characterized for weight loss, geometric density, and grain size as determined on fracture surface using scanning electron microscopy (SEM).

The dielectric measurements were carried out on an automated Hewlett-Packard system (as described in the reference.[15] The dielectric constant and loss were measured pseudo-continuously for each sample at various frequencies (100 Hz, 1 KHz, 10 Kz, 100 KHz) as the samples were cooled from +150°C to -150°C at a cooling rate of 4°C/min. Dielectric aging studies typically extend to over 1000 hrs. To facilitate evaluation of a large number of samples, "relative" percent aging values were determined from capacitance readings taken at 24 hrs and on de-aged specimens.[17]

Transmission electron microscopy (TEM) characterization was performed on samples with selected engineered variations. Slices were cut from fired disks using a diamond saw followed by grinding to a thickness of ~ 30 μm using silicon carbide. A copper support grid was glued onto the surface of each polished specimen using epoxy resin. Electron transparent regions were obtained by atom-beam milling the samples with an Ion Tech argon beam thinner operating at an accelerating voltage of 5 kV and at an incidence angle of 15-30 degrees. Finished TEM specimens were coated with a thin layer of carbon in order to prevent them from charging within the electron microscope. TEM observations were made with a JEOL-200CX microscope and a Philips 420 STEM both equipped with a LINK systems energy dispersive x-ray spectrometer (EDS).

Grain boundaries were examined in the bright field (BF) TEM imaging mode using a phase contrast technique (as described in refs. (18 and 19)). The technique being performed by forming a conventional BF image of a grain boundary, defocussing the illumination (to form a parallel incident beam) and recording a series of micrographs encompassing both overfocus and underfocus conditions of the objective lens. In this technique the presence of a second phase at the grain boundary results in a pair of dark or bright lines (which are in fact a pair of Fresnel fringes) delineating the boundary. If no boundary film is present, micrographs simply appear out-of-focus. The essential condition for this technique is that the boundary is "edge on" relative to the direction of the incident electron beam. In this case an estimate of the brain boundary thickness can also be made. Grain boundaries were also examined by a high resolution lattice fringe imaging technique.

As previously noted, the complex lead-based relaxors possess a B-site cation ordering. This ordering corresponds to an F-centered $2a_o \times 2a_o \times 2a_o$ superstructure on the B-site sublattice.[3,20,21,22] The B-site ordering gives rise to superlattice reflections of the type $(h + 1/2, k + 1/2, l + 1/2)$. Dark field imaging of these superlattice reflections reveal order domains ~ 10 nm.

Physical and Dielectric Properties

The general characteristics of PMN:PT samples as a function of thermal history are summarized in Table I. All the samples possessed densities greater than 95% theoretical (8.11 g/cm^3). The weight loss during sintering was confined to the range of 0.5-1.5 wt% with slightly higher losses occuring in samples processed at higher temperatures. The annealed samples and samples fired in $BaZrO_3$ sand showed only marginal differences in weight loss. Both reagent grade and high purity samples that contained excess PbO lost approximately 0.5 wt% more than was added. It should be mentioned that the x-ray analysis of PMN ceramic samples were phase pure with no evidence of pyrochlore or PbO phases.

For all PMN-based ceramics studied the K_{max} values are relatively high and this is believed to be owing to the overall care in processing. There is a consistent influence of powder purity on the dielectric constant K_{max} ~ 28,000 compared to K_{max} ~ 24,500, given similar thermal process conditions for high purity and reagent grade respectively and are shown in Fig. 1. This shows both a lower dielectric maximum and a shift of T_{max} for the reagent grade powder processed.

A wider range of grain sizes were achieved through intermediate firing temperatures, but for simplicity only a few from the extremes were selected for detailed structural characterization. Physical and dielectric properties for a wider range of grain sizes can be found in ref. (15). Lack of large grain sizes (> 10 μm), in this and related work, is attributed to the fine and uniform stoichiometric starting powders and PbO control making them less susceptible to abnormal grain growth.

The magnitude of dielectric constant K_{max} versus grain size (G.S.) is presented in Table I, and shown in Fig. 2 (from ref. 15). Clearly, the value of K_{max} increases with increasing grain

size. In addition, further thermal annealing resulted in a dramatic increase in K, without grain growth or significant difference in weight loss or shifts in T_{max} for grain sizes > 1.0 μm.

Dielectric aging characteristics of the ceramic samples were also studied. It was found that the aging rate of stoichiometry prepared samples were generally low with no detectable aging found in the high purity samples in agreement with other reports.[23] However, samples prepared with excess PbO, though driven-off through volatility during sintering, still exhibited the highest degree of aging even for the high purity samples, see Fig. 3.

In summarizing, processing parameters which affecting the dielectric properties are grain size, powder purity, annealing, and non-stoichiometric batching.

Micro/Nanostructural Characterization

Grain boundaries examined in samples prepared in this study using both the bright-field (BF) TEM under-focus/one-focus fresnel fringe technique and the high resolution lattice imaging revealed the existence of grain boundary phase in all the materials characterized in this study. A typical high resolution image of the grain boundary phase in the course grain reagent grade sample is illustrated in Fig. 4a and b. As shown {100} planes (0.407 nm) have been imaged in adjacent edge-on grains clearly showing a discontinuity between the two sets of lattice planes. Thicknesses of these intergranular glassy phases were found to be approximately ~ 2 ± 1 nm with little measurable variation in thickness either along lengths of individual boundaries or throughout each sample or between samples including those with the excess PbO additions. A direct chemical analysis of the grain boundary phase could not be obtained owing to the small scale of the boundaries. However, the phase is most likely Pb-rich owing to the low melting point of this constituent and the recent SIMS study (secondary ion mass spectroscopy) by Wang and Schulze.[24] These PbO-glassy phases are the residual of a fugitive sintering mechanism not well understood at this time.

Although no apparent differences in grain boundaries were observed, compositional and phase variations were found at grain boundary triple points. Second phases were found at all triple points in the course grained materials prepared from reagent grade powders regardless of firing condition or composition (excess up to 2 wt% PbO). A representative example of triple junction phase is shown in Fig. 5. The EDS analysis revealed that the second phase was rich in lead and other impurity elements such as Al, Si, P, and S as shown in Fig. 6a. Similar findings to the observations made by Gorton et al.[13] Diffraction analysis, Fig. 6b, of the lead oxide phase(s) could not be indexed to any known lead-oxide phase. The diffuse concentric rings on which diffracted spots are superimposed implying that fine crystalline phases ~ 10-15 nm are present. The "dirty" triple junctions were observed in all the reagent grade fine grain samples. We also draw attention to the rounded grain boundaries at the triple points suggesting that a phase was

liquid during sintering. Interestingly, the triple points examined in the high purity ceramics were "clean," that is free of second phases as illustrated in Fig. 5b.

In addition to second phase(s) at triple points, various intragranular phases were observed, though x-ray powder diffraction indicated phase pure samples. Figure 7a illustrates an example of an intragranular particle found in a high purity sample. The phase was identified from electron diffraction patterns as MgO, <100> zone axis patterns and EDS analysis shown in Figs. 7b and c. In the reagent grade PMN ceramics intragranular phases of rich in Mg and Si were grown, Mg_2SiO_4 has been identified from electron diffraction patterns. The Mg_2SiO_4 is believed to be produced during the pre-calcination of the $Mg_{0.93}Nb_{1.86}Ti_{0.21}O_6$ powder where SiO_2 is an impurity. The size and morphology of the MgO-rich phases were irregular and randomly distributed, making any quantitative assessment of the volume fraction difficult. These MgO-rich phases are related to dispersion problems of MgO in forming columbite phase.

In addition to the observed intragranular and intergranular microstructural features of nanostructural features of the PMN grains were also examined. As well documented, there exists non-stoichiometric B-site cation order domains (~ 10 nm) within the PMN grains.[20,21,22] Comparing the superlattices on electron diffraction patterns and the dark-field images revealed no noticeable differences in size between the various PMN ceramics prepared.

So to reiterate, the presence and absence of the intergranular triple points with reagent grade and high purity powder were the only significant microstructural changes observed with the processing variables. Small nanostructural changes are still believed to occur but too small to be characterized with techniques used here.

DISCUSSION

Rationalizing the complexity of the polarization mechanism of the relaxor ceramic with regard to composition, phases, defect chemistry, in relation to dielectric properties is an extremely difficult problem. Our aim is to outline the trends and plausible explanations.

Let us first discuss the PMN-perovskite grain. The PMN grain is an ensemble of nanoscale polar regions and chemical order domains both on the order of 10 nm. The polar regions may exist up to temperatures ~ 350°C where it is believed the whole grain becomes paraelectric while the ensemble of chemical ordered domains remain. Below this critical temperature the polar regions are thermally active and begin to interact with one another and frustrate each others local equilibrium and is the conceptual basis of a dipolar glass description.[16] The chemical order domains result from the atomic ordering of the Mg and Nb ions. This is further complicated by the belief that ordering growth is self-limited in PMN, i.e., after long heat treatments no noticeable change to the scale of ordering has taken place. The ordering has been

suggested to be non-stoichiometric in nature with an ordering between Mg- and Nb-cations, close to a 1:1 ratio. Of course, these suggestions are made from inferred experimental results and are not totally conclusive. However, such a suggestion can account for the self-limiting of the order size in that there has to be a segregation of Mg- and Nb-rich regions. The Mg-rich ordered regions are believed to be are surrounded by a Nb-rich sea in order to maintain the stoichiometry. This leave us with a fundamental question; how would these regions compensate the charge from such non-stoichiometric ordering? This problem has been partly addressed by a proposed defect chemistry models involving lead and oxygen vacancies and the covalency of the lead cation but as yet no completely satisfying explanation exists.[13,25]

We now consider the more traditional microstructural aspects of the PMN-based ceramic. Here the ceramic is considered as an ensemble of micron-scaled PMN grains with a few other minor phases. The perovskite grains have been observed to be laced with a continuous amorphous intergranular phase—most probably PbO-based. The other intragranular phases observed in this study included Mg-rich grains in the form of MgO in high purity and a Mg_2SiO_4 spinel phase previously as pointed out.

These MgO and PbO phases found in the microstructure and the non-stoichiometric ordering at the nano-level implies a further complexity in the defect chemistry of the PMN ceramic which still have to be solved.

The Processing Parameter Effects on the PMN Ceramic

Powder Purity and Dopants

From the above results and previously published data there is an influence on both dielectric properties and microstructure with powder purity and other dopants.[13]

It is interesting that the only observed microstructural differences are found at the triple points, however, applying simple dielectric mixing laws to these discrete volumes we are unable to account for the difference in dielectric properties. The intergranular grain boundary is observed to be of similar thickness between the high purity and reagent grade powders so the differences in dielectric property are thought to be the result of impurity doping of the PMN:PT grain. As already discussed by Chen et al., donor and acceptor doping have differing effects on the nanoscale ordering in PMN grains.[26] Donor doping with La^{+3} enhances the scale of chemical ordering, whereas acceptor doping with Na^{+1} reduces the scale of ordering. However, in their study tremendous amounts of dopant were used to observe this effect. These results further imply that the ordering in PMN is non-stoichiometric. The important thing to learn from that study is aliovalent doping influences the underlying order domain size.

The above results show the dielectric constant is certainly enhanced with higher purity powders—the impurities being Na, Al, Si, P, and S from EDS and spectrographic analyses. We believe anion substitution is extremely unlikely with P and S, but cation substitution of Al^{+3} and

Na^+ can be expected. The substitution of Si^{+4} is not expected, since Si prefers four-fold coordination and not the octahedra six-fold coordination as present in perovskites. There are examples of Al^{+3} and Na^+ doping in $Pb(Zr,Ti)O_3$ and PMN perovskites, respectively.(27) So, the important impurities in reagent grade powder are the Al^{+3} and Na^+ acceptor doping the B-site and A-site. The acceptor doping then would decrease the size of non-stoichiometric order domains of PMN.

To quantitatively account for changes in the dielectric constant and changes in the ordering is beyond the present theory. However, we are able to demonstrate the sensitivity of an individual superparaelectric region with small changes in size. Assuming the order domains localize the superparaelectric regions as hypothesized earlier, then a change in the order domain size also changes the size of the superparaelectric region.(28) This in turn effects the flipping frequency, ω, of the polarization in the superparaelectric region as the flipping frequency is related by the simple expression:

$$\omega = \omega_D \exp - \frac{H}{K_B T} \qquad (5)$$

where ω_D = Debye frequency ~ 10^{12} Hz,

H = height of energy barrier and is directly related to volume of the superparaelectric region, and

K_BT ~ the thermal energy.

Then for the same thermal energy, K_BT, we can compare the flipping frequency in two ordered regions of differing diameters, d_1 and d_2. For just a 10% decrease (i.e., 2 unit cells in a 10 nm region) changes the flipping frequency from 10^4 to 10^6 Hz can be predicted using equation (5). In the case of acceptor doping there is an increase in the number of small high frequency regions relative to pure PMN so a change in the distribution of superparaelectric regions is expected wh may account for the observed decrease in K_{max} and shift of T_{max}.

Non-Stoichiometric Batching Effects on PMN Ceramics

PMN-based materials batched with excess amounts of the constituent powders have various effects on the dielectric properties, these are discussed below.

Excess PbO

As stated in the introduction, excess PbO has two major effects on the dielectric behavior, one is intrinsic, the other is extrinsic. The intrinsic effect is dielectric aging and the extrinsic effect is owing to the series mixing of a continuous low dielectric PbO-based phase lowering the dielectric constant of the ceramic.

Accounting for the dielectric aging with the addition of excess PbO is a difficult problem. Traditionally, we expect aging to be induced when aliovalent cations are substituted into the crystal structure inducing defect dipoles.[17,29] These defect dipoles then align with the ferroelectric spontaneous polarization and locally breaks the degeneracy between other possible polar orientations. The ferroelectric polarization then prefers this lower energy orientation over the other orientations, the polarization becomes "aged" into this direction with time and locally becomes less polarizable. For an understanding of the aging with excess PbO we turn to a defect chemistry hypothesis below.[17]

For a constant lead activity, the formation of doubly ionized oxygen vacancies V_O can be represented by the reaction:

$$O_O^x \leftrightarrow \frac{1}{2}O_2 + V_O^{\cdot\cdot} + 2e' \tag{6}$$

$$K_{V_O^{\cdot\cdot}} = n^2[V_O^{\cdot\cdot}]PO_2^{\frac{1}{2}}.$$

for a low oxygen partial pressure, PO_2. If the PO_2 is high, then the formation of V_{Pb} can be expressed as:

$$\frac{1}{2}O_2 \rightarrow O_O^x + V_{Pb}'' + 2h^{\cdot} \tag{7}$$

$$\therefore K_{V_{Pb}''} = p[V_{Pb}''][PO_2]^{-\frac{1}{2}}.$$

For the other extreme of PO_2 constant, then

$$Pb(g) \rightarrow Pb_{Pb}^x + V_O^{\cdot\cdot} + 2e' \tag{6}$$

$$K_{V_O^{\cdot\cdot}} = n^2[V_O^{\cdot\cdot}]a_{Pb}^{-1}.$$

where there is high lead activity, a_{Pb}. In the case of low lead activity

$$Pb_{Pb}^{x} \rightarrow Pb(g)\uparrow + V_{Pb}'' + 2h^{\cdot} \qquad (7)$$

$$K_{V_{Pb}''} = p^2[V_{Pb}''] a_{Pb}$$

a_{Pb} will be directly related to the lead partial pressure, Pb_{Pb}, assuming a volatile species of Pb.

The relative concentrations of these defects will be dependent on T, PO_2, and Pb_{Pb}, although the predominant defect at any specific thermodynamic condition has still to be determined experimentally. Regardless, with an increase of excess PbO in batching we suggest an increase in the a_{Pb} and this has an opposite effect on eqs. (6) and (7). Thus inducing an imbalance between the $[V_{Pb}'']$ and $[V_O^{\cdot\cdot}]$ and creating defect dipoles which could promote the aging process.

The extrinsic influence of excess PbO is to increase the volume fraction of low dielectric constant material at the grain boundaries and thus lowering the total dielectric constant. A more detailed discussion on this effect will be discussed with grain size and intergranular phases together below.

Excess MgO

In the early 1980's, MgO was added as a means of controlling the pyrochlore formation as observed in the introduction. The dominant effect of MgO to well-prepared PMN ceramics is the induction of aging, Fig. 8.[17] The aging suggests an intrinsic influence of the MgO related to the defect chemistry. It may be possible to substitute Mg on the A-site in small amounts making PbO excess. The above arguments for PbO excess would then apply. There is no direct evidence for Mg occupying the 12-coordinated A-site; but higher weight losses during sintering with MgO excess and also the presence of aging both give this possibility. Another, and more feasible possibility is the excess substitution of Mg on the B-site, thus perturbing the overall 1:2 ratio of Mg and Nb cation and effectively acting as an acceptor dopant. More detailed aging rate studies are needed to substantiate the differences in the aging between excess PbO and excess MgO.

Excess Nb_2O_5

Excess Nb_2O_5 promotes pyrochlore formation and changes in the dielectric constant appears to be predominantly extrinsic owing to dilute of the perovskite dielectric constant. Chen et al., found the reduced dielectric constant in such ceramics obeyed simple dielectric mixing laws.[30] For low volume fractions of pyrochlore phase in PMN and also for converse case of low volume fraction of PMN in pyrochlore the dielectric mixing laws suggested by Weiner showed a good fit. For intermediate amounts of pyrochlore in PMN a close fit with logarithmic rules was formed. Aging effects of Nb_2O_5 additions were not discussed by Chen.[30]

Grain Size Dependence

The origin of the grain size dependence in the PMN-based relaxors is an important question. The extrinsic contribution from the continuous intergranular glassy phase reduces the dielectric constant by dielectric mixing. From our TEM studies it is clear that despite changing powder-purity, sintering temperature, and annealing and controlling lead dissolution a remanent glassy intergranular phase is always present in the ceramics produced here. This PbO glassy phase is $\sim 2 \pm 1$ nm in thickness in these well-prepared materials. There may be slight variations in the thickness of this grain boundary phase owing to the different crystallographic orientations between adjacent grains, but no evidence of inhomogeneous distributions in grain boundary phase on the scale's observed in modified PZT.[31]

In modeling the dielectric mixing between grain and intergranular phase one has to use the most appropriate mixing rule. A generalized expression for a multiphasic dielectric is:

$$R^n = \sum_i V_i k_i^n \qquad (8)$$

Diphasic mixing reduces the expansion to two terms i = 1 and 2 for the respective dielectric phases, V_i is the volume fraction and K_i is the dielectric constant.

For the case where n = + 1 we obtain $K = V_1K_1 + V_2K_2$ which corresponds to parallel dielectric mixing.

For the case n = - 1 we obtain the expression

$$\frac{1}{R} = \frac{V_1}{K_1} + \frac{V_2}{K_2} \qquad (9)$$

which corresponds to the series mixing. The case n = o corresponds to the empirical logarithmic law:

$$\log R = V_1 \log K_1 + V_2 \log K_2. \qquad (10)$$

Although, in general the microstructure is a mixture of parallel and series intergranular boundaries, it is the series boundaries which dominate the magnitude of the dielectric constant. The overall dielectric behavior for cases where the matrix dielectric constant $K_1 >> K_2$ the intergranular phase dielectric constant and the volume fractions of each phase are such that

$V_1 >> V_2$, the so-called brick-wall approximation applies. This reduces the series law to include the volume fraction of series grain boundary phase only.[34]

$$\frac{1}{K} = \frac{V_1}{K_1} + \frac{V_2}{3K_2}. \tag{11}$$

With PMN:PT based ceramics the PMN-grains have extremely high dielectric constants ≥ 20,000 compared to an intergranular lead glass phase assumed $K_2 \sim 20$.[32] Also, the volume fraction of the intergranular phase is small compared to the grain, as the thickness, t_{gb}, of the grain boundary phase is very small compared to the grain size t_{gb} a modification to the brick-wall model can be made such that:

$$\frac{1}{K} = \frac{1}{K^g} + \frac{1}{R.\,K^{g.b}} \quad and \quad R = \frac{t_g}{t_{g.b}} \tag{12}$$

where: K^g = dielectric constant of the grain

$K_{g.b}$ = dielectric constant of grain boundary and R is the thickness ratio between grain size, t_g and grain boundary thickness, $t_{g.b}$

Now the argument to distinguish between an extrinsic PbO layer or an intrinsic change to the relaxor grain to account for grain size dependence goes as follows. If the grain size dependence is solely controlled by changing R, the thickness ratio, the grain boundary contribution to dielectric constant $K^{g.b}$ is temperature independent (for temperatures in the range studied here). So the only temperature dependence for the ceramic dielectric constant, K, comes from the grains themselves, K^g. The dielectric temperature dependence of the grains would be expected to be identical to the single crystals K^{cryst} and so it follows:

$$K^g = K^{cryst} \tag{13}$$

But,

$$\frac{1}{K^{cryst}} = \frac{1}{K^{cryst}_{max}} + \frac{\left(T - T^{cryst}_{max}\right)^2}{2\delta^2_{cryst} K^{cryst}_{max}} \tag{14}$$

Where: K^{cryst} = dielectric constant of single crystal PMN:PT.,
K^{cryst}_{max} = maximum dielectric constant of single crystal PMN:PT,
T_{max} = temperature at maximum dielectric constant, and
δ_{cryst} = diffuseness coefficient from single crystal PMN.

Combining equations (10), (11), and (12) leads to

$$\frac{1}{R} = \left(\frac{1}{K^{cryst}_{max}} + \frac{1}{R}\frac{1}{K^{g.b}}\right) + \frac{(T - T_{max})^2}{2\delta^2_{cryst} K^{cryst}_{max}} \tag{15}$$

However, it is also possible to represent the inverse dielectric constants temperature dependence of the ceramic as follows:

$$\frac{1}{R} = \frac{1}{R_{max}} + \frac{(T - T_{max})^2}{2\delta^2 R_{max}} \tag{16}$$

where: K_{max} = the maximum dielectric constant of ceramic, and
δ = diffuseness coefficient of ceramics.

Equating the equations (13) and (14) we have

$$\frac{1}{R_{max}} = \frac{1}{K^{cryst}_{max}} + \frac{1}{R} \cdot \frac{1}{K_{g.b}} \tag{17}$$

and

$$\delta^2 R_{max} = \delta^2_{cryst} K^{cryst}_{max} = \text{constant} \tag{18}$$

Equation (18) suggests that $\delta^2 K_{max}$ is a constant for all grain sizes provided the grain size dependence of K is only owing to the change in ratio R of grain size and grain boundary thickness. A plot of $\delta^2 K_{max}$ versus grain size (1/tg) for PMN:PT (0.93/0.07) is shown in Fig. 9. A very weak slope indicates that the extrinsic grain size dependence is not the complete explanation of the phenomenon. However, the slope is very weak in grain sizes > 1.0 μm indicating the extrinsic contribution is dominating. Recent evidence in PMN further indicates an intrinsic effect is also present.[35] Papet et al. showed a shift of the Curie maximum to higher temperatures with smaller grain size and also a dielectric constant K ~ 300 measured from PMN particles ~ 70 nm in a 0-3 composite.

In the grain size range studied here > 1.0 μm as the extrinsic mechanism dominates this allows the application of equation (15), to the grain size dependence of K_{max}. Figure 10 shows the $1/K_{max}$ variation of inverse grain size (1/tg). If this data is fitted to equation (17), the slope is related to $t^{g.b}/K_g$. Then using $K^{g.b}$, ~ 20, typical values for lead glasses.[32] This approach predicts a thickness of the grain boundary phase 1.8 nm which is a good agreement to the TEM measured grain boundary thickness ~ 2.0 ± 1.0 nm. The intercept of Fig. 10 shows a K_{max} ~ 29,000 for single crystal values of PMN:PT (0.07). Using Fig. 9 we can also suggest values of δ ~ 38 for single crystal PMN:PT.

This approach of characterizing K, δ, and $t^{g.b}$ from grain size data is very useful as it can aid the processor to eliminate variations in the grain boundary extrinsic contribution in relaxor ferroelectrics.

Annealing Treatments

Annealing PMN-based samples without grain growth were found to enhance the dielectric constant. The major effect of annealing is the reduction or redistribution of lead oxide grain boundary phase just small reduction in this enhanced the overall dielectric constant. It is possible that a slight intrinsic change to the order domain distribution can also take place and so similar arguments involving an increase in size and the raising of dielectric constant can be applied. The influence and sensitivity of each intrinsic or extrinsic effect is most important depends on the annleaing temperatures. Temperatures below 800°C are more likely to be changing intrinsic effects whereas higher temperatures would be reducing the volume of PbO in the grain boundaries.

SUMMARY AND CONCLUSIONS

Subtle changes in processing procedures can significantly affect dielectric properties of PMN-PT ceramics. Reasons for this is the complexity of interaction between atomic (defect chemistry), nanostructural and microstructural features making up the PMN ceramic as summarized in Fig. 11. In most ceramics the processor is concerned with either the

microstructural or atomic structural levels in engineering the required properties. Although the nanostructural levels gives the relaxor its particular properties, this additional level makes the processing much more difficult than other electronic ceramics. In that small size changes in the nanostructure strongly influences the effect of the intrinsic relaxor behavior.

This paper has demonstrated which processing variables affect the particular structural levels and in turn give rise to which intrinsic or extrinsic changes. Intrinsic changes cover those which influence the relaxor mechanism directly at the atomic and nanostructural levels. Where as extrinsic changes are more related to the microstructural levels influences on the dielectric properties.

With the present knowledge of processing PMN as reviewed in the introduction the major extrinsic influence is the ratio of grain boundary thickness and grain size. A technique was developed which, for grain sizes ≥ 1.0 μm, can use with annealing treatments to eliminate the maximum amount of intergranular phase for a range of grain sizes to obtain the maximum dielectric properties. Grain size dependency in relaxors is believed to be both explained by the extrinsic contribution recent work on PMN implies a second intrinsic mechanism is important to lower particle and grain sizes. This mechanism will become more apparent as PMN thin films are produced but the processing of these thin films will have to be developed in a similar manner to the ceramic processing.

REFERENCES

1. G.A. Smolenskii. *J. Phys. Soc. Jpn.*, 28 (1970), Suppl. 26.
2. L.E. Cross. *Ferroelectrics*, 76 (1987), 241.
3. C.A. Randall, A.S. Bhalla, T.R. Shrout, and L.E. Cross. *Mat. Res. Bull.*, 5, No. 4 (1990), 829.
4. T.R. Shrout and J.P. Dougherty. *Ceram. Trans.*, 8 (1990).
5. K. Uchino, M. Tatsumi, I. Hayashi, and T. Hayashi. *Jap. J. Appl. Phys.*, 24 (1985), 733-735.
6. M. Inada. *Jap. Nat'l. Tech. Rep.*, 27[1] (1977), 95-102.
7. M. Lejune and J.P. Boilot. *Ceram. Int.*, 8[3] (1982), 99-104.
8. S.L. Swartz and T.R. Shrout. *Mat. Res. Bull.*, 18 (1983), 663-667.
9. S.J. Jang. Ph.D. Thesis, Pennsylvania State University (1980).
10. M. Negase. Matsushita Electric Co. Wireless Lab Report, (1968), IDI-6137.
11. S. Swartz and T.R. Shrout. *Mat. Res. Bull.*, 17 (1982), 1245-1250.
12. E. Goo and G. Thomas. *J. Am. Ceram. Soc.*, 69 (1981), C188-C190.

13. A.J. Gorton, J. Chen, H. Chen, D. Smyth, and M.P. Harmer. Proceedings 6th IEEE Int'l. Symp. Appl. Ferroelectrics, (1988), 150-153.
14. P. Papet, J.P. Dougherty, and T.R. Shrout. (Submitted to *Mat. Res. Bull.* (1990)).
15. T.R. Shrout, U. Kumar, M. Megherhi, W. Yang, and S.J. Jang. *Ferroelectrics*, 76 (1989), 474-487.
16. D. Viehland, S.J. Jang, and L.E. Cross. (Submitted to *J. Appl. Phys.* (1990)).
17. T.R. Shrout, W. Huebner, A.D. Hilton, and C.A. Randall. *Ferroelectrics*, 93 (1989), 361.
18. D.R. Clarke. *J. Appl. Phys.*, 49, No. 4 (1978), 2407.
19. O.L. Kvaneek, T.M. Shaw, and G. Thomas. *J. Appl. Phys.*, 50, No. 6 (1979), 4223.
20. H.B. Krause, J.M. Cowley, and J. Wheatley. *Acta Cryst.*, A35 (1979), 1015.
21. J. Chen, A. Gorton, H.M. Chan, and M.P. Harmer. *J. Am. Ceram. Soc.*, 69, No. 12, C303 (1986).
22. A.D. Hilton, C.A. Randall, D.J. Barber, and R.W. Whatmore. Inst. Phys. Conf. Series, No. 90, Chapter 9 (1987), 315.
23. W.Y. Pan, E. Furman, G.O. Dayton, and L.E. Cross. *J. Mat. Sci. Lett.*, 5 (1986), 630.
24. H.C. Wang and W.A. Schulze. *J. Am. Ceram. Soc.*, 73[4] (1990), 825.
25. D.M. Smyth, M.P. Harmer, and P. Peng. Proceedings of the Center for Dielectric Studies Symposium on the Improvement of Multilayer Capacitor Reliability, (1989), 231-240.
26. J. Chen, H.M. Chan, and M.P. Harmer. *J. Am. Ceram. Soc.*, 72[4] (1989), 593.
27. R. Gerson. *J. Appl. Phys.*, 31 (1960), 1615.
28. C.A. Randall and A.S. Bhalla. *Jap. J. Appl. Phys.* 29, No. 2 (1990), 327.
29. W.Y. Pan. *J. Am. Ceram. Soc.*, 71, No. 1 (1988), C17.
30. J. Chen and M.P. Harmer. *J. Am. Ceram. Soc.*, 73[1] (1990), 68.
31. C.A. Randall, D.J. Barber, and R.W. Whatmore. *J. Mat. Sci.*, 21 (1987), 925.
32. W.D. Kingery. Introduction to Ceramics, published by John Wiley and Sons, Inc., pp. 706 (1960).

Figure Captions

Figure 1. Typical difference between dielectric constant (100 Hz) and dielectric loss temperature dependence in PMN:PT (0.93:0.07) made from high purity (H.P.) and reagent grade (R.G.) powder.

Figure 2. Variation of the dielectric constant temperature dependence (100 Hz) with grain size in PMN:PT (0.93:0.07) ceramics.

Figure 3. Typical example of the aged and deaged dielectric behavior as a function of temperature (at 100 Hz, 1 KHz, 10 KHz, and 100 KHz) for course grain (~ 6 μm) high purity but excess PbO ceramic.

Figure 4. a) Lattice image of course grained PMN:PT grains close to a grain boundary, showing a grain boundary phase ~ 2 nm.

b and c) Under-overfocus micrographs of grain boundary phase in PMN:PT ceramics, reversal in contrast implies presence of grain boundary phase (ref. 18).

Figure 5. a) Glassy phase found at triple point in reagent grade PMN:PT ceramic.

b) Clean triple points in high purity PMN:PT ceramics.

Figure 6. a) Triple point in reagent grade PMN:PT ceramic.

b) EDS of triple point in reagent grade PMN:PT ceramic.

c) Electron diffraction pattern reveals some diffraction spots.

Figure 7. a) Rare intergranular phase of MgO in high purity PMN:PT (0.93:0.07) ceramic.

b) <001> diffraction pattern of MgO.

Figure 8. Variation of aging rate with the batch of deficient and excess MgO in PMN:PT (0.93:0.07) ceramics.

Figure 9. Variation of $\delta^2 K_{max}$ and grain size for PMN:PT (0.93:0.07) reagent grade ceramics.

Figure 10. Variation of $1/K_{max}$ and grain size for PMN:PT (0.93:0.07) reagent grade ceramics.

Figure 11. Schematic diagram showing variations and interactions of the structural levels in the PMN:PT ceramic system.

Table I. (from Ref. 15)

Firing Condition	Wt. Loss%	ρ[g/cm^3]	Grain Size	K_{max}	T_{max}°C	δ(°C)
950°C -0.5 hrs	0.5	7.4	1.5 µm	11,500	24	58
-4 hrs	0.7	7.83	2.0 µm	13,000	22.8	50
-48 hrs	0.6	7.88	2.0 µm	20,300	---	39
1050°C -0.5 hrs	0.8	7.88	2.0 µm	12,600	20.6	57
(Zirconate Sand)	(0.97)			(14,800)		(47)
-4 hrs	0.5	7.91	3.0 µm	15,700	20.5	44
-20 hrs	1.1	7.89	3.0 µm	18,800	22.2	43
1150°C -0.5 hrs	0.7	7.87	3.0 µm	13,500	19.7	48
(Zirconate Sand)	(0.87)			(15,100)		(47)
-4 hrs	1.0	7.88	3.0 µm	17,800	---	43
1250°C -0.5 hrs	1.1	7.84	5.0 µm	17,500	---	44
-4 hrs	1.2	7.82	6.5 µm	20,800	18.4	42
-20 hrs	1.45	7.76	9.0 µm	22,800	17.9	39
1300°C -0.5 hrs	1.1	7.82	6.0 µm	21,000	18.7	41

Processing Conditions and General Characteristics of 0.93 PMN:0.07 PT Ceramics.

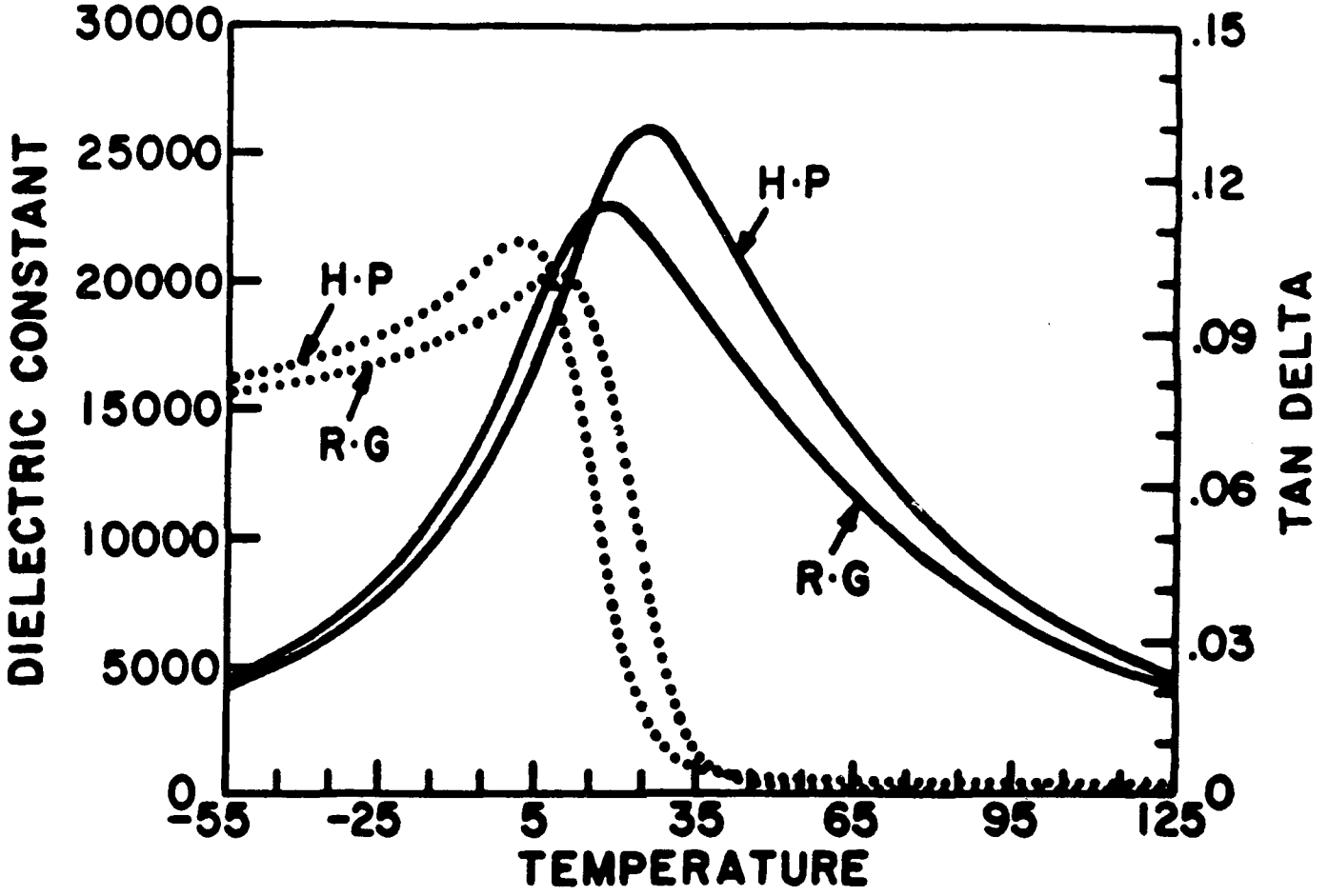

Figure 1. Typical difference between dielectric constant (100 Hz) and dielectric loss temperature dependence in PMN:PT (0.93:0.07) made from high purity (H.P.) and reagent grade (R.G.) powder.

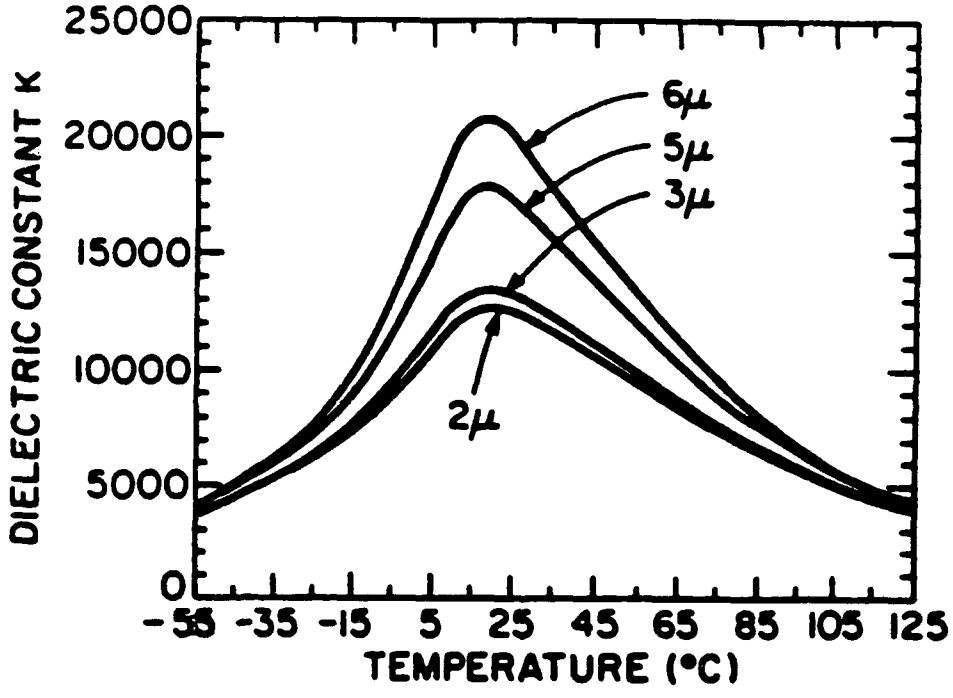

Figure 2. Variation of the dielectric constant temperature dependence (100 Hz) with grain size in PMN:PT (0.93:0.07) ceramics.

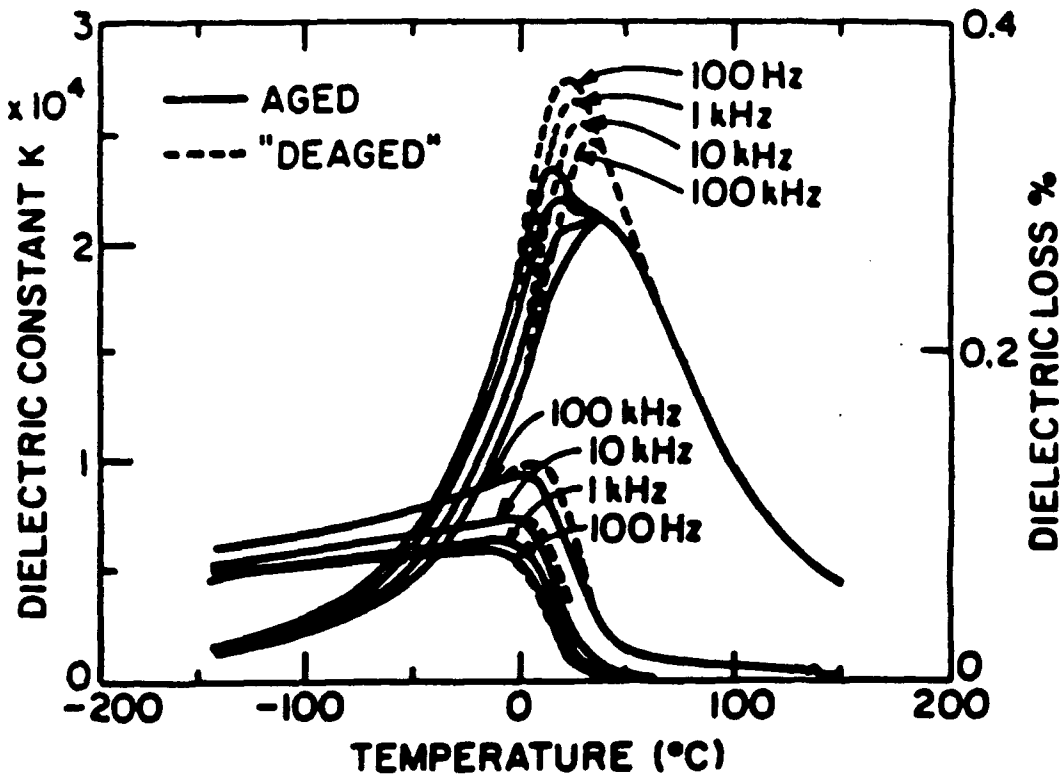

Figure 3. Typical example of the aged and deaged dielectric behavior as a function of temperature (at 100 Hz, 1 KHz, 10 KHz, and 100 KHz) for course grain (~ 6 μm) high purity but excess PbO ceramic.

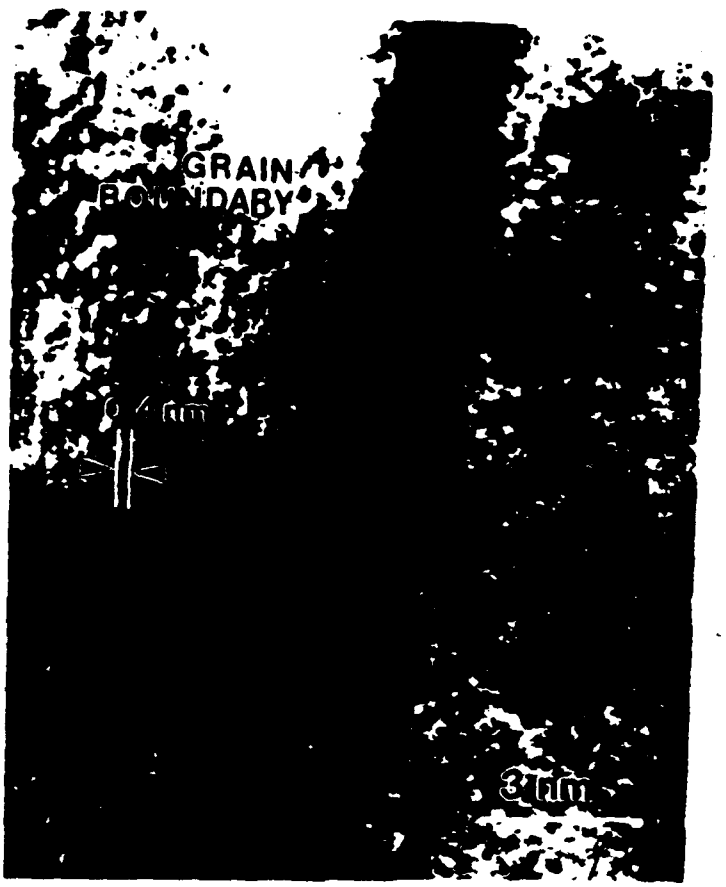

Figure 4. a) Lattice image of course grained PMN:PT grains close to a grain boundary, showing a grain boundary phase ~ 2 nm.

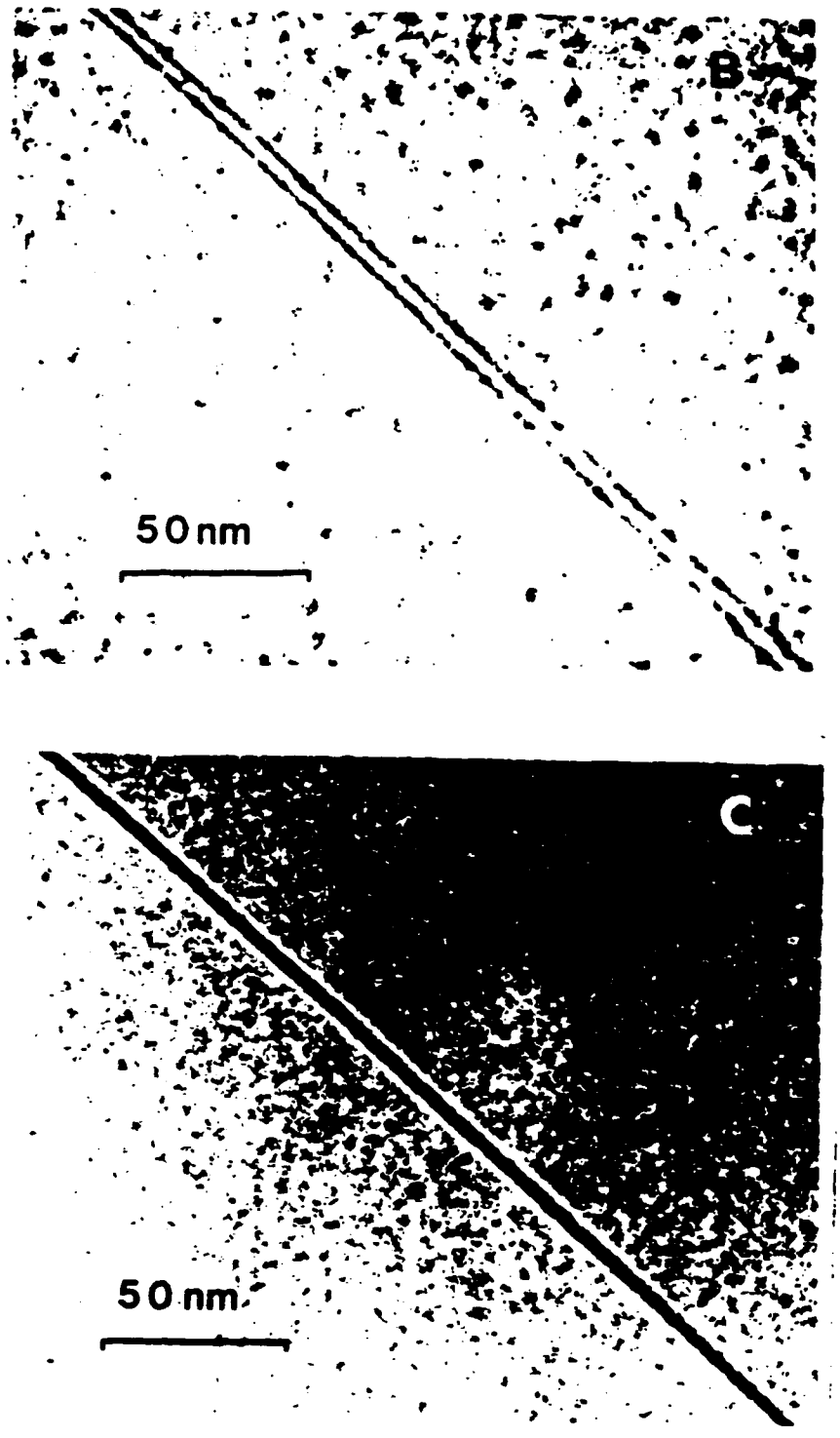

Fig 4. b) and c) Under-overfocus micrographs of grain boundary phase in PMN:PT ceramics, reversal in contrast implies presence of grain boundary phase (ref. 18).

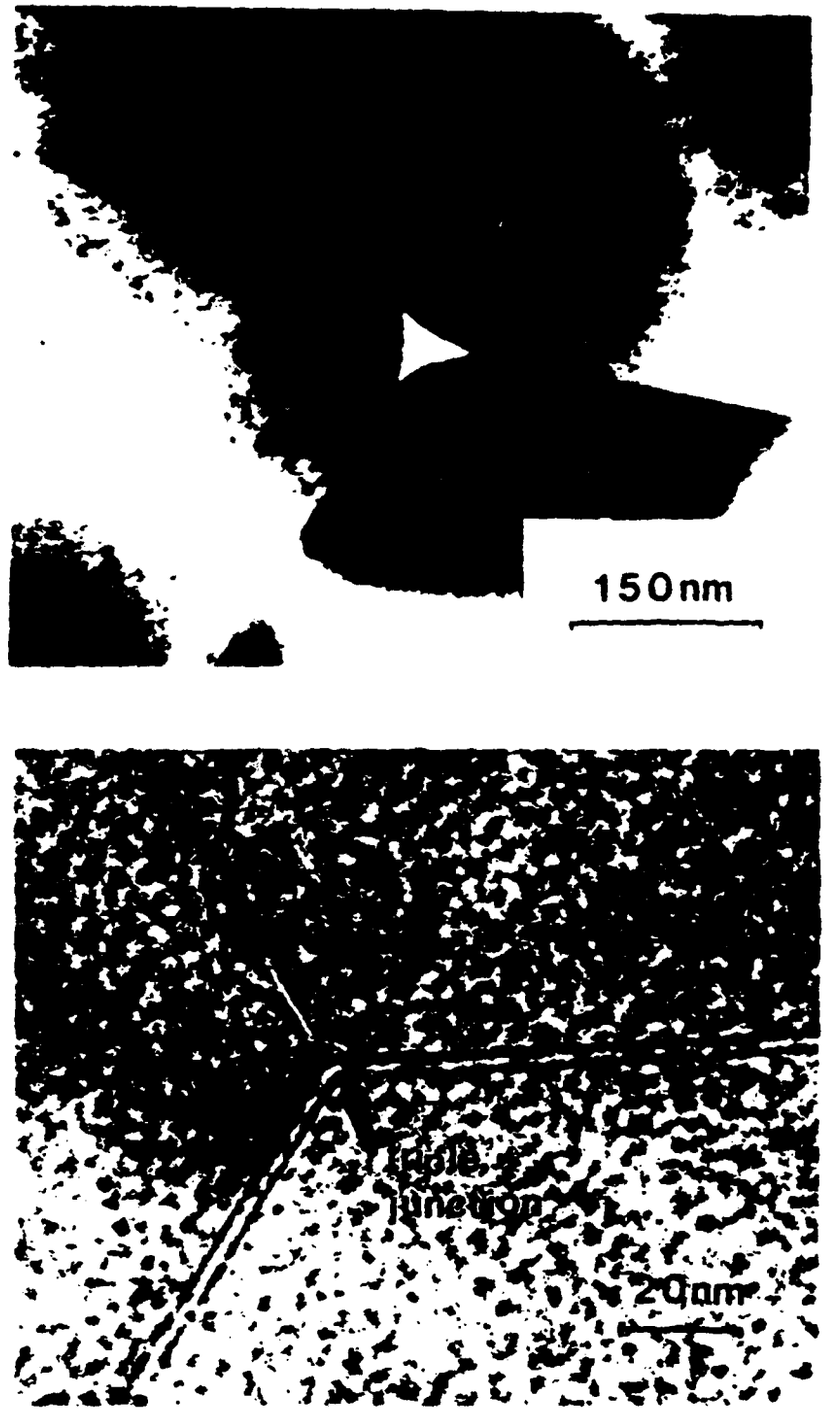

Figure 5. a) Glassy phase found at triple point in reagent grade PMN:PT ceramic.

b) Clean triple points in high purity PMN:PT ceramics.

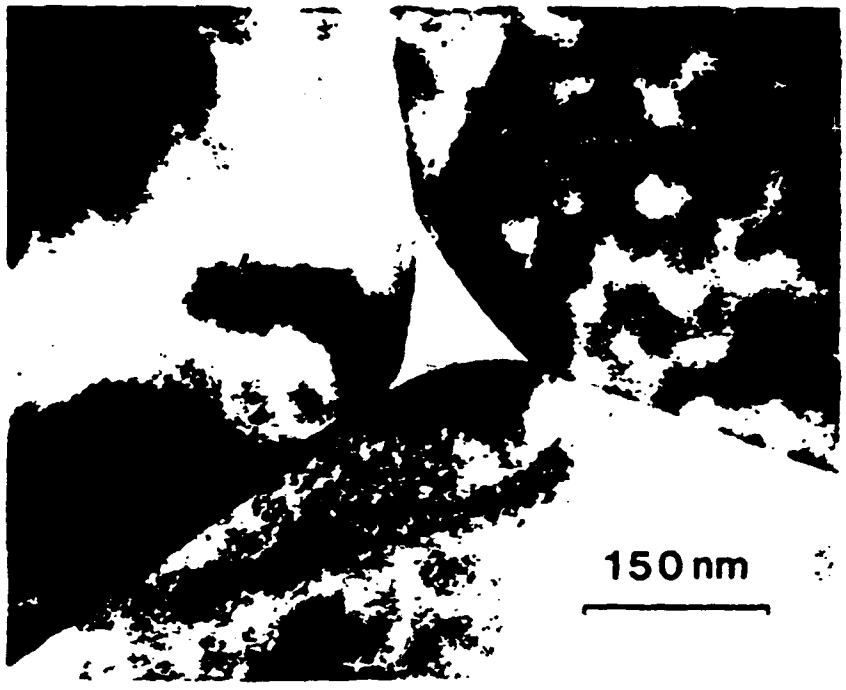

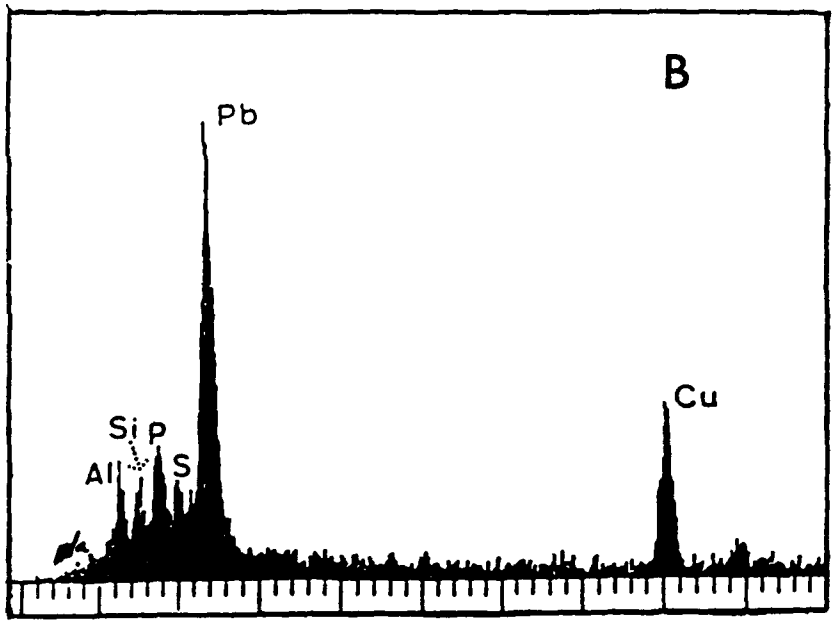

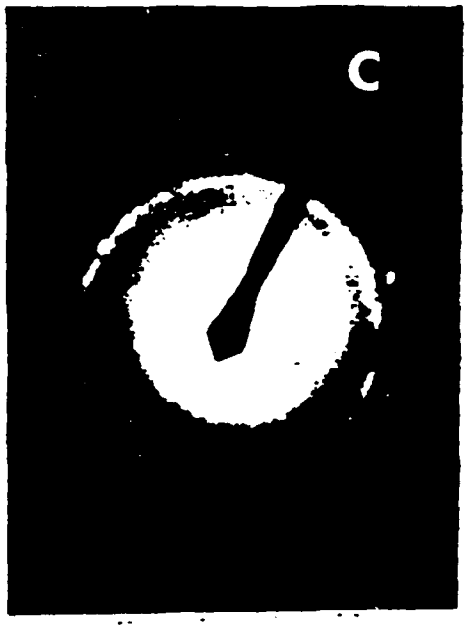

Figure 6 a) Triple point in reagent grade PMN:PT Ceramic.
b) EDS of triple point in reagent grade PMN:PT ceramic
c) Electron diffraction pattern from triple point.

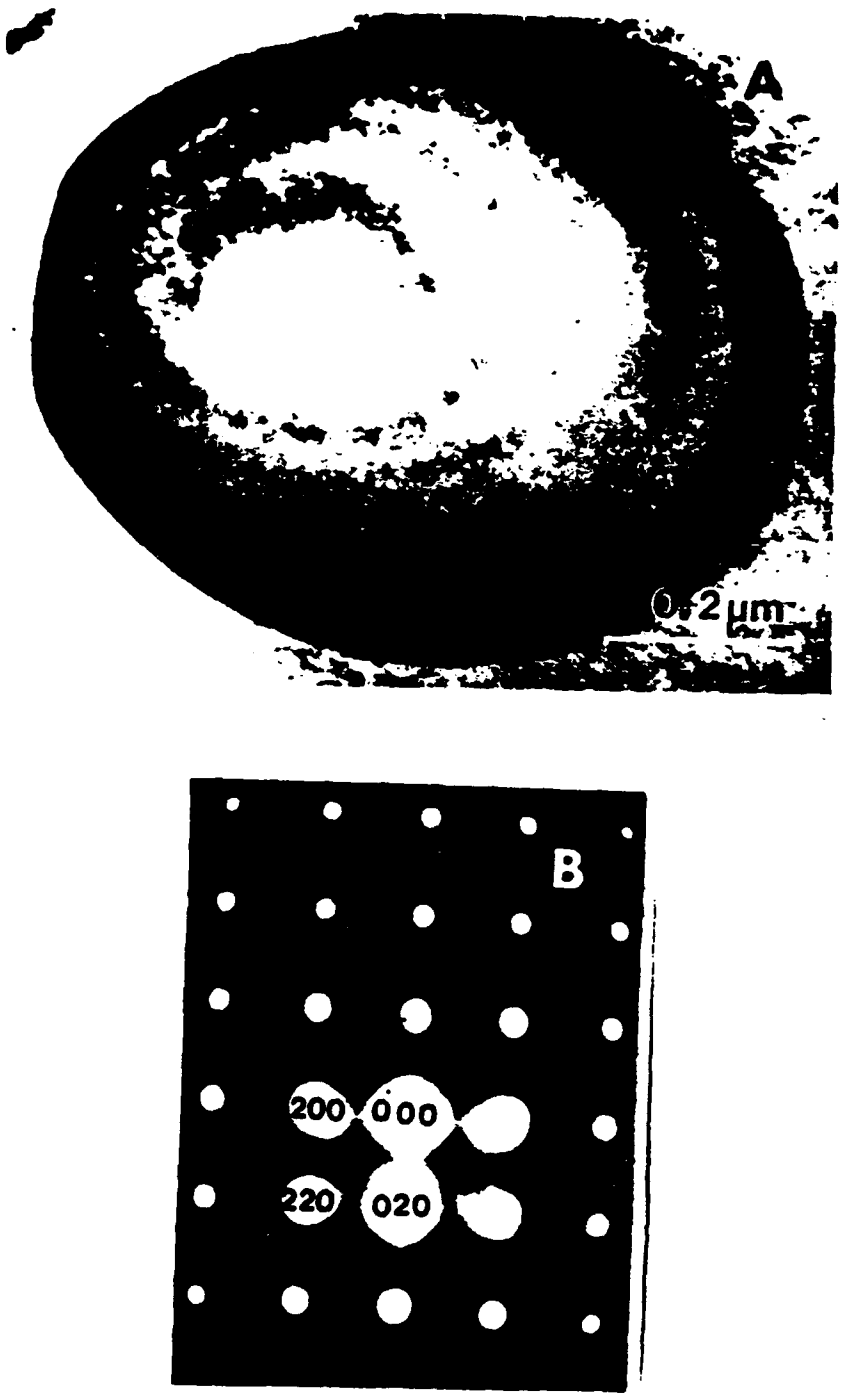

Figure 7. a) Rare intergranular phase of MgO in high purity PMN:PT (0.93:0.07) ceramic.

b) <001> diffraction pattern of MgO.

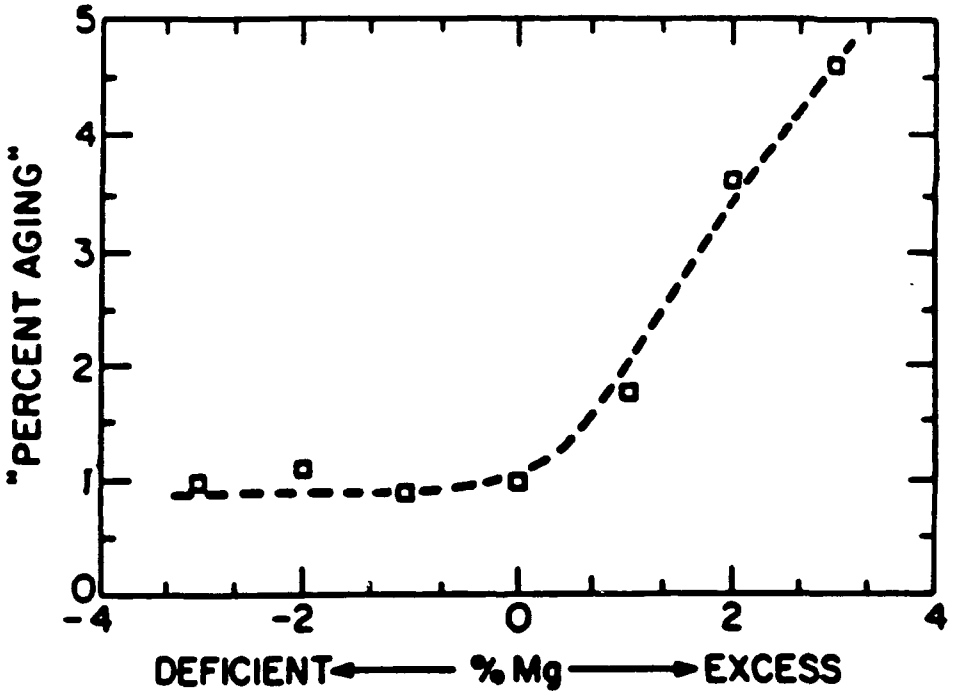

Figure 8. Variation of aging rate with the batch of deficient and excess MgO in PMN:PT (0.93:0.07) ceramics.

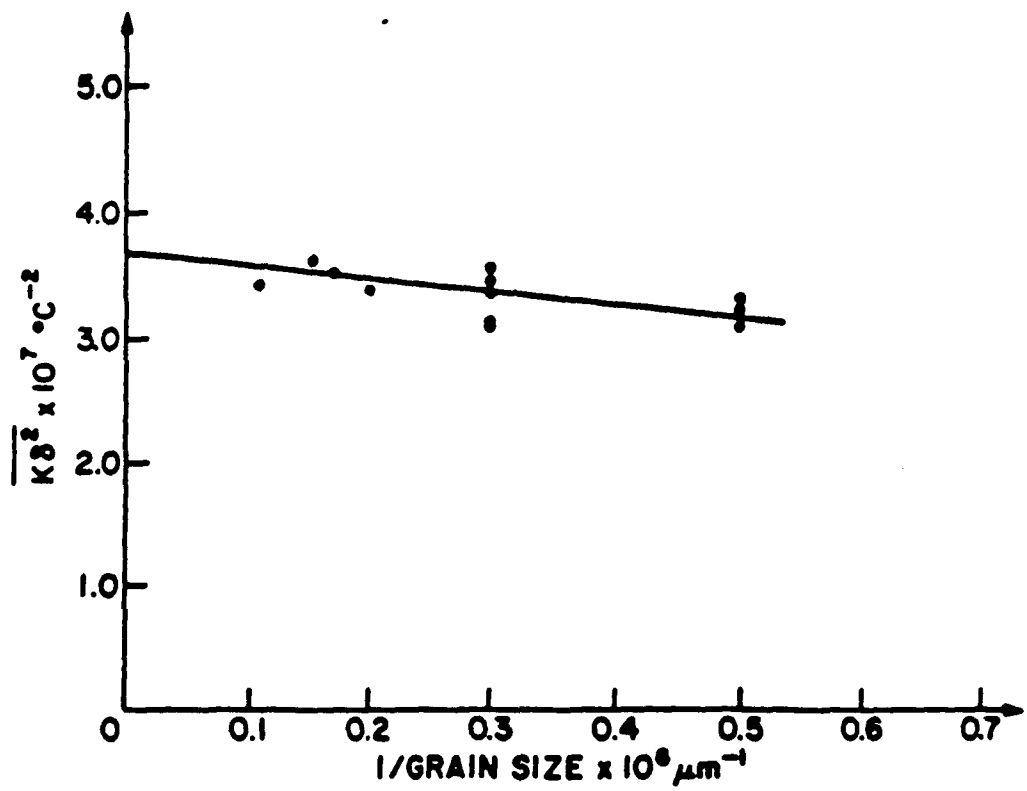

Figure 9. Variation of $\delta^2 K_{max}$ and grain size for PMN:PT (0.93:0.07) reagent grade ceramics.

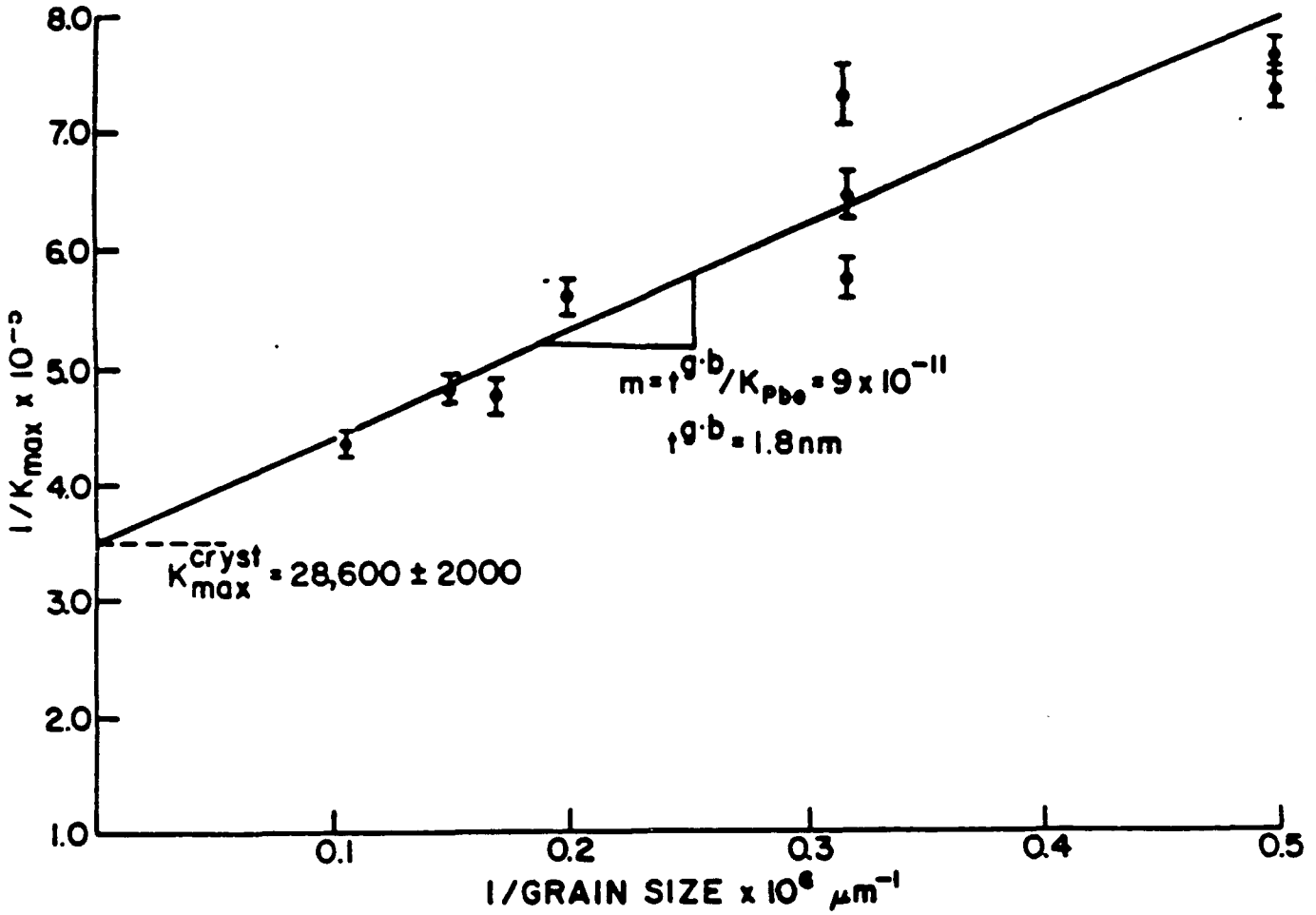

Figure 10. Variation of $1/K_{max}$ and grain size for PMN:PT (0.93:0.07) reagent grade ceramics.

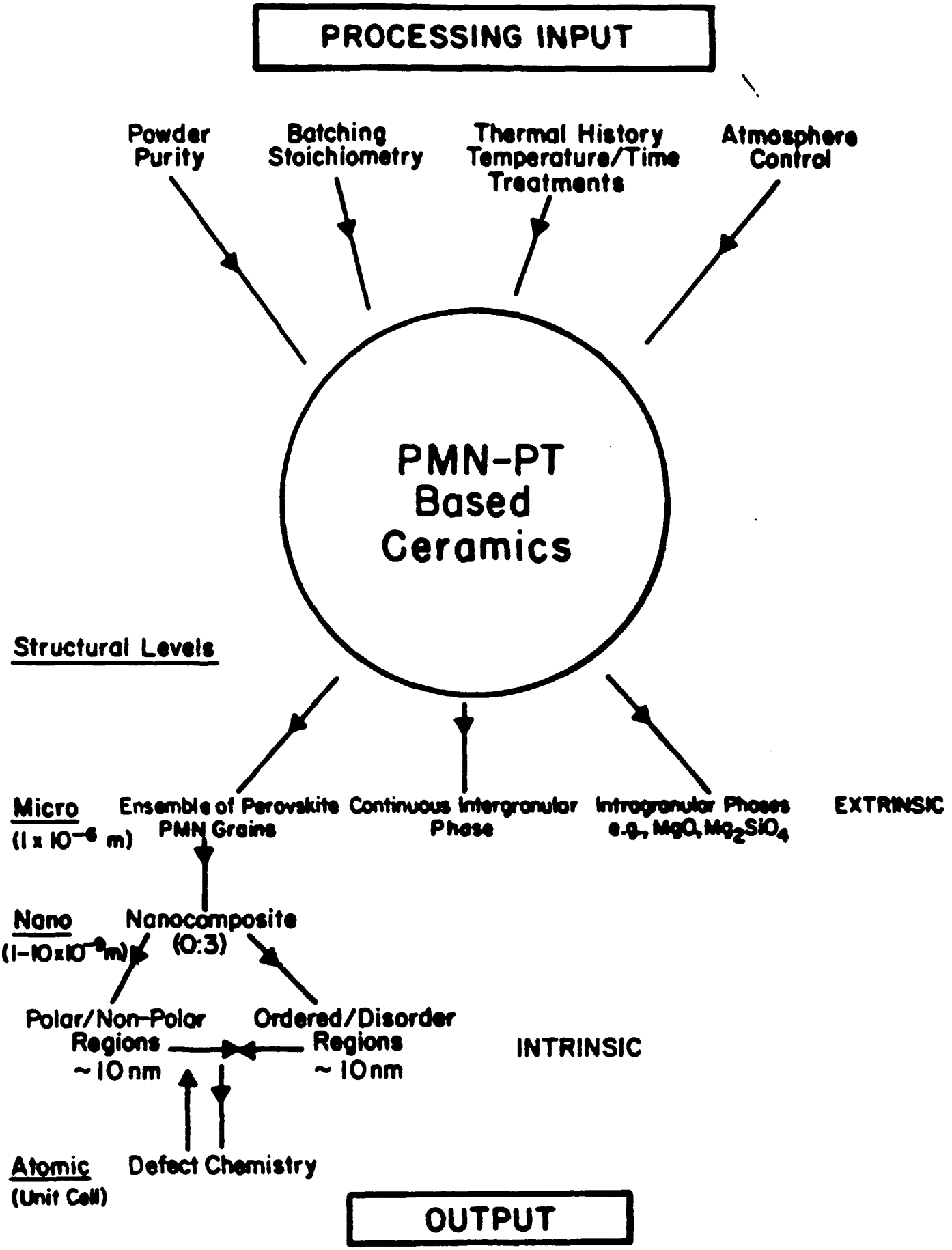
PROCESSING INPUT
Powder Purity
Batching Stoichiometry
Thermal History Temperature/Time Treatments
Atmosphere Control
PMN-PT Based Ceramics
Structural Levels
Micro
(1 x 10⁻⁶ m)
Ensemble of Perovskite PMN Grains
Continuous Intergranular Phase
Intragranular Phases e.g., MgO, Mg2SiO4
EXTRINSIC
Nano
(1-10x10⁻⁹m)
Nanocomposite (0:3)
Polar/Non-Polar Regions ~10 nm
Ordered/Disorder Regions ~10nm
INTRINSIC
Atomic
(Unit Cell)
Defect Chemistry
OUTPUT

APPENDIX 40

journal

J. Am. Ceram. Soc., 73 [6] 1783–84 (1990)

Effects of Sm_2O_3 and $Gd_2O_3 + Nd_2O_3$ on Electromechanical Properties of $PbTiO_3$ Ceramics

W. R. Xue,* Walter A. Schulze,*,† and Robert E. Newnham*

Materials Research Laboratory, The Pennsylvania State University, University Park, Pennsylvania 16802

The electromechanical properties of $PbTiO_3$ ceramics, modified by substitution of Sm or Gd + Nd (same average atomic radius as Sm) for Pb, were studied in the range of 6% to 14% substitution. The modified $PbTiO_3$ ceramics were stable, and the Curie temperature decreased linearly over this composition range. The 10% Sm composition had a large anisotropy in the coupling factor ratio, k_t/k_p, and a similar, but weaker, effect developed for 12% (1/2 Gd + 1/2 Nd). This indicates that other than average ion size may influence the electromechanical coupling factor ratio. [Key words: electromechanical properties, lead titanate, samarium, neodymium, gadolinium.]

I. Introduction

LEAD TITANATE ceramics are very useful piezoelectric materials because of their relatively small dielectric constant, high Curie temperature, and large piezoelectric anisotropy. Transducers made from $PbTiO_3$ can be used at high temperatures and high frequencies.[1,2] Two new types of $PbTiO_3$ ceramics have been investigated recently.[3,4] One was modified by the partial substitution of alkaline-earth metals for Pb and the second by rare-earth metals for Pb.

In 1981, Yamashita reported on $PbTiO_3$ ceramics modified with alkaline-earth metals.[3] The coupling factor ratio, k_t/k_p, of this material is 12, an exceptionally high value. In 1982, Takeuchi described transducers with k_t/k_p as high as 15, made by poling $(Pb_{0.88}Sm_{0.08})(Ti_{0.98}Mn_{0.02})O_3$ ceramics at 150°C and 60 kV/cm.[4]

To obtain electroceramics with a k_t/k_p ratio as high as possible and to examine the influence of the substitution cation radius, we have investigated the effects of Sm and Gd + Nd on the electromechanical properties of $PbTiO_3$. The ionic radii for the three rare-earth ions are Sm^{3+}, 0.096; Gd^{3+}, 0.094; and Nd^{3+}, 0.098 nm (0.96, 0.94, and 0.98 Å, respectively). Hence, doping $PbTiO_3$ with a 50:50 mixture of $Gd^{3+} + Nd^{3+}$ should mimic the behavior of Sm^{3+}-doped $PbTiO_3$ if ionic size is the critical factor.

II. Experimental Procedure

Two composition ranges were studied: $(Pb_{1-1.5x}Sm_x)(Ti_{0.98}Mn_{0.02})O_3$ and $(Pb_{1-1.5y}(Gd_{0.5} + Nd_{0.5})_y)(Ti_{0.98}Mn_{0.02})O_3$. In the Sm series, ceramic specimens were prepared with $x = 0.06$, 0.08, 0.10, 0.12, and 0.14. Samples with Gd + Nd substitutions were prepared with $y = 0.08$, 0.10, and 0.12. The raw materials were processed by ball-milling in plastic jars using zirconia balls. Calcining was conducted at 900°C for 1 h, and then the powder was crushed again. A small amount of aqueous poly(vinyl alcohol) solution was added, and the mixture was molded into disks 20 mm in diameter by 2 mm in thickness. They were sintered at 1100° to 1200°C for 2 h in a PbO atmosphere. The lattice constant was measured by X-ray diffraction using Cu$K\alpha$ radiation. Sputtered gold electrodes were applied, and poling was conducted in vegetable oil at 150°C using an electric field of 50 kV/cm for 5 min. The temperature dependence of the dielectric constant was measured at 10, 100, and 1000 kHz over the range from 50° to 500°C using a multifrequency inductance–capacitance–resistance (LCR) meter. Impedance circle diagrams were used for measuring piezoelectric characteristics at room temperature.[5] The piezoelectric coefficient d_{33} was measured at 100 Hz using a d_{33} meter.[‡]

III. Results and Discussion

Table I lists the tetragonal parameters a and c. The c/a ratio decreases very slightly with increasing Sm content. Unit-cell dimensions for the Gd + Nd series are similar to those for Sm. Curie temperatures of the Sm- and (Gd + Nd)-doped ceramics are also listed in Table I. The Curie temperature decreases approximately linearly with increasing Sm or Gd + Nd content. The Curie temperature of (Gd + Nd)-substituted $PbTiO_3$ is nearly the same as that of the Sm-substituted material with the same content.

The piezoelectric coefficient d_{33} increases with increasing Sm or Gd + Nd content, but not in a linear fashion. Comparing these two systems, the d_{33} values of the Sm system are slightly higher than those of the Gd + Nd system. Table I lists the elctromechanical coupling factors k_p and k_t. The planar coupling coefficent k_p decreases with increasing Sm, reaching its smallest value at 10% Sm; it then begins to increase. The thickness coupling factor k_t increases with increasing Sm up to 10%, and then remains approximately constant with further increases in Sm content. For (Gd + Nd)-doped ceramics, k_p decreases with increasing Gd + Nd content, whereas k_t differs from the Sm trend and decreases with increasing dopant. The coupling factor ratio k_t/k_p reaches maximum values of 17 for 10% Sm and 10 for 12% (Gd + Nd). The increase in the ratio for the Gd + Nd dopant results from k_p decreasing more rapidly than k_t, while the ratio for the Sm-doped material drops because of the reduction of k_p.

IV. Summary

$PbTiO_3$ ceramics modified by substitution of Sm or Gd + Nd for Pb are stable in the range 6% to 14% substitution. The Curie temperature decreases linearly over this range.

The ratio of the electromechanical coupling factor k_t/k_p is highest at the 10% Sm composition. Even though the Gd + Nd addition mimics very closely the Sm radius, the k_t/k_p ratio did not change as much as with Sm and, unlike the Sm-doped material, k_t dropped with increasing dopant. These

D. M. Smyth—contributing editor

Manuscript No. 198126. Received September 11, 1989; approved January 26, 1990

*Member, American Ceramic Society.
†On leave from Nanjing Institute of Chemical Technology, China.
‡Now with Ceramics Department, Alfred University, Alfred, NY.

‡Berlincourt d_{33} PiezoMeter, Channel Products, Inc., Chesterfield, OH.

Table I. Lattice Parameter, Piezoelectric Coefficients, and Curie Temperature of Modified $PbTiO_3$ Ceramics

Composition	a (Å)*	c (Å)*	c/a	T_c (°C)	d_{33} ($\times 10^{-12}$ C/N)	k_p (%)	k_t (%)	k_t/k_p
0%	3.905	4.152	1.063	490				
+6% Sm	3.904	4.142	1.061	393	54	4.5	32.0	7.1
+8% Sm	3.911	4.145	1.060	357	61	3.2	43.4	13.6
+10% Sm	3.909	4.138	1.059	321	68	2.5	42.7	17.1
+12% Sm	3.895	4.124	1.059	282	72	6.3	42.7	6.8
+14% Sm	3.894	4.123	1.059	255	74	6.4	44.5	7.0
+4% (Gd + Nd)	3.906	4.140	1.060	354	59	6.0	44.0	7.3
+5% (Gd + Nd)	3.898	4.124	1.058	326	62	3.8	36.0	9.5
+6% (Gd + Nd)	3.899	4.129	1.059	297	65	2.8	29.0	10.4

*1 Å = 10 nm.

results suggest that factors other than ionic radius affect the coupling and coupling anisotropy.

References

[1]I. Uedo and S. Ikegami, "Piezoelectric Properties of Modified $PbTiO_3$ Ceramics," *Jpn. J. Appl. Phys.*, 7, 236 (1968).

[2]Y. Matsuo, M. Fujimura, and H. Sasaki, "Lead Titanate Ceramics Doped with Manganese Oxide," *J. Am. Ceram. Soc.*, **48**, 111 (1965).

[3]Y. Yamashita, K. Yokoyama, H. Honda, and T. Takahashi, "Piezoelectric Properties of Modified $PbTiO_3$ Ceramics Containing Alkaline Earths," *Jpn. J. Appl. Phys.*, **20** [4, Suppl.] 183 (1981).

[4]H. Takeuchi, S. Jyomura, E. Yamamoto, and Y. Ito, "Electromechanical Properties of (Pb,Ln)(Ti,Mn)O_3 Ceramics (Ln = Rare-Earths)," *J. Accoust. Soc. Am.*, **72**, 1114 (1982).

[5]R. Holland and E. P. EerNisse, "Accurate Measurement of Coefficients in a Ferroelectric Ceramic," *IEEE Trans. Sonics Ultrason.*, **SU-16**, 173 (1969).

[6]E. Sawaguchi, T. Mitsuma, and Z. Ishii, "Double Hysteresis Loop of $(Pb_xCa_{1-x})TiO_3$ Ceramics," *J. Phys. Soc. Jpn.*, **11**, 1298 (1956). □

APPENDIX 41

Ferroelectrics Letters. 1990, Vol. 12, pp. 29-34
Reprints available directly from publisher
Photocopying permitted by license only

SOLUTION-SOL-GEL PROCESSING OF LEAD MAGNESIUM NIOBATE THIN FILMS†

P. RAVINDRANATHAN, S. KOMARNENI*, A. S. BHALLA, L. E. CROSS AND R. ROY

Materials Research Laboratory, The Pennsylvania State University, University Park, PA 16802, USA.

(Received for Publication June 27, 1990)

Abstract Lead magnesium niobate (PMN) thin films were prepared by a solution sol-gel (SSG) technique. X-ray diffraction analysis indicated that the perovskite phase of PMN formed at a temperature as low as 775°C. A highly oriented film along (111) direction was obtained on silicon substrate . The orientation and crystallization rate were strongly influenced by the type of substrate and heating conditions.

INTRODUCTION

Lead magnesium niobate (PMN), $Pb(Mg_{1/3}Nb_{2/3})O_3$ with perovskite structure has recently received considerable imporance in the area of electronic ceramics because of its excellent dielectric and ferroelectric properties.[1] The preparation and properties have been investigated in both single crystal and ceramic forms. However, there are only few reports about the preparation of PMN thin films in the literature.[2,3] One of the problems with PMN ceramics is the difficulty in producing a single phase material consisting of only the perovskite phase. Depending on the processing conditions, a second phase of pyrochlore may be present which reduces the dielectric constant of the material. We have reported earlier the preparation and properties of PMN ceramics using solution sol-gel method.[4,5]

The use of sol-gel method can offer many advantages in the preparation of electronic ceramics such as purity, homogeneity, ease of forming a variety of structures, low processing temperature and unique combination of properties. In this paper, we describe the preparation of PMN thin films by a solution-sol-gel method.

EXPERIMENTAL PROCEDURE

Fig.1 illustrates the flow diagram for the preparation of solutions and films using a SSG method. The concentration of the solution was 0.08 mole/litre. This solution was stored in a glove box to prevent hydrolysis from the humid air. The homogeneous solution of PMN was used for spin coating on silicon wafer [111], platinum film which was sputtered on [111] silicon and [100] MgO single

*Also with the Department of Agronomy

†Communicated by Dr. George W. Taylor

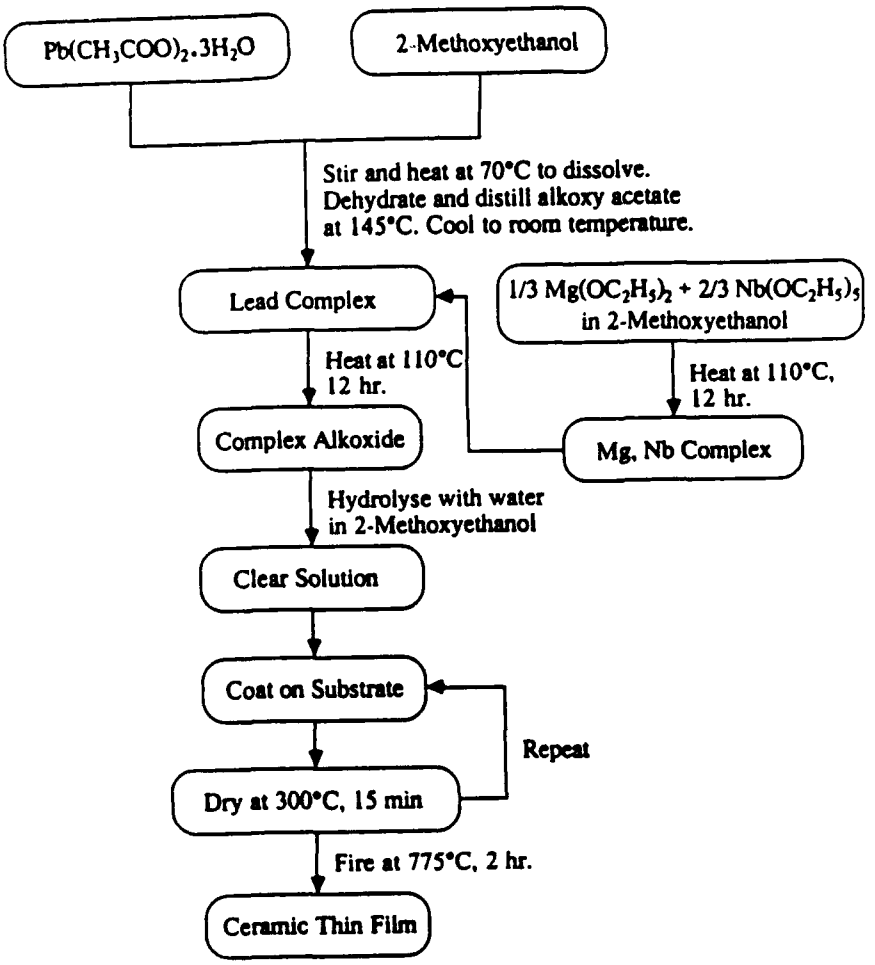

FIGURE 1. Flow diagram for the processing of PMN thin films.

crystal [100] substrates. The substrates were cleaned by standard semiconductor processing techniques.[6] Finally, the substrates were rinsed with 2-methoxyethanol and dried using precision duster. This substrate cleaning procedure was found to improve film quality. Hydrolysed solutions were applied to all the substrates which were then spun at a speed of 2000 rpm for 45 seconds. After each spin coating deposition, the substrates were heated in a furnace at 300°C for 15 minutes. After the final deposition, the films were calcined at various temperatures in air between 700 to 850°C at intervals of 25°C for 30 to 120 minutes. The films were calcined at several heating rates also. In the fast firing, the furnace was set at a desired temperature and the sample was placed in a platinum foil and introduced into the furnace. In the slow firing, the samples were heated at 5°C/minute.

The hydrolysed solution was kept in a beaker to form a gel. The dried gels were calcined at 775°C for 120 minutes. Thermal analysis of the gel was carried out in air with a heating rate of 10°C/minute. The films were charaterized by x-ray diffraction (XRD) analysis. The thickness and the grain size of the films were observed by a scanning electron microscope (SEM).

RESULTS AND DISCUSSION

The thermal analysis of the gel showed an endotherm at 108°C which corresponds to removal of water associated with the gel and an exotherm at 341°C corresponding to the decomposition of organics. About 18.8% weight loss occured in the temperature range of 30° - 330°C. The removal of all organics occurs at about 330°C. The films and the gel were heated first at 350°C for 120 minutes and then at 775°C for 120 minutes. The gel calcined at 775°C for 120 minutes showed the formation of perovskite phase (~98%).

The films deposited on the various substrate were calcined at different temperatures revealed that the optimum temperature is 775°C. The XRD pattern of the film calcined at 775°C for 120 minutes on Si substrate is shown in figure 2. The amount of perovskite phase can be calculated using the X-ray intensity of the (111) or (110) peak of the perovskite phase and the intensity of the (222) peak of the pyrochlore phase as has been reported earlier.[2,4] The amount of perovskite phase was found to be only 83%. The XRD pattern indicates the formation of highly oriented film along [111] direction. There are also some peaks corresponding to the pyrochlore phase. As pointed out earlier the problem with PMN ceramics is the difficulty in producing a single phase material consisting of only the perovskite phase. With our earlier observation[7] and other reports it is concluded that the formation of perovskite phase from pyrochlore phase may be a kinetic problem. The amount of perovskite phase formed increased as the number of layers deposited on silicon substrate increased. The heating rate, however, did not affect the orientation of the film on silicon substrate. The same orientation along [111] direction was also observed on platinum sputtered silicon . The films fired with a heating rate of 1500°C/ minute formed highly oriented films along [110] direction on platinum sputtered silicon and the amount of perovskite phase was found to be >96% . With MgO substrate, the film calcined at 800°C for 30

minutes showed the formation of only a small amount of perovskite phase with [100] orientation. The complete formation of perovskite phase was not observed by us here and this observation is in disagreement with that reported by Okuwada et al.[2]

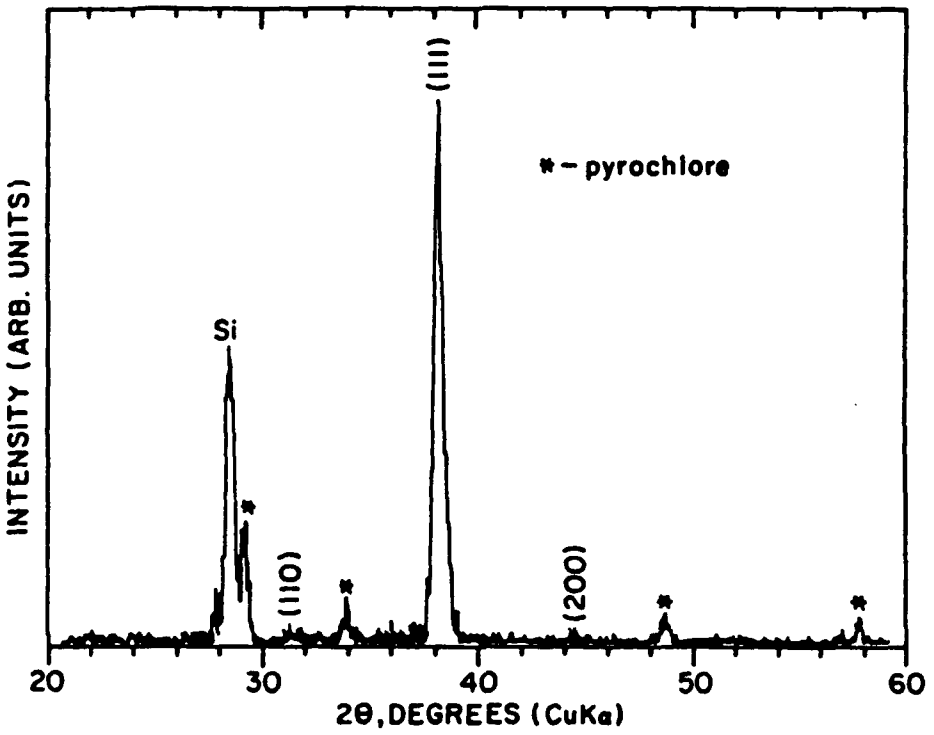

FIGURE 2. XRD pattern of PMN film calcined at 775°C for 120 minutes on silicon substrate.

The reason for this difference is not totally clear but it may be due to difference in the precursor solutions. All the films showed a thickness of about 0.3 to 0.5 μm. A typical SEM of PMN film on silicon substrate is show in figure 3. This film was made by five repeated coatings and calcined at 775°C. The thickness of the film was found to be 0.3 μm. The grain size was < 0.1 μm.

CONCLUSION AND FUTURE WORK

Lead magnesium niobate thin films with perovskite structure were prepared by solution sol-gel method. The film calcined at 775°C for 2 hr showed >95% of

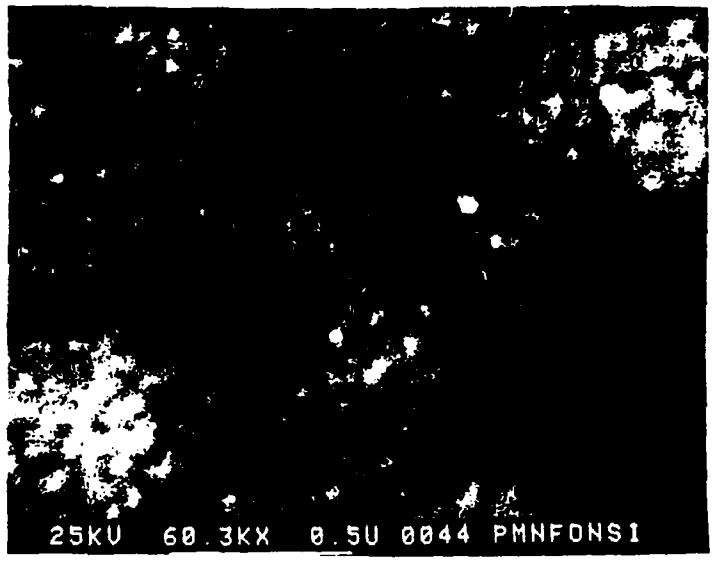

FIGURE 3. Scanning electron micrograph of PMN film on silicon substrate.

perovskite phase. A highly oriented film along *[111] direction* was obtained on silicon substrate. The heating rate was found to affect the orientation of the thin film on platinum sputtered silicon substrate. Further work on the preparation of the PMN-PT films by the SSG method reported here and their electrical property measurements are in progress.

Acknowledgements

This research was supported by the Office of Naval Research Contract No. N00014-86-K-0767.

REFERENCES

1. K. Uchino, Ceram. Bull., 65, 647 (1986).
2. K. Okuwada, M. Imai and K. Kakuno, Jpn. J. of Appl. Phys., 28, 1271 (1989).
3. L. C. Veith, G. M. Vest and R. W. Vest, Abst. of the 91st Annual Meeting of the Am. Ceram. Soc., Indiana, 294 (1989).

4. P. Ravindranathan, S. Komarneni, A. S. Bhalla, R. Roy and L.E. Cross, "Ceramic Transactions", Ceramic Powder Science, Ed. Gary L. Messing, Edwin R. Fuller, Jr., and H. Hausner, Am. Ceram. Soc., 182 (1988).
5. P. Ravindranathan, S. Komarneni, A. S. Bhalla and R. Roy, Ferroelectrics Letts., (accepted).
6. D. P. Partlow and J. Greggi, J. Mater. Res., 2, 595 (1987).
7. P. Ravindranathan, S. Komarneni and R. Roy, J. Am. Ceram. Soc., 73, 1024 (1990).

APPENDIX 42

Particle and grain size effects on the dielectric behavior of the relaxor ferroelectric $Pb(Mg_{1/3}Nb_{2/3})O_3$

Philippe Papet, Joseph P. Dougherty, and Thomas R. Shrout
Center for Dielectric Studies, Materials Research Laboratory, The Pennsylvania State University, University Park, Pennsylvania 16802

(Received 24 May 1990; accepted 20 August 1990)

The role of particle and grain size on the dielectric behavior of the perovskite relaxor ferroelectric $Pb(Mg_{1/3}Nb_{2/3})O_3$ [PMN] was investigated. Ultrafine powders of PMN were prepared using a reactive calcination process. Reactive calcination, the process by which morphological changes take place upon reaction of the component powders, produced particle agglomerates less than 0.5 μm. Through milling, these structures were readily broken down to ~70 nanometer-sized particulates. The highly reactive powders allowed densification as low as 900 °C, but with corresponding grain growth in the micron range. Such grain growth was associated with liquid phase sintering as a result of PbO–Nb_2O_5 second phase(s) pyrochlore. Sintering, assisted by hot uniaxial pressing, below the temperature of liquid formation of 835 °C, allowed the fabrication of highly dense materials with a grain size less than 0.3 μm. The dielectric and related properties were determined for samples having grain sizes in the range of 0.3 μm to 6 μm. Characteristic of relaxors, frequency dependence (K and loss) and point of T_{max} were found to be related to grain and/or particle size and secondarily to the processing conditions. Modeling of particle size/dielectric behavior was performed using various dielectric properties of 0–3 composites comprised of varying size powder in a polymer matrix. An intrinsic-microdomain perturbation concept was proposed to interpret observed scaling effects of the relaxor dielectric behavior in contrast to normally accepted extrinsic grain boundary models.

I. INTRODUCTION

Lead magnesium niobate, $Pb(Mg_{1/3}Nb_{2/3})O_3$, belongs to a family of complex $Pb(B'B'')O_3$ perovskites which are known as relaxor ferroelectrics. First discovered by Smolenskii,[1,2] these materials exhibit broad and anomalously large dielectric maximas which make them ideal candidates for multilayer capacitors (MLCs) and electrostriction actuators, electro-optics.[3,4] The following materials are distinguished from "normal" ferroelectrics by the presence of a broad diffuse and dispersive phase transition. The dielectric constant (K) peaks at T_m, but because of the dispersion in the Curie temperature can be defined only in reference to the frequency at which the measurements are made. The spontaneous polarization, P_s, is not lost at T_m but gradually decays to zero with increasing temperature above T_m. Relaxor materials show no evidence of optical anisotropy or x-ray line splitting (pseudo-cubic structural changes), even well below T_m.

The most widely accepted models for the understanding of relaxor ferroelectric phenomena come from Smolenskii[5] and Cross.[6] The generally accepted inhomogeneous microregion model postulated by Smolenskii *et al.* bases the origin of the diffuse phase transition on local compositional fluctuations associated with B-site cation disorder, resulting in a distribution of Curie temperatures. Cross further enhanced the understanding of relaxor dielectric behavior, suggesting that localized polar microregions are analogous to spin cluster behavior in superparamagnets. Cross's "superparaelectric" concept accounts for many of the observed properties of relaxors including the frequency dependence of the permittivity, dielectric aging, and also metastable switching from micro → macrodomain. More recently, Randall *et al.* proposed a connection between localized B-site cation ordering and relaxor behavior.[7] Common to all the above models is the fact that the structural origin of relaxor behavior is on the scale of 10–100 nm.

As relaxor-based materials continue to play an increasing role in electro-ceramics, it is important that one understands the role of microstructural relationships on the overall relaxor dielectric behavior. This importance is exemplified in applications such as multilayer capacitors, thin films, and actuators, where microstructural features such as grain sizes are approaching the scale of the origin of relaxor behavior. The objective of this work was to investigate the role of grain size and particle size in PMN ceramics as it approaches the associated nanoscale region of relaxor dielectric behavior.

II. EXPERIMENTAL

In order to investigate the influence of particle and grain size as they approach the associated scale of relaxor ferroelectrics, one must start with nanosized pow-

ders. Such powders are generally achievable utilizing only sophisticated chemical techniques.[8] In this study, PMN powder was prepared using a co-precipitation process, similar to that reported in Ref. 9. However, in the process, to get phase purity required relatively high calcination temperatures (≥850 °C) to ensure perovskite formation and hence resulted in particle sizes >1 μm. Alternatively, very fine PMN powder was produced via solid state reaction using a reactive calcination process in conjunction with high energy milling. Characteristic of lead-based perovskites, a large volumetric expansion occurs upon reaction. At this point, the morphological development results in a spongy skeletal type structure, which is susceptible to milling. This process, known as reactive calcination, is well described in a previous paper for numerous lead based perovskite compounds.[10]

For the case of PMN, the component powders used were Hammond $2PbCO_3$–$Pb(OH)_2$ (99%) and $MgNb_2O_6$ columbite, prepared by prereacting Fisher Scientific $MgCO_3$ (99%) and Fansteel Metals Nb_2O_5 (99.5%) at 1200 °C/4 h. The columbite precursor method, first utilized by Swartz and Shrout,[11] helps eliminate the potential of unwanted lead-niobate pyrochlore phase(s).

The powder mixture was calcined at 650 °C/4 h in order to obtain the point of maximum volume expansion. High energy milling was performed using a Union Process Model-01 attritor mill. For this, the power was mixed with de-ionized H_2O and polyelectrolyte dispersant (Rohm and Haas Tamol 901). The reactively calcined and milled powders were characterized for surface area, particle size, average agglomeration number AAN(50), and phase purity by x-ray diffraction. The powder was found to contain a small amount of pyrochlore; hence, another powder was calcined at 900 °C/4 h to completely eliminate possible effects of pyrochlore, and milled as above. Characteristics of the various powders are reported in Table I. The reactively calcined powder was very fine with a calculated particle size of 0.45 μm. Clearly, it appears that the milling treatment was very efficient in this case, producing a calculated particle size of the milled powder (70 nm) in a range generally achievable using only chemical synthesis techniques. For all process conditions, the degree of agglomeration as given by AAN(50), which represents an estimate of the number of primary particles in each agglomerate,[12] was found to be similar and overall low.

The absence of a structural and corresponding abrupt ferroelectric phase transition in relaxor ferroelectrics eliminated the possibility of alternative powder characterization methods, e.g., differential thermal analysis (DTA) and x-ray diffraction, to look at possible size effects on the transition as observed in normal ferroelectrics.[13] Hence, various sized powders were used to prepare 0–3 polymer composites[14] in which the dielectric behavior of the powders themselves could be determined, utilizing various dielectric mixing models. The preparation of 0–3 composites consisted of homogeneously mixing prepared powders (−35 vol.%) with a polymer (epoxy resin) to obtain a composite where the grains of powder were embedded in a 3-dimensionally interconnected polymer matrix.

To investigate the effects of particle size on sintering behavior and subsequent grain size, disks (10 mm diameter) were prepared using polyvinylbutyral binder followed by burnout. The resultant green densities were in the range of 58–60% of theoretical density. Both conventional sintering in the temperature range 900–1100 °C and hot uniaxial pressing in the range of 800–900 °C were used, the latter being required to prevent anomalous grain growth associated with the presence of a liquid phase as a result of PbO–Nb_2O_5-pyrochlore formation, to be discussed later. Weight loss due to PbO volatility was limited to less than 1%.

The fired samples were characterized for geometric density and grain size using scanning electron microscopy (SEM) of fractured surfaces and transmission electron microscopy (TEM). Selected samples of varying microstructures were polished and electroded using sputtered-on gold. The dielectric properties were

TABLE I. Physical characteristics of calcined powders.

Samples	Calcined temperature	Milling time	Specific surface area m^2/g	Calculated particle size[a] (nm)	Measured (median) particle size[a] (μm)	AAN(50)[b]
650 UM	650 °C (4 h)	Unmilled	1.65	450	1.5 (sedigraph)[c]	37
650 M	650 °C (4 h)	4 h	10.07	70	0.2 (TEM)	23
900 UM	900 °C (4 h)	Unmilled	0.54	1400	4.6 (sedigraph)	35
900 M	900 °C (4 h)	4 h	4.07	180	0.6 (TEM)	37

[a]Equivalent spherical diameter (ESD) determined through the equation $D = 6/\rho SA$, where ρ is the theoretical density, SA the specific surface area, and D the calculated primary particle size.
[b]AAN(50) = $(MPS)^3/(ESD)^3$.
[c]Model 5000 sedigraph, micromeritics, Norcross, GA.

measured pseudo-continuously from 120 °C to −60 °C at various frequencies (100 Hz, 1, 10, 100 kHz) using a Hewlett-Packard automated system.

Characteristic of the dielectric temperature behavior in relaxors, values of K_{max}, T_m, and relative frequency dispersion which characterize the broadness of the dielectric peak, were determined, including the 0–3 composites.

III. RESULTS AND DISCUSSION

The sintering behavior of the reactively calcined (650 °C) (milled and unmilled) and the high temperature calcined powders (900 °C) are shown in Fig. 1. As presented, the reactively calcined powders began to sinter as low as 700 °C, reaching >90% theoretical density near 900 °C. As expected, reactivity was enhanced by milling. Figure 1, however, demonstrates that the sintering behavior of the powders was not related to particle size only, since the 900 °C milled powder was finer than the 650 °C (unmilled), yet the latter densified more readily. This difference was again noted in the grain growth behavior. As presented in Table II, 900 °C calcined/milled samples (900M) exhibited smaller grain sizes than the reactively calcined materials. Both the sintering and grain growth behavior were correlated to the presence of pyrochlore in the reactively calcined powders, resulting in liquid phase formation corresponding to a $PbO–Nb_2O_5$ eutectic 835 °C, as previously reported.[15]

Based on the above, to produce densification of the reactively calcined powder without grain growth, hot uniaxial pressing was thus required at temperatures less than 835 °C. Grain sizes as low as 0.3 μm were achieved. Densities ≥95% theoretical were obtained; the density was slightly dependent on the pressure. Although pyrochlore was observed in the reactively calcined powders, none remained after sintering. In the case of 900M powder only ~89% density was reached by hot uniaxial pressing at 870 °C; the grain size was close to 0.45 μm. A representative TEM photomicrograph of a hot pressed fine grain PMN sample is shown in Fig. 2. Though the thermal process conditions were at low temperatures, the microstructures were well developed with only a few dislocations and inclusions observed.

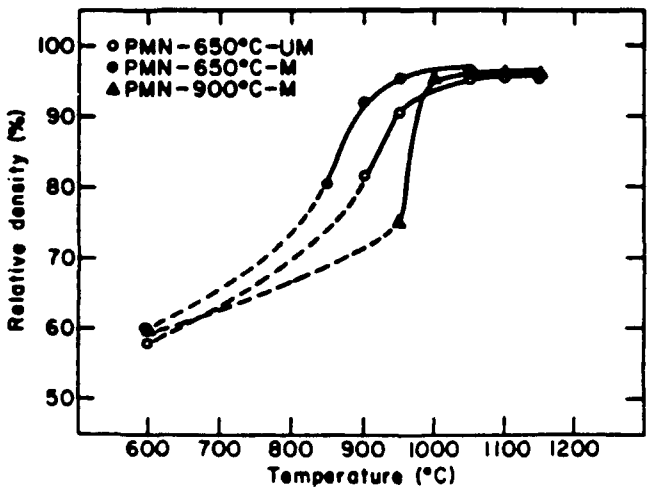

FIG. 1. Relative density versus sintering temperature for the conventionally sintered samples using milled (M) and unmilled (UM) powders.

Dielectric properties

The physical and dielectric properties of PMN samples as a function of sintering conditions are reported in Table II. To compute the maximum dielectric constant (K_{max} or K_m) versus grain size, we first have to take into account porosity. We estimated the real value of K_m, without porosity, using Wiener's mixture rule for diphasic solids containing an isolated spherical minor phase given as[16]:

$$K - K_1/K + 2K_1 = V_2(K_2 - K_1)/K_2 + 2K_1, \quad (1)$$

where K is the average dielectric constant, K_1 and K_2 the dielectric constant of phases 1 and 2, respectively, and V_2 the volume fraction of phase 2, which is assumed to be constituted of spheres embedded in a matrix of phase 1. Assuming the porosity is not interconnected, we have:

$$K_1 = K(1 + V_2/2)/(1 - V_2) \quad (2)$$

where K is the experimental value directly measured.

The calculated values of K_m versus grain size are plotted in Fig. 3, which shows the monotonic decrease of K_m as the grain size decreases. In fact, as we can see in Fig. 4, the dielectric constant is decreased at all temperatures when the grain size is reduced. Note also that the degrees of dielectric dispersion in both K and loss are greatly diminished with decreasing grain sizes, as evident for the 0.3 μm sample.

The dielectric peaks for ultrafine PMN powder (<0.3 μm) embedded in powder: polymer composites were difficult to distinguish because of the very low dielectric constant of the polymer ($K \sim 3.7$), consequently dominating the composite dielectric behavior. In other words, the flatness of the dielectric versus temperature behavior did not permit distinguishing K_m or T_m.

The dielectric values were measured to be a K of ~10 for the 650M powder composite (~22 vol.%) and ~38 for the 900M composites. The values of the dielectric constant for the ultrafine PMN powders were estimated using the logarithmic rule[17]:

$$\text{Ln } K_{composite} = V_{poly} \text{ Ln } K_{poly} + V_{PMN} \text{ Ln } K_{PMN} \quad (3)$$

TABLE II. Physical and dielectric properties of sintered PMN samples.

Samples	Firing conditions	Density (%)	Grain size (μm)	K_{max} (1 kHz)[a]	T_m (°C)
650M	Hot-pressed (18 MPa) 810 °C, 2 h	85	0.3	4600 (5400)	+1
	Hot-pressed (21 MPa) 825 °C, 2 h	91	0.3	5900 (6500)	−3
	As above Annealed 24 h at 600 °C	91	0.3	7500 (8200)	−2.2
	As above Annealed 1 week at 600 °C	91	0.3	7100 (7800)	−2.3
	Hot-pressed (25 MPa) 825 °C, 2 h	95	0.3	6400 (6700)	−0.7
	Hot-pressed (18 MPa) 890 °C, 2 h	98	1.1	11200 (11400)	−5.4
	Conventional 900 °C, 2 h	92	2	11200 (12200)	−6.2
	Conventional 950 °C, 2 h	95	4	15400 (16200)	−8.2
	Conventional 1050 °C, 2 h	97	5.6	16600 (17100)	−8.4
650UM	Conventional 950 °C, 2 h	91	2.9	13300 (14600)	−5.2
	Conventional 1050 °C, 2 h	95	4.7	16800 (17700)	−7.4
	Conventional 1100 °C, 2 h	96	6.2	17300 (18000)	−7.6
900M	Hot-pressed (MPa) 860 °C, 2 h	89	0.45	7200 (8100)	−3.4
	Conventional 1000 °C, 2 h	95	2.6	13300 (14000)	−11.6
	Conventional 1050 °C, 2 h	96	4.6	14700 (15300)	−11.9

[a] K_{max} value in parentheses calculated using Eq. (2).

where V_{poly} and K_{poly} are the volume fraction and dielectric constant of the polymer phase, respectively. The logarithmic mixing rule was selected because it gave the best fit to standard samples and previous results of high K dielectric polymer composites.[18,19] The standard composites were comprised of coarse PMN powder processed from well-sintered compacts of known dielectric constants. Values of $K_{PMN} \sim 330$ and 2800 were determined, respectively, for the 650M and 900M powders. These results further underline the decreasing of K with the grain size, as shown in Fig. 3.

Similar dielectric grain size dependency in other lead-based relaxors has been explained by the presence of a low polarizable phase boundary.[20,21] Naturally, with decreasing grain size the volume of the low polarizable second phase increases with a corresponding decrease in the dielectric constant. The origin of a low polarizable (low K) second phase may be due to different factors. First, it is very common to observe using TEM analysis the presence of a very thin layer of second phase on the order of 1–2 nm located around each grain, believed to be PbO-based regardless of process conditions.[22,23] This phase is also found at triple point boundaries along with impurities derived from the raw materials or introduced during processing.

Recently, Wang and Schulze[24] systematically examined the role of a PbO grain boundary phase on the dielectric properties of PMN. The dielectric constant was found to decrease with increasing amounts of PbO introduced during processing. Though little grain size variations were observed, the dielectric dependency was explained according to the series mixing theory used for diphasic systems where $K_g \gg K_{gb}$, being simplified in the following expression:

$$\frac{1}{K} = \frac{1}{K_{grain}} + \frac{1}{RK_{gb}} \quad (4)$$

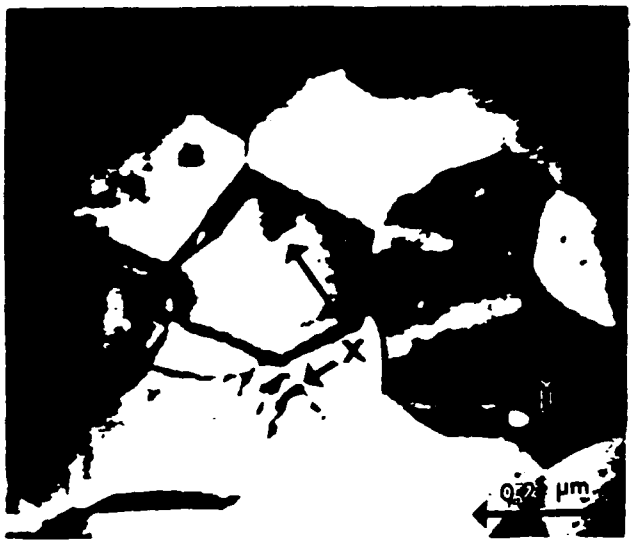

FIG. 2. TEM photomicrograph of the fractured surface of a hot-pressed 650M sample at 825 °C (21 MPa). x = dislocations, i = inclusion.

where K is the microstructurally dependent value at T_m, K_{xtal} the single crystal value, K_{gb} the grain boundary value, and R the ratio of the grain size to grain boundary thickness. Assuming a K_{xtal} of 20 000 and K_{gb} in the order of 10 to 20, the dielectric analysis revealed a grain boundary layer in the range of 1 to 5 nm, increasing according to the amount of excess PbO added.

Using the above expression and K_{xtal} and K_{gb} values of 20 000 and 20, respectively, assuming a 1 nm grain boundary thickness as schematically depicted in Fig. 5(a) (the lower limit for stoichiometric PMN), the microstructurally dependent K value was determined as a function of grain size and presented in Fig. 3 as the series model. As shown, good agreement between the experimentally determined values, regardless of process

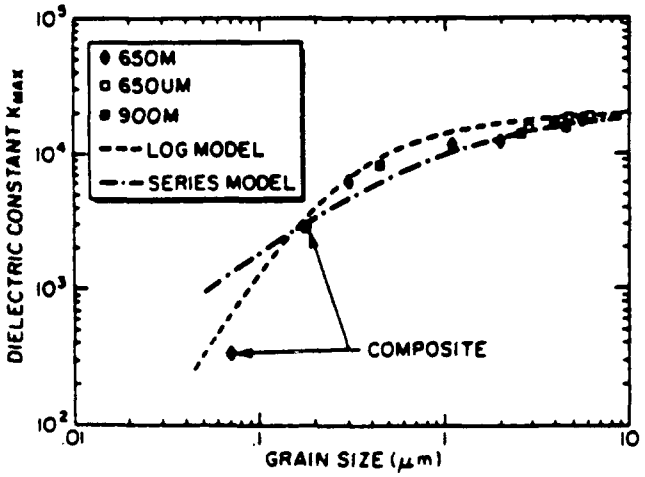

FIG. 3. Maximum of the dielectric constant K_{max} versus grain and/or particle size.

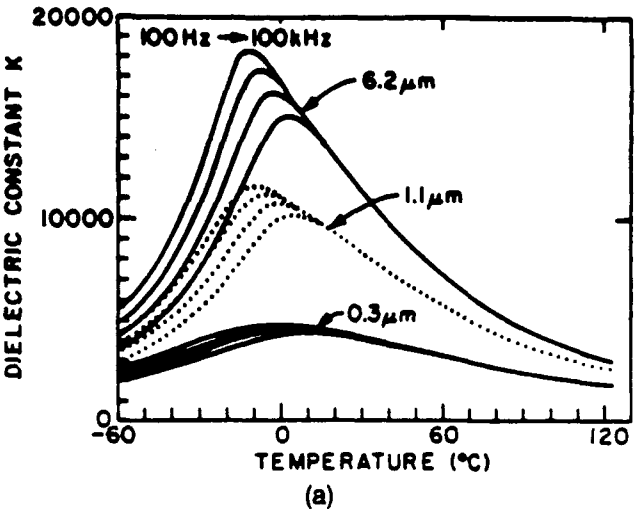

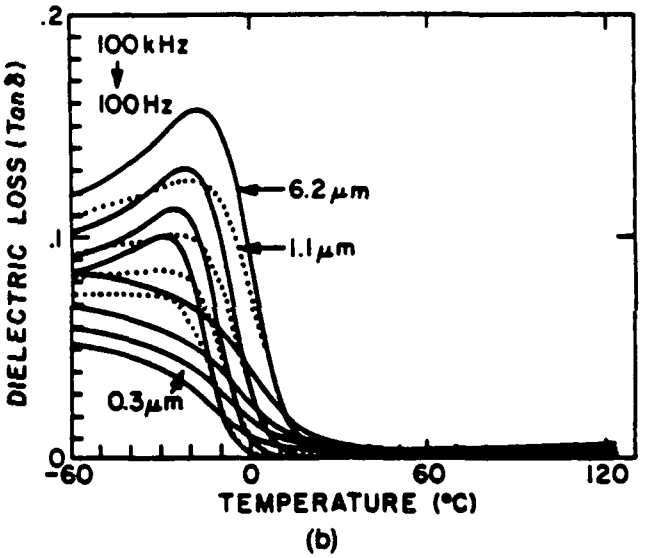

FIG. 4. Grain size effects on the dielectric properties: (a) dielectric constant versus temperature and (b) dielectric loss versus temperature.

conditions, was observed down to about the 1 μm grain size level. Deviations below 1 μm may be a result of limitations in the series diphasic mixing model used. As the volume of the low K phase increases, the model approaches the parallel case.

Though a low K grain boundary phase appears to explain adequately the observed grain size dependency, this concept cannot account for the extremely low dielectric values of the fine grain samples and the PMN powders where no grain boundaries are present. Limitations of the grain boundary concept are further shown by the observed shifts in T_m, as reported in Table II and shown in Figs. 4(a) and 6. The shifts in T_m were not only grain size dependent, but process related as well.

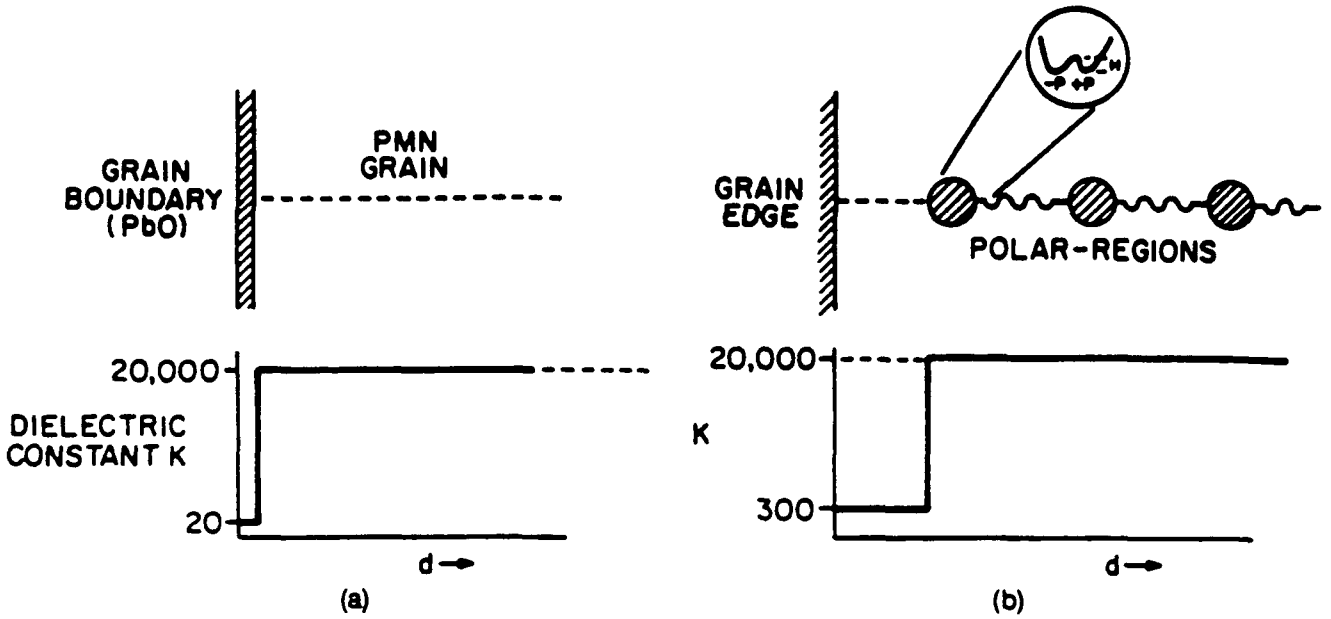

FIG. 5. Schematic one-dimensional representation of dielectric structure-property relationships for PMN: (a) PbO grain boundary concept and (b) microdomain perturbation concept.

Alternatively to the low K PbO-grain boundary phase, a second source of low polarizable phase region may be a consequence of the low processing temperatures used and high energy milling treatment of the powders, resulting in less developed crystallinity and/or defects (e.g., dislocations) located on grain or particle surfaces. The exact nature of surfaces of dielectric powders in relation to process conditions, unfortunately, is not well understood at this time.

An additional parameter that can lead to modification of the dielectric properties is stress. Studies on the pressure dependence of PbO-based relaxor materials show that by applying an isostatic pressure both K_m and T_m decrease.[25,26] Similar particle/grain size effects have been found for other perovskites where, with decreasing particle or grain size, the effective surface tensional stresses are believed to play an important role.[13]

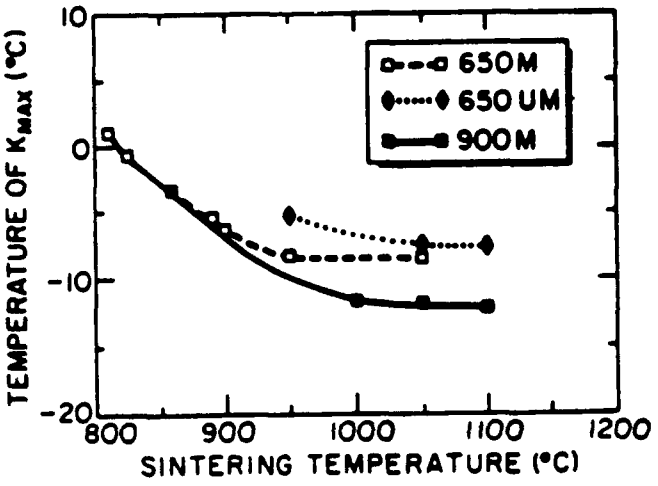

FIG. 6. Temperature of K_m versus sintering temperature.

In support of stress effects, Shrout *et al.*[20] found that by annealing sintered samples of PMN-based dielectrics, a dramatic increase in K was found. In this work, thermal annealing of a low K hot-pressed sample was tried, to emphasize further the effect of stress. By annealing for different periods of time at only 600 °C so as not to allow any microstructural charges or PbO loss, it was noted that for 24 h of thermal treatment, K_m did increase (see Table II). Annealing for one week, however, resulted in K_m decreasing slightly in comparison with the 24-h annealed sample. This result suggests the formation of a small amount of pyrochlore phase due to the long thermal treatment, though not detected by x-ray diffraction. However, in opposition to the role of stress on the dielectric behavior is the fact that T_{max} increases, not decreases, with decreasing grain size. It is also difficult to justify significant levels of internal stress in an isotropic material that doesn't exhibit a phase change upon cooling from thermal processing (calcining or sintering).

The particle and grain size dependency of the dielectric behavior in PMN can possibly be explained based on the intrinsic underlying mechanism(s) of relaxor behavior itself. Recent work by Viehland *et al.*[27] in advancing the understanding of Cross's superparaelectric theory suggests a microdipole-dipole cooperative interaction between superparaelectric regions which enhances K and accounts for the dispersive response. This interactive, or coherence, length maximizes near T_m on the order of 10–20 nm. Schematically shown in Fig. 5(b), coupling between microregions (superpara-

electric potentials) would be perturbed at grain boundaries or particle surfaces, resulting in essentially a low polarizable region. Naturally, as the scale of a PMN particle or grain approaches the interaction length, little volume or core of dielectrically active polar microregions would exist.

In terms of dielectric analysis, the series model given in Eq. (4), where R is now the ratio of grain size to the noninteracting "shell" region and K_{gb} replaced with K_{Shell}, again can be applied. Inserting values of K_{Shell} of ~300 and using an inactive shell region on the order of 15 nm, the dielectric constant of PMN (polycrystalline and/or particle) was determined as a function of size. The K_{Shell} value of ~300 was selected, being on the order of an incipient ferroelectric and as the value found for PMN at cryogenic temperatures (~1 K) where domain (micro and macro) effects would be frozen out.[28]

The calculated values as a function of grain and/or particle size are again equivalent to those determined for the series model shown in Fig. 3, being bent downward (below ~0.1 μm) if one assumes the grain size, in actuality, consists only of the "core" resulting in a closer fit to the experimental values.

In addition to the series model, dielectric values of PMN as a function of grain and/or particle size were determined based on Lichtenecker's logarithmic mixing rule given in Eq. (3) and now in the following expression:

$$\text{Ln } K_{PMN} = V_{Shell} \text{ Ln } K_{Shell} + V_{Core} \text{ Ln } K_{Core} \qquad (5)$$

where V_{Shell} and K_{Shell} and V_{Core} and K_{Core} are the volume and dielectric constants of the inactive "shell" and core regions, respectively. Inserting values of K_{Core} of 20 000, the single crystal K_{max} value of PMN, and a K_{Shell} of ~300 as above, the dielectric constant of PMN as a function of scale was calculated and represented by the log model in Fig. 3, showing excellent agreement to the experimentally found data. The logarithmic model's more realistic agreement may be related to the relatively large volume of the "shell" region and less disparity between the levels of K for the core and shell regions, both criteria for the series model.

As presented above, the intrinsic-microdomain perturbation concept, in general, can be used to interpret observed microstructural dependencies in PMN, including the scale of particles themselves.

Variations in the transition temperature T_{max} with scale can also be explained based on the above concept. For small grains and/or particles, the thermally active larger micropolar regions (volumes) are preferentially "locked-in." The larger regions are associated with the lower frequencies; hence, statistically more higher frequency regions (smaller volume) are thermally active at a given temperature and contribute to the dielectric polarizability. In effect, the Curie maxima appear to shift upward toward the high frequency realm; or in other words, T_m increases. This behavior is further shown in Fig. 4(b), where the dielectric loss and level of frequency dispersion is greatly reduced for the fine grain samples. Additional variations in the dielectric behavior presented in Table II and shown in Fig. 6 appear to be process related. Both the level of K_{max} and associated T_m appear to be a function of the calcination and milling conditions along with the sintering temperature. Such effects may be associated with defects introduced during milling or less developed crystallinity (lower processing temperatures) which may further perturb the shell region and its interaction with the core. The increased dielectric constant as a result of thermal annealing may effectively enhance the polarizability of the shell region through the elimination of defects. On a more intrinsic nature, process conditions may result in variations (size and distribution) of the nonstoichiometric ordered regions of Mg:Nb which are believed to localize the superparaelectric regions and hence the underlying relaxor behavior, as reported by Randall *et al.*[7] Defects and lower thermal processes would tend to enhance the nonstoichiometric ordering, increasing the diffuseness of the dielectric behavior, as was observed. Observation of the diffuseness change by TEM or any other characterization technique would be quite complex and could be a separate study.

IV. CONCLUSION

The dielectric properties of the relaxor $Pb(Mg_{1/3}Nb_{2/3})O_3$ were found to be dependent on the grain and/or particle size and secondarily on the overall process conditions (calcine and sintering conditions). The grain/particle dependency revealed that the dielectric constant K decreased, being less dispersive with decreasing scale, particularly as the size of the dielectric approached the underlying scale associated with relaxor ferroelectric behavior.

In addition to the observed K dependency, the temperature T_{max} increased with decreasing grain size. An intrinsic-microdomain perturbation concept was proposed to interpret the observed scaling and process related effects. In contrast to previous low polarizable grain boundary models, this model produced a better fit to the small grain/particle data.

ACKNOWLEDGMENTS

The authors wish to thank Beth Jones for her technical skills and Dr. P. Dougier and Dr. C. Randall for their encouragement and helpful discussions. We also thank Rhone-Poulenc Recherches, France, for making this work possible.

REFERENCES

[1]G. A. Smolenskii and A. I. Agranovskaya, Sov. Phys.-Tech. Phys. 3, 1380 (1958).
[2]G. A. Smolenskii and A. I. Agranovskaya, Sov. Phys.-Solid State 1 (10), 1429 (1959).
[3]T. R. Shrout and J. P. Dougherty, *Ceram. Trans.*, edited by M. Yan and H. C. Ling (Amer. Ceram. Soc., Columbus, OH, 1990), Vol. 8.
[4]S. Nomura and K. Uchino, Ferroelectrics 27, 31–34 (1982).
[5]G. A. Smolenskii, J. Phys. Soc. Jpn. (Suppl.) 28, 26 (1970).
[6]L. E. Cross, Ferroelectrics 76, 241–267 (1987).
[7]C. A. Randall, A. S. Bhalla, T. R. Shrout, and L. E. Cross, J. Mater. Res. 5, 829 (1990).
[8]E. Matijević, Mater. Res. Bull. XII, 18 (1989).
[9]P. Ravindranathan, S. Komarneni, and R. Roy, J. Am. Ceram. Soc. 73 (4), 1024 (1990).
[10]T. R. Shrout, P. Papet, S. Kim, and G. S. Lee, J. Am. Ceram. Soc. (1990).
[11]S. L. Swartz and T. R. Shrout, Mater. Res. Bull. XVII, 1245 (1982).
[12]J. H. Adair, A. J. Rose, and L. G. McCoy, *Advances in Ceramics*, edited by K. M. Nair (Am. Ceram. Soc., Columbus, OH, 1984), Vol. II, pp. 142–156.
[13]K. Uchino, "Particle/Grain Size Dependence of Ferroelectricity," Am. Ceram. Soc. Meeting, Indianapolis, IN (1989).
[14]R. E. Newnham, D. P. Skinner, and L. E. Cross, Mater. Res. Bull. XIII, 525 (1978).
[15]M. Lejeune, Ph.D. Thesis, Université de Limoges, France (1986).
[16]D. A. Payne and L. E. Cross, in *Ceramic Microstructures '76*, edited by R. M. Fulrath and J. A. Park (Westview Press, Boulder, CO, 1977), pp. 584–597.
[17]K. Lichtenecker, Phys. Z. 27, 115 (1926) (in German).
[18]H. Anderson, C. Tompkins, and F. Frantz, Tech. Rept., ECOM-02450-F, Fort Monmouth, NJ (1967).
[19]R. T. Jacobsen, Proc. Elect. Comp. Conf., 343 (1971).
[20]T. R. Shrout, U. Kumar, M. Megherbi, N. Yang, and S. J. Jang, Ferroelectrics 76, 479 (1987).
[21]D. N. Huang, Z. W. Yin, and L. E. Cross, Proc. 6th IEEE Int. Symp. Appl., Ferroelectrics, 159 (1986).
[22]A. J. Gorton, J. Chen, H. Chan, D. Smyth, and M. P. Harmer, Proc. 6th IEEE Int. Symp. Appl., Ferroelectrics, 150 (1986).
[23]A. Hilton, Ph.D. Thesis, University of Essex, England (1989).
[24]H. C. Wang and W. A. Schulze, J. Am. Ceram. Soc. 73 (4), 825 (1990).
[25]N. Yasuda, S. Fujimoto, and H. Terasawa, IEEE Trans. Ultr. Ferro. and Freq. Control 36, 402 (1989).
[26]B. J. Jin, Z. Y. Yin, X. Q. Wang, and S. H. Hu, Ferroelectrics 93, 391 (1989).
[27]D. Viehland, S. J. Jang, M. Wuttig, and L. E. Cross, Ferroelectrics (to be published).
[28]D. A. Ackerman, D. Moy, R. C. Potter, A. C. Anderson, and W. N. Lawless, Phys. Rev. B 23 (8), 3886 (1981).

APPENDIX 43

THERMAL DEGRADATION OF RELAXOR-BASED PIEZOELECTRIC CERAMICS

J. T. Fielding, Jr., S. J. Jang, T. R. Shrout,
Materials Research Laboratory
The Pennsylvania State University
University Park, PA

Abstract

The thermal degradation of dielectric and piezoelectric properties was investigated for relaxor ferroelectric compositions in the (1-x)$Pb(Mg_{1/3}Nb_{2/3})O_3$-(x)$PbTiO_3$ family near the morphotropic phase boundary. Degradation of the radial coupling factor k_p, piezoelectric charge coefficient d_{33}, and mechanical quality factor Q_m were observed to be less than expected based on temperature dependence of the polarization. It was suggested that the micropolar nature of the polarization allows restoration of piezoelectric properties after thermal exposures.

Introduction

Ferroelectric ceramics are utilized extensively in transducer applications. Presently, the lead zirconate titanate (PZT) family of ceramics are the most widely used owing to their excellent dielectric and piezoelectric properties at the morphotropic phase boundary (MPB). The anomalously large properties can be explained by the coexistence of tetragonal and rhombohedral phases, allowing increased domain reorientability and easier polarization.[1]

Excellent piezoelectric and dielectric properties are found in the relaxor ferroelectric based systems, such as.(1-x)$Pb(Mg_{1/3}Nb_{2/3})O_3$-$PbTiO_3$(x)(PMN-PT), (1-x)$Pb(Zn_{1/3}Nb_{2/3})O_3$-(x)$PbTiO_3$(PZN-PT), (1-x)$Pb(Ni_{1/3}Nb_{2/3})O_3$-Pb(Zr,Ti)O_3 (PNN-PZT), which also exhibit morphotropic phase boundaries.[2] The large dielectric properties and broad transition of complex perovskites with the general formula $Pb(B_1B_2)O_3$ were reported by Smolenskii in 1958.[3] These relaxor ferroelectric materials exhibit a broad phase transition and frequency dispersion of the maximum permittivity and dissipation factor. The development of phenomenological theory for relaxor ferroelectrics has been presented by Cross and others.[4]

Curiously, relaxor MPB transitions from ferroelectric to paraelectric occur in the narrow temperature range 150-180°C, considerably lower than those found for PZT based piezoelectrics. The lower T_C and hence narrower temperature usage range of relaxor based piezoelectrics is further complicated owing to their macro-micro depolarization behavior below T_{max}, which is not observed in normal piezoelectrics. It was believed that the effect of thermal degradation on this depolarization mechanism may limit the usefulness of relaxor based piezoelectrics in transducer applications.

Of interest for this work is the solid solution system (1-x)$Pb(Mg_{1/3}Nb_{2/3})O_3$-(x)$PbTiO_3$. The end member PMN is a relaxor ferroelectric, exhibiting a large dielectric constant and broad transition near -15 °C. $PbTiO_3$ is a normal ferroelectric with a transition at 490 °C. Choi et al. found the maximum piezoelectric properties in the PMN-PT system occur at the compositions with x~0.30-0.325 mole % $PbTiO_3$.[5] The PMN-PT phase diagram in the MPB region is shown in figure 1. Curvature of the MPB is observed with a proposed rhombohedral to tetragonal transition occurring at lower PT contents. This effectively lowers the T_c and maximum device operating temperatures to depolarization.

The loss of polarization, measured using pyroelectric measurement techniques, is useful in determining the critical temperature for thermal depolarization. Evaluating the dicontinuity in the behavior of the pyroelectric coefficient p (p=dP/dT, where P is polarization and T is temperature) and polarization, transition temperatures can be determined. Td is designated the depolarization temperature, where the spontaneous polarization vanishes.

The objective of this work was to examine the effect of exposure to elevated temperatures on dielectric and piezoelectric properties near the MPB and to discuss the mechanisms of thermal degradation involved as compared to normal ferroelectric materials, such as found in the lead zirconate system, which are nominally rated at 1/2 T_c for thermal usage.

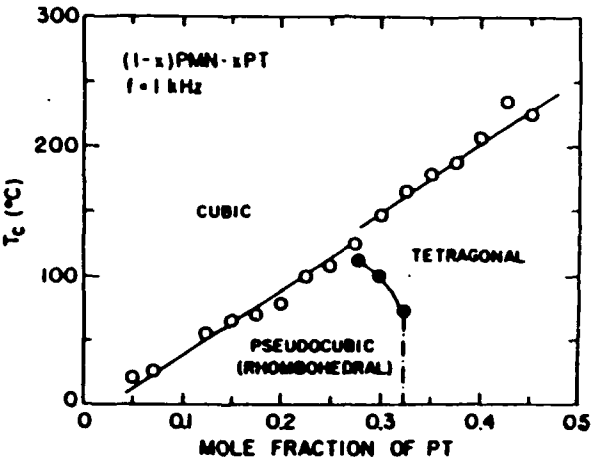

Figure 1. The phase diagram for the morphotropic phase boundary region for (1-x)$Pb(Mg_{1/3}Nb_{2/3})O_3$-(x)$PbTiO_3$ PMNsolid solution system. After Choi et al.[5]

Experimental

Sample Preparation

The (1-x)$Pb(Mg_{1/3}Nb_{2/3})O_3$-(x)$PbTiO_3$ compositions near the MPB with x = 0.28, 0.315, 0.365, and 0.4 were processed using the columbite precursor method described by Swartz and Shrout[6] with reagent grade raw materials. Rhombohedral compositions with x=0.28,0.315 are designated R-1 and R-2, respectively. Tetragonal compositions exhibitiing non-relaxor or normal behavior wiith x=0.365, 0.4 are designated T-1 and T-2.

Starting materials were mixed and vibratory milled using deionized water and polyelectrolyte dispersant for 18 hours. After drying, the mixture was calcined at 1100 °C for 4 hours to ensure columbite formation and phase purity. The columbite phase was formed in the reaction: $((1-x)/3)(MgO+Nb_2O_5)+(x)TiO_2 \Rightarrow (Mg_{1-x}Nb_{2-x}Ti_x)O_4$ Structure was confirmed by XRD analysis. Prior to reaction with PbO, the calcined powder was pulverized using a hammermill through a 0.5 mm screen to break up aggregates. $PbCO_3$ was added and then vibratory milled for 18 hours. After drying, the mixture was calcined at 800 °C for 4 hours. Information on structure and pyrochlore content was determined using XRD. The calculated pyrochlore content was less than 2%. The calcined material was then vibratory milled for 18 hours and dried. Acrylic binder was added to provide mechanical strength in the pressing operation.

Disks of 16 mm diameter were uniaxially pressed using a steel die at a pressure of 70 MPa. Binder burnout was accomplished using a heating rate of 2 °C/min. to 300 °C. Discs were sintered using closed high density alumina crucibles at 1250 °C for 4 hours. A PbO source material comprised of $PbZrO_3$ was used to maintain PbO

stoichiometry in the discs during sintering. Fired discs were lapped to 0.9 mm thickness and Au electrodes were applied using sputtering.

A commercial "soft" piezoelectric composition (UPI-501A, Ultrasonic Powders, Inc.) with well characterized properties was used for comparison. Disks were prepared using similar techniques as above.

Electrical Measurements

Dielectric properties were measured using a multifrequency LCR meter3 (Model 4274A, Hewlett Packard Co.). Values for the transition temperature T_{max} and peak dielectric constant K_{max} were determined using an automated measurement system consisting of a environmental chamber, interface and computer. The dielectric constant and dissipation factor were measured at a heating rate of 4 °C/min. at frequencies between 0.1 and 100 KHz.

The static Byer-Roundy technique for pyroelectric measurements was used to determine the pyroelectric coefficient, spontaneous polarization and depoling temperature, T_d. A heating rate of 2 °C/min. was used. Sample polarization was performed by applying a d.c. field of 20 kV/cm while cooling from above the transition temperature to -50 °C.

Resonant frequency measurements were made using a network analyzer (Model 3577A, Hewlett Packard Co.) configured for reflection . Appropriate standards were used in the calculation of radial coupling factor k_p and mechanical quality factor, Q_m.[7] The piezoelectric charge coefficient, d_{33}, was measured using a Berlincourt d_{33} meter (Model CP 3300, Channel Products, Chagrin Falls, OH). The elastic compliance s11E and poisson ratio σ were calculated according to the method described by Bogdanov.[8]

To determine the minimal thermal exposure time required to stimulate reproducible degradation of properties, the time dependence of thermal degradation mechanisms was also examined. From the pyroelectric data it was observed that 40-50% of the polarization is lost at temperatures approximately 75% of T_d. For rhombohedral compositons this temperature is in the region between the two pyroelectric peaks. Samples were held at temperatures approximately 75% of their respective T_{max} for periods of 0.5, 2, 6, 12, and 24 hours under short circuit conditions. The dielectric and related properties were measured 48 hours after removal from the test chamber.

Prior to thermal exposure, measurements were made 48 hours after poling to allow for aging that might normally occur. Dielectric constant, dissipation factor, d_{33}, piezoelectric coupling factor k_p were measured. Disks were thermally degraded under short circuit conditions in a temperature chamber using exposure times of 30 minutes and temperatures between room temperature and T_{max}. Dielectric and related properties were measured 24 and 48 hours after removal from the test chamber to determine the level of thermal degradation.

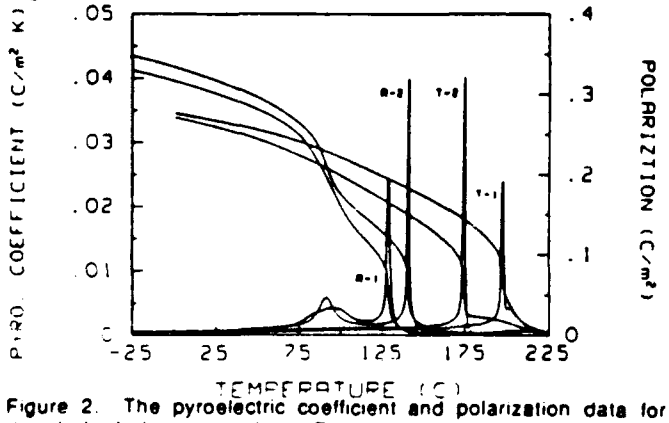

Figure 2. The pyroelectric coefficient and polarization data for rhombohedral compositions R-1, R-2 (x= 0.28, 0.315) and tetragonal compositions T-1, T-2 (x= 0.4, 0.365).

Results and Discussion

Pyroelectric coefficients and polarization behavior of the various materials are shown is in figure 2. Maximum pyroelectric coefficients were obtained at 135 °C and 139 °C for rhombohedral compositions R-1 and R-2; and 199 °C and 179 °C for tetragonal compositions T-1 and T-2. Polarization decreases continuously upon heating above room temperature. For rhombohedral compositions a discontinuous change is observed at the rhombohedral to tetragonal transition, approximately 90 °C, representing a 25 and 40% loss of polarization for compositons R-1 and R-2, respectively.

Initial values of dielectric properties, including unpoled and poled dielectric constant and dissipation factor, of the compositions evaluated are listed in Table I. The transition temperatures for dielectric and pyroelectric measurements are also listed. The values of T_{max} and T_d found are close together. Initial room temperature values of d_{33}, k_p, Q_m, N_p, Y_{11}^E, and σ are listed in Table II.

Table I. Dielectric Properties of Compostions Evaluated

Composition	x	K	D	K_{max}	T_{max} (°C)	Td (°C)
R-1	0.28	1800 (2500)*	0.018 (0.027)	33000 (33600)	139 (139.7)	129.0
R-2	0.315	2650 (2830)	0.015 (0.030)	43000 (43200)	144 (142.8)	141.3
T-1	0.40	2200 (2000)	0.011 (0.014)	29000 (30000)	202 (198.9)	197.7
T-2	0.365	3770 (2800)	0.011 (0.016)	28500 (30200)	180 (176.5)	174.8
PZT-5A		1720 1380	0.019 0.023			

*Unpoled values in parentheses.

Table II. Piezoelectric and Elastic Properties of Compositions Evaluated

Composition	x	d_{33} (pC/N)	k_p	Q_m	N_p (Hz m)	Y_{11}^E ($x10^{10}N/m^2$)	σ
R-1	0.28	395	0.58	120	2140	7.34	0.30
R-2	0.315	630	0.64	92	1990	7.38	0.23
T-1	0.40	318	0.45	95	2320	8.29	0.325
T-2	0.365	528	0.57	94	2130	6.75	0.34
PZT-5A		445	0.65	78	2020	6.26	0.32

The degradation of dielectric and piezoelectric properties with time indicated that maximum service temperature was more important than the time at temperature. The degradation of properties was only moderately sensitive to exposure time. The degradation of K, k_p and d_{33} for times between 0.5 and 24 hours was examined. The rhombohedral compositions exhibited a greater degradation of properties than the tetragonal ones.

The effect of of thermal degradation at different temperatures on the dielectric constant is shown in figure 3. Rhombohedral compositions show a large increase in K up to temperatures near the transition temperature, then a decrease. The PZT composition shows an increase in K and then a decrease above 75% T_C, similar to the behavior exhibited by compostion R-1. The observed increase in K is probably due to an extrinsic contribution. Tetragonal compositons show a minimal degradation up to temperatures near T_c. Examining the percent change in K as a function of transition temperature, shown in figure 3b, the tetragonal compositons exhibit minimal temperature degradation nearly up to T_C.

The effect of temperature on radial coupling factor k_p is shown in

figure 4. The coupling factor vanishes at the depoling temperature T_d. At temperatures below T_d, the degradation of the coupling factor is less than expected for the loss in polarization observed in the pyroelectric data. The degradation as a function of transition temperature, shown in Figure 4b, shows that the rhombohedral composition R-1 and PZT exhibit pronounced degradation at temperatures beyond 80% T_c. This also indicates a extrinsic contribution to the polarization.

The thermal degradation of the piezoelectric charge coefficient d_{33} is observed in figure 5. Again the degradation is less than expected for the loss in polarization observed in the pyroelectric runs. When the change in d_{33} is evaluated as a funtion of transition temperature, as shown in figure 5b, degratdation becomes significant at temperatures above 80% T_c for composition R-2 and PZT.

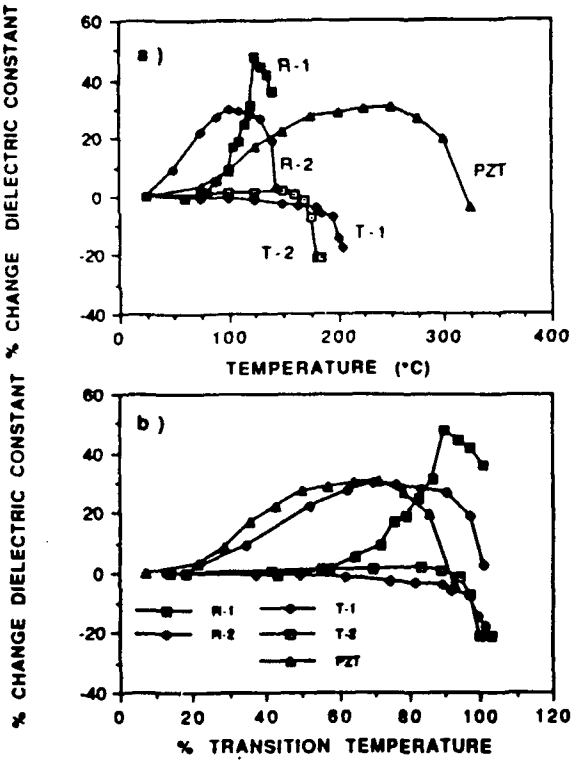

Figure 3. The % change in dielectric constant for rhombohedral compositions R-1, R-2 and tetragonal compositions T-1, T-2: a) as a function of temperature ; b) as a function of % transition temperature.

The effect of temperature on the mechanical quality factor Q_m is shown in figure 6. The tetragonal compostions exhibit increasing Q_m with temperature up to nearly T_d, and then a large increase. The rhombohedral compositons exhibit a rapidly decreasing Qm above 75 °C. The Q_m for PZT remains insensitive to temperature up to nearly T_C. Calculations of elastic constants showed that Y_{11}^E increased slightly (3%) at the transition temperature. The elastic constants for the tetragonal compositions were relatively insensitive to temperature.

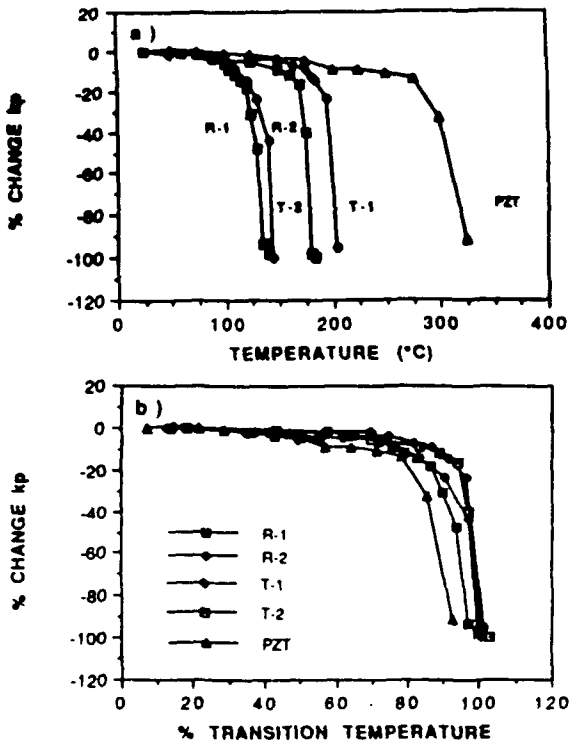

Figure 4. The % change in radial coupling factor k_p for rhombohedral compositions R-1, R-2 and tetragonal compositions T-1, T-2: a) as a function of temperature ; b) as a function of % transition temperature.

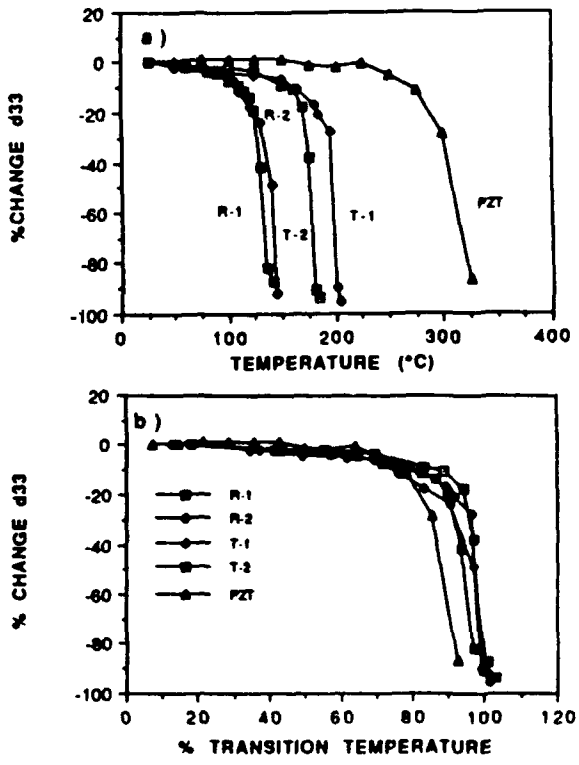

Figure 5. The % change in d_{33} piezoelectric charge coefficient for rhombohedral compositions R-1, R-2 and tetragonal compositions T-1, T-2: a) as a function of temperature ; b) as a function of % transition temperature.

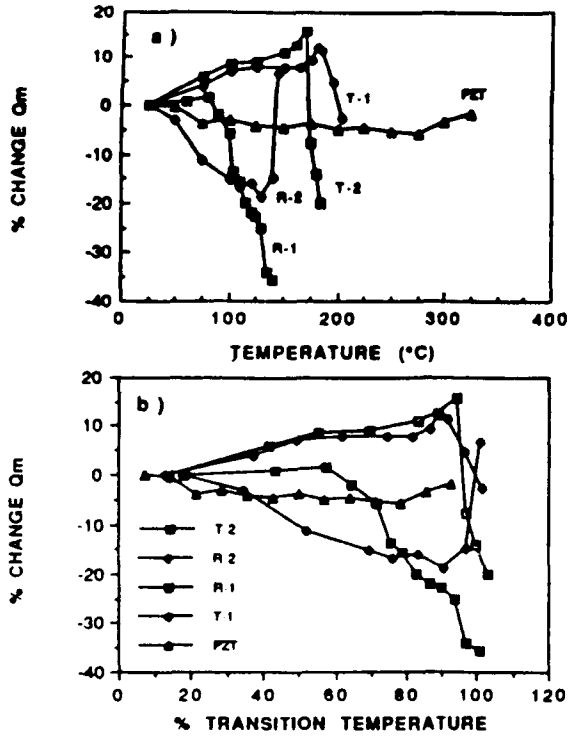

Figure 6. The % change in mechanical quality factor, Q_m, for rhombohedral compositions R-1, R-2 and tetragonal compositions T-1, T-2: a) as a function of temperature ; b) as a function of % transition temperature.

The effect of temperature on radial frequency constant Np is shown in figure 7. The frequency is constant is relatively insensitive to temperature up to temperatures near the transition for tetragonal compostions and rhombohedral compositon R-1. The relative insensitivity of Np as a function of transition temperature is shown in figure 7b. The PZT commercial composition exhibits a greater temperature dependence than the relaxor-based PMN MPB compositions.

The degradation of piezoelectric properties in the relaxor ferroelectrics was less than expected from an examination of the polarization behavior alone. At temperatures below the depoling temperature, T_d, the properties are nearly restored after equilibrating at room temperature. This may be due to the polarization mechanisms associated with the relaxor materials. The macropolar regions measured at room temperature become smaller and uncoupled in an nonpolar matrix at elevated temperatures. This would agree with the pyroelectric data. But at exposure temperatures below T_d, upon cooling the micropolar regions are still aligned and coalesce to reform macropolar regions, exhibiting only a small degradation in piezoelectric properties.

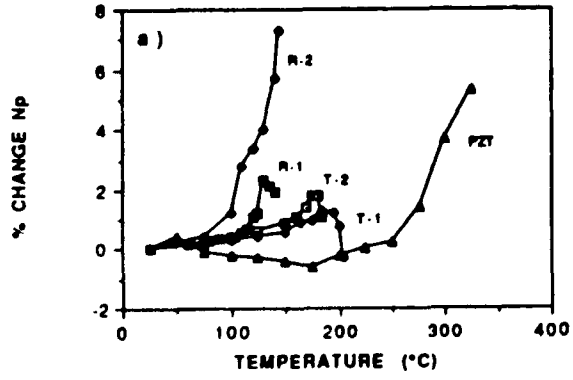

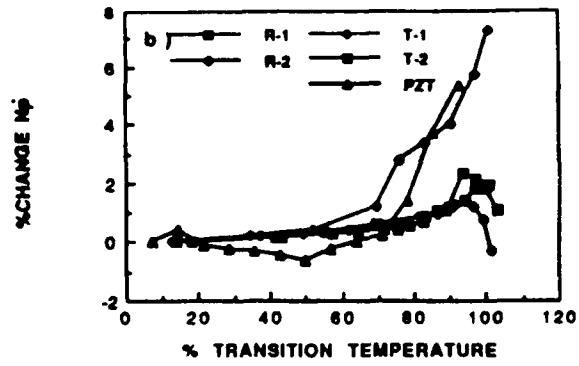

Figure 7. The % change in radial frequency constant N_p for rhombohedral compositions R-1, R-2 and tetragonal compositions T-1, T-2: a) as a function of temperature ; b) as a function of % transition temperature.

Summary

Due to the difference in polarization arrangements in normal and relaxor based piezoelectrics, it was desired to establish the temperature dependence of critical piezolectrc properties. Using this data operating temperature ranges can be established. The transition temperatures are considerably lower thant those found in PZT based piezoelectrics, but the degree of degradation as a function of transition temperature is similar. The thermal degradation of piezoelectric and dielectric properties was investigated for four compositions near the morphotropic phase boundary in the $(1-x)Pb(Mg_{1/3}Nb_{2/3})O_3$-$(x)PbTiO_3$ complex perovskite system. A commercial PZT based piezoelectric was used to contrast the degradation in properties. The effect of temperature on dielectric constant is negligible for tetragonal compositions. For rhombohedral compositions, there is a large increase up to approximately 75% of T_C and then K decreases. The radial coupling factor and d33 piezoelectric charge coefficient are insensitive to temperature up to 90% of T_C. Above this temperature there is a rapid loss finishing in complete depolarization at T_d.

References

1. B. Jaffe, W.R. Cook, H. Jaffe, Piezoelectric Ceramics, Ch 7 New York Academic Press 1971.
2. S.T. Chung, K. Nagata and H. Igarishi,"Piezoelectric and Dielectric Properties of PNN-PZN-PZ-PT System Ceramics," Ferroelectrics, 94, 243-247, 1989.
3. G.A. Smolenskii and A.I. Agranovuskaya, "Dielectric Polarization of a Number of Complex Compounds", Soviet Physics-Solid State 1, 1429-1437 (1959).
4. L.E. Cross, "Relaxor Ferroelectrics," Ferroelectrics, 76, 241-267 (1987).
5. S.W. Choi, T.R. Shrout, S.J. Jang and A.S. Bhalla, "Dielectric and Pyroelectric Properties of PMN-PT Solid Solution", Ferroelectrics, 100, pp229, 1990.
6. S.L. Swartz and T.R. Shrout, "Fabrication Of Perovskite Lead Magnesium Niobate", Materials Research Bulletin, 17, 1245 (1982).
7. IRE Standards on Piezoelectric Crystals: Measurement of Piezoelectric Ceramics, 61 IRE14.S1 Proceed. IRE 49 1161-69 (1961).
8. S.V. Bogdanov and A.M. Timonin, "On a Method of Calculating Piezomoduli from the Radial Vibrations of a Disk", Izv.Akad. Nauk SSSR, Tom 21 (3) p 397 1957 (in Russian).

APPENDIX 44

RELAXOR BASED FINE GRAIN PIEZOELECTRIC MATERIALS

N. Kim, S. J. Jang, and T. R. Shrout
Materials Research Laboratory
The Pennsylvania State University
University Park, PA. 16802

Abstract

The dielectric and piezoelectric properties of polycrystalline ceramics of relaxor ferroelectric lead magnesium niobate-lead titanate modified with La_2O_3, $(1-x)(Pb_{0.985}La_{0.01}\square_{0.005}(Mg_{1/3}Nb_{2/3})$-$(x)PbTiO_3$, have been investigated. The compositional range of $0.2 \leq x \leq 0.4$, being near the morphotropic phase boundary, was characterized.

Lanthanum doping resulted in reduction of grain size, enhanced density, and shifted the dielectric maximum temperature downwardly. The final microstructures of all compositions were fine ($\leq 1\mu m$) with uniform grain size distributions. Room temperature dielectric constants Ks of 5,000 and piezoelectric constants $d_{33(s)}$ of 500 pC/N were found for compositions near the morphotropic phase boundary ($x \approx 0.33$).

Based on this investigation, La doped PMN-PT compositions appear to be promising candidate materials for high dielectric constant fine-grained piezoelectric applications.

Introduction

Perovskite lead magnesium niobate $Pb(Mg_{1/3}Nb_{2/3})O_3$, hereafter abbreviated PMN, belongs to a class of ferroelectric materials which exhibit a diffuse phase transition known as relaxor ferroelectrics[1]. The dielectric behavior of these materials have been widely investigated in both single crystal and polycrystalline ceramic forms since first synthesized by Soviet workers in the late 1950's.

PMN forms a solid solution with the normal ferroelectric $PbTiO_3$ (PT) (Curie temperature, $T_c \sim 490$ °C), allowing its transition to be raised to near room temperature with only small amounts of PT (< 10 mole %). Within the PMN-PT solid solution series, there exists a morphotropic phase boundary (MPB) near 33 mole % PT, separating rhombohedral and tetragonal phases[2]. In single crystals as well as the polycrystalline materials, compositions near the MPB exhibit unusually large dielectric and piezoelectric properties, similar to those observed in other lead based ferroelectrics such as $Pb(Zr_xTi_{1-x})O_3$ (PZT) and relaxor-$PbTiO_3$ systems, e.g., $Pb(Ni_{1/3}Nb_{2/3})O_3$-$PbTiO_3$ (PNN-PT) and $Pb(Zn_{1/3}Nb_{2/3})O_3$-$PbTiO_3$ (PZN-PT). It is interesting to note that all relaxor-PT MPB compositions have T_{max}'s in the range of 150 °C ~ 180 °C, giving rise to a question of the underlying mechanism which is not fully understood at this time.

In recent years, device technology has being greatly developed for various applications and the scale of such devices including multilayer capacitors, electrostrictors, and piezoelectric transducers are getting smaller. Thus, fine grain size (< 1 μm) materials with high dielectric constant and piezoelectric activity are desired.

In conventional PZT piezo-materials, smaller grains tend to clamp out extrinsic contributions such as domain wall motion. Microstructural dependency on the properties is not expected in PMN-based ceramics since the underlying phenomena associated with relaxor ferroelectric behavior is on the order of ~ 10 nm^3. Observed grain size effects in relaxor materials have been attributed to a low dielectric constant grain boundary phases which dilute the properties, however, can be annealed out.

In previous work[4, 5], La additions to PMN and its solid solution were shown to promote densification while inhibiting grain growth and reducing the level of PbO volatility, similar to that found in La-doped lead zirconia titanate ceramics. Also, through hot isostatic pressing, optically transparent materials have been achieved, allowing the determination of various optic and electro-optic properties. This purpose of work was to use La to inhibit grain growth of MPB compositions for fine grain size piezoelectric materials.

Experimental Procedure

Several compositions of lead magnesium niobate-lead titanate solid solution were selected across PMN-PT morphotropic phase boundary. Polycrystalline ceramic samples were prepared by solid state reaction using the columbite method described in previous referrence[4]. In this work, a small amount (1 mole %) of La was found to inhibit grain growth. Since it lowers T_{max} ~25 °C/mole %, we desired the minimal amount of La so as to broaden out working temperature range. To obtain a fine powder size, the calcined materials were vibratory milled. The milled particle size was 0.5 μm with a surface area 1.6 m^2/g.

Discs were prepared using polyvinyl alcohol (PVA) binder followed by burnout prior to sintering. Pellets of 16 mm in diameter and 2~3 mm thick were pressed at 10 MPa. The binder was burned out by a slow

Table 1. Physical Properties of La-doped PMN-PT ceramics

Composition PMN-PT (X : Y)	Firing (°C/hour)	Density (g/cm^3)	Theoretical density (g/cm^3)	Grain size (μm)
100:0	1100/4	7.80	8.15	2.0
	1200/4	7.82	"	3.2
93:07	1100/4	7.78	8.15	1.2
	1200/4	7.81	"	2.4
80:20	1100/4	7.78	8.14	0.7
	1200/4	7.81	"	1.6
75:25	1100/4	7.82	8.13	0.7
	1200/4	7.84	"	1.5
70:30	1100/4	7.78	8.12	0.7
	1200/4	7.81	"	1.7
65:35	1100/4	7.76	8.10	0.7
	1200/4	7.82	"	1.8
60:40	1100/4	7.80	8.09	0.6
	1200/4	7.85	"	1.5

heating process at 350 °C for 180 minutes and then 600 °C for 180 minutes. Samples were placed on platinum foil in closed alumina crucibles and sintered at temperatures of 1100 °C and 1200 °C for 4 hours. The desired PbO rich atmosphere was maintained by placing small amounts of an equimolar powder mixture of PbO and ZrO_2 in a small platinum boat. A heating rate of 900 °C/1 hour was used to further help prevent the loss of PbO.

Weight loss, geometrical density and grain size were determined for all the various compositions and firings. Powder X-ray diffraction (XRD) patterns of calcined and sintered powders were analysed for the presence of pyrochlore. The grain sizes were determined using the line intercept method on fractured or polished surfaces monitored by SEM. The observed grain sizes were similar from both fractured and polished surfaces as found in La-doped PZT ceramics.

In preparation for dielectric and piezoelectric measurements, samples were ground and electroded with sputtered goled. An air dry silver paste was also applied to the goled sputtered surface to insure good electrical contact. The dielectric measurements were carried out with an automated system consisting of a temperature control box and LCR meter. Dielectric constant and dissipation factor were measured pseudo-continuously at various frequencies as the samples were heated from -50 °C to 200 °C at a rate of 2 to 4 degrees per minutes.

In the case of piezoelectric measurements, optimum poling was performed on selected samples by cooling from above the transition temperature in a stirred oil bath to room temperature in air with an applied electric field of 30 kV/cm. The piezoelectric d_{33} coefficients were measured on disk samples using a Berlincourt d_{33} meter. The planar coupling factor, k_p, mechanical quality factor, Q_m, and frequency constant, N_p, were calculated using a resonance method which is based on the IEEE standard on piezoelectricity. In this set up, an impedance analyzer (Model 4192A, Hewlett Packard, Inc.) was controlled by a desk top computer (Model 9816, Hewlett Packard Inc.). By examing the variation of conductance verse frequency and capacitance frequency, the pertinent material parameters were determined. These values were then used to calculate piezoelectric coefficients.

Results and Discussion

Physical Properties

Physical properties for selected PMN-PT-La samples are reported in Table 1. As tabulated, the resulting densities were greater than 95 % theoretical, being 8.15 g/cm^3 for PMN-La. Densities increased with firing temperature up to 1200 °C due to removal of free PbO and porosity. As reported in Table 1, the addition of La to PMN-PT solid solutions was found to inhibit grain growth as expected. A narrow range in grain sizes (0.5 ~ 3 μm) was found for all the various compositions and firings. Typical SEM photomicrographs of fractured surfaces with fine grain (<1 μm) are shown in Figure 1. This behavior can be explained by solid solution impurity drag mechanism[6]. This proposed model implies that more La ions concentrate near grain boundaries than inside bulk grains and react with defects in the grain boundaries such as pyrochlore, lead vacancies, oxygen vacancies, and impurities and substantially reducing the grain boundary mobility or grain growth rate. This kind of behavior was also observed in several systems in PLZT[7], Bi-doped PZT[8], and La-doped $PbNb_2O_6$ ceramics[9].

Extensive work was carried out to achieve fine grain and high density ceramics, especially for compositions near MPB. Annealing studies were performed in order to optimize longer sintering times and annealing to eliminate PbO in the grain boundaries without changing firing temperatures. As listed in

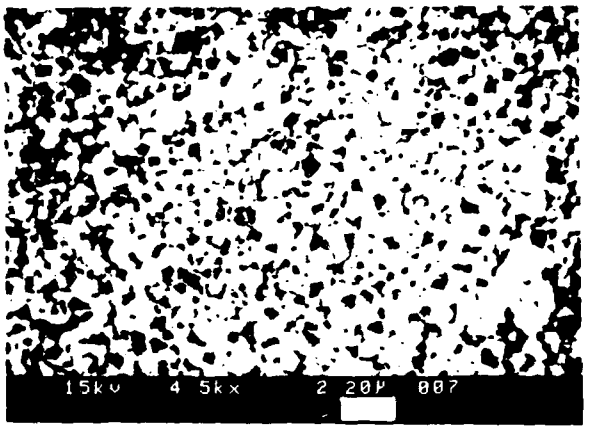

Figure 1. SEM photomicrographs of fractured surface of La-doped PMN-PT (70:30) (sample fired 1100 °C/10 hour).

Table 2. Physical properties of La-doped PMN-PT ceramics near MPB for optimizing fine-grained materials

Composition PMN-PT (X:Y)	Firing (°C/hour)	Weight Loss after firing (wt %)	Annealing (°C/hour)	Weight Loss after anneal (wt %)	Density (g/cm^3)	Grain size (μm)
75:25	1100/4	1.5	--	--	7.78	0.8
70:30	1100/4	1.4	--	--	7.80	0.7
75:25	1100/4	1.5	900/10	0.2	7.80	0.8
70:30	1100/4	1.4	900/10	0.15	7.84	0.7
75:25	1100/10	1.8	--	--	7.88	1.0
70:30	1100/10	2.0	--	--	7.87	0.9
75:25	1100/10	1.7	900/10	0.09	7.9	1.2
70:30	1100/10	2.0	900/10	0.1	7.92	1.0

Table 2, the densities were found to increase after annealing and long firing time without significantly changing grain size. In addition, all samples after annealing showed slight weight losses. This is believed to be due to the free PbO in the grain boundaries and the triple points[10]. In the PMN-PT-La solid solution region, the microstructures were found to be similar with fine grain size (< 1 μm) for the compositions studied up to 40 mole % PT. Also, ceramics containing higher amounts of La (≥ 1 mole %) were found to possess similar grain sizes and microstructures. This indicates that only a small addition of La is sufficient to inhibit grain growth and hence less affecting the dielectric and related behavior.

Dielectric Behavior

Unpoled and poled dielectric behavior of fine-grained (<1 μm) ceramics are plotted in Figures 2 and 3. Upon poling, no significant change of K_{max}'s were observed, while slightly shifting T_{max}'s to higher temperatures. However, the dielectric constants at room temperature (K_{RT}) were found to change significantly after poling. The K_{RT} near MPB increased upon poling, in contrast of a reduction observed with both rhombohedral (80/20/1) and tetragonal (60/40/1) phase regions. These observation may be explained as follows. Compositions near MPB are considered mixed phases (rhombohedral and tetragonal) and therefore have numerous poling directions. Thus, these compositions can allow higher piezoelectric coupling during poling, giving rise to an increased dielectric constant (K_{RT}) upon poling as presented in the following equation, $K^T = K^S/(1 - k_p)^2$, where "K^T and K^S" are the poled (free) and unpoled (clamped) dielectric constant, respectively and "k_p" is the piezoelectric planar coupling factor[11]. High k_p was indeed observed with compositions near MPB. In case of rhombohedral and tetragonal phases, other effects would strongly dominate than piezoelectric coupling such as intrinsic anisotropy or induced strain in which both effects result in reduction of the dielectric constant upon poling.

The dielectric losses at room temperature were also found to be reduced upon poling in all compositions. It is believed that the dielectric loss generally comes from macrodomain wall motions. The domains can fixed by electric field poling, resulting in less domain wall motions and thus less dielectric losses.

Piezoelectric Property

The observed piezoelectric properties (d_{33}, Q_m, k_p, and N_p) of fine-grained (< 1 μm) ceramics as a function of PT are plotted in Figures 4 and 5. As shown, high piezoelectric coefficients were found for compositions near MPB. The maximum piezoelectric d_{33} coefficient and planar coupling factor k_p were observed near MPB, in contrast of minimum frequency constant N_p. However, the mechanical quality factor Q_m's were found to be similar along all compositions. This is probably due to the "soft" nature of La-doped PMN-PT ceramics as found in PZTs.

The piezoelectric coefficient d_{33} increased with firing temperature, indicating a slight grain size dependence as presented in Table 4, as similar to that found in undoped PMN-PT ceramics, which was believed due to PbO grain boundary phases[10].

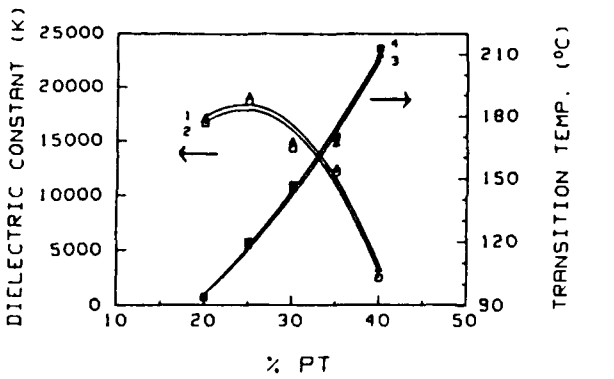

Figure 2. Max. dielectric constant (K_{max}) at 1 kHz and Temp. of dielectric max. (T_{max}) (1, 3: unpoled and 2, 4: poled) as a function of $PbTiO_3$.

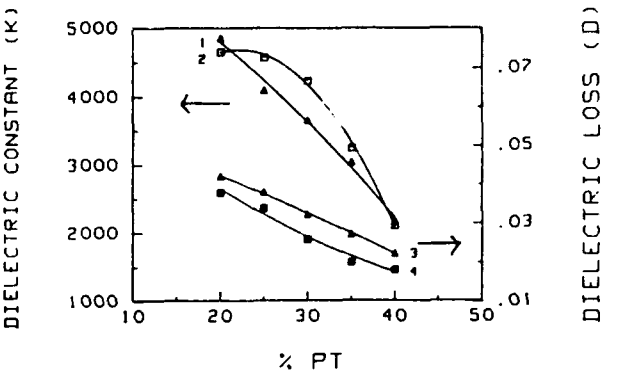

Figure 3. Dielectric constant . (K_{RT}) and dielectric loss at room temp. (1, 3: unpoled and 2, 4: poled) as a function of $PbTiO_3$.

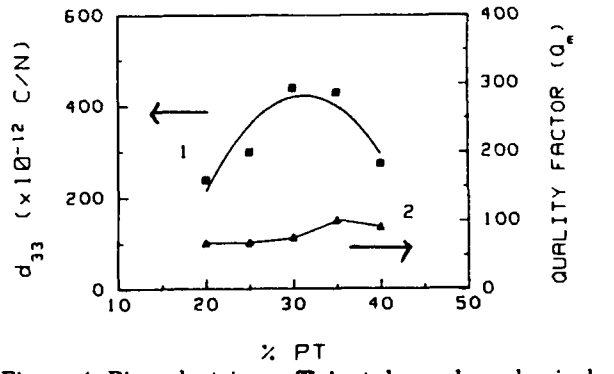

Figure 4. Piezoelectric coefficient d_{33} and mechanical quality factor Q_m as a function of $PbTiO_3$.

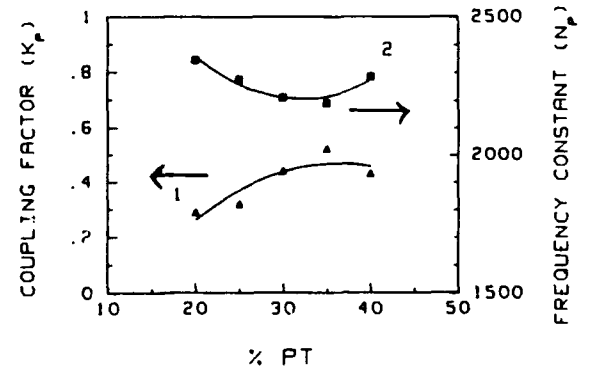

Figure 5. Piezoelectric planar coupling factor k_p and frequency N_p as a function of $PbTiO_3$.

Annealing

Extensive work was carried out on compositions near MPB in order to optimize the dielectric and piezoelectric properties without changing grain size (<1 μm). As presented in Tables 5 and 6, the dielectric and piezoelectric properties were found to increase after long firing and annealing similar to that observed in $Pb(Zn_{1/3}Nb_{2/3})$-$BaTiO_3$-$PbTiO_3$ (PZN-BT-PT) ceramics[12]. This is believed to be due to the amorphous PbO grain boundary phases, which affect poorly not only dielectric but also piezoelectric properties.

After long time firing and annealing, the best values obtained in composition (70/30/1) near MPB as follows: the maximum dielectric constant reached ~ 20,000 with a room temperature dielectric constant of 4,600 (poled), maintaining a fine and uniform grain size (< 1 μm). The piezoelectric coefficients obtained were d_{33}=510 pC/N, k_p=0.56, Q_m=63, and N_p=2,180.

The observed piezoelectric properties are similar to that of "soft" PZT ceramics, however, which have generally large grain sizes (3 ~ 10 μm) due to their high firing temperatures. It is believed that high piezoelectric properties with fine-grained ceramics can be possible in La-doped PMN-PT system.

Table 3. Piezoelectric coefficient d_{33} of La-doped PMN-PT ceramics

Composition PMN-PT (X:Y)	Firing (°C/hour)	Grain size (μm)	d33 (pC/N)
80:20	1100/4	0.7	210
	1200/4	1.6	360
75:25	1100/4	0.7	240
	1200/4	1.5	480
70:30	1100/4	0.7	310
	1200/4	1.7	560
65:35	1100/4	0.7	270
	1200/4	1.8	440
60:40	1100/4	0.6	200
	1200/4	1.5	250

Summary

Lanthanum was used to inhibit grain growth in PMN-PT solid solution compositions near MPB in order to fabricate fine grain size (<1 μm) piezo ceramics. As expected, anomalously high piezoelectric properties were observed with compositions near MPB, giving rise to confirm again the position of MPB. Annealing studies were carried out to optimize the dielectric and piezoelectric properties without changing the grain size. The dielectric and piezoelectric properties were greatly improved after long firing and annealing, being related to the reduction in the amorphous PbO grain boundary phase(s) as observed in other systems. Grain size dependencies are not anticipated in relaxor feroelectrics because the origin of macro-micro domain appearence is on the nanoscale well below grain size's.

The observed high piezoelectric properties with compositions near MPB are similar to those of larger grain size "soft" PZT ceramics. Through the use of La modifications, PMN-PT based ceramics with well developed fine grain microstructures for device applications such as multilayer capacitors, actuators, and piezoelectric transducers appear promising.

References

[1] L. E. Cross, S. J. Jang, R. E. Newnham, S. Nomura, and K. Uchino, "Large electrostrictive effects in relaxor ferroelectrics," *Ferroelectrics*, 23, p. 187, 1983.

[2] S. W. Choi, T. R. Shrout, S. J. Jang, and A. S. Bhalla, "Dielectric and pyroelectric properties in the PMN:PT system," *Ferroelectrics*, 100, p. 29, 1990.

[3] C. A. Randall, A. S. Bhalla, T. R. Shrout, and L. E. Cross, "A discussion of complex lead perovskite ferroelectrics with regard to B-site cation order," to be published, 1990.

[4] N. Kim, W. Huebner, S. J. Jang, T. R. Shrout, "Dielectric and Piezoelectric Properties of Lanthanum-modified Lead Magnesium Niobate-Lead Titanate Ceramics," *Ferroelectrics*, 93, p. 341, 1989.

[5] N. Kim, D. A. McHenry, S. J. Jang, T. R. Shrout, "Fabrication of Optically Transparent Lead Magnesium Niobate Polycrystalline Ceramics using Hot Isostatic Pressing," *J. Am. Cerm. Soc.*, 73[4] p. 928, 1990.

[6] R. J. Brook, "Impurity Drag effect and grain growth kinetics," *Scr. Met.*, 2[7] p. 355, 1968.

[7] R. A. Langman, R. B. Runk, and S. R. Butler, "Isothermal grain growth of pressure sintered PLZT ceramics," *J. Am. Cerm. Soc.*, 56[9], p. 486, 1973.

Table 4. Unpoled and poled dielectric properties of La-doped PMN-PT (70:30) ceramics

Firing Condition (°C/hour)	Unpoled State				Poled State			
	K_{RT}	tanδ	K_{max}	T_{max}	K_{RT}	tanδ	K_{max}	T_{max}
1100/4	3,730	0.031	14,000	144 °C	4,330	0.026	13,700	146 °C
1100/4 & anneal 900/10	3,650	0.032	16,500	144 °C	4,240	0.025	15,800	147 °C
1100/10	3,520	0.031	19,800	143 °C	4,300	0.027	19,300	145 °C
1100/10 & anneal 900/10	3,750	0.032	20,500	143 °C	4,600	0.028	19,900	145 °C

Table 5. Piezoelectric properties of La-doped PMN-PT ceramics near MPB

Firing (°C/hour)	Composition PMN-PT	Grain size (μm)	d_{33} (pC/N)	k_p	Q_m	N_p (mHz)
1100/4	75:25	0.8	230	0.28	70	2300
	70:30	0.7	370	0.39	68	2250
1100/4 & anneal 900/10	75:25	0.8	275	0.30	68	2290
	70:30	0.7	440	0.44	68	2235
1100/10	75:25	1.0	350	0.38	67	2280
	70:30	0.9	480	0.51	65	2210
1100/10 & anneal 900/10	75:25	1.2	400	0.43	67	2265
	70:30	1.0	510	0.56	63	2180

[8] G. H. Haertling, "Grain growth and densification of hot pressed lead zirconate - lead titanate ceramics containing Bismuth," *J. Am. Cerm. Soc.*, 49[3], p. 113, 1966.

[9] G. S. Lee, Y. S. Kim, S. J. Jang, and T. R. Shrout, "Grain Growth control and Properties of Impurity doped Lead Barium Niobate Piezoelectric ceramics," presented at 92th Am. Cerm. Soc. Meet., at Dallas, TX., 1990.

[10] A. D. Hilton, C. A. Randall, D. J. Barber, and T. R. Shrout, "TEM studies of $Pb(Mg_{1/3}Nb_{2/3})O_3$ - $PbTiO_3$ ferroelectric relaxors," *Ferroelectrics*, 93, p. 379, 1989.

[11] B. Jaffe, W. R., Cook, and H. Jaffe, "*Piezoelectric ceramics*," Academic Press, New York, 1971.

[12] J. Belsick, "Phase relations, dielectric and piezoelectric properties of ceramics in the system lead zinc niobate - barium titanate - lead titanate," M.S. Thesis, The Pennsylvania State University, 1989.

APPENDIX 45

Ferroelectrics Letters, 1990, Vol 12, pp. 55-62
Reprints available directly from publisher
Photocopying permitted by license only

PREPARATION AND CHARACTERIZATION OF INDIUM BASED COMPLEX PEROVSKITES - Pb(In1/2Nb1/2)O3 (PIN), Ba(In1/2Nb1/2)O3 (BIN), AND Ba(In1/2Ta1/2)O3 (BIT).†

F.G. JONES, C.A. RANDALL, S.J. JANG, and T.R. SHROUT
Center for Dielectric Studies
Materials Research Laboratory
The Pennsylvania State University
University Park, PA 16802

(Received for Publication August 22, 1990)

Abstract The processing of order-disorder perovskites $Ba(In_{1/2}Nb_{1/2})O_3$ (BIN), $Ba(In_{1/2}Ta_{1/2})O_3$ (BIT), and the lead analogue $Pb(In_{1/2}Nb_{1/2})O_3$ (PIN) was investigated with an emphasis on improving and expanding our knowledge of microwave dielectric materials. Both BIN and BIT were shown to be paraelectric perovskites. The processing and annealing of PIN were related to the perovskite and its transformation to pyrochlore. Dielectric and physical characteristics were examined by X-ray diffraction profiles (XRD), scanning electron microscopy (SEM), and dielectric behavior. Attempts to enhance B-site cation order in PIN by thermal annealing were unsuccessful due to a pyrochlore formation.

INTRODUCTION

Recently, dielectric materials for microwave resonators have become of interest in satellite communications. These materials require relatively high dielectric constant, low dielectric loss, as well as a temperature stability in the microwave frequency regime of 50MHz to 20GHz. Wakino (1986)[1] has outlined a number of possible candidate materials that are predominately in the paraelectric perovskite family. These include $CaTiO_3$, $BaZrO_3$, $Ba(Zn_{1/3}Ta_{2/3})O_3$, $Ba(Mg_{1/3}Ta_{2/3})O_3$ and numerous solid solutions. In the selection of low loss materials, it is important to consider what relaxation processes contribute to dielectric loss. Dielectric losses in paraelectric materials are caused by lattice defects and anharmonic lattice vibrations. Whereas, losses in ferroelectric materials such as $BaTiO_3$ and $LiNbO_3$ arise from domain wall motion and piezoelectric grain resonance.[2] Recently, Lanagan (1987) [3] suggested antiferroelectrics for microwave dielectrics as they exhibit no piezoelectric grain resonance and minimal contribution of domain walls to the permittivity. Because of the antiferroelectric behavior of these materials, it is theoretically possible to achieve high dielectric constant, yet low loss. Of particular interest also, Wakino et. al. (1986)[4] has shown a correlation of microwave loss to cation order in the perovskite structure.

Based on the above contributions to dielectric loss, the order-disorder

This paper was originaly presented at the Seventh International Meeting of Ferroelectricity, Saarbrucken, F.R. Germany, August 28 to September 1, 1989.

†Communicated by Dr. George W. Taylor

perovskites[5] $Ba(In_{1/2}Nb_{1/2})O_3$ - (BIN), $Pb(In_{1/2}Nb_{1/2})O_3$ (PIN) and their tantalate analogues were herein proposed as potential candidates for microwave dielectrics. However, to date, a great deal of controversy exists over the dielectric and structural characteristics of BIN and PIN ceramics. Though paraelectric behavior would be expected, both BIN and BIT have been reported to exhibit dielectric anomalies suggesting ferroelectric behavior[6]. In the case of PIN, the order-disorder characteristics and corresponding change in dielectric behavior from ferroelectric to antiferroelectric (ordered state) have been well documented in single crystals[7,8,9,10], however, little work has been done in the fabrication of polycrystalline materials. Attempts to make polycrystalline PIN and PIT have resulted in uncharacteristically poor dielectric properties owing to the presence of parasitic pyrochlore phase(s) [11,12].

It was the objective of this work to utilize improved fabrication techniques to prepare the proposed perovskites, and to confirm their dielectric and structural characteristics.

EXPERIMENTAL PROCEDURE

From the perovskite ABO_3 structural field plot of average electronegativity versus tolerance factor, shown in figure 1, we note that both BIN and BIT are in a region at high perovskite stability, whereas, both PIN and PIT are amongst those compounds which are difficult to form without the presence of pyrochlore phase(s) [13]. From previous studies of lead based complex perovskites, it has been shown that by pre-reacting the B-site oxides and subsequent reaction with PbO, the formation of the perovskite phase is greatly enhanced[14]. Hence, in this work, high purity In_2O_3 was pre-reacted with Nb_2O_5 to form the wolframite $InNbO_4$ followed by reaction with PbO, as presented in the following:

$$In_2O_3 + Nb_2O_5 \xrightarrow{850^oC/4hrs.} 2\ InNbO_4$$

$$2PbO + InNbO_4 \xrightarrow{900^oC/4hrs.} 2Pb(In_{1/2}Nb_{1/2})O_3$$

The calcined powders were characterized by X-ray diffraction to determine phase purity. The reacted powder was then vibratory milled to enhance reactivity followed by disk preparation using a 3wt.% PVA solution. Following binder burnout, the disks were embedded in coarse PIN sand and sintered at 1050°C for 4hrs. in closed alumina crucibles. The firing sand was essential for the control of PbO and In_2O_3 losses due to volatility, and minimization of pyrochlore formation. Note: preliminary work found that PIT could not be fabricated in the perovskite structure without at least or no less than 35% pyrochlore.

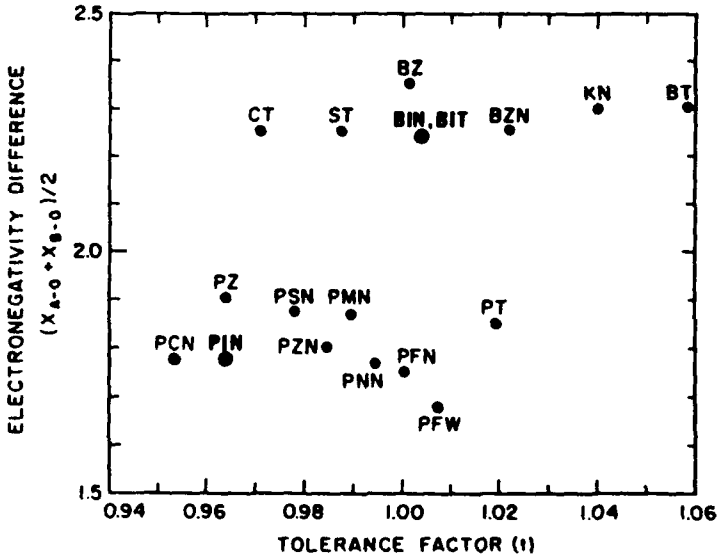

FIGURE 1. Plot of average electronegativity (χ) versus tolerance factor (t).

Where : BT= $BaTiO_3$, KN= $KNbO_3$, BZN =$Ba(Zn_{1/3}Nb_{2/3})O_3$
BIN= $Ba(In_{1/2}Nb_{1/2})O_3$, BIT= $Ba(In_{1/2}Ta_{1/2})O_3$,
Bz= $BaZrO_3$, St= $SrTiO_3$, CT= $CaTiO_3$, PT= $PbTiO_3$,
PMN= $Pb(Mg_{1/3}Nb_{2/3})O_3$, PSN= $Pb(Sc_{1/2}Nb_{1/2})O_3$, PZ= $PbZrO_3$
PFN= $Pb(Fe_{1/2}Nb_{1/2})O_3$, PNN= $Pb(Ni_{1/3}Nb_{2/3})O_3$, PZN= $Pb(Zn_{1/3}Nb_{2/3})O_3$
PIN= $Pb(In_{1/2}Nb_{1/2})O_3$, and PCN= $Pb(Cd_{1/3}Nb_{2/3})O_3$

The phase stability of both BIT and BIN perovskites allowed them to be readily processed using conventional mixed oxides of $BaCO_3$, In_2O_3, Nb_2O_5, or

Ta_2O_5 . The powders were vibratory mixed/milled followed by calcination at 1350°C for 4hrs. The reacted powder was processed as above and fired 1650°C for 4hrs., again using firing sands. Due to the refractory nature of BIT and temperature limitations of the furnace, the partially sintered material was again milled and resintered to enhance densification.

Sintered samples were characterized for density, phase purity, and grain size (using SEM of fractured surfaces). Samples were polished and electroded using sputtered gold electrodes. The dielectric properties of the samples were measured at frequencies 100Hz to 100KHz with an automatic capacitance bridge (Hewlett-Packard 4274A)[15]. The temperature was varied over the temperature range of -150°C to 230°C while samples were being measured.

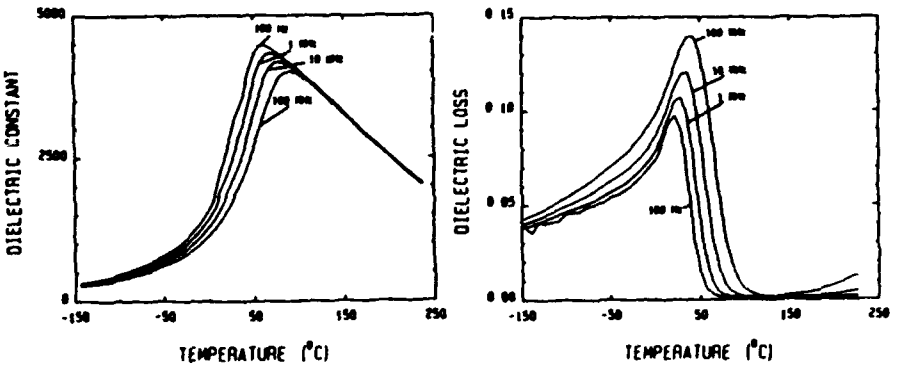

FIGURE 2. Plot of the dielectric constant and loss vs.temperature for disordered PIN.

RESULTS AND DISCUSSION

By utilizing the processing methods described above, high density (>95% theoretical) PIN ceramics possessing less than (<3%) pyrochlore, as determined by X-ray diffraction, were obtained. The grain size was found to be ~ 1-3μm. The dielectric behavior of PIN was found to be typical of relaxor ferroelectrics possessing a broad and strongly frequency dependent dielectric constant maximum with Tc~61°C (@ 1KHz), as shown in Figure 2. A Kmax of

4500 was nearly that reported for single crystals. Also characteristic of relaxors, linear 1/K vs. $(T-Tc)^2$ behavior was observed (see Figure 3), with a diffuseness coefficient δ of 114K.

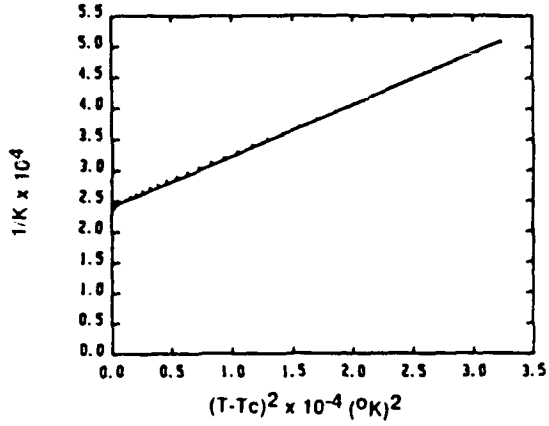

FIGURE 3. Dependence of 1/K on $(T-Tmax)^2$ for PIN.

Attempts to order PIN through various thermal treatments, as reported for single crystals, were futile. Though annealing from 400 to 1100°C for 0 to 72hrs. was performed in firing sands to prevent PbO and In_2O_3 losses, pyrochlore formation occurred. Figure 4 shows schematically a plot of annealing temperature vs. time indicating the competition between the ordering process and perovskite-pyrochlore transformation. Attempts to grow PIN grains to enhance the ability to order, again was met by pyrochlore formation. Grain growth was attempted by sintering at temperatures close to the melting temperature of ~ 1290°C for short durations of time (5 - 15 min.); however, minimal perovskite grain growth was observed. A sharp increase in perovskite - pyrochlore transformation (>20%) was evidenced by large (>15μm) trigonal shaped pyrochlore grains. Similar problems of pyrochlore transformation also were found in attempts to grain grow $Pb(Zn_{1/3}Nb_{2/3})O_3$ based materials by Kumar (1988)[16], reflecting the thermodynamic stability of pyrochlore in these systems.

In contrast to PIN, both BIN and BIT were readily produced in perovskite

form. Sintered densities of ≥ 95 and 85% of theoretical were obtained, respectively. The grain size of these ceramics was found to be approximately 2-3μm. As anticipated, the dielectric properties (see Figure 5) revealed paraelectric type behavior with dielectric constants of K~40 and 38 for BIN and BIT and correspondingly low loss (<0.0009 at 100KHz). The temperature coefficient of capacitance was determined to be ~ -139ppm/C^{o} for BIN and ~-124ppm/C^{o} for BIT. X-ray diffraction revealed no superstructure lines and thus no cation order. Ordering of these materials through thermal annealing were not attempted. Annealing samples at temperatures as low as 600^{o}C for 40hrs., which was successful for single crystals, did not increase ordering, yet substantial pyrochlore formation occurred.

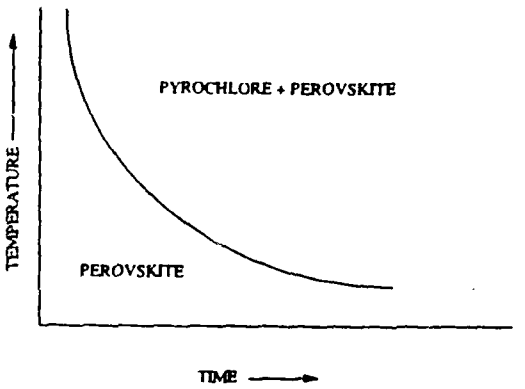

FIGURE 4. The annealing temperature vs. time plot showing the competition between ordering and perovskite-pyrochlore transformation.

SUMMARY

1) High density (>95%) and low pyrochlore (<3%) PIN was produced by using the B-site precursor method described above, and using firing sands in the sintering process to control PbO and In_2O_3 losses. However, ordering and grain growth kinetics were found to compete with the perovskite - pyrochlore transformation. This makes the highly ordered antiferroelectric PIN as a single phase material to be a difficult processing challenge, and thus an unsuccessful choice as a potential

15. Swartz, S.L., Shrout, T.R., Schulze, W.A., and Cross, L.E., J. Amer. Cer.Soc.,67,(5), 311, (1984).
16. Kumar, U., Dielectric, Pyroelectric, Electrostrictive, and Relaxor Preoperties of Lead Zinc Niobate -Barium Titanate Ceramic Solid Solutions, Penns. State University, Ph.D. thesis, (1989).

microwave dielectric.

2) BIN and BIT ceramics with densities of (95%) and (85%) were produced by conventional ceramic methods. Sands were again used in the processing to control In_2O_3 losses. Both ceramics exhibited classic paraelectric behavior.

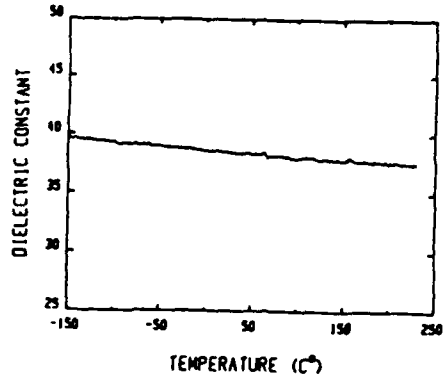

FIGURE 5. Plot of dielectric constant vs. temperature for disordered BIN for frequency range of 100Hz. to 100KHz.

REFERENCES

1. Wakino, K., Minai, K., and Tamura, H. J., Amer.Cer.Soc.,67 , 278, (1984).
2.3. Lanagan, M.T., Microwave Dielectric Properties of Antiferroelectric Lead Zirconate, Penns. State University, Ph.D. thesis, (1987).
4. Wakino, K.,Murata, M., and Tamura, H., J.Amer.Cer.Soc.,69 ,(1), 34, (1986).
5. Galasso, F.S. ,Structure, Properties and Preparation of Perovskite Type Compounds, Pergamon, New York, 1969.
6. Groves, P., Phase Transitions, 5, 197, (1985).
7. Bokov, A.A., Raevskii, I.P., Smotrakov, V.G., and Talysheva, I.M., Sov. Phy. Sol. Stat. 26, 369, (1984).
8. Groves, P., J. Phys. C: Solid State Phys. 19, 5103, (1986).
9. Kuprianov, M.F., Turik, A.V., Zaitsev, S.M., and Fesenko, E.G., Phase transitions, 4, 65, (1983).
10. Prokopalo, O.I., Raevskii, I.P.,Malitskaya, M.A., Popov, Yu. M., Bokov, A.A., and Smotrakov, V.G., Ferroelectrics, 45, 89, (1982).
11. Kochetkov, V.V., and Venevtsev, Yu.N., Izvestiya Akademia Nauk SSSR, Neorganicheskii Materialy, 15, 10, 1833, (1979).
12. Groves, P., Ferroelectrics, 65, No.1-2, 67, (1985).
13. Shrout, T.R., and Halliyal, A., Am. Ceram. Soc. Bull.,66, [4] 704 (1987).
14. Swartz, S.L. and Shrout, T.R., Mater. Res. Bull., 17, 1245 (1982).

APPENDIX 46

National Institute of Standards and Technology Special Publication 804, Chemistry of Electronic Ceramic Materials, Proceedings of the International Conference held in Jackson, WY, August 17-22, 1990, issued January 1991.

CONVENTIONALLY PREPARED SUBMICRON ELECTRO-CERAMIC POWDERS BY REACTIVE CALCINATION

Thomas R. Shrout
Pennsylvania State University
Materials Research Laboratory
University Park, PA 16802

ABSTRACT

It is the physiochemical nature of lead-based perovskites $Pb(B)O_3$ that upon reaction of the component oxides a large volumetric expansion occurs. In addition to perovskites, Pb- and Bi-based pyrochlores ($A_2B_2O_7$) and the layered structure compound $Bi_4Ti_3O_{12}$ also exhibit similar physiochemical behavior. At the temperature of maximum expansion, the associated morphological development results in a porous skeletal type structure consisting of fine particulates that can be readily broken down further by milling. The level of expansion and ease of comminution was shown to be strongly dependent on the starting powder size, using perovskite $Pb(ZrTi)O_3$ as the example. Using this concept of "reactive calcination," the state of optimum soft agglomeration and subsequent milling can allow for fully reacted powder with submicron particle size.

INTRODUCTION

With the continuing miniaturization of electronics including ceramic devices such as multilayer capacitors, ultrasonic transducers, sensors, piezo motors, and electrostrictive actuators, the importance of fine and phase pure starting powders becomes ever so more evident. Such powders also allow the potential for novel applications such as ferro-fluids which require finely dispersed submicron powders in a liquid medium.(1) Fundamentally, submicron to nano-sized powders are of interest in the understanding of the role of "scale" on intrinsic physical phenomena such as ferroelectricity and related behavior.(2)

Numerous methods to produce submicron powders have been developed with emphasis on the perovskite ABO_3 family of materials. Methods include chemical synthesis techniques such as co-precipitation of alkoxides, molten salt, and hydrothermal. However, most chemical synthesis techniques are relatively costly and do not lend themselves for mass production.

Recently, submicrometer powders of Pb-based perovskites including $PbTiO_3$, $PbZrO_3$, $Pb(Zr_{.53}Ti_{.47})O_3$ and $Pb(Mg_{1/3}Nb_{2/3})O_3$ were prepared by a reactive calcination process.(3) Using only reagent-grade raw materials and conventional processing techniques, highly reactive powders were produced by reacting the materials near the temperature of maximum volumetric expansion. At this point, the associated morphological development results in a skeletal-type

structure consisting of ultra-fine particulates than can be readily broken down by milling (see Fig. 1). Powder sizes < 0.1 μm were produced allowing enhanced densification and correspondingly small grain sizes.[4,5]

The objective of this work was to further optimize the "reactive calcination" process of lead-based perovskite through control of the starting powder characteristics. It was a further objective to explore the potential of reactive calcination in non-PbO perovskites and other electro-ceramic structural families through knowledge of their physiochemical behavior.

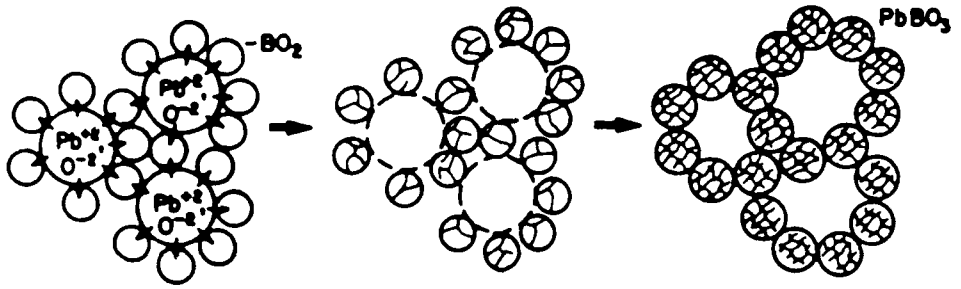

Figure 1. Schematic representation of the perovskite $PbBO_3$ formation and associated morphological changes.[3]

EXPERIMENTAL PROCEDURE

The Pb-based perovskite material chosen to examine the role of component powder characteristics on reactive calcination was the solid solution $Pb(Zr_{.53}Ti_{.47})O_3$ (PZT). Non-perovskite materials investigated included the pyrochlores $Pb_2Nb_2O_7$ and $Bi_2Ti_2O_7$ and $Bi_4Ti_3O_{12}$ layer structure compound. The non-PbO perovskite $(Na_{1/2}Bi_{1/2})TiO_3$ was also studied.

Reagent-grade raw materials were used to prepare the compounds as described in ref. 3. The component powders were characterized by determining their as-received surface area and particle size.

Since intermediate reactions occur in the formation of the complex perovskite PZT, the B-site precursor method developed by Swartz and Shrout[6] was used whereby the ZrO_2 and TiO_2 oxide were pre-reacted prior to reaction with PbO as follows:

$$0.53\ ZrO_2 + 0.47\ TiO_2 \xrightarrow{\sim 1400\,^{\circ}C\ /\ 4hr} Zr_{.53}Ti_{.47}O_2 \quad \text{(rutile)} \qquad [1]$$

$$PbO + Zr_{.53}Ti_{.47}O_2 \rightarrow PZT \quad \text{(perovskite)} \qquad [2]$$

Variations in particle sizes of both the PbO and Zr,TiO_2 oxides were prepared by vibratory or attrition milling. The powder size schemes for reactive calcination of PZT are schematically shown in Fig. 2.

Stoichiometric mixtures of the component oxides for all the compounds studied were prepared by vibratory mixing in ethyl alcohol or de-ionized H_2O and polyelectrolyte dispersant at a pH where minimal dissolution of Pb^{+2} occurs.(7) Upon drying, the powders were pressed into disks of similar packing densities.

The possibility and/or extent of reactive calcination was determined by the degree of volumetric expansion and corresponding temperature reaction range. This was performed by placing pressed disks in a furnace (open air) and heated at a rate of ~ 100°C/hr. Above 500°C, disks were quenched at 25 to 50°C intervals by being pulled directly from the furnace and allowed to cool in air. Sample geometries were used to determine the degree of volumetric expansion or shrinkage. The disks were then crushed and powder XRD analysis performed to determine the amount of phase reaction and subsequent particle characteristics. SEM microstructural analysis of selected powder compacts (before and after crushing) were also examined to examine morphological development during reaction.

Based on these results, large quantities of (~ 1 kg) PZT packed powders were prepared. The powders were calcined for 4 hrs approximately 50°C below the maximum expansion (to allow for kinetics) and at higher temperatures to demonstrate the point of optimum skeletal formation and subsequent consequence on milling efficiency. Slurries of the calcined powders were prepared as before and attrition milled while samples were removed at various intervals. The milled powders were then characterized by specific surface area. The primary particle size was determined through the equation

$$D = \frac{6}{pSA} \qquad [3]$$

where p is the theoretical density, SA the surface area, and D the calculated primary particle size.

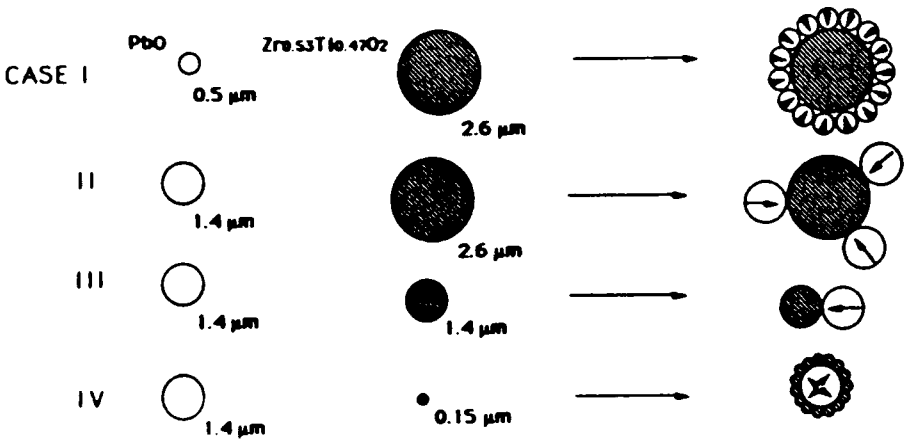

Figure 2. Component powder size schemes for the formation of perovskite PZT.

RESULTS AND DISCUSSION

Instinctively, one expects that ceramic powder compacts should shrink on reaction as a consequence of higher product densities, as found for non-PbO perovskites. The volumetric expansion observed during the formation of Pb-based perovskites is reportedly the result of molar volume differences in the component oxides and subsequent perovskite phase. Attempts to predict relative volume expansions for various compounds clearly suggests the expansion behavior is also dependent on the particle packing and size characteristics as proposed in Fig. 2.

The importance of particle characteristics on reactive calcination is clearly evident in Fig. 3, showing the impact of PbO particle size on the volume expansion during the formation of perovskite PZT. As presented, fine PbO (Case I) resulted in shrinkage prior to a relatively small volume expansion and associated formation of the perovskite phase. The shrinkage is believed to be the result of the highly reactive nature of the fine PbO particle/agglomerates which sinter prior to reaction with the coarser Zr,TiO_2 particles. The impact of Zr,TiO_2, particle size, clearly shows that the finer material enhanced the formation of perovskite PZT, but the reactive nature of the fine powder and less open skeletal structure lead to densification at relatively low temperatures (Case IV). For Case III, where PbO and Zr,TiO_2 are of similar size, resulted in the largest volume expansion. Of particular interest is that once the skeletal structure was formed, densification did not occur even up to temperatures of 1000°C. Hence, inhomogeneous densification (low coordination number of reaction regions) was optimized. The importance of this behavior is clearly evident in Fig. 4, whereby the ease in which the skeletal structures can be broken down is given in terms of a milling factor. As shown, the skeletal sructure associated with Case III was readily broken down by milling with an order of magnitude decrease in particle size in only one hour. A large volume change found over an extensive temperature range (Case III), thus, allows for a broader calcination process window. Further implications of the morphological development of these materials will be presented in the summary.

The morphological behavior presented above was not found to be unique to Pb-perovskites but was also observed in the Pb-based pyrochlore phase $Pb_2Nb_2O_7$ as shown in Fig. 5. Analogous to Pb, the Bi-based perovskite $Na_{0.5}Bi_{0.5}TiO_3$, pyrochlore $Bi_2Ti_2O_7$ and layer structure $Bi_4Ti_3O_{12}$ compounds also exhibited similar behavior, but to a lesser degree. It is important to note that at the point of maximum volumetric expansion corresponds to the formation of the expected phase.

CONCLUSION

The volumetric expansion and morphological development associated with the formation of Pb-based perovskites was found to be strongly dependent on the starting powder characteristics, using perovskite $Pb(ZrTi)O_3$ as the example. The resulting porous skeletal structure of perovskite particulates was found to be readily broken down into submicron particles by milling. In addition to Pb-based perovskites, Pb- and Bi-based pyrochlores ($A_2B_2O_7$), the layered structure compound $Bi_4Ti_3O_{12}$ and $(Na_{1/2}Bi_{1/2})TiO_3$ perovskite were also found to exhibit

similar physiochemical behavior. Using this concept of "reactive calcination" the point of maximum expansion can be used as a characterization tool to determine the optimum state of soft agglomeration to provide highly reactive powders.

Further investigation and modeling of particle size and packing effects on reactive calcination are still required.

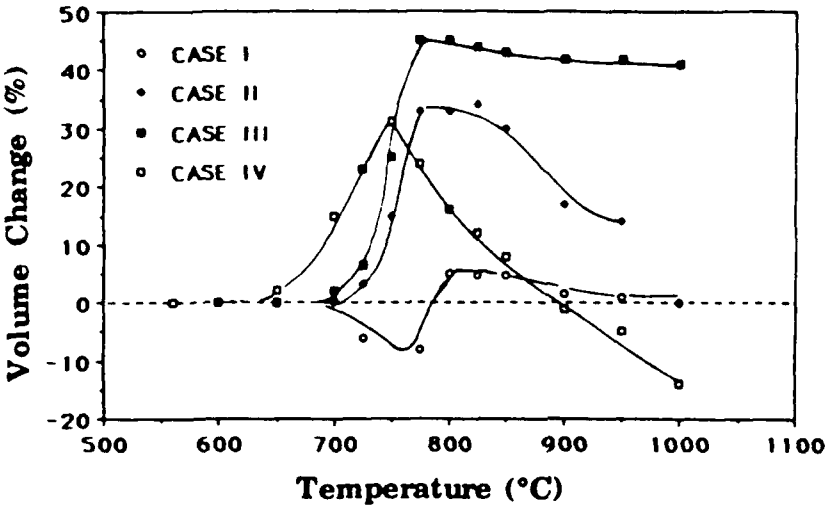

Figure 3. Volumetric expansion-shrinkage characteristics of PZT as a function of temperature for various component sizes.

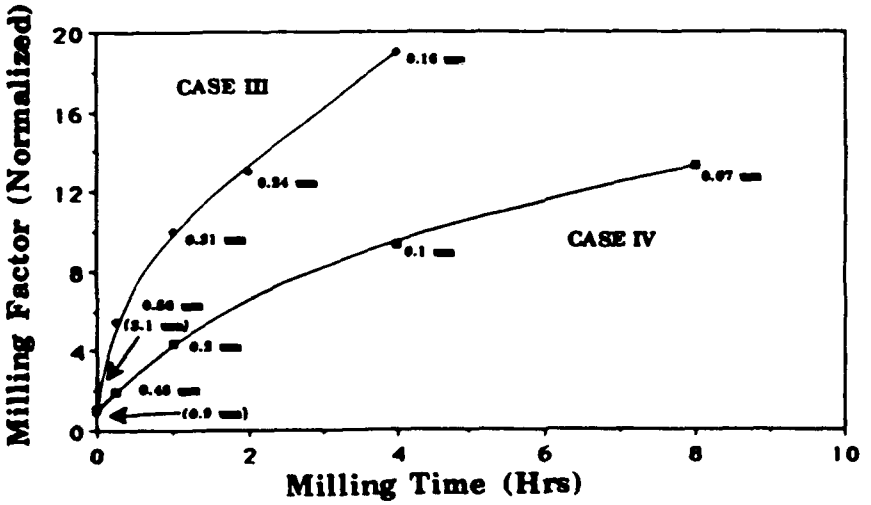

Figure 4. Milling factor (normalized) for reactively calcined PZT (Cases III (3.1 μm) and IV (0.9 μm)) as a function of milling (attrition) time.

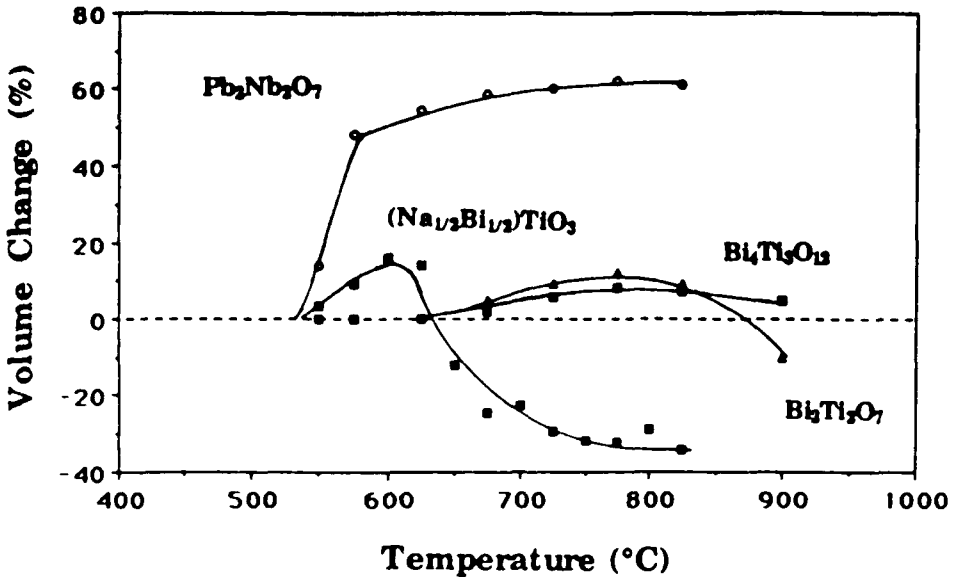

Figure 5. Volumetric expansion-shrinkage characteristics of $Pb_2Nb_2O_7$, $Bi_2Ti_2O_7$ (pyrochlore), $Na_{0.5}Bi_{0.5}TiO_3$ (perovskite) and $Bi_4Ti_3O_{12}$ (larger structure).

ACKNOWLEDGEMENTS

The author wishes to thank Beth Jones for her technical skills and Drs. Venkataramani, G.S. Lee, and J.H. Adair for their helpful discussions.

REFERENCES

1. J.U. Muller and K. Barner. "Polydisperse Suspensions of $BaTiO_3$ Particles," *Ferroelectrics*, 108, 83-88 (1990).
2. K. Uchino, E. Sadamaga, and T. Hirose. "Dependence of the Crystal Structure on Particle Size in Barium Titanate," *J. Am. Ceram. Soc.*, 72[8], 1555-1558 (1989).
3. T.R. Shrout, P. Papet, S. Kim, and G.S. Lee. "Conventionally Prepared Submicrometer Lead-Based Perovskite Powders by Reactive Calcination," *J. Am. Ceram. Soc.*, 73[3], 1862-1867 (1990).
4. P. Papet, J.P. Dougherty, and T.R. Shrout. "Particle and Grain Size Effects on the Dielectric Behavior of the Relaxor Ferroelectric $Pb(Mg_{1/3}Nb_{2/3})O_3$," (to be published in *J. Mat. Res.*).
5. S. Kim, G.S. Lee, and T.R. Shrout. "Fabrication of Fine Grain Piezoelectric Ceramics Using Reactive Calcination," (to be published in *J. Mat. Sci.*).
6. S.L. Swartz and T.R. Shrout. "Fabrication of Perovskite Lead Magnesium Niobate," *Mater. Res. Bull.*, 17, 1245-1250 (1982).
7. M. Pourbaix. Atlas of Electrochemical Equilibria in Aqueous Solutions, National Association of Corrosion Engineers (1974).

APPENDIX 47

FABRICATION OF FINE GRAIN PIEZOELECTRIC CERAMICS USING REACTIVE CALCINATION

S. Kim, G.S. Lee, and T.R. Shrout
Materials Research Laboratory
The Pennsylvania State University
University Park, PA 16802

and

S. Venkataramani
General Electric Co.
Schenectady, NY 12301

ABSTRACT

Fine grain piezoelectric ceramics with the formula $Pb(Zr_{.53}Ti_{.47})O_3$ (PZT) were prepared by a reactive calcination process. Using conventional materials and processing techniques, highly reactive powders of PZT were achieved by calcining to or near the point of maximum volume expansion whereby associated morphological changes resulted in highly reactive powder. Upon milling, powders < 0.3 μ were readily obtained allowing densification at temperatures < 1000°C. Using the B-site precursor method, whereby the ZrO_2 and TiO_2 oxides were pre-reacted prior to reaction with PbO, further enhanced the reactivity by eliminating intermediate reactions and subsequent phase(s) which can hinder densification and overall homogeneity. Highly dense piezoceramics with grain sizes ~ 1-2 μ exhibiting dielectric and piezoelectric characteristics comparable to conventionally prepared large grain size materials were obtained.

INTRODUCTION

Modified lead zirconate titanate (PZT) ceramics are choice materials still widely used for various piezoelectric applications.[1-4] In general, conventionally prepared PZT ceramics are calcined and sintered at relatively high temperatures, ≥ 900°C and 1200°C, respectively, to insure complete phase formation, and the desired piezoelectric properties. Problems associated with the high processing temperatures include PbO loss through volatilization and hence poor overall uniformity. In recent applications, such as multilayer actuators[5,6] it is desirable to use lower sintering temperatures to incorporate less costly internal electrodes, as well as to achieve finer grain size structures. The latter is particularly important in high frequency devices such as biomedical transducers.[7]

Processing methods employed to enhance the reactivity of PZT have included various chemical techniques (sol-gel, molten salt, and hydrothermal) to prepare homogeneous and fine

powders, as well as high energy milling, and hot pressing.[1-3,8-13] Though the above methods have been successful in reducing the firing temperature and subsequent grain size, they are in general, expensive and not amenable to large scale production.

Previous investigations on the role of calcination and its effect on sintering of PZT ceramics found that densification could be enhanced by partially reacting the component powders near the point of maximum volume expansion, an effect generally observed in the formation of lead based $Pb(B)O_3$ perovskites.[14] The enhanced densification was attributed to a reactive sintering process,† associated with the on-going completion of the PZT formation reaction.

The reaction sequence of PZT, however, is quite complex with several intermediate phases being formed. Associated with these phases, that include $PbTiO_3$, are volume expansions and morphological transformations that may actually hinder or lead to inhomogeneous densification if the oxide mixture is not properly processed. Based on the work by Swartz and Shrout[15] on related lead-based perovskites, it was proposed that by pre-reacting the B-site oxides TiO_2 and ZrO_2 --> $ZrTiO_4$ prior to reaction with PbO only a single reaction step and subsequent volume expansion would occur and thus lead to more homogeneous densification.

In this study the concept of reactive sintering in conjunction with conventional materials and processing techniques was proposed to prepare highly reactive PZT powder and fine grain piezoelectric ceramics. Reactive sintering was investigated for both mixed oxide and B-site precursor powder methods. The dielectric, piezoelectric, and physical characteristics were determined for both systems.

EXPERIMENTAL PROCEDURE

Powder Preparation

The PZT composition selected for this study being near the morphotropic phase boundary was $Pb(Zr_{0.53}Ti_{0.47})O_3$. Raw materials used for the experiments were reagent grade PbO,* TiO_2,** and ZrO_2.***+ The powders were weighed in a nalgene container and vibratory milled++ for 24 hrs with ethyl alcohol using ZrO_2 milling media. A small amount of dispersant was added

---

†The term "reactive sintering" is herein defined as a process by which densification is enhanced as the result of an accompanying phenomena, e.g., chemical reaction, which is greatly beneficial to diffusion and the overall sintering phenomena.

*Hammond Lead Products, Inc., PbO (yellow, 99%) Hammond, IN.

**Whittaker, Clark, and Daniels, TiO_2 Grade (99%) Pittsburgh, PA.

***Harshaw/Filtrol Partnership, ZrO_2 (electronic grade) Cleveland, OH.

+Sweco, Inc., Model M-18-5, Florence, KY.

to provide efficient milling. The slurry was dried in an oven at 80°C and calcined near the point of maximum volume expansion experimentally described in the next section. To further increase the reactivity of the powder, approximately one-half of the calcined powder was vibratory milled. The two types of materials designated PZT-AS (as-calcined) and PZT-M (milled) are used hereafter.

A PZT mixture was also prepared using zirconate titanate (ZT) powder, where ZT was prepared from ZrO_2 and TiO_2 in the ratio of 53:47. The mixture was prepared as above and calcined at 1400°C for 4 hrs. The calcined ZT powder was hammer milled and sieved through 60 mesh, followed by the addition of PbO and calcined again near the point of maximum volume expansion. Again, part of the powder was milled, designated ZTP-M and ZTP-AS (for the as-calcined material).

Calcination and Sintering Studies

To determine the "optimum" calcination temperature, powders of uncalcined PZT-AS and ZTP-AS were pressed (~ 34 MPa) into disks 1.25 cm in diameter and 3-4 mm thick. The disks were heated in an electric furnace up to 1000°C with a heating rate of 2°C/min, with samples removed from the furnace at 50°C intervals. The sample dimensions were measured to determine volume expansion and/or shrinkage. X-ray powder diffraction of the samples was used to characterize the completion of the reaction sequences. The calcination temperature used for the large batches (~ 1 kg) was selected to be ~ 50°C less than the point of maximum expansion of the disks to allow for differences due to kinetics. The PZT and ZTP powders were calcined at 725°C for 4 hrs. As stated, halves of the two batches were vibratory milled subsequent to calcination to further enhance reactivity. The powders were again characterized for specific surface area, particle size, and agglomeration. For comparison of particle size(s) and the degree of agglomeration, scanning electron microscope (SEM) photomicrographs of the powders were taken. Disks were prepared using a 3 wt% PVA being pressed into a disk of 1.25 cm diameter at ~ 70 MPa. The green densities of all the disks were in the range of 4.5-4.8 g/cm^3. After binder burnout, the pellets were sintered at 850°C-1200°C in closed alumina crucibles for one hour. A PbO atmosphere was maintained using $PbZrO_3$ powder. The pellets were characterized for geometric density and grain size as determined on fractured surfaces by SEM.

Dielectric and Piezoelectric Properties

Samples having densities greater than 90% theoretical (ρ_{theo} ~ 8 g/cm^3) were polished and electroded with sputtered on gold with air dry silver applied to insure better contact during poling and electrical property measurements. Disks were poled in a silicon oil bath at 120°C with an applied field of 50 to 60 KV/cm for 3 to 10 minutes. Values of the piezoelectric constant, d_{33}, measured using a Berlincourt d_{33} meter, were checked to insure completion of poling.

The dielectric constant (K) and dissipation factor (loss) of the ZTP and PZT samples were measured using a Hewlett-Packard (Model 4274A) LCR meter. The piezoelectric planar coupling

coefficient (k_p) and mechanical quality factor, Q_m, were determined using a Hewlett-Packard (Model 3577A) network analyzer in reference to the IRE standard.[16] Values were measured 24 hrs after poling.

RESULTS AND DISCUSSION

The volume expansion/shrinkage curves as a function of calcining temperature for P+Z+T and ZT+P mixtures are shown in Fig. 1. As presented, the PZT mixture exhibited two volume expansions near 650°C and 750°C, whereas the ZTP, as anticipated, exhibited only one near 800°C. As previously reported,[14] the two expansion maximums observed for P+Z+T reflect the formation of PT (~ 650°C) and intermediate PZT phase(s) (~ 750°C), respectively. The volume expansions are reportedly believed to be due to a molar volume increase of the reaction phase(s) in contrast to the starting oxides. Naturally, the expansion behavior is dependent on the forming pressure, heating rate, etc. The sequence of x-ray diffraction patterns shown in Fig. 2a, also confirms the formation of the intermediate phases PT and PZT. Above 750°C, the completion of perovskite PZT phase began to take place with the diffraction peak(s) becoming sharper with increasing temperature. In the ZTP case (see Fig. 2b) no reaction took place until ~ 750°C, where the formation of PZT began and completed at ~ 800°C as reflected by the strong diffraction peaks.

Simplified reaction sequences of the two types of PZT mixtures can be summarized in the following:

P+Z+T [PZT-AS]	P+ZT [ZTP-AS]
$PbO + TiO_2 \xrightarrow{\sim 650^\circ C} PbTiO_3$	
$PbO + PbTiO_3 + ZrO_2 \xrightarrow{\sim 750^\circ C} Pb(Zr_xTi_{1-x})O_3$ (intermediate PZT)	$PbO + ZrTiO_4 \xrightarrow{\sim 800^\circ C} PZT$
$PbTiO_3 + Pb(Zr_xTi_{1-x})O_3 \xrightarrow{> 750^\circ C} PZT$	

Though the reported reaction sequence(s) for P+Z+T are in actuality more complex than presented, the importance of the B-site precursor method in eliminating intermediate reactions and associated morphological changes was apparent. This technique helps prevent the possibility of problems associated with unreacted ZrO_2 and competing volume expansions with densification during firing. The single calcines of the PZT-AS and ZTP-AS at 725°C/4 hrs, though below the

point of volume expansion(s) shown in Figs. 2a and 2b, were found to be single phase perovskite PZT. The process by which powders are reacted at a point of maximum volume expansion due to associated morphological changes is hereafter designated as "reactive calcination."

The powder characteristics of the milled and unmilled reactively calcined PZT and ZTP powders are reported in Table I. Also included are the powder characteristics of the ZT precursor powder. As presented, the equivalent particle size, as determined from the surface area, was smaller for the ZTP powder, though they were calcined at the same conditions. Upon milling, a significant reduction in particle size and corresponding increase in surface area was observed with a slight increase in agglomeration. It is interesting to note that the PZT-AS and ZTP-AS powders milled to approximately the same particle size reflecting the limit of milling efficiency. SEM analysis confirmed the calculated particle sizes and degree of agglomeration.

Densities of the sintered disks as a function of firing temperature (850°C-1200°C) for the PZT and ZTP materials are plotted in Fig. 3. Virtually no increase in density occured below 900°C for the PZT-AS and milled (PZT-M) powders, whereas densification (> 85% theoretical) occured as low as 850°C for ZTP. As expected, milling increased the reactivity of the powders and subsequent densification. Densities > 90% theoretical were achieved for the ZTP-M material as low as 950°C, whereas temperatures of 1000°C and 1200°C were required for the PZT-M and PZT-AS, respectively. The average grain size for PZT and ZTP samples fired at 1000°C and 1200°C are reported in Table II. Typical SEM photomicrographs of fractured (intergranular) surfaces of the sintered samples are shown in Fig. 4. Grain sizes for PZT-AS and ZTP-AS samples fired at 1000°C were found to be ~ 2 μ, increasing in size to ~ 3 μ at the higher firing temperature. Samples processed with the milled powders were found to be somewhat smaller. Grain sizes in the neighborhood of ~ 1.5 μ with a fired density > 95% theoretical were obtained for the ZTP-M material fired at only 1000°C for 1 hr.

In addition to physical characteristics, the dielectric and piezoelectric properties of PZT-M and ZTP-M ceramics fired at 1000°C and 1200°C are reported in Table II. For comparison, data for conventionally prepared $Pb(Zr_{.53}Ti_{.47})O_3$ from Jaffe et al.,[1] was reported. Okazaki and Nagata[17,18] found that both the dielectric and piezoelectric properties (K, d_{33}, k_p, etc.) increase with density and grain size. This behavior was also observed whereas the lower density and finer grain sized materials possessed lower values. However, the largest deviations were found to occur between the PZT and ZTP materials regardless of density or grain size. The PZT materials, whether originally milled or not, possessed significantly lower dielectric constants and piezoelectric d_{33} values. This difference reflects inhomogeneity in the PZT material in that the properties, such as the dielectric K, are very dependent on the Zr:Ti ratio near the morphotropic phase boundary. Also of importance, the piezoelectric properties d_{33} and k_p, for the ZTP materials fired at 1000°C were inferior to those fired at 1200°C, though possessing similar densities and grain sizes. The

lower values are believed to be related to the crystallinity of the materials being less developed. The associated defects thus result in a stiffening out of the extrinsic polarizability (domain wall motion).[19] As found for other perovskites,[20] longer sintering times may anneal out various crystalline defects resulting in less grain size dependency.

CONCLUSIONS

Using reagent grade materials and conventional processing techniques, fine grain PZT ceramics were fabricated based on reactive calcination. By reacting the component powders (PbO, ZrO_2, and TiO_2) near the point of maximum volume expansion, very fine (< 0.3 μ) and highly reactive powders were readily made. Such powders could be densified at temperatures less than ~ 1000°C. Being fully reacted, enhanced densification was simply due to the reactive nature of fine powders and not due to a reactive sintering process as originally proposed. The reactive calcination process was further enhanced by first pre-reacting the B-site oxides (ZrO_2 and TiO_2) prior to reaction with PbO. This step eliminated intermediate phase reactions which hindered densification and resulted in a more homogeneous material.

Highly dense piezoceramics with fine grain size structure < 2 μ exhibiting dielectric and piezoelectric properties comparable to conventionally prepared large grain size materials were obtained. Further investigations, however, of the mechanisms and morphological changes that take place during calcination are still required. The role of grain size and associated dependency of the dielectric and piezoelectric properties also needs to be addressed.

REFERENCES

1. B. Jaffe, W.R. Cook, Jr., and H. Jaffe, Piezoelectric Ceramics, Academic Press, NY (1971).
2. R.C. Buchanan, Ceramic Materials for Electronics, pp. 154-222, Marcel Dekker, Inc., NY (1986).
3. L.M. Levinson, Electronic Ceramics Properties, Devices, Applications, pp. 371-492, Marcel Dekker, Inc., NY (1987).
4. T. Shiosaki, "Recent Developments in Piezoelectric Materials," Ferroelectrics, 91, 39-51 (1989).
5. K. Uchino, "Electrostrictive Actuators: Materials and Applications," Cer. Bull., 65, 4 (1986).
6. W. Wersing, H. Walth, and M. Schnoller, "PZT-Based Multilayer Piezoelectric Ceramics with Ag:Pd-Internal 'Electrodes'," Ferroelectrics, 87, 271-294 (1988).

7. W.A. Smith, A.A. Shavlov, and B.A. Auld, "Design of Piezocomposites for Ultrasonic Transducers," Ferroelectrics, 91, 155-162 (1989).
8. L.M. Brown and K.S. Mazdiyasni, "Cold-Pressing and Low Temperature Sintering of Alkoxy-Derived PLZT," J. Amer. Cer. Soc., 55[1], 541-44 (1932).
9. J.B. Blum and S.R. Gurkovich, "Sol-Gel Derived $PbTiO_3$," J. Mat. Sci., 20, 4479-83 (1985).
10. M. Suzuki, S. Uedaira, H. Masuya, and H. Tamura, "Hydrothermal Synthesis of Lead Titanate Fine Powders," Ceramic Powder Science, II, A, eds., G. Messing, E. Fuller, Jr., and H. Hausner, 163-170 (1988).
11. J.H. Adair, T.R. Shrout, and K. Osseo-Asare, "Hydrothermal Synthesis of Perovskite Ceramic Powders," presented at Int. Meet. on Advanced Materials, MRS, Tokyo, Japan (1988).
12. K.C. Beal, "Precipitation of Lead Zirconate Titanate Solid Solutions under Hydrothermal Cnditions," Advances in Ceramics, Vol. 21: Ceramic Powder Science, 33-41 (1987).
13. S. Tashiro, N. Saski, Y. Tsuji, H. Igarashi, and K. Okazaki, "Sintering of Submicron Powders Prepared by Ball Milling," Jap. Jour. of Appl. Phys., 26, 142-44 (1987).
14. S. Venkataramani, "Calcining and its Effects on Sintering and Properties of Lead Zirconate Titanate Ceramics," Ph.D. Thesis, The Pennsylvania State University, University Park, PA (1981).
15. S.L. Swartz and T.R. Shrout, "Fabrication of Perovskite Lead Magnesium Niobate," Mat. Res. Bull., 17, 1245-50 (1982).
16. I.R.E. Standards on Piezoelectric Crystals: Measurements of Piezoelectric Ceramics (1961).
17. O. Okazaki and K. Nagata, Mechanical Behavior of Materials, pp. 404-12, The Society of Materials Science, Japan (1972).
18. K. Okazaki and K. Nagata, "Effects of Grain Size and Porosity on Electrical and Optical Properties of PLZT Ceramics," J. Amer. Cer. Soc., 56, 82-86 (1973).
19. X.L. Zhang, X. Chen, L.E. Cross, and W.A. Schulze, "Dielectric and Piezoelectric Properties of Modified Lead Titanate Zirconate Ceramics from 4.2 to 300 K," J. Mat. Sci., 18, 968-972 (1983).
20. T.R. Shrout, U. Kumar, M. Megherhi, N. Yang, and S.J. Jang, "Grain Size Dependence of Dielectric and Electrostriction of $Pb(Mg_{1/2}Nb_{2/3})O_3$-Based Ceramics," Ferroelectrics, 76, 479-487 (1989).

LIST OF FIGURES

Table I
Component and reacted powder characteristics.

Component Powders	S.A. m^2/g	Equivalent Particle Size (μm)	+Median Particle Size (μm) (Sedigraph)	AAN(50)
PbO	0.54	1.20	5.9	120
TiO_2	8.40	0.17		
ZrO_2	21.4	0.05	0.9	5,800
Reacted Powders				
[$ZrTiO_3$]-precursor	1.2	1.00	3.5	43
PZT-AS	0.50	1.50	3.8	16
PZT-M	2.97	0.25	1.1	85
ZTP-AS	1.09	0.68	1.8	18
ZTP-M	2.70	0.27	0.8	26

+Micromeretic Sedigraph (Model 5000).

Table II
Dielectric and piezoelectric properties of PZT and ZTP.

	Firing Temp. (°C)	Density (g/cm^3)	Average Grain Size (μm)	K (RT, 1 KHz)	D.F (%)	Piezo d_{33} ($x10^{-12}$ C/N)	k_p (%)	Q_m
*$Pb(Zr_{0.53}Ti_{0.47})O_3$	>1200	7.5	5-10	~700	---	~200	45	---
PZT-AS	1000	6.3	2.0	---	---	---	---	---
	1200	7.4	2.6	440	1.4	200	46	330
ZTP-AS	1000	7.8	2.1	890	1.6	180	25	240
	1200	7.9	2.8	800	0.7	250	50	380
PZT-M	1000	7.3	0.9	560	1.5	170	29	210
	1200	7.8	1.8	480	0.9	190	46	350
ZTP-M	1000	7.7	1.5	790	2.6	190	34	200
	1200	7.8	2.4	740	1.7	250	49	270

*Jaffe, Cook, and Jaffe[1]

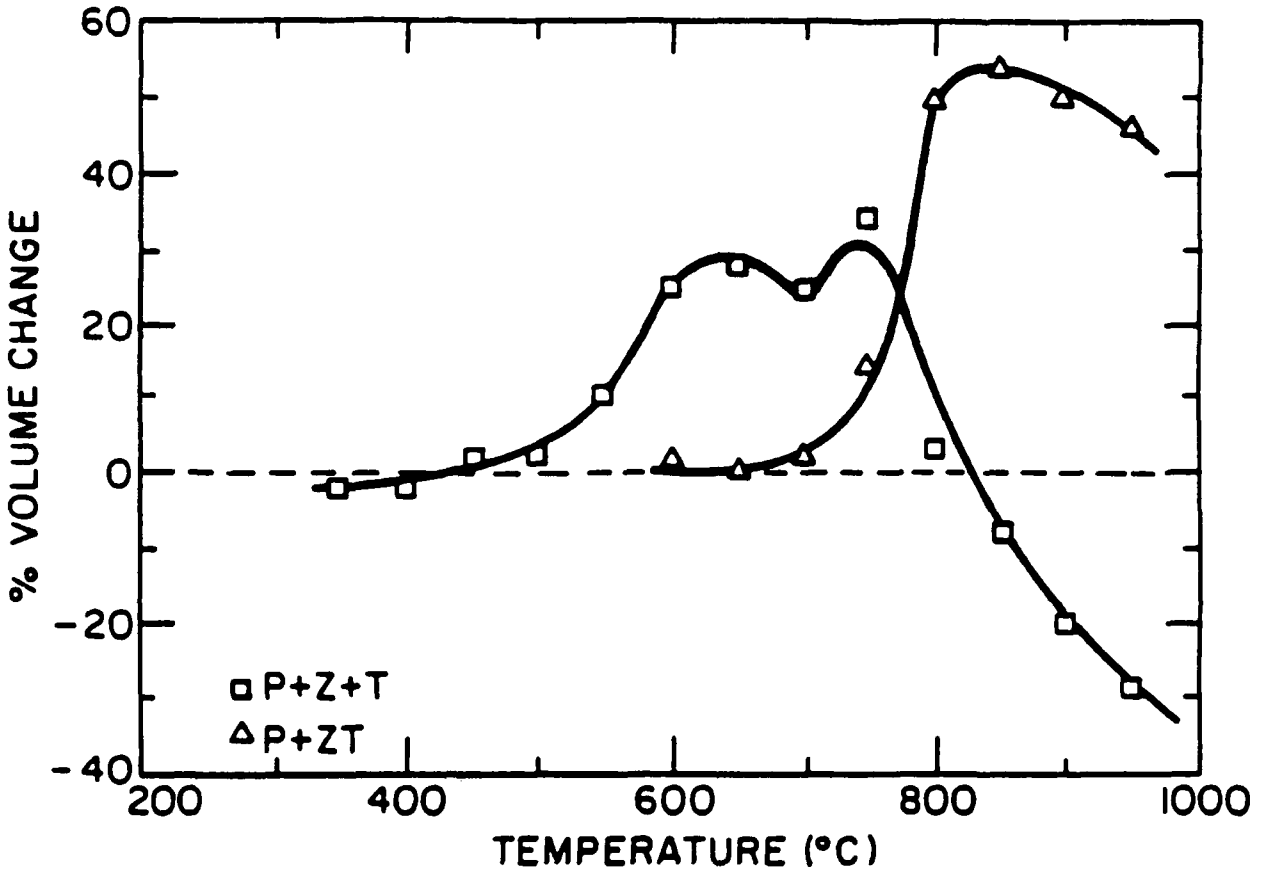

Figure 1. Volumetric expansion/shrinkage characteristics for P+Z+T (PZT) and ZT+P (ZTP) mixtures as a function of temperature.

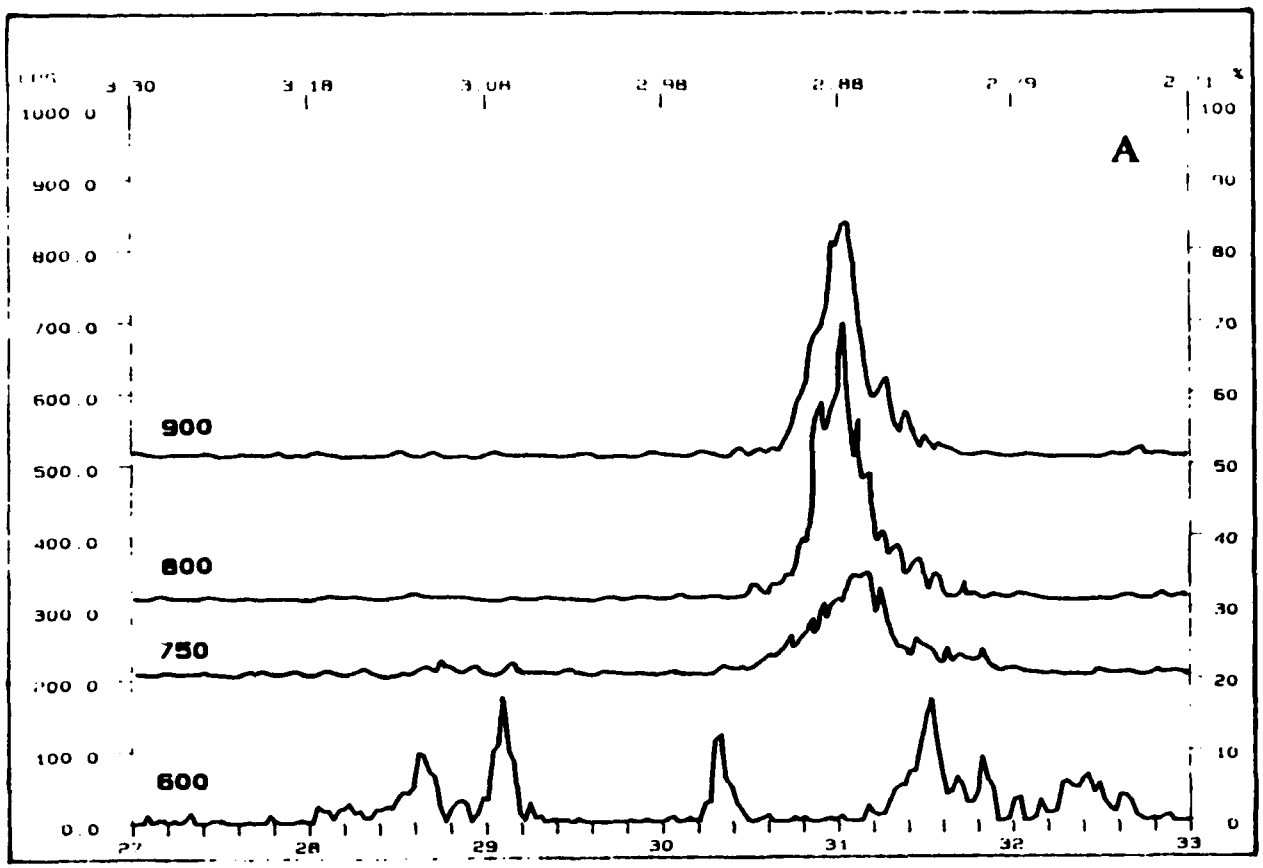

Figure 2. X-ray powder diffraction patterns for (a) P+Z+T and (b) ZT+P formation processes.

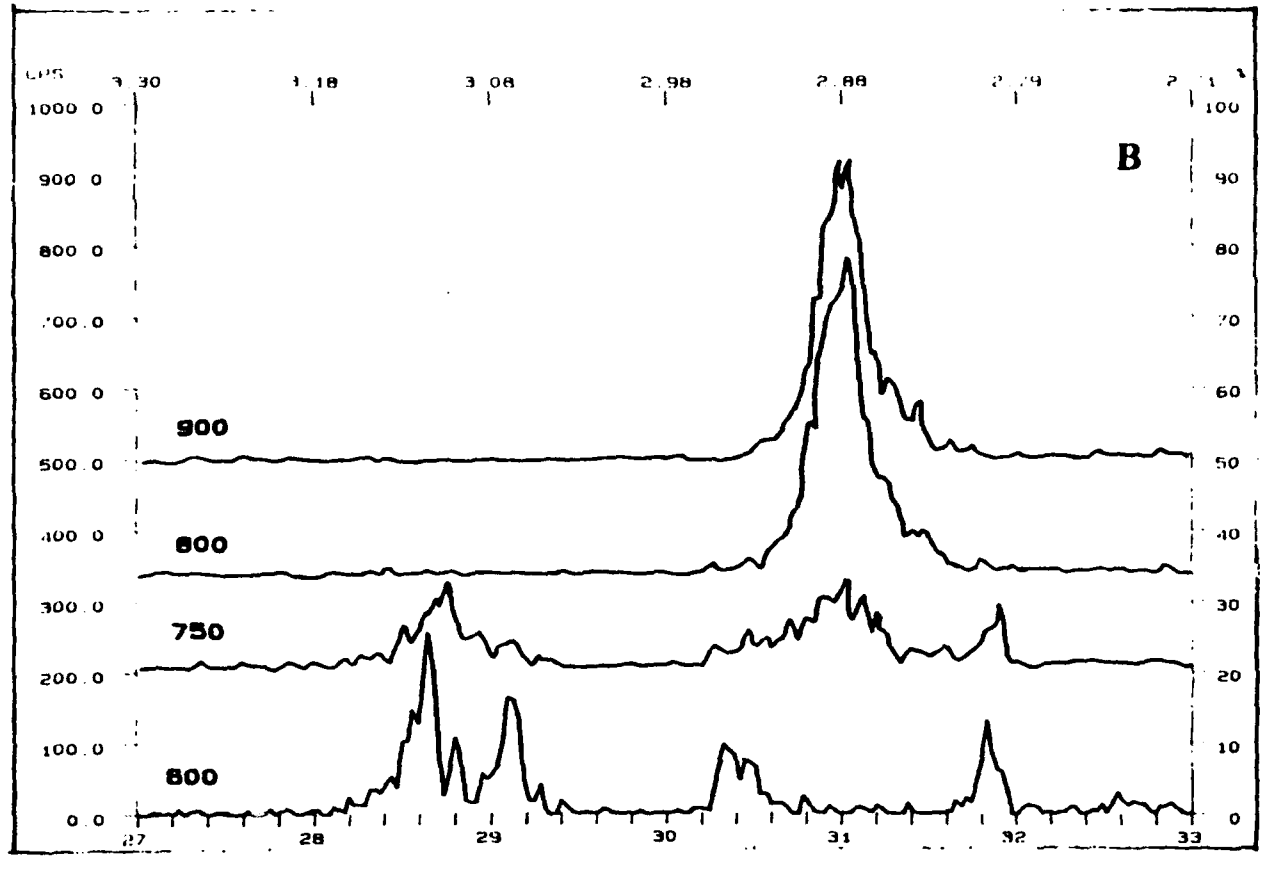
CPS
3.30
3.18
3.08
2.98
2.88
2.79
1000.0
900.0
800.0
700.0
600.0
500.0
400.0
300.0
200.0
100.0
0.0
100
90
80
70
60
50
40
30
20
10
0
B
900
800
750
600
27
28
29
30
31
32
33

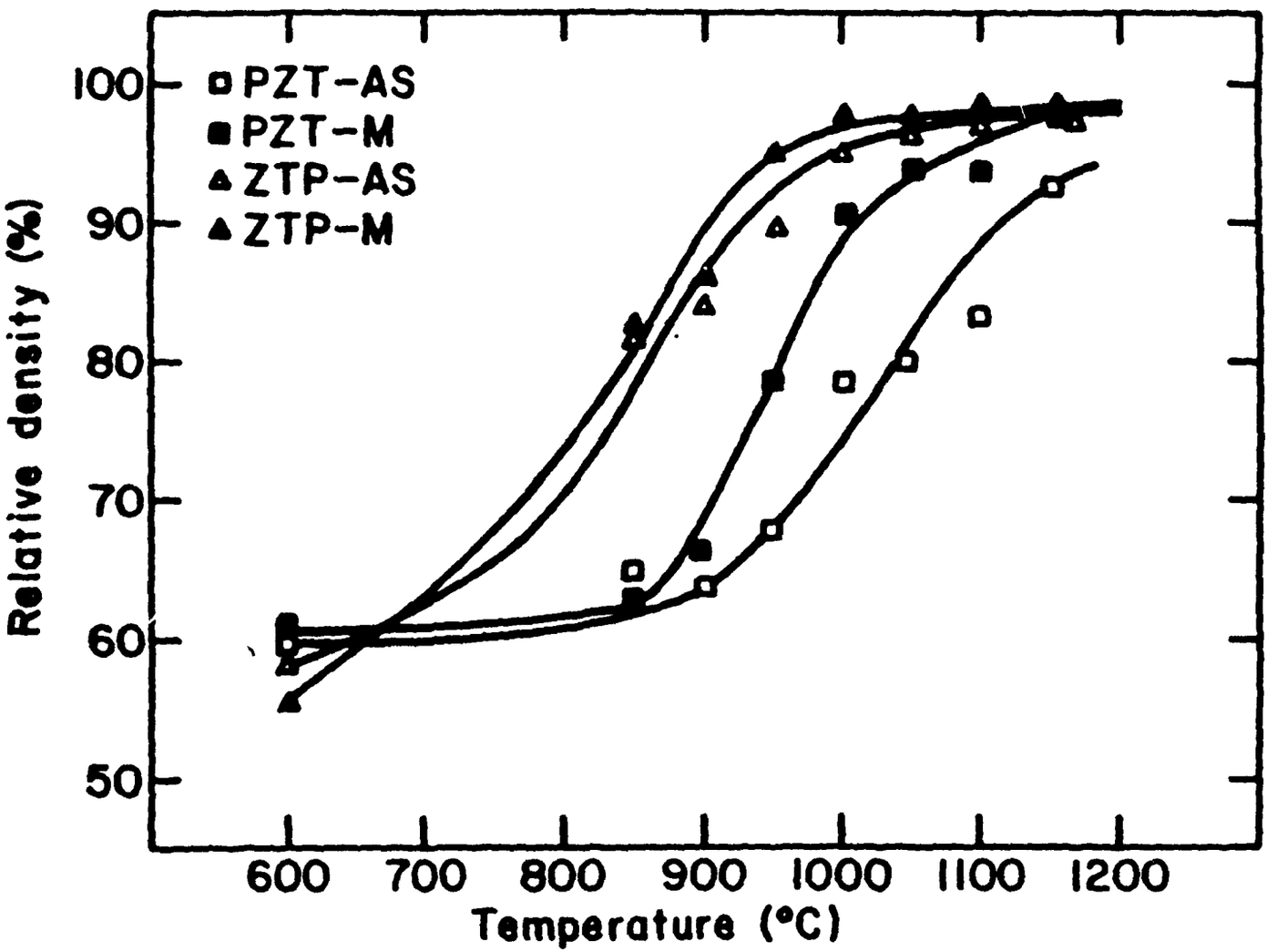

Figure 3. Sintering behavior of milled and as-calcined PZT and ZTP powders.

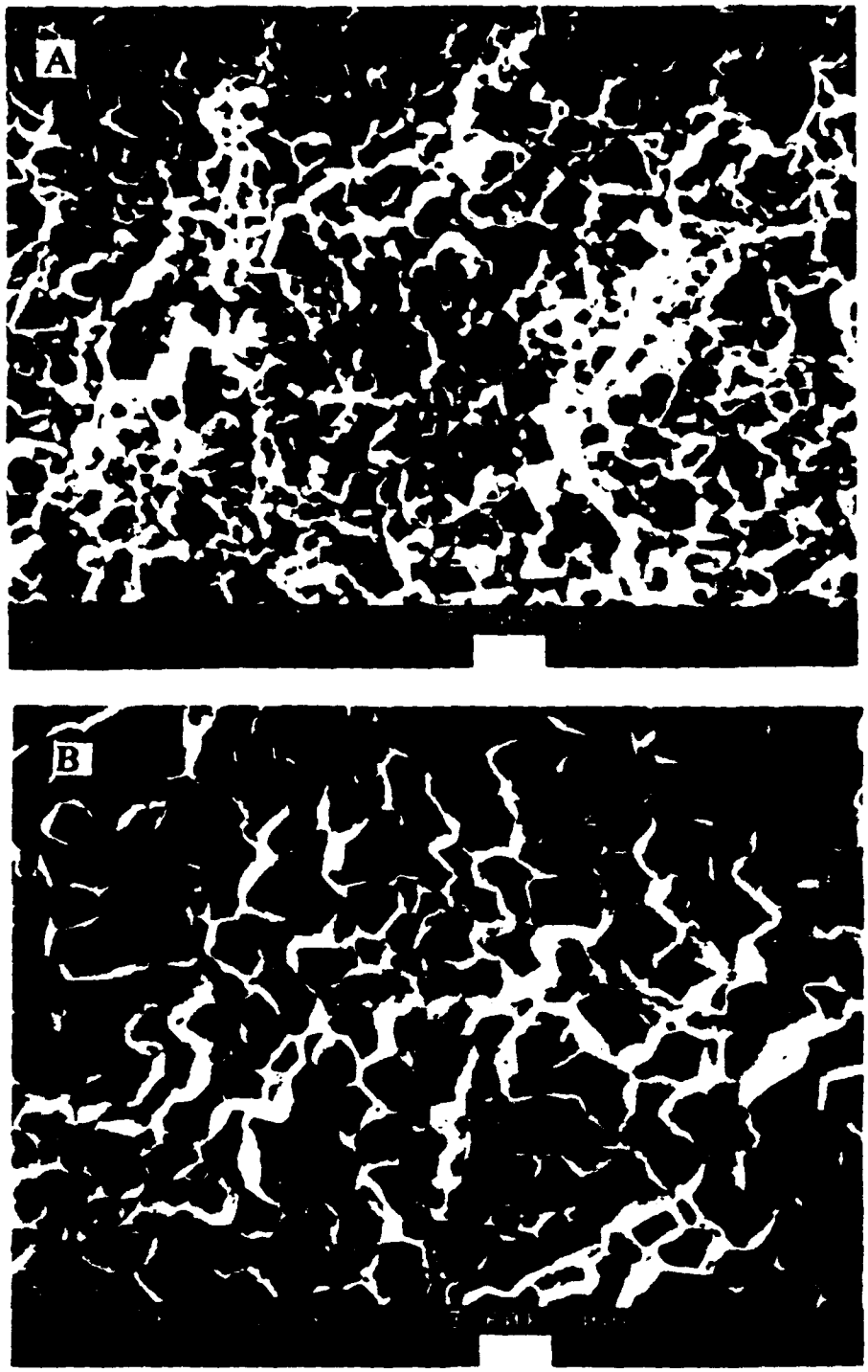

Figure 4. SEM photomicrographs of ZTP-M samples fired at (a) 1000°C and (b) 1200°C, respectively (fracture surfaces).

APPENDIX 48

CONVENTIONALLY PREPARED SUBMICRON LEAD-BASED PEROVSKITE POWDERS BY REACTIVE CALCINATION

T.R. Shrout, P. Papet, S. Kim, G.S. Lee
Materials Research Laboratory
The Pennsylvania State University
University Park, PA 16802

ABSTRACT

Submicron powders of various lead-based perovskites, including $PbTiO_3$, $PbZrO_3$, $Pb(Zr_{.53}Ti_{.47})O_3$ and $Pb(Mg_{1/3}Nb_{2/3})O_3$ were prepared by a reactive calcination process. Using only reagent grade raw materials and conventional processing techniques, highly reactive powders were produced by reacting the materials near the point of maximum volume expansion. At this point, the morphological development results in a skeletal type structure consisting of ultra-fine particulates that can be readily broken down further by milling. Powder sizes less than 0.3 microns and as small as 70 nanometers generally only achieveable using chemical processing techniques, were achieved. The highly reactive powders allowed densification to occur at temperatures as low as ~ 900°C with correspondingly small grain sizes. A model describing the physiochemical behavior and associated morphological development of Pb-based perovskites was herein proposed.

INTRODUCTION

Lead-based perovskites having the general formula $Pb(B)O_3$ encompass a large family of materials utilized in a wide range of applications including: multilayer capacitors, piezoelectric sensors and transducers, electrostrictive actuators, pyroelectric detectors, and optical devices.[1-6] Included are simple perovskites such as $PbTiO_3$ and $PbZrO_3$, and solid solutions therein (PZT) and more recently complex perovskites $Pb(B_1B_2)O_3$ such as $Pb(Mg_{1/3}Nb_{2/3})O_3$ [PMN] which belong to the family known as relaxor ferroelectrics.[7]

To continually optimize the performance of Pb-based perovskites, various methods to produce submicron powders for enhanced reactivity, uniformity, and reduced grain size have been developed. Methods include chemical synthesis techniques such as co-precipitation of alkoxides,[8-10] molten salt,[11] and hydrothermal.[12-14] However, most chemical synthesis techniques are relatively costly and do not lend themselves for mass production. Comminution of conventionally prepared calcined powders to submicron levels have been achieved through high energy milling, but generally results in excessive contamination and require extended milling times.[15,16]

Enhanced reactivity and subsequent densification of conventionally prepared Pb-based perovskites has been reported being related to the calcination conditions. Venkataramini[17] found that enhanced densification of PZT could be achieved by only partially reacting the component powders. The enhanced densification was believed to be the result of a reactive sintering process* which occurred during the final stages of perovskite formation. Though no explanation was given, Takagi et. al[18] observed enhanced densification for partially calcined Pb-based perovskites which reportedly possessed a PbO-rich surface layer on the B-site component oxides.

It is the physiochemical nature of Pb-based perovskites that upon reaction of the component oxides a large volume expansion occurs. This corresponding expansion is believed to be associated with the formation of phase(s) possessing a larger molar volume than the individual components or "topology" of the reaction which leads to rapid coarsening of the highly reactive product layer resulting in a porous skeletal type structure.[17,19] Schematically shown in Fig. 1, perovskite formation through the reaction of PbO and B-site oxide(s) involves the uni-directional diffusion (transfer) of PbO ($Pb^{+2}$and O^{-2} ions) through the product layer.[20] Studies on the reaction formation of PZT showed that drastic morphological changes occur at or near the associated volume expansion(s) which may result in particle sizes smaller than that of the initial starting powders. Further, it is our belief that at such a point of expansion, the reacted powders will require less energy to allow further reduction in size, that is, the skeletal structure can be readily broken down.

The objective of this work was to demonstrate the possibility of obtaining submicron Pb-based perovskite powders, through knowledge of their physiochemical behavior while utilizing only conventional processing techniques. Proposed mechanism(s) for enhanced densification are also discussed.

EXPERIMENTAL PROCEDURE

The lead-based materials chosen for this study included the simple perovskites $PbTiO_3$ [PT], $PbZrO_3$ [PZ], the solid solution $Pb(Zr_{.53}Ti_{.47})O_3$ [PZT] and the complex perovskite $Pb(Mg_{1/3}Nb_{2/3})O_3$ [PMN]. Reagent grade raw materials of lead carbonate hydroxide $2PbCO_3{\cdot}Pb(OH)_2$ or PbO (yellow)[a], magnesium carbonate hydroxide $MgCO_3{\cdot}Mg(OH)_2$[b],

*The term "reactive sintering" is herein defined as a process by which densification is enhanced as the result of an accompanying phenomena, e.g., chemical reaction, phase transformation, etc., which is greatly beneficial to diffusion and the overall sintering phenomena.

[a]Hammond Lead Products, White Lead HLP-A or PbO (yellow) 99%), Hammond, IN.

[b]Fischer Scientific Co., Magnesium Carbonate (purified grade), Pittsburgh, PA.

titanium dioxide (TiO_2)[c], niobium pentoxide (Nb_2O_5)[d], and zirconium dioxide (ZrO_2)[e] were used to prepare the compounds. The component powders were characterized by determining their as-received surface area, and particle size. Equally important as particle size, the degree of agglomeration of the powders was estimated from the ratio of the median equivalent spherical volume from the particle sizing technique to the average volume calculated from specific surface area (esd--equivalent spherical diameter) measurements. The ratio, designated as the average agglomeration number (AAN(50)) represents an estimate of the number of primary particles in each agglomerate.[21]

The powder characteristics are reported in Table I. No particle size and thus AAN(50) values for the magnesium carbonate hydroxide powder were reported due to its intrinsically poor dispersion characteristics. As presented and confirmed by SEM photomicrographs (not shown) the magnesium carbonate and zirconium dioxide powders were highly agglomerated.

Since intermediate reactions may occur in the formation of PZT and PMN when starting from individual oxides, the B-site oxides were pre-reacted following the established B-site precursor method developed by Swartz and Shrout.[22] The precursor method was as follows:

$$0.53\ ZrO_2 + 0.47\ TiO_2 \xrightarrow{\sim 1400^\circ C/4\ hr} Zr_{0.53}Ti_{0.47}O_2 \quad \text{(Rutile)} \qquad (1)$$

$$MgO + Nb_2O_5 \xrightarrow{\sim 1100^\circ C/4\ hr} MgNb_2O_6 \quad \text{(Columbite)} \qquad (2)$$

Once formed, reaction of the precursor with PbO eliminates (or suppresses) intermediate phases while going directly to the perovskite phase as given in the following expressions.

$$\begin{array}{lll} & - Zr_{.53}Ti_{.47}O_2 \text{ -----> } Pb(Zr_{.53}Ti_{.47})O_3\ [PZT] & \\ PbO + \text{B-site precursor} & & \text{(Perovskite)} \quad (3) \\ & - 1/3MgNb_2O_6 \text{ -----> } Pb(Mg_{1/3}Nb_{2/3})O_3\ [PMN] & \end{array}$$

For this study, the $Zr_{.53}Ti_{.47}O_2$ and $MgNb_2O_6$ precursors were prepared by either vibratory[f] or attrition[g] mixing/milling stoichiometric amounts of the component raw materials in

---

[c]Whittaker, Clark, and Daniels, TiO_2 (USP grade-99%), Pittsburgh, PA.

[d]Fansteel Nb_2O_5 (technical grade), North Chicago, IL.

[e]Harshaw/Filtrol, ZrO_2 (electronic grade), Cleveland, OH.

[f]Sweco, Inc., Model M-18-5, Florence, KY.

[g]Union Process, Inc., Model 01, Akron, OH.

ethyl alcohol or deionized H_2O and polyelectrolyte dispersant.[h] Upon drying, the powders were calcined in alumina crucibles. The calcined slugs were pulverized using a hammermill through a 0.2 mm screen. The powders were examined by x-ray diffraction (XRD) to insure phase purity. The powder characteristics of the precursors are also reported in Table I, possessing relatively large particle sizes (~ 2-3 μ) being only slightly agglomerated.

Stoichiometric mixtures of PbO and the B-site components were prepared as above. The source of PbO, either lead carbonate hydroxide or PbO (yellow) was based on ease of dispersion in deionized H_2O or alcohol, respectively. To determine the calcining temperature at which maximum volume expansion occurs, disks approximately 0.5" (1.3 cm) in diameter and 3-5 mm thick were pressed. The disks were placed in a furnace (open air) and heated at a rate of 120°C/hr. Above 500°C, disks were quenched at 50°C intervals being pulled directly from the furnace and allowed to cool in air. Sample geometries were used to determine the degree of expansion or shrinkage. The disks were then crushed and x-ray powder diffraction analysis performed to determine the degree and amount of phase(s) reaction. Based on these results, large quantities (~ kg) of loosely packed powders were prepared. The powders were calcined for 4 hrs approximately 50°C below the temperature of maximum expansion to allow for kinetics. The powder characteristics and XRD of the reacted materials were determined to evaluate the effect of thermal history. Determination of the ferroelectric (PT, PZT) and anti-ferroelectric (PZ) phase transitions (T_c) by differential thermal analysis (D.T.A.) was also used to confirm the completeness of the perovskite phase formation. No analysis was performed on PMN wing to the characteristic diffuse phase transition of relaxor ferroelectrics.

Slurries of the calcined powders in ethyl alcohol or deionized H_2O were prepared as before and attrition or vibratory milled 4 or 48 hrs, respectively. Preliminary investigations revealed that longer milling times did not significantly result in further size reduction. No attempt to determine optimum milling times having were made. The milled powders were then characterized for specific surface area. Due to the fact that the powder size(s) were below or near the limits of the particle sizing technique, particle size was determined through the equation:

$$D = \frac{6}{\rho S.A.} \qquad (4)$$

where ρ is the theoretical density, S.A. the specific surface area, and D the calculated primary particle size. TEM analysis was used to confirm particle size as well as the degree of agglomeration and morphology.

---

[h]Rohm and Haas, Tamol-901, Philadelphia, PA.

Preliminary sintering studies of disks pressed with milled powders of PMN and PZT were performed to determine the influence of highly reactive powders on the sintering kinetics.

RESULTS AND DISCUSSION

The change in volume of the uncalcined powder compacts as a function of temperature are plotted in Fig. 2. Only one distinct volume expansion maximum was found for individual mixtures, corresponding to only one reaction, that being perovskite formation. As shown, the temperature of volume expansion occurred ~ 600-650°C for PT, 750-800°C for PZ, 800-850°C for PZT, and 700-750°C for PMN. Naturally, the point of maximum volume expansion and corresponding temperature range is dependent on homogeneity, packing density and powder characteristics which may effect the overall kinetics of reaction. Also shown in Fig. 2, x-ray diffraction results confirmed the single step reaction to the perovskite phase as proposed earlier in equation (3). Though commonly reported in the formation of perovskite PMN, no pyrochlore phase(s) were observed.[22,23]

Instinctively, one expects that the powder compacts should shrink on heating as a consequence of higher product densities. As stated earlier, the associated volume expansion is believed to be associated with uni-directional PbO diffusion (Pb^{+2} and O^{-2} ions) occuring at a reaction layer at B-site oxide contact surfaces (see Fig. 1). A more descriptive schematic of the reaction process and associated morphological changes is presented in Fig. 3, whereby the larger PbO particles are assumed to be surrounded by the smaller B-site component oxides. Upon reaction, an expansion comes from the fact that the reaction perovskite phase possesses a different molar volume than that of one or both of the individual component oxides. This volume change/reaction enhances the formation of defects and fissures, consequently creating additional opportunities for surface and boundary diffusion.[24] This continuously changing structure thus results in a skeletal type structure comprised of "spongy" particulates confirmed experimentally by SEM for a reacted PMN powder compact as shown in Fig. 4a. With further thermal energy, the highly reactive particulates rapidly coarsen, resulting in an increase in porosity. This further volume increase schematically presented in Fig. 3 and experimentally in Fig. 4b, is the result of inhomogeneous densification owing to the low coordination number of the reaction regions, as observed in other ceramic systems.[25] It is at these critical stages of morphological development, that can result in particulate sizes significantly finer than the starting powders and whereby can be readily broken down further with milling. To describe this phenomena, the term "reactive calcination" is herein defined as the process by which highly reactive powders of the desired phase(s) are produced due to morphological changes in the starting raw materials.

The physical characteristics of the various powders (large batches) reactively calcined near the point of maximum volume expansion are reported in Table II. Except for the PMN powder, which contained ~ 10% pyrochlore, all the powders were fully reacted. It is important to realize that it is desirable that the perovskite formation reaction be complete prior to the firing/sintering step, since further morphological changes may hinder densification and overall homogeneity. Also presented in Table II, all the powders had relatively large surface areas (> 1-2 m^2/g) and fine primary particle sizes. Though calcined below the temperature of maximum volume expansion the large powder batches possessed correspondingly similar surface areas. Upon milling, the powder surface areas increased more than double with particle sizes as fine as 70 nanometers for PMN. Perovskite powders having particle sizes, generally only achieveable using sophisticated chemical processing techniques were thus obtained.

Though more complex, the finest powders were achieved for the PMN which possessed the largest volume expansion during reaction. The calculated particle sizes were confirmed by TEM analysis, as reported in Table II. Representative TEM photomicrographs of PZ and PT powders are shown in Fig. 5. Commonly observed for ultra-fine powders, the PZ, PMN, and PZT materials were agglomerated owing to the influence of van der Waals attractive intermolecular interactions which take on a greater importance as particle size decreases.[26] Interestingly, the PT powder was less agglomerated (see Fig. 5c)! This behavior was believed to be related to the large polarization that develops upon cooling through the paraelectric-ferroelectric transition (T_c) and hence modifies the surface charge. However, more understanding of the relationship between surface charge and polarizability is required.

The results of the sintering study performed on the reactively calcined PMN and PZT materials are summarized in Fig. 6. As found, the submicron prepared powders densified at temperatures 100-200°C lower than that generally reported for conventionally processed materials.[1,2,54,5] Also shown, milling further enhanced the reactivity and subsequent densification of PMN and PZT ceramics with densities > 90% theoretical obtained at firing temperatures as low as 900°C. The resulting grain sizes for dense samples were also found to be relatively small in the $\leq 1\ \mu$ range.

It was previously suggested that the improved densification of PbO-based perovskites was the result of a reactive sintering process, whereby densification was enhanced owing to the on-going completion of phase formation. In this work, however, x-ray diffraction analyses clearly indicated that the powders were crystalline and stoichiometrically single phase. In addition, D.T.A. results of T_c's (see Table II) were found to be in agreement with reported values.[2] Thus, the enhanced sintering comes simply from the fact that highly reactive powders could be produced by a reactive calcination process being realized as a result of morphological changes associated

with the formation of PbO-based perovskite materials. Further it was these morphological developments that allowed additional reactivity through particle size reduction by milling.

CONCLUSION

In this work the physiochemical behavior during the formation of lead-based perovskites ($PbBO_3$) was investigated and modeled. Based on this model, it was proposed that highly reactive powders could be prepared by reacting the component materials near the point of maximum expansion. At this point, the associated morphological development results in a spongy/skeletal type structure consisting of ultra-fine particulates that can be readily broker. down further by milling. Using this concept of "reactive calcination" fully reacted perovskite powders (simple and complex) of $PbTiO_3$, $PbZrO_3$, $Pb(ZrTi)O_3$, and $Pb(Mg_{1/3}Nb_{2/3})O_3$ with particle sizes < 0.3 μ and as low as 70 nanometers, were achieved using only reagent grade raw materials. The highly reactive powders allowed densification at temperatures 100-200°C lower than that reported for conventionally prepared materials.

Naturally, the reactive calcination process of PbO-based perovskites can be further optimized by investigating the role of the component powder characteristics overall homogeneity, packing density and subsequent milling conditions.

The possibility of using reactive calcination and subsequent milling to prepare highly reactive powders of additional perovskites, ferrites (spinels and garnets) and other systems prepared from multiple components needs to be explored.

REFERENCES

1. J.M. Herbert, Ceramic Dielectrics and Capacitors, Electrocomponent Science Monographs, Vol. 6, Gordon and Breach, NY (1985).
2. B. Jaffe, W.R. Cook, Jr., and H. Jaffe, Piezoelectric Ceramics, Academic Press, NY (1971).
3. K. Uchino, "Electrostrictive Actuators: Materials and Applications," Cer. Bull., 65, 4 (1986).
4. R.C. Buchanan, Ceramic Materials for Electronics, pp. 154-222, Marcel Dekker, Inc., NY (1986).
5. L.M. Levinson, Electronic Ceramics Properties, Devices, Applications, pp. 371-492, Marcel Dekker, Inc., NY (1987).
6. R.E. Whatmore, P.C. Osbond, and N.M. Shorrocks, "Ferroelectric Materials for Thermal IR Detectors," Ferroelectrics, 76, 351-367 (1987).

7. L.E. Cross, "Relaxor Ferroelectrics," Ferroelectrics, 76, 241-267 (1987).
8. P. Ravindranathan, S. Komarnani, a.S. Bhalla, R. Roy, and L.E. Cross, "Sol-Gel Processing of Lead Magnesium Niobate (PMN) Powder and its Characterization," Ceramic Powder Science, II, A, eds., G. Messing, E. Fuller, Jr., and H. Hausner, 182-189 (1978).
9. L.M. Brown and K.S. Mazdiyasni, "Cold-Pressing and Low Temperature Sintering of Alkoxy-Derived PLZT," J. Amer. Cer. Soc., 55[1], 541-44 (1932).
10. J.B. Blum and S.R. Gurkovich, "Sol-Gel Derived $PbTiO_3$," J. Mat. Science, 20, 4479-83 (1985).
11. R.H. Arendt, J.H. Rosolowski, and J.W. Szymaszek, "Lead Zirconate Titanate Ceramics from Molten Salt Solvent Synthesized Powders," Mater. Res. Bull., 14[5], 703-709 (1979).
12. M. Suzuki, S. Uedaira, H. Masuya, and H. Tamura, "Hydrothermal Synthesis of Lead Titanate Fine Powders," Ceramic Powder Science, II, A, eds., G. Messing, E. Fuller, Jr., and H. Hausner, 163-170 (1988).
13. J.H. Adair, T.R. Shrout, and K. Ossea-Asare, "Hydrothermal Synthesis of Perovskite Ceramic Powders," presented at Int. Meet. on Advanced Materials, MRS, Tokyo, Japan (1988).
14. K.C. Beal, "Precipitation of Lead Zirconate Titanate Solid Solutions under Hydrothermal Conditions," Advances in Ceramics, Vol. 21: Ceramic Powder Science, 33-41 (1987).
15. Shinjiro Tashiro, Norio Saski, Yuuji Tsuji, Hideji Igarashi, and Kiyashi Okazaki, "Sintering of Submicron Powders Prepared by Ball Milling," Jap. Jour. of Appl. Phys., 26, 142-44 (1987).
16. C. Greskovich, "Milling Treatise on Materials Science and Technology," Vol. 9, Ceramic Fabrication Processes, F.F.Y. Wang, ed., Academic Press, NY (1976).
17. S. Venkataramini, "Calcining and its Effects on Sintering and Properties of Lead Zirconate Titanate Ceramics," Ph.D. Thesis, The Pennsylvania State University, PA (1981).
18. T. Takagi, K. Anetami, and K. Shimiza, "Lead-containing Oxide Powder," U.S. Pat. 4,812,426 (1989).
19. D.A. Buckner and P.D. Wilcox, "Effects of Calcining on Sintering of Lead Zirconate-Titanate Ceramics," Amer. Cer. Soc. Bull., 51, 218-222 (1972).
20. V.V. Prisedskii, L.G. Klevtsova, and V.V. Klimov, "Mechanism and Kinetics of Reactive Diffusion During the Formation of Lead Titanate and Lead Zirconate," Izv. Akad. Nauk. SSSR, Neorg. Mat. 10, 2166-2172 (1974).

21. J.H. Adair, A.J. Roese, and L.G. McCoy, Particle Size Analysis of Ceramic Powders, Advances in Ceramics, Vol. II, Processing for Improved Productivity, M.M. Nair, eds., The American Ceramic Society, Columbus, OH (1984).

22. S.L. Swartz and T.R. Shrout, "Fabrication of Perovskite Lead Magnesium Niobate," Mat. Res. Bull., 17, 1245-50 (1982).

23. T.R. Shrout and Arvind Halliyal, "Preparation of Lead-Based Ferroelectric Relaxors for Capacitors," Amer. Cer. Soc. Bull., 66, 704-711 (1987).

24. W.D. Kingery, H.K. Bowen, and D.R. Uhlmann, Introduction to Ceramics, p. 425, John Wiley and Sons, NY (1976).

25. D.W. Budworth, "A Random Packing Geometrical Model of Sintering," Ceramic Microstructures, eds., R.M. Fulrath and J.A. Pask, 255-260, Westview Press, Boulder, CO (1977).

26. G.Y. Onoda, Jr. and L.L. Herd, eds., Ceramic Processing Before Firing, pp. 35-37, John Wiley and Sons, NY (1978).

LIST OF FIGURES

Table I
Component Powder Characteristics.

Material	Specific Surface Area (m^2/g) (esd μm)	+Median Particle Size (μm)	AAN(50)
White Lead ($2PbCO_3 \cdot Pb(OH)_2$)	0.82 (1.2)	3.5	25
PbO (yellow)	0.54 (1.2)	5.9	120
Magnesium Carbonate ($MgCO_3 \cdot Mg(OH)_2$)	24.5 (0.12)	---	---
Titanium Dioxide (TiO_2)	8.4 (0.17)	0.44	17
Niobium Pentoxide (Nb_2O_5)	2.0 (0.67)	1.4	9
Zirconium Dioxide (ZrO_2)	21.4 (0.05)	0.9	5,800
Precursors			
$Zr_{.53}Ti_{.47}O_2$	1.2 (1.0)	3.5	45
$MgNb_2O_6$	0.9 (1.3)	2.5	7

+Micromeretic Sedigraph (Model 5000)

Table II
Physical characteristics of reactive calcined perovskite powders.

Material	Calcine Condition	Phase(s)	T_c	Specific Surface Area (m^2/g)-(esd) [as-calcined]	[milled]	Particle Size (TEM)	Agglomeration (subjective)
$PbTiO_3$	625°C/4 hr	Perov	490°C	1.8 (0.4)	3.7 (0.2 μ)	~ 0.3 μ	Little
$PbZrO_3$	725°C/4 hr	Perov	320°C	2.0 (0.4)	5.1 (0.15 μ)	~ 0.3 μ	Extensive
$Pb(Mg_{1/3}Nb_{2/3})O_3$	650°C/4 hr	Perov + (10% Pyr)	---	1.6 (0.5 μ)	10 (0.07 μ)	~ 0.2 μ	Extensive
$Pb(Zr_{.53}Ti_{.47})O_3$	725°C/4 hr	Perov	350°C	1.1 (0.7 μ)	2.7 (0.3 μ)	~ 0.4 μ	Moderate

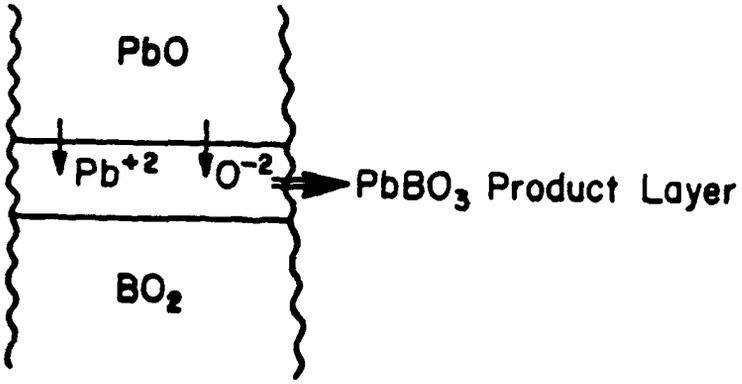
PbO
Pb^{+2}
O^{-2}
$PbBO_3$ Product Layer
BO_2

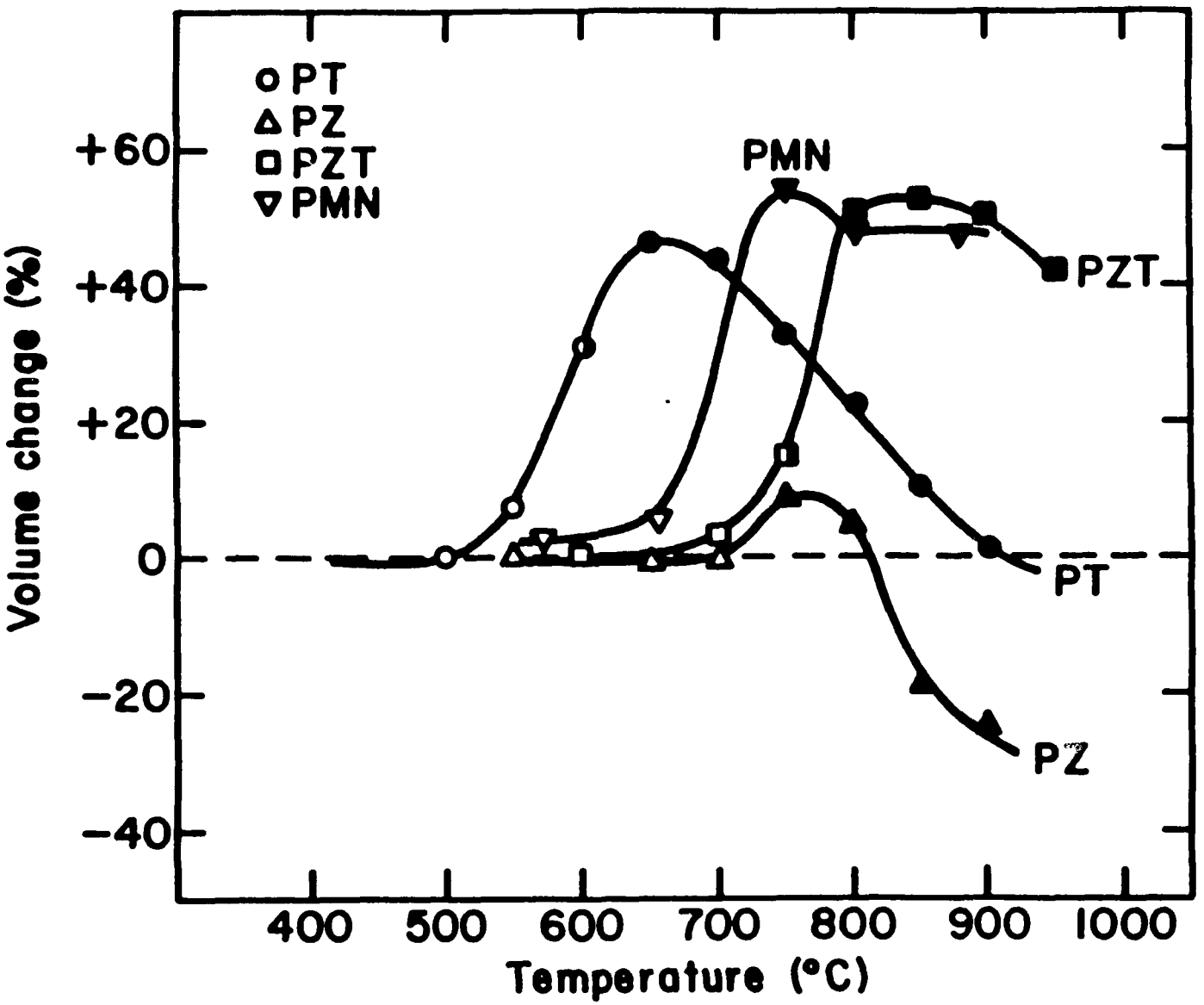
PT
PZ
PZT
PMN
+60
+40
+20
0
-20
-40
Volume change (%)
400
500
600
700
800
900
1000
Temperature (°C)
PMN
PZT
PT
PZ

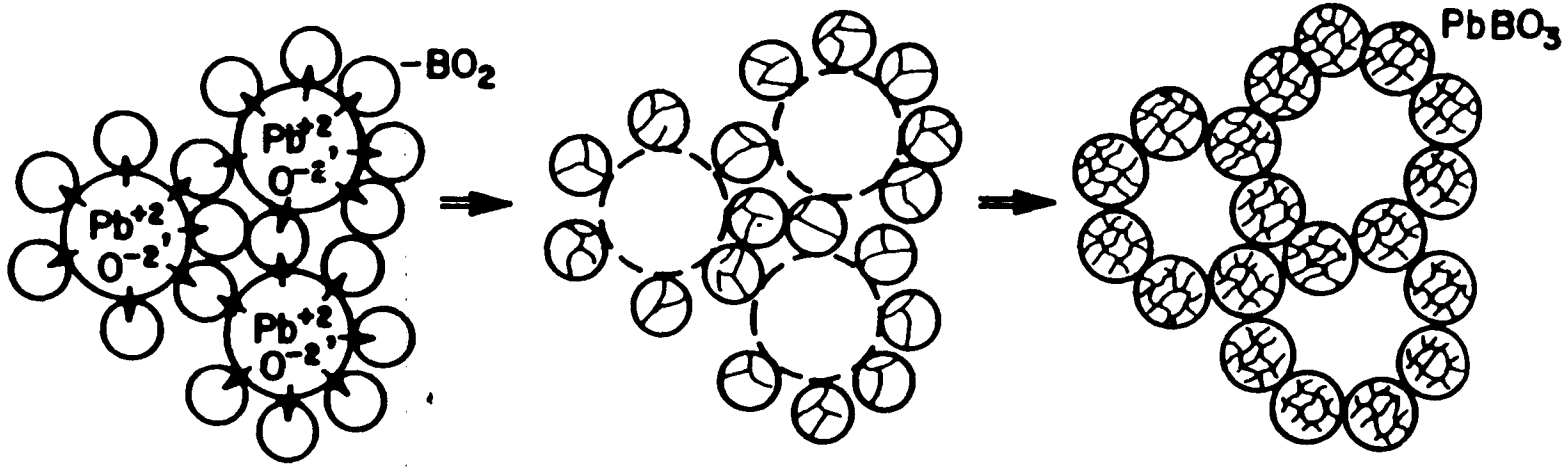
$-BO_2$
Pb^{+2}
O^{-2}
Pb^{+2}
O^{-2}
Pb^{+2}
O^{-2}
$PbBO_3$

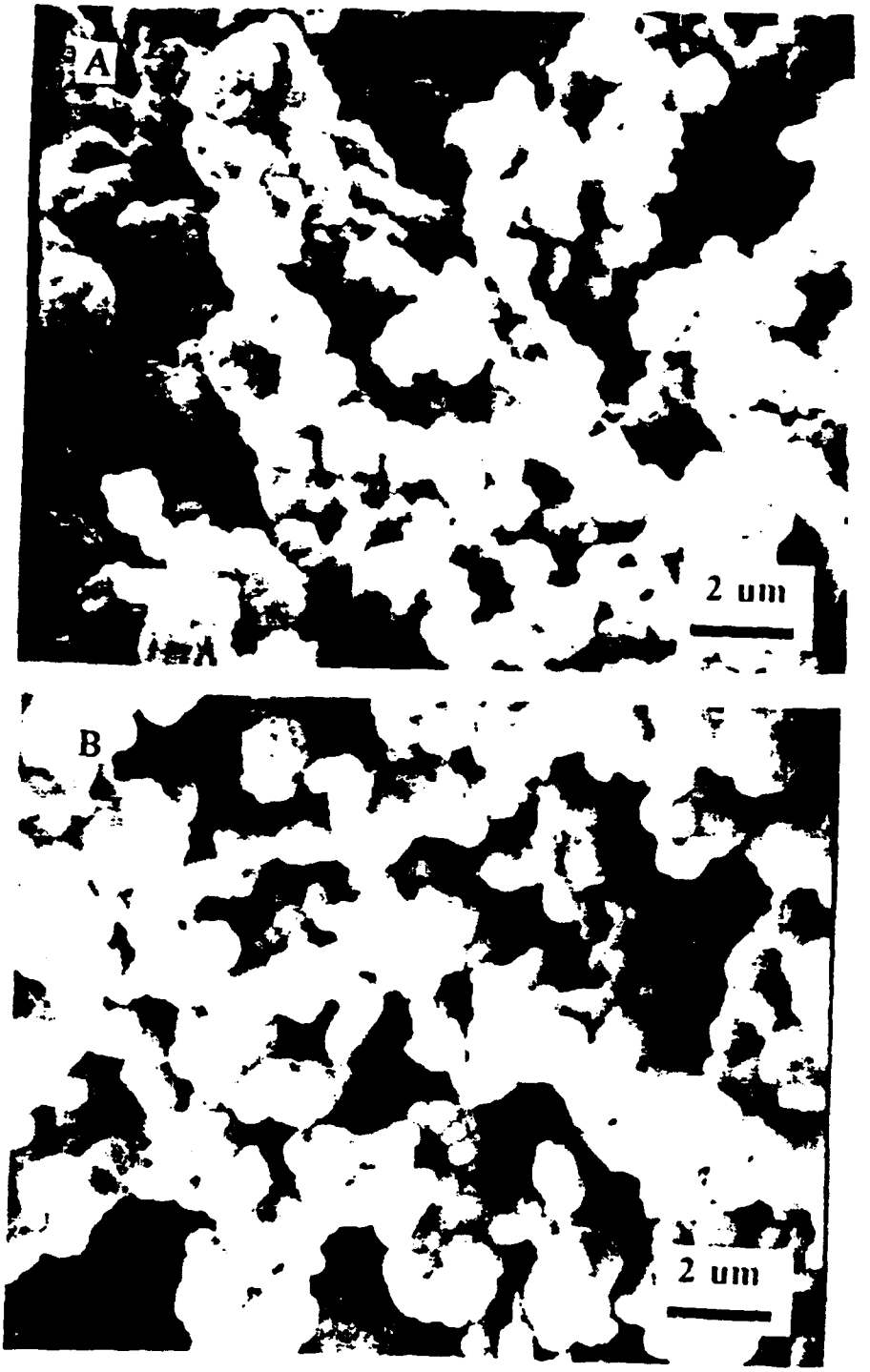
A
2 um
B
2 um

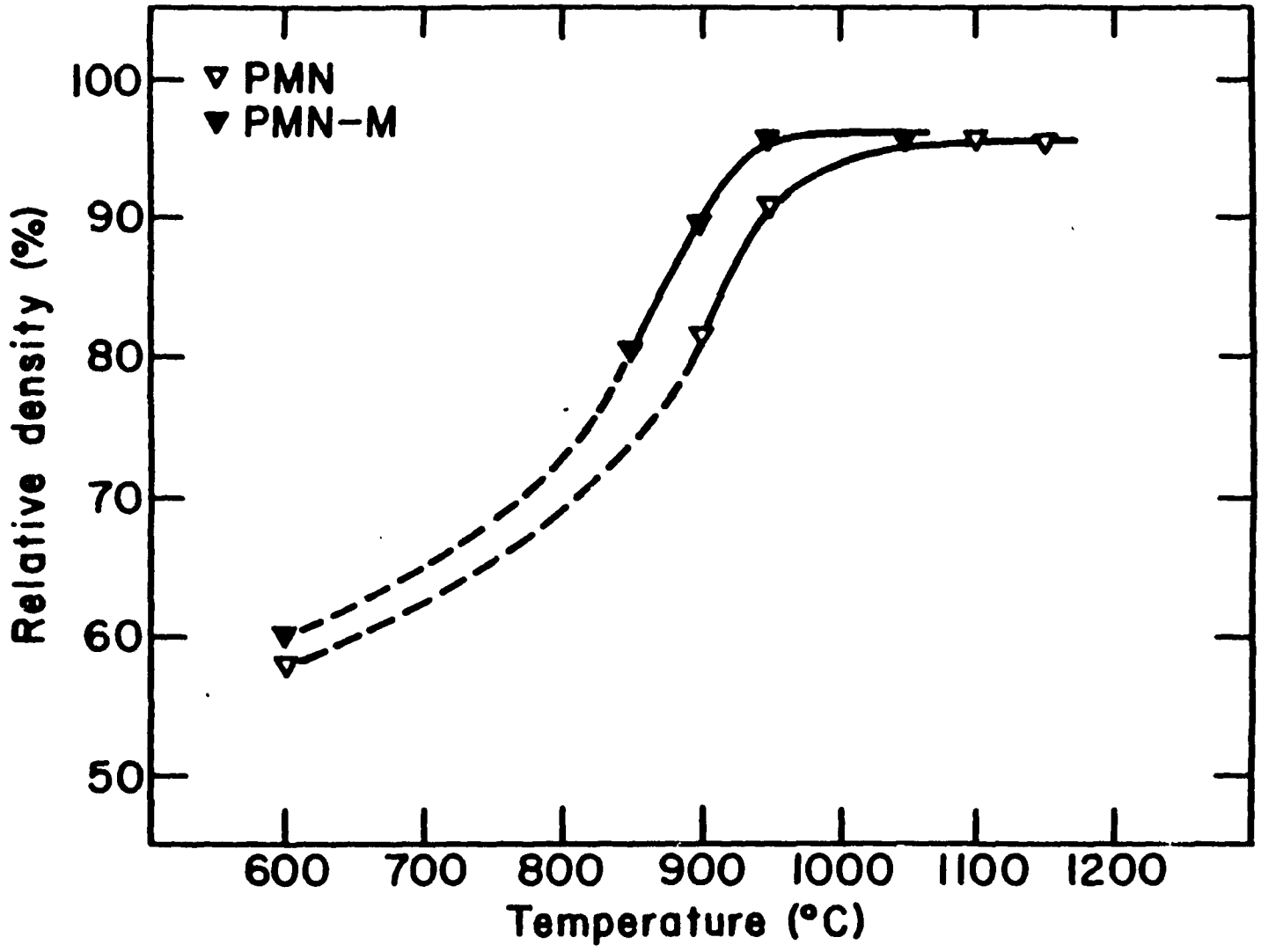
▽ PMN
▼ PMN-M
100
90
80
70
60
50
Relative density (%)
600
700
800
900
1000
1100
1200
Temperature (°C)

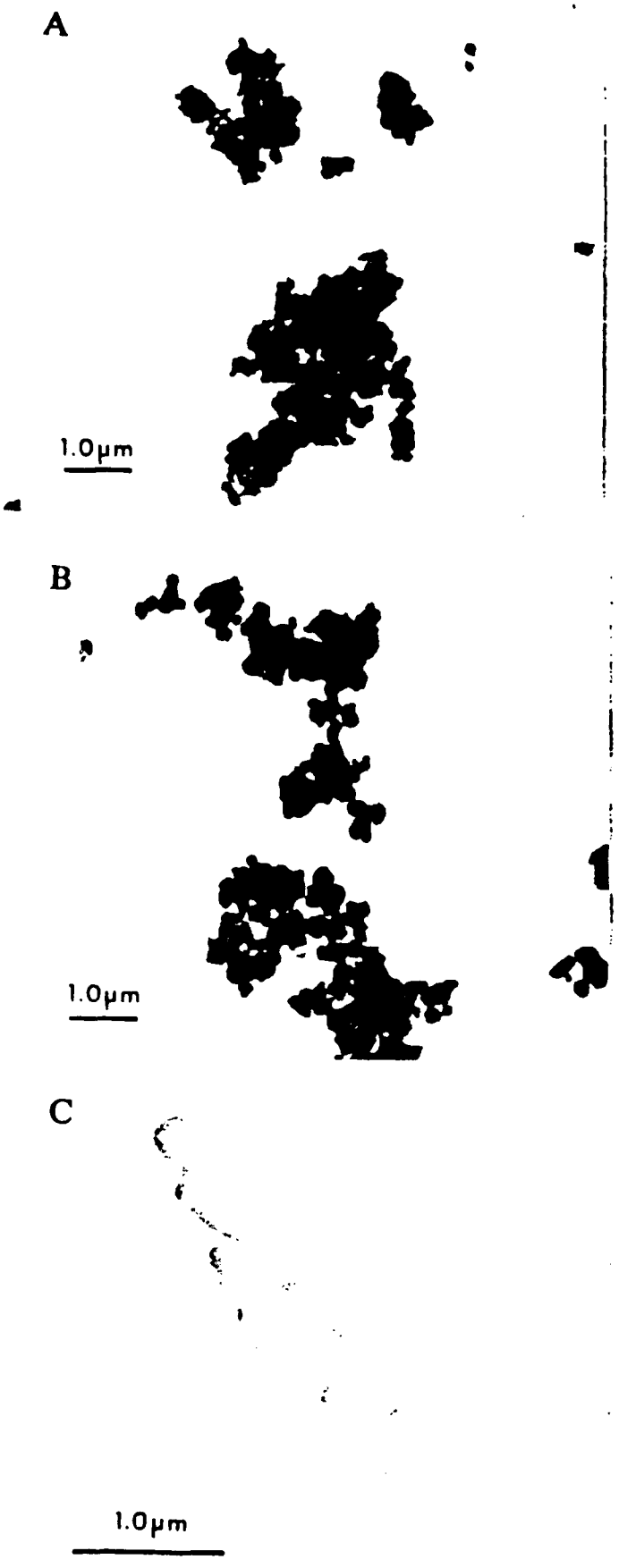
A
1.0μm
B
1.0μm
C
1.0μm

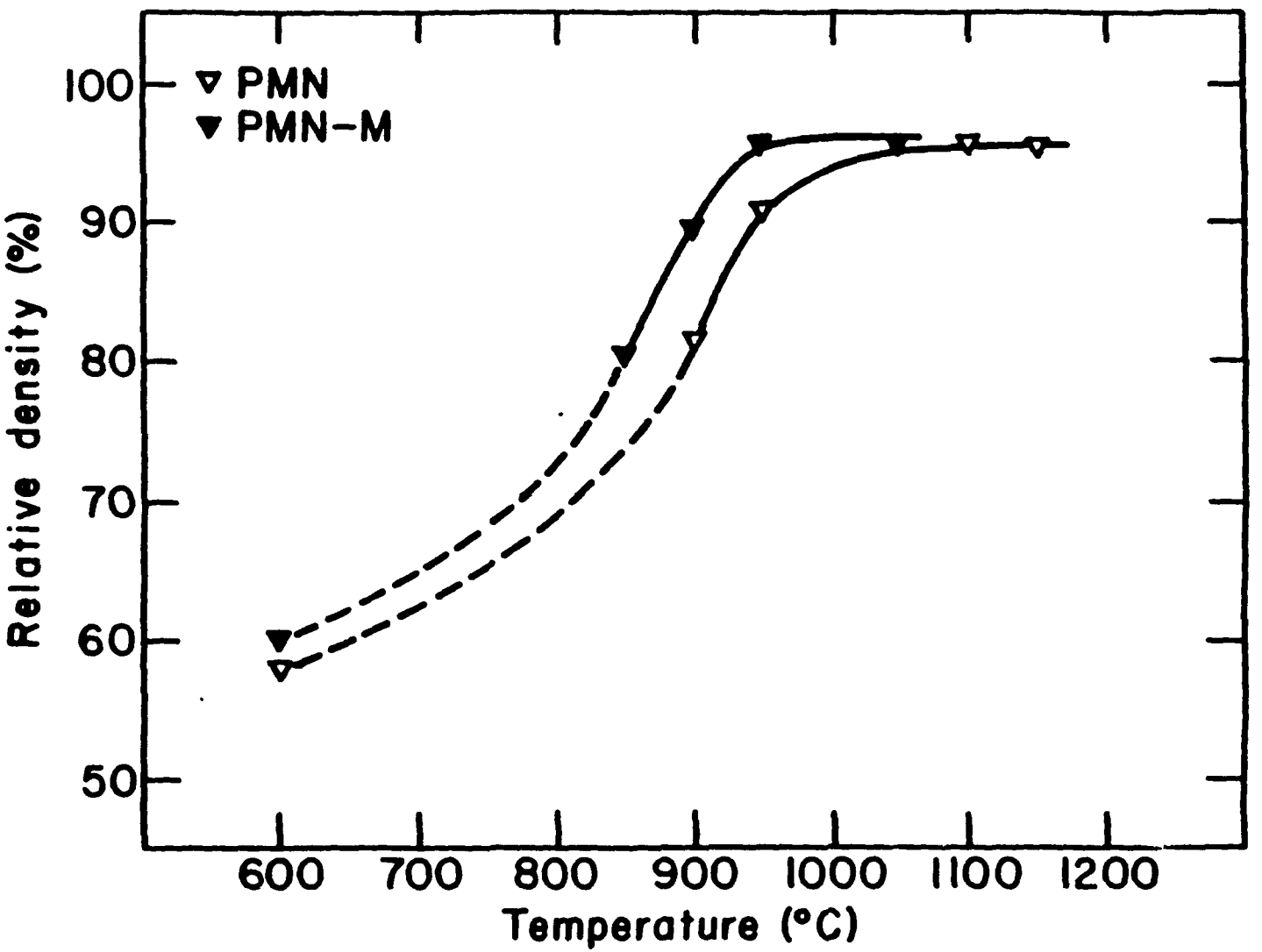
PMN
PMN-M
Relative density (%)
100
90
80
70
60
50
600
700
800
900
1000
1100
1200
Temperature (°C)

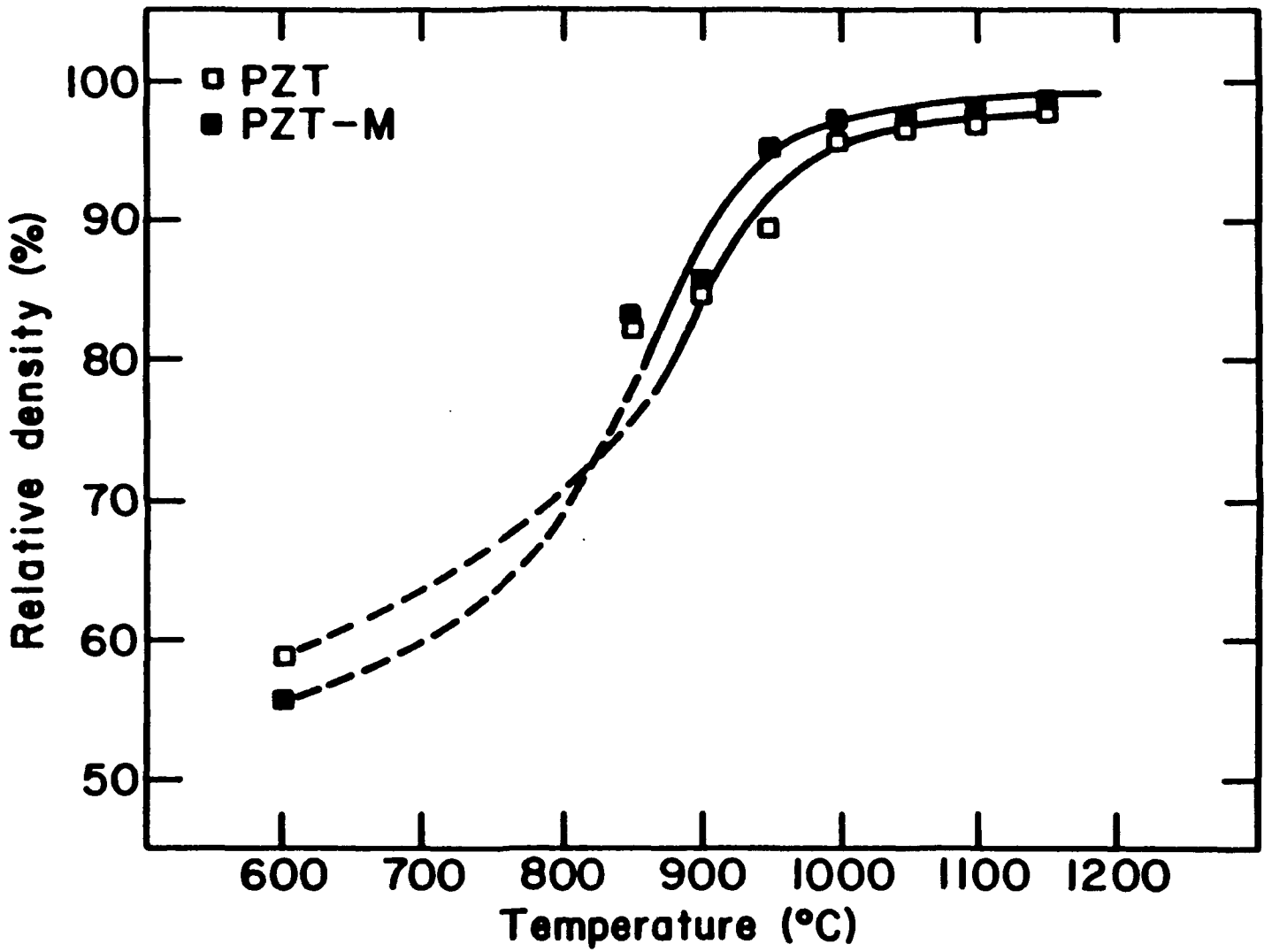
PZT
PZT-M
Relative density (%)
100
90
80
70
60
50
600
700
800
900
1000
1100
1200
Temperature (°C)

APPENDIX 49

II-15

FABRICATION OF POROUS ELECTROCERAMIC STRUCTURES BY REACTIVE CALCINATION

THOMAS R. SHROUT, YOUNG S. KIM, and JOSEPH FIELDING, JR.
Pennsylvania State University, 150 Materials Research Laboratory, University Park, PA 16802, USA.

S. VENKATARAMANI
General Electric Co., Schenectady, NY 12301

ABSTRACT: It is the physiochemical nature of lead-based perovskites $Pb(B)O_3$ and pyrochlores $Pb_2(B_2)O_{6-7}$ that upon reaction of the component oxides a large volumetric expansion occurs. The degree of expansion is strongly dependent on the starting powder characteristics (size, distribution, etc.). The corresponding morphological development allows the ability to obtain highly porous skeletal type ceramic structures. Using this concept of "reactive calcination" a high degree of controlled porosity (> 40%) without utilizing fugitive phase organic or volatile components can be obtained as a result of inhomogeneous densification. Potential applications include PZT/polymer composites for hydrophones, piezoelectrically active filters/membranes, and other devices (sensors) whereby a large "active" surface area is desired.

1. INTRODUCTION

Studies on the physiochemical nature and formation process of Pb- and Bi-based perovskites (ABO_3) and pyrochlores ($A_2B_2O_{6-7}$) including the layered structure $Bi_4Ti_4O_{12}$ have demonstrated the possibility of "smart processing." By monitoring the point of maximum volume expansion during the reaction process, the temperature of phase formation and state of optimum agglomeration (soft) can be determined.[1] As expected, the point and degree of expansion has been found to be strongly dependent on the starting powder characteristics such as size.[2] Using the concept of "reactive calcination" has allowed the ability to produce submicron to nano sized powders of a variety of commercially viable materials with only reagent raw grade materials Fundamentally, the ability to produce fine powders has helped the understanding of the role of scale, both particle and grain size, on ferroelectric and related behavior.[3,4]

In addition to fine powders, the same morphological development associated with the formation of Pb- and Bi-based materials allows the ability to obtain highly porous skeletal type ceramic structures owing to inhomogeneous densification.[5,6] It was the objective of this work to demonstrate the potential of using reactive calcination to fabricate ceramic structures with controlled porosity without utilizing fugitive phases (organics) or foaming techniques. Potential applications for such ceramic structures would include piezoelectric/polymer composites for hydrophones, and active filters/membranes, and devices such as sensors, whereby a large "active" surface area is desired.

2. EXPERIMENTAL

The material chosen to explore the potential of reactive calcination on fabricating highly porous structures was the solid solution $Pb(Zr_{.53}Ti_{.47})O_3$ (PZT). Reagent grade raw materials used are described in Ref. 2. Since intermediate reactions occur during the formation of the complex perovskite PZT, the B-site precursor method after Swartz and Shrout[7] was used whereby the refractory B-site oxides ZrO_2 and TiO_2 were pre-reacted prior to reaction with PbO as follows:

$$0.53\ ZrO_2 + 0.47\ TiO_2 \xrightarrow{\sim 1400°C/4\ hrs.} Zr_{.53}Ti_{.42}O_2\ (rutile)$$

$$PbO + Zr_{.53}Ti_{.47}O_2 \longrightarrow PZT\ (perovskite)$$

As reported in Ref. 2, and shown in Fig. 1, the volumetric expansion-shrinkage behavior during the formation of PZT is strongly dependent on the component powder characteristics. Based on this work, component powders of comparable size (~ 1.4 μm) (Case III) were selected to achieve maximum volumetric expansion. To allow for a finer pore structure, component powders with large size differences (PbO >> ZT) approximately 10:1 (Case IV), were also used. Following mixing in de-ionized H_2O and polyelectrolyte dispersant at a pH where minimal dissolution of Pb^{+2} occurs, the dried powders were pressed into disks.

To induce expansion, the disks were then placed in an open furnace and heated at a rate of ~ 100°C/hr to a temperature near the point of maximum volumetric expansion. Upon cooling, sample geometries revealed that the degree of expansion was > 45% for Case III and ~ 25% for Case IV. The expanded disks were then fired in closed alumina crucibles in the range of 1050°C to 1200°C for 2 hrs. to achieve well developed microstructures, i.e., grain growth. $PbZrO_3$ powder was used to prevent PbO volatility. The fired disks were physically characterized for weight loss, geometric density, and pore/channel size (SEM). The samples were electroded (Au-sputter) and poled at 30 Kv/cm at 120°C for 5 minutes. Following poling, the dielectric and piezoelectric properties were determined.

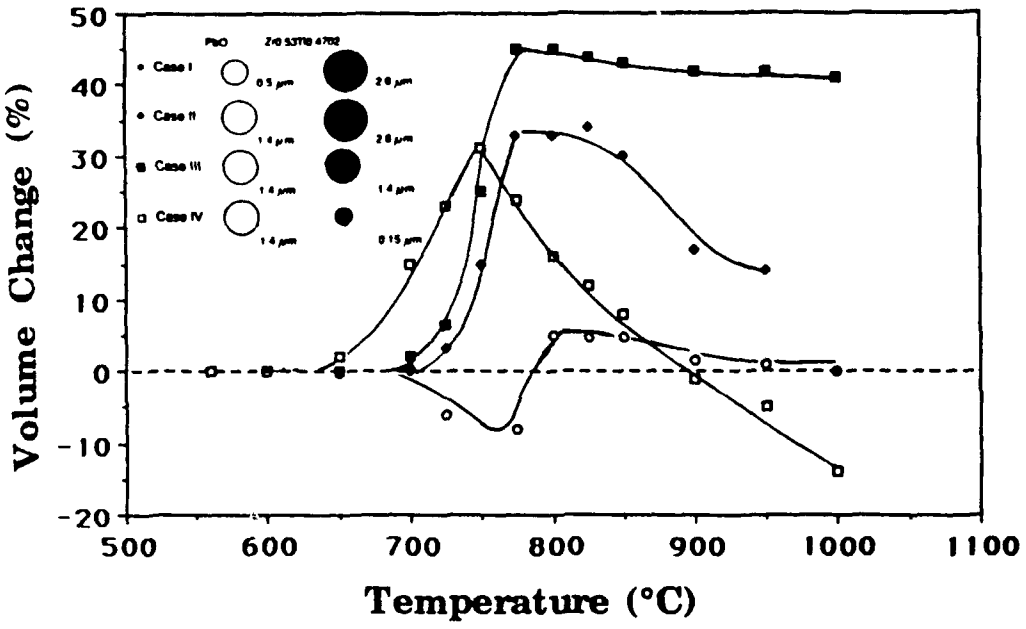

Figure 1. Volumetric expansion-shrinkage characteristics of PZT as a function of temperature for various component sizes (ref. 2).

3.0 RESULTS AND DISCUSSION

Physical characteristics of the fired PZT samples are reported in Table I. As presented, little densification occured even at temperatures as high as 1200°C. As expected, this behavior is the result of lowering the effective coordination number of reaction regions leading to inhomogeneous densification. Densities as low as 60% (Case III) with well developed microstructures, facetted grains (~ 4 μm) were achieved (see Fig. 2) Similar microstructures were observed for the more reactive PZT powder (Case IV) reaching densities ~ 86% theoretical at 1200°C and only 80% 1050°C—1100°C (see Fig. 2b).

The ability to handle and pole the highly porous samples further testifies to their well developed microstructures and overall mechanical integrity. In contrast to porous PZT compacts prepared via organic fugitive phases (plastic spheres) for composite hydrophones,[8] the microstructures presented in this work possess uniform columnar (grain to grain) connectivity as compared to the sharp angular and constricting connectivity associated with the geometry of the fugitive phase. In addition, volatilization of the fugitive phase can lead to disruption of the delicate microstructure.

The uniformity and connectivity of the PZT skeletal structure is also substantiated by the dielectric and piezoelectric properties reported in Table I. The relatively high K and d_{33} values reflect significant parallel connectivity of the PZT grains allowing poling. Naturally, with increasing porously the mechanical Q decreased.

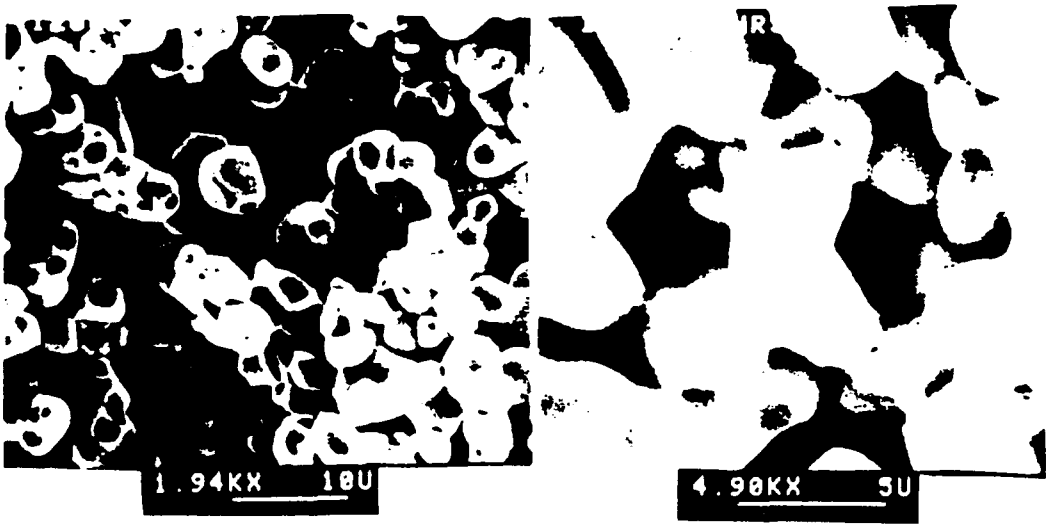

Figure 2. SEM photomicrographs of sintered reactively calcined PZT disks a) Case III—1200°C/2 hrs—left, b) Case IV—1050°C/2 hrs—right.

TABLE I.
Characteristics of Inhomogeneity Densified PZT Disks.

Sample	Firing Conditions	Density (% Theo.)	Grain Size (μm)	*Dielectric (1 kHz) K	Loss	d_{33} ($\times 10^{-12}$ C/N)	k_p (%)	Q
*PZT	≥ 1200°C	~95%	≥ 5	~700	~.01	200	45	~300
PZT (Case III)	1200°C	60%	~4	250	.01	70	13	~70
PZT (Case IV)	1050/1100°C	80%	~3	500	.01	100	15	~110
	1200°C	86%	~4	550	.01	135	23	150

*Jaffe, Cook, and Jaffe.[9]

4.0 SUMMARY

Potential applications using the reactive calcination process and subsequent inhomogeneous densification are as follows:

1) **Piezoelectric Composite Hydrophones:**
The highly porous PZT skeletal structures can be back-filled with a polymer resulting in 3:3 composites, being similar to other PZT/polymer composites developed for hydrophones.[10]

2) **Piezoelectrically Active Filters/Membranes:**
The ability to control the level and scale of porosity in a piezoelectrically active skeletal structure offers the potential for an active filter membrane. Enhancement of the filtering process may arise from the resonating structure acting as a micro-pump and/or de-clogging device.

3) **Sensors:**
The large "active" surface area through reactive calcination offers an alternative fabrication method for sensors, e.g., PZT humidity sensors.[11]

5.0 REFERENCES

1. T.R. Shrout, P. Papet, S. Kim, and G.S. Lee. "Conventionally Prepared Submicron Lead-Based Perovskite Powders by Reactive Calcination," *J. Am. Ceram. Soc.*, 73[7], 1862-1867 (1990).

2. T.R. Shrout. "Conventionally Prepared Submicron Electro-Ceramic Powders by Reactive Calcination," Proc. 1st Int'l. Meeting on the Chemistry of the Electronic Ceramic Materials, Jackson Hole, WY (1990).

3. S. Kim, G.S. Lee, S. Venkataramani, and T.R. Shrout. "Fabrication of Fine Grain Piezoelectric Ceramics Using Reactive Calcination and Milling," (to be published in *J. Mat. Sci.*).

4. P. Papet, J.P. Dougherty, and T.R. Shrout. "Particle and Grain Size Effects on the Dielectric Behavior of the Relaxor Ferroelectric $Pb(Mg_{1/3}Nb_{2/3})O_3$," *J. Mat. Res.*, 10 (1990).

5. S. Venkataramani. "Calcining and its Effects on Sintering and Properties of Lead Zirconate Titanate Ceramics," Ph.D. Thesis, Pennsylvania State University (1981).

6. D.W. Budworth. "A Random Packing Geometrical Model of Sintering," Ceramic Microstructures, eds., R.M. Fulrath and J.A. Pask, 255-260, Westview Press, Boulder, CO (1977).

7. S.L. Swartz and T.R. Shrout. "Fabrication of Perovskite Lead Magnesium Niobate," *Mat. Res. Bull.*, 17, 1245-1250 (1982).

8. K. Rittenmyer, T. Shrout, W.A. Schulze, and R.E. Newnham. "Piezoelectric 3-3 Composites," *Ferroelectrics*, 41, 189-195 (1982).

9. B. Jaffe, W.R. Cook, Jr., and H. Jaffe. *Piezoelectric Ceramics*, Academic Press, NY (1971).

10. R.E. Newnham, L.J. Bowen, K.A. Klicker, and L.E. Cross. "Composite Piezoelectric Transducers," *Mat. in Eng.*, 2, 93-106 (1980).

11. H. Asakura, H. Yamamura, and K. Uchino. "Humidity Sensitive Actuator," *Ferroelectrics*, 93, 205-210 (1989).

MISCELLANEOUS PAPERS

APPENDIX 50

Ferroelectrics, 1990, Vol. 107, pp. 191–193
Reprints available directly from the publisher
Photocopying permitted by license only

GROWTH AND CHARACTERIZATION OF FERROELECTRIC/POLAR SINGLE CRYSTAL FIBERS

J.K. YAMAMOTO, C.A. RANDALL, S.A. MARKGRAF, A.S. BHALLA
Materials Research Laboratory, The Pennsylvania State University, University Park, Pennsylvania, U.S.A.
and
M.A. SAIFI
Bell Communications Research, Red Bank, New Jersey, U.S.A.

Abstract The growth of several ferroelectric and polar compounds have been grown using a modified float zone technique. The growth technique is described and the results of property measurements are presented.

INTRODUCTION

Growth of single crystal fibers with light guiding structures is both of scientific and technological interest. The technological aspect has gained an added importance because of the rapid deployment of optical fibers in communication systems. For such systems fiber geometry compatible devices may be possible from single crystal fibers. The fiber geometry may also find improved applications in sensor devices, where crystals grown by bulk methods are presently in use.

The first attempt to grow single crystals by a laser powered modified float zone technique was accomplished by Gasson and Cockayne.[1] They were able to grow 5mm diameter Al_2O_3, $MgAl_2O_4$ and other refractory compositions. Burrus and Stone later applied a similar technique to grow 50μm to 125μm diameter Nd:YAG single crystal fibers.[2] More recently, the technique has been used to grow optically nonlinear materials such as $LiNbO_3$ and β-BaB_2O_4.[3,4] This poster will describe the growth of several oxide ferroelectric compositions and present the results of different characterization techniques to assess crystal quality and qualitative ferroelectricity.

LASER HEATED PEDESTAL GROWTH (LHPG) TECHNIQUE

The LHPG technique is a modified float zone technique where the melt is supported by the surface tension of the molten zone, Figure 1. Radiation from a 50 watt CO_2 laser is introduced into the growth chamber and is directed through a series of optical components

and incident upon a concave parabolic mirror. The ceramic preform or single crystal feed rod is placed vertically in line with the major axis of the parabolic mirror. The hot zone is located at the parabolic focal point. The vertical motion of the feed rod and the pulled crystal are controlled by high precision pulling heads. Further details concerning the technique can be found in the literature.[5]

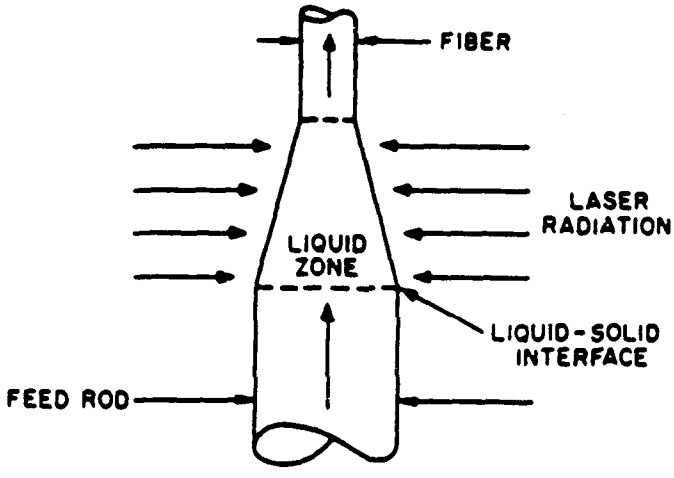

Figure 1. Schematic of the Melt Zone

EXPERIMENTAL

The feed rods were made by either a mixed oxide method or via an organometallic route. The powders were pressed into 3 cm diameter pellets and sintered. The ceramic preforms were then cut to the appropriate size.

Crystals from a number of different structural and compositional families as well as congruently and incongruently melting compounds were grown to test the capabilities of this technique. These included members from the perovskite, tungsten bronze, pyroniobate and fresnoite-type families, Figure 2.

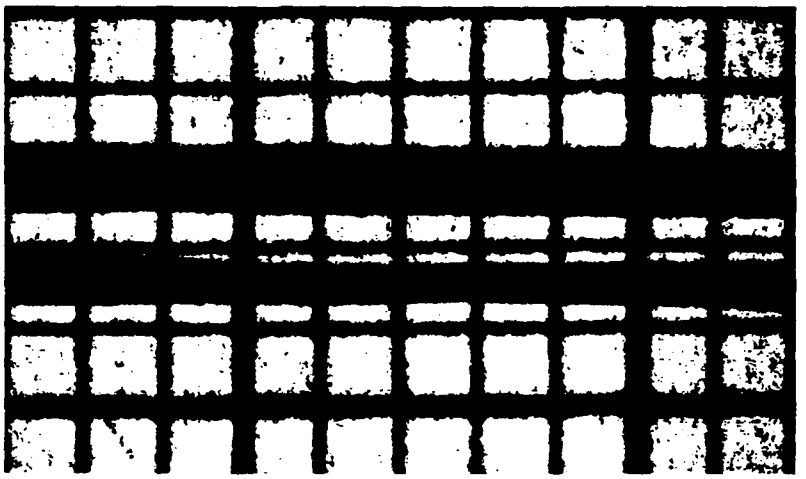

Figure 2. Examples of pyrotitanate single crystal fibers, $La_2Ti_2O_7$ (top) and $Nd_2Ti_2O_7$ (bottom).

CONCLUSION

The LHPG technique has proven to be a powerful technique in the growth of shaped crystals. Both congruently and incongruently melting compositions can be grown with this technique and therefore offers the possiblity of studying materials that are difficult to grow by other methods.

REFERENCES

1. D.B. Gasson and B. Cockayne, J. Mater. Sci., 5, 100 (1970).
2. C.A. Burrus and J. Stone, Appl. Phys. Lett., 26 , 318 (1975).
3. Y.S. Luh, M.M. Fejer, R.L.Byer, and R.S. Feigelson, J. Cryst. Growth, 85 , 264 (1987).
4. D.Y. Tang, R.K. Route, and R.S. Feigelson, J. Cryst. Growth, 91, 81 (1988).
5. R.S. Feigelson, in Crystal Growth of Electronic Materials, edited by E. Kaldis (Elsevier Science Publishers, New York, 1985), Chapter 11, pp.127-145.

APPENDIX 51

Solid State Communications, Vol. 75, No. 10, pp. 821–824, 1990. 0038-1098/90 $3.00 + .00
Printed in Great Britain. Pergamon Press plc

INCOMMENSURATE PHASE IN $Ba_2TiSi_2O_8$

S.A. Markgraf, C.A. Randall and A.S. Bhalla

Materials Research Laboratory, The Pennsylvania State University, University Park, PA 16802, USA

and

R.J. Reeder

Department of Earth and Space Science, S.U.N.Y. at Stony Brook, Stony Brook, NY 11794, USA

(*Received* 5 *February* 1990 *by G. Burns*)

Transmission electron microscope examination of $Ba_2TiSi_2O_8$ has revealed a new incommensurate phase. The incommensurate reflections occur along $\langle 1\,0\,0 \rangle$, and in the $h\,k\,1/2$ level. At elevated temperatures the incommensurate reflections disappear: it is suggested that the property anomalies previously reported in this material at 160°C are due to the onset of the incommensuration. Differences and similarities with other related compounds are discussed.

1. INTRODUCTION

FRESNOITE, $Ba_2TiSi_2O_8$ (BTS), is a relatively rare mineral found in sanbornite-bearing metamorphic rocks [1]. It has been studied primarily for its polar properties, where much of the work was centered on the possibility of using BTS in surface acoustic wave devices [2]. Fresnoite-based materials can be fabricated through the polar glass-ceramic process [3]. A comparative study between single crystals of BTS and the related polar glass-ceramics revealed an unusual anomaly at 160°C [4]. The most striking signature of this anomaly was found in the pyroelectric behavior. With increasing temperature the pyroelectric coefficient increases steadily until 160°C, whereupon it decreases rapidly, passing through zero at 190°C. A broad peak in the dielectric constant and the piezoelectric coupling coefficient were also indications of the anomaly. Although these anomalies suggested a phase transition at 160°C in BTS, single-crystal structure refinements at 25 and 300°C resulted in satisfactory residuals within the same space group [5]. This result seemed to rule out the possibility of a phase transition, and although several possible explanations were presented (cancellation of primary and secondary effects [4], anomalies in the elastic constants [5], which have since been observed by Chang and Bhalla [6]), the cause of the anomaly remained unclear.

The germanium analog of BTS, $Ba_2TiGe_2O_8$ (BTG), has two phase transitions: a ferroelastic phase transition at 850°C, and an unusual low-temperature transition at −50°C on cooling, 0°C on heating. An incommensurate modulation of the structure exists throughout the temperature range 850°C to −50°C [7].

Transmission electron microscope (TEM) examination of single crystals of BTS has revealed a previously unreported set of superlattice reflections. We show that these reflections are incommensurate. This communication reports on the incommensurate phase in BTS, its relationship with the 160°C anomaly, and its correspondence to similar compounds.

2. EXPERIMENTAL

Several different samples were used in this study. Single crystals of BTS were grown by the Czochralski technique, and with a miniature float zone technique from ceramic feed stock and Czochralski-grown BTS seeds. Ceramic samples were prepared through a conventional mixed-oxide technique.

The samples were ion-beam thinned and examined initially at room-temperature with a Philips 420 TEM. All samples showed identical diffraction patterns; therefore we will only discuss the Czochralski-grown sample. This crystal was also examined on a J.E.O.L. 200 CX Electron Microscope equipped with a Gatan model 628 hot stage.

The crystal used in the previous structure refinements of Markgraf *et al.* [5] was reexamined with an X-ray precession camera operating with filtered MO radiation.

3. RESULTS

Previous studies on single crystals of BTS showed a tetragonal cell in space group $P4bm$ (C_{4v}^2),

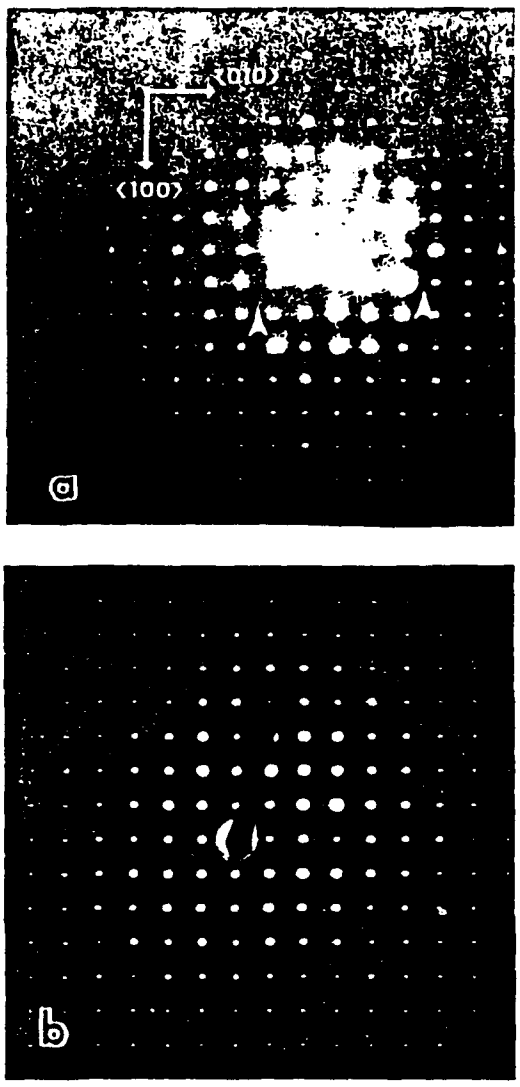

Fig. 1. BTS single crystal zone axis ⟨0 0 1⟩ electron diffraction pattern: (a) room temperature; (b) elevated temperature.

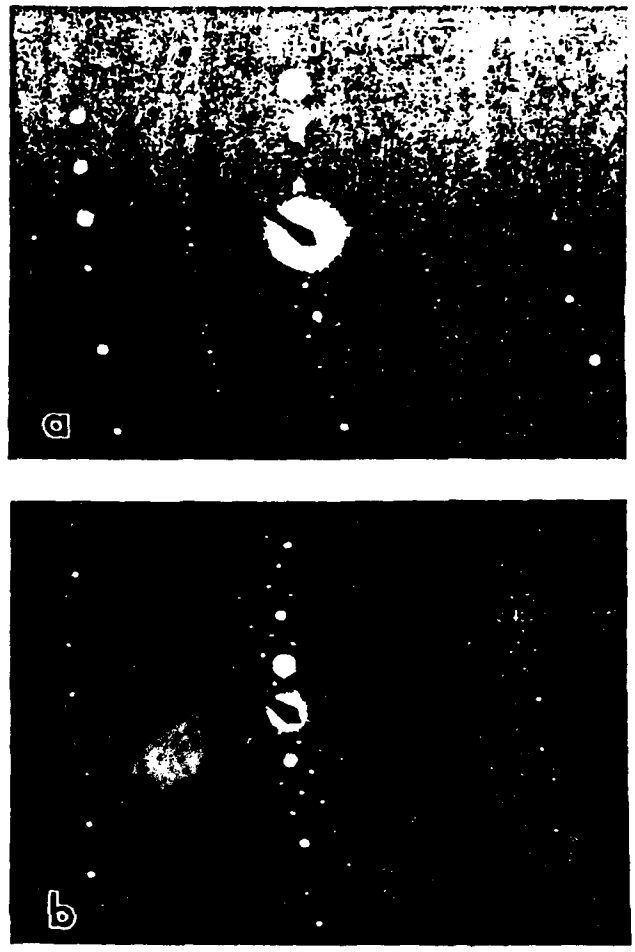

Fig. 2. BTS single crystal *tilted* zone axis ⟨0 0 1⟩ electron diffraction pattern: (a) room temperature; (b) elevated temperature.

$a = 8.52$ Å, $c = 5.21$ Å. Figure 1 presents a zone axis ⟨0 0 1⟩ electron diffraction pattern from a BTS single crystal. The arrows mark the weak reflections we consider as incommensurate. These reflections occur at $(1 + \delta)a^*/3$, where $\delta = 0.20$, although the accuracy of this measurement is not high. Electron diffraction patterns on tilted [0 0 1] samples show incommensurate reflections in the $hk1/2$ level (Fig 2). These reflections effectively double the c lattice parameter. Figure 3 shows the room-temperature three-dimensional reciprocal lattice of BTS.

The single crystal used in the structure analysis of Markgraf *et al.* [5] was examined with a X-ray precession camera for reflections in the $hk1/2$ level. An extremely long exposure (six weeks) confirmed the presence of the incommensurate reflections in this sample.

Heating the sample *in situ* within the electron microscope revealed that the incommensurate reflections become progressively weaker, until they are no longer observable (Figs. 1 and 2). The incommensurate reflections reappear with no noticeable difference in position or intensity upon cooling to room-temperature. The specimen/furnace assembly utilized in this hot-stage can lead to large thermal difference between the temperature at the observation area and the thermocouple readout from the microscope furnace. We are therefore reluctant to compare the transition temperature obtained from the microscope hot-stage with the temperature obtained from property anomalies; they are however within the same range (Fig. 1b was obtained with a furnace temperature of 345°C, Fig. 2b was obtained with a furnace temperture of 210°C on a subsequent run).

Dark-field imaging using several incommensurate reflections showed the presence of domains (Fig. 4). These domains are very fine, on the order of 100 nm in size, and show very weak contrast. On the lower

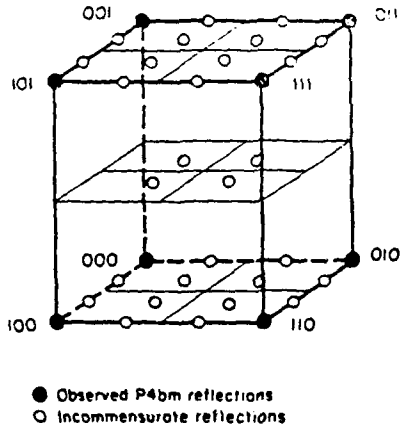

Fig. 3. Three-dimensional view of the observed reciprocal lattice found in BTS at room temperature with electron diffraction. The thick lines outline the prototypic tetragonal unit cell, the thin lines serve as a guide for the eye.

energy microscope (Philips: 120 kV) we observed only a mottled background: with the higher energy microscope (J.E.O.L: 200 kV) the contrast was much better. Unfortunately we could not isolate reflections along just the ⟨1 0 0⟩ direction or the ⟨0 1 0⟩ direction for dark-field work. We had hoped to determine if different domains were excited by using reflections either along ⟨1 0 0⟩ or ⟨0 1 0⟩.

4. DISCUSSION

Previous work has shown that BTS has the same structure at room-temperature and at 300°C [5]. Because of the structural similarity above and below 160°C, no structural explanation was available for the unusual anomaly observed in BTS. However, the temperature behavior of the incommensurate reflections leads us to the conclusion that the anomaly in BTS is the result of a prototypic to incommensurate type of phase transition. Prototype-to-incommensurate phase transitions are commonly subtle in their signature.

There are several unexplained features of our TEM analysis. The incommensurate reflections are strongest in the center of the $h\,k\,0$ diffraction pattern. From a kinematical treatment this indicates that the cause of the incommensuration may be compositional in nature [8]. Incommensurates with displacive origins may show the incommensurate reflections becoming stronger with increasing distance from the center of the diffraction pattern. However it seems unlikely that the cause of the incommensuration is due to a modulation of the composition. Rather it is more likely that the Debye-Waller parameters, ignored in the above analysis, play a major role in the intensity of the incommensurate reflections. It should be noted that not all incommensurate crystals, wherein the modulation is well understood, follow a simple compositional *versus* displacive guideline (e.g. Rb_2ZnCl_4, $Ba_2NaNb_5O_{15}$[10]) in their diffraction behavior.

We are uncertain of the cause of the domains formed by dark field imaging the incommensurate reflections. Analysis is difficult due to their high density and weak contrast. One possibility is that they represent discommensurations. Discommensurations are the crystallographic equivalent of antiphase boundaries, in that they are imaged with satellite reflections, or in this case incommensurate reflections. Microscopically discommensurations represent walls separating commensurate regions. The dark areas on Fig. 4 would than be regions with a different modulation vector, areas not excited by the incommensurate reflections chosen. Unfortunately, because of the resolution of the micrographs, we are not able to correlate the density of the domains with δ, or analyze their interactions for some understanding of the symmetry of the modulation vector(s).

As mentioned previously the germanium analog of BTS has an incommensurate phase, and this incommensurate phase is coupled with a ferroelastic phase transition occurring at 850°C. This behavior is attributed to the buckling of the pyrogermanate group. Adding silicon to the germanium endmember suppresses the ferroelastic phase transition, until at approximately 40 atomic percent silicon the phase is no longer ferroelastic at room-temperature [11]. It is therefore surprising to find an incommensurate phase in BTS, especially without the appearance of ferroelasticity.

Aspects of the incommensurate phase in BTS are similar to those observed in BTG. The most obvious similarity is the occurrence of the reflections at $h\,k$ 1/2 in both compounds. Only superlattice reflections are present in this level, and these reflections are quite strong relative to superlattice reflections in the $h\,k\,0$ level. An important difference in the two incommensurate phases is that in BTG the modulation is along the prototypic ⟨1 1 0⟩ direction, whereas in BTS it is found along ⟨1 0 0⟩.

Although the strain present in BTS is evidently not great enough to induce ferroelastic behavior, it is apparently enough to cause slight structural distortions and the concomitant incommensurate phase. The cause for these distortions is a matter of speculation. One possibility is that barium in the ten-fold site causes a strain in the basal plane containing the Si_2O_7 and TiO_5 linkage. Certainly it is the basal plane that contains much of the strain in BTS. Chang and Bhalla [6] have shown that only the c_{11}, c_{12}, and c_{66} elastic constants are affected by the phase transition. Other indications of this strain can be found in an optical

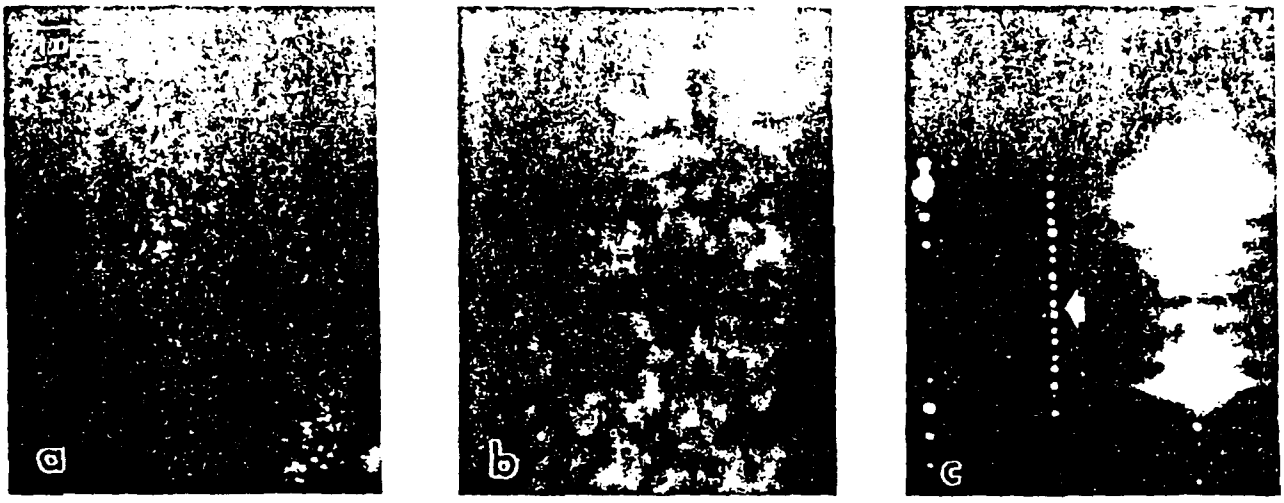

Fig. 4. Dark-field image using several hk 1/2 incommensurate reflections at room temperature: (a) observed contrast; (b) enlargement of region (a); (c) incommensurate reflections utilized are arrowed.

conoscopic examination of BTS. The interference figure expected for a uniaxial crystal is slightly distorted, showing the effects of strain, and giving a hint of biaxial character. One test of this argument would be through examination of $(Ba, Sr)_2TiSi_2O_8$. Strontium, with a smaller ionic radius, should not cause as much strain in the structure. Similar arguments have been advanced to explain the incommensurate phase in several melilite compounds [12, 13], which have a closely related structure.

5. CONCLUSION

An incommensurate phase is described in $Ba_2TiSi_2O_8$ for the first time. The incommensuration has also been confirmed to occur in samples previously examined with X-rays. It is postulated that the incommensurate phase is responsible for the property anomalies observed at 160°C through a prototype-to-incommensurate type of phase transition. The modulation in BTS occurs in a different direction than that found in the germanium analog, although both show superlattice reflections in the hk 1/2 level. The modulation is suggested to be associated with the large barium cation causing distortions in the basal Si_2O_7 and TiO_5 linkage.

Acknowledgement – We would like to thank Z.P. Chang for the donation of the Czochralski-grown crystal.

REFERENCES

1. J.T. Alfors, M.C. Stinson & R.A. Matthews, *Am. Mineral.* **50**, 314 (1965).
2. J. Melngailis, J.F. Vetelino, A. Jhunjhunwala, T.B. Reed, R.E. Fahey & E. Stern, *Appl. Phys. Lett.* **32**, 203 (1978), and references therein.
3. A. Halliyal, A.S. Bhalla, R.E. Newnham & L.E. Cross, *J. Mater. Sci.* **16**, 1023 (1981).
4. A. Halliyal, A.S. Bhalla, S.A. Markgraf, L.E. Cross & R.E. Newnham, *Ferroelec.* **62**, 27 (1985).
5. S.A. Markgraf, A. Halliyal, A.S. Bhalla, R.E. Newnham & C.T. Prewitt, *Ferroelec.* **62**, 17 (1985).
6. Z.P. Chang & A.S. Bhalla, *Materials Letters* **8**, 418 (1989).
7. S.A. Markgraf & A.S. Bhalla, *Phase Trans.* **18**, 55 (1989).
8. J.W. Steeds, D.M. Bird, D.J. Eaglesham, S. McKernan, R. Vincent & R.L. Withers, *Ultramicroscopy* **18**, 97 (1985).
9. H. Bestgen, *Solid State Commun.* **58**, 197 (1986).
10. G. Van Tendeloo, S. Amelinckx, C. Manolinkas & W. Shulin, *Phys. Status Solidi (a)* **91**, 483 (1985).
11. H. Schmid, P. Genequand, H. Tippman, G. Pouilly & H. Guéda, *J. Mater. Sci.* **13**, 2257 (1978).
12. B.S. Hemingway, H.T. Evans, G.L. Nord, Jr., H.T. Haselton, R.A. Robie & J.J. McGee, *Can. Mineral.* **24**, 425 (1986).
13. F. Seifert, M. Czank, B. Simons & W. Schmahl, *Phys. Chem. Minerals.* **14**, 26 (1987).

APPENDIX 52

Phase Transitions, 1989, Vol. 18, pp. 55-76
Reprints available directly from the publisher
Photocopying permitted by license only

LOW-TEMPERATURE PHASE TRANSITION IN $Ba_2TiGe_2O_8$

STEVEN A. MARKGRAF and AMAR S. BHALLA

Materials Research Laboratory
The Pennsylvania State University
University Park, PA 16802 USA.

(Received 8 July 1988; in final form 3 November 1988)

Previous work on $Ba_2TiGe_2O_8$ crystals has shown an unusual low-temperature (~223 K on cooling, ~273 K on heating) phase transition. Precession x-ray photographs on $Ba_2TiGe_2O_8$ single crystals show an incommensurate modulation along **b***, and, for the first time, also along **a***. Single crystal intensity data confirm the average structure in space group Cmm2. There is positional disorder in the pyrogermanate groups, and this is the probable cause for the modulated structure. The low-temperature phase transition is proposed to be a lock-in transition, with the modulation along **a*** locking in at a value of $\frac{1}{3}$. Several properties, as well as other unusual features of the low-temperature phase transition, are discussed in light of the proposed lock-in transition. Domain studies show that the ferroelastic domains are unstable in the low-temperature phase.

KEY WORDS: $Ba_2TiGe_2O_8$, ferroelastic crystal, incommensurate crystal, lock-in phase transition.

1 INTRODUCTION

The mineral fresnoite, $Ba_2TiSi_2O_8$ (hereafter denoted as BTS), was first described in 1965 by Alfors, Stinson, and Matthews (1965). Since then it has received more attention from materials scientists than from the geological community. The interest is primarily because of the piezoelectric and pyroelectric properties of the crystal, and the relative ease with which large transparent crystals may be synthesized. The germanium analog, $Ba_2TiGe_2O_8$ (hereafter denoted as BTG), has been investigated for its polar properties and for insight into its ferroelastic phase transition at ~1123 K. The initial interest in fresnoite-type crystals at the Materials Research Laboratory was in the ability to form polar glass-ceramics from them. Polar glass-ceramics are a unique subgroup of traditional glass-ceramics in that during recrystallization of the glass an oriented microstructure is obtainable. The oriented microstructure permits the polar properties of the crystal to be utilized without the difficulty of synthesizing a single crystal. The properties of polar glass-ceramics are well reviewed in the work of Halliyal (1984).

Recent work by Halliyal, Bhalla and Cross (1986) have indicated a low-temperature phase transition previously unreported in BTG. This phase transition was first

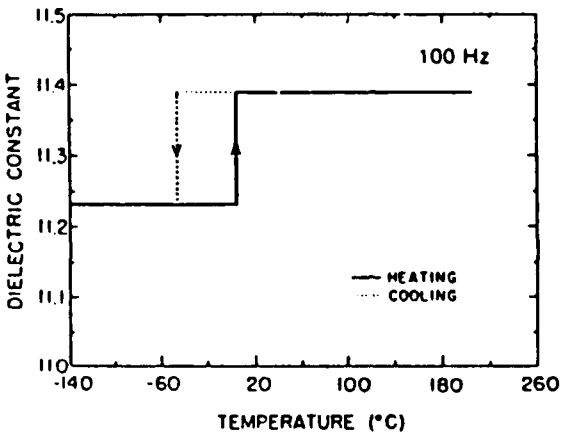

(a)

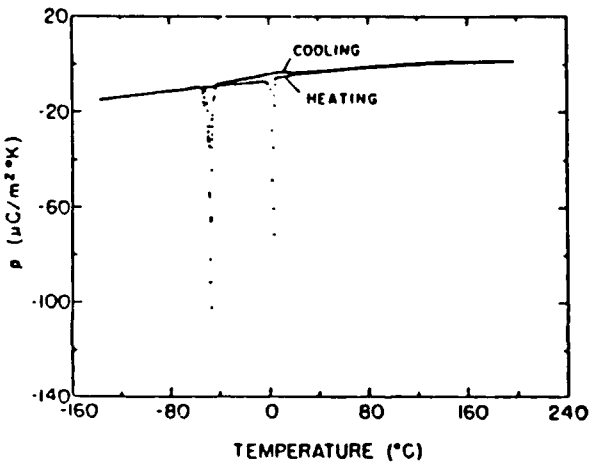

(b)

Figure 1 Dielectric (a) and pyroelectric (b) properties of BTG single crystal as a function of temperature. After Halliyal *et al.* (1985)

observed through pyroelectric and dielectric measurements. The permittivity along c shows a very small decrease at the transition, dropping from 11.4 to 11.2 (Figure 1a). The dissipation factor showed little change throughout the temperature range investigated. At ~223 K (on cooling) the pyroelectric coefficient shows a very sharp peak, whereas on heating the peak occurs at ~273 K (Figure 1b) (Halliyal *et al.* (1985)). Below 223 K the crystal is still polar; in fact the slope of the pyroelectric coefficient appears identical above and below the sharp peak. Polar glass-ceramics made from germanium-deficient compositions did not show the low-temperature phase transition. Halliyal *et al.* (1985) interpreted this transition as manifestation of a

possible divertable ferroelectric. The low-temperature phase would be in either point group m or 1 for the case of a divertable ferroelectric. Divertable ferroelectrics are relatively rare, and there is some interest in them for use in optical devices. In addition the phase transition, if it were ferroelectric, would most likely be improper, because the permittivity and dissipation factor did not show strong signals at the transition. The work of Halliyal *et al.* (1985) was preliminary, and further investigation was necessary to clear up several aspects of this transition.

Crystal Structure and Phase Relations in the $Ba_2TiSi_2O_8$-$Ba_2TiGe_2O_8$ *System*

The crystal structure of BTS was reported concurrently by Masse, Grenier and Durif (1967) (synthetic sample) and Moore and Louisnathan (1967, 1969) (mineral specimen). Both found essentially the same features: BTS crystallizes in space group P4bm (C_{4v}^2), with $a = 8.52$ Å, $c = 5.21$ Å, $V = 378$ Å^3, $Z = 2$. The silicon ions occur in pyrosilicate groups corner-linked to TiO_5 square pyramids. This linkage is parallel with the basal {001} plane (see Figure 2 for the tetragonal cell).

BTG, the germanium end member, was first synthesized and described as isostructural with BTS by Masse and Durif (1967). Upon further investigation by Kimura, Doi, Nanamatsu and Kawamura (1973) it was demonstrated that the crystal occurs in the orthorhombic system. These workers assigned the crystal to space group Iba2

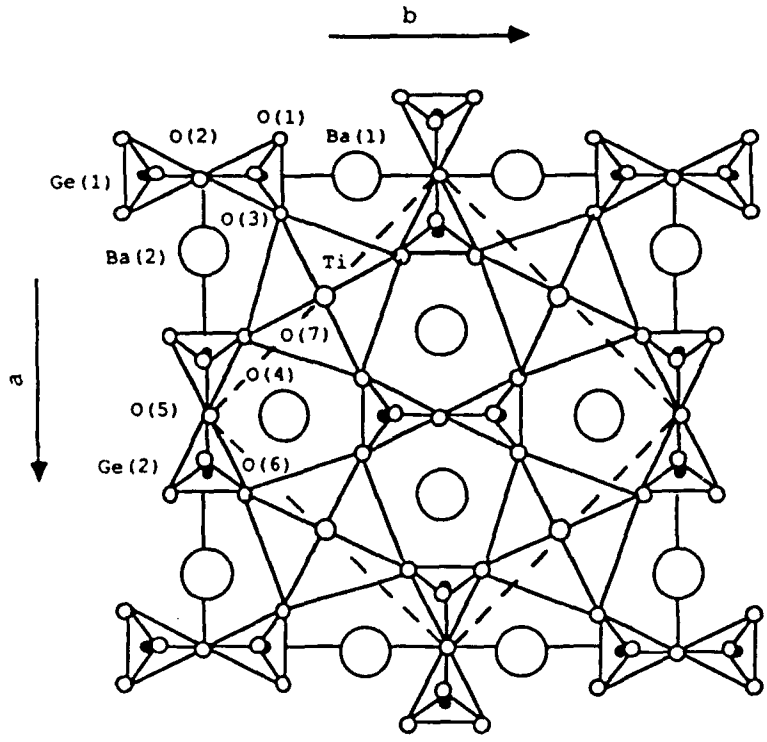

Figure 2 {001} projection of BTG crystal structure. Dashed line shows the prototypic P4bm cell.

(C_{2v}^{21}), with $a = 12.30$ Å, $b = 135.2$ Å, $c = 10.70$ Å, V = 17,794 Å^3. The b parameter is approximately 11 × a, and the given c parameter is twice the c cell edge of the BTS cell. Kimura *et al.* (1973) presented photographs of domains later shown to be ferroelastic in nature (Kimura, Utsumi and Nanamatsu, 1976). A room-temperature "average" structure, ignoring the superstructure in the b and c cell parameters, was determined by Iijima, Marumo, Kimura and Kawamura (1981), using space group Cmm2 (C_{2v}^{11}), $a = 12.31$ Å, $b = 12.292$ Å, $c = 5.366$ Å, $Z = 4$ (Figure 2). These workers also reported that the superlattice reflections responsible for the assignment of Iba2 disappear at the ferroelastic phase transition.

A convenient method of describing ferroic phase transitions has been developed by Abrahams and Keve (1971). It involves writing the atomic coordinates in terms of the symmetry elements lost upon passing through the phase transition. From the study of Iijima *et al.* (1981), the 1123 K transition in BTG may be described as:

$$(x_2, y_2, z_2) = (\tfrac{1}{2} - y_1, \tfrac{1}{2} - x_1, z_1) + \Delta$$

where (x_1, y_1, z_1) represent the atomic coordinates in one orientation state, and (x_2, y_2, z_2) are the atomic coordinates in the second orientation state. The Δ term represents the movement the atoms must undergo in order to switch from orientation state 1 to orientation state 2. For BTG Δ is approximately 0.005 Å for most atoms. Another important feature of ferroelastic crystals is the knowledge of the prototypic structure. Analysis of the high-temperature structure (at 1163 K) in space group P4bm was accomplished on BTG by Iijima, Marumo, Kimura and Kawamura (1982). Their results show that the prototypic structure of BTG is isostructural with BTS.

Some work has been reported on mixed solid-solution $Ba_2TiGe_2O_8$-$Ba_2TiSi_2O_8$ crystals. BTG accepts approximately 40 to 50 atomic % Si into the tetrahedral site before accommodating the tetragonal structure at room temperatures (Schmid, Genequand, Tippmann, Pouilly and Geudu, (1979); Iijima *et al.* (1982)). The ferroelastic transition temperature is lowered with increasing Si content, as shown by Iijima *et al.* (1982) reporting a transition temperature of 523 K for $Ba_2Ti(Si_{0.4}Ge_{0.6})_2O_8$. Although Iijima *et al.* (1982) were able to grow small transparent crystals in the solid-solution region, attempts by Schmid *et al.* (1978) to synthesize mixed composition crystals resulted in inhomogeneous Si-Ge distributions. Structural information available on a $Ba_2Ti(Si_{0.75}Ge_{0.25})_2O_8$ crystal (Iijima *et al.*, 1982) shows it is tetragonal and isostructural with BTS.

2 CRYSTAL GROWTH OF $Ba_2TiGe_2O_8$

Stoichiometric amounts of electronic grade $BaCO_3$, electronic grade GeO_2, and 99.99% pure TiO_2 were weighed, dry-mixed, prereacted at 973 K for 24 hours, and melted in a thick-walled platinum crucible. An inductance furnace was used to pull the crystal. The platinum crucible was insulated with alumina spheres inside a zirconia-felt-lined alumina crucible. An alumina cap was placed over the assemblage to act as an after-heater. The seed was a $\langle 100 \rangle_{\text{tetragonal}}$ $Ba_2TiSi_2O_8$ crystal. The crystal was

pulled in air with a pulling rate of 2 mm/hour, without crucible rotation. After crystal growth was completed a white condensate was found on the chamber walls. Previous workers (Drafall and Spear, 1978) have shown this condensate to be a germanium phase, probably amorphous GeO_2.

The resulting boule (hereafter denoted BTG 10/13) was pale yellow in color and approximately 2 cm in diameter and 2 cm high. It has been suggested that the pale yellow color in BTS crystals is because of the presence of reduced titanium (Haussühl, Eckstein, Recker and Wallrafen, 1977). As is common in BTG crystals, cracking (both micro and macro) occurred throughout the crystal. A small amount was crushed for powder x-ray diffraction characterization. The x-ray powder pattern agreed with the published pattern for BTG (JCPDF #35-213; indexed as tetragonal). The density of a large piece of the BTG 10/13 boule was measured using the Archimedes method (medium: deionized water). A density of 4.80 g/cm^3 was determined, in good agreement with other workers (4.84 g/cm^3; Kimura *et al.*, 1973). Another BTG boule available, kindly provided by Dr. Z. P. Chang of the Materials Research Laboratory, was small and clear. This crystal was grown on 3/16, and any discussion of it will carry this notation (BTG 3/16). The importance of this crystal is that it does not show the low-temperature phase transition.

3 DOMAIN STUDIES

Experimental

Samples investigated included plates perpendicular to [001], [100] and [010], [110] and [1$\bar{1}$0]. The plates were oriented with a back-reflection Laue camera, parallel polished with 12 μm, 3 μm, 1 μm and 0.3 μm Al_2O_3 grit, and fine polished with cerium oxide. A feature common to these samples was the inability to obtain a very good surface finish. The orientation for the {110} plates was approximate. One of the {110} plates (parallel to the growth direction) showed a propensity to thermal shock when removed from the sample holder.

Two samples from the BTG 3/16 boule were prepared for optical investigation: [001] and [110] plate. Samples were prepared as described above.

Room-temperature studies were performed on a Leitz polarizing microscope. The BTG 10 13 samples were investigated as a function of temperature. The high-temperature (298 to 1173 K) experiments were accomplished using a Leitz Hot Stage placed on the Leitz microscope. The low-temperature (298 to 200 K) work was done on a Nikon polarizing microscope equipped with a standard U.S.G.S. heating/cooling fluid inclusion stage.

Results

The BTG 10/13 [001] plate shows a large number of ferroelastic domains, approximately 50-100 μm in size, as shown in Figure 3. Each adjacent domain has the **a** and **b** axes interchanged, hence the term 90° twins. It should be noted that in the 10/13 sample the ferroelastic twinning is pervasive, whereas in the 3/16 crystal the twins are

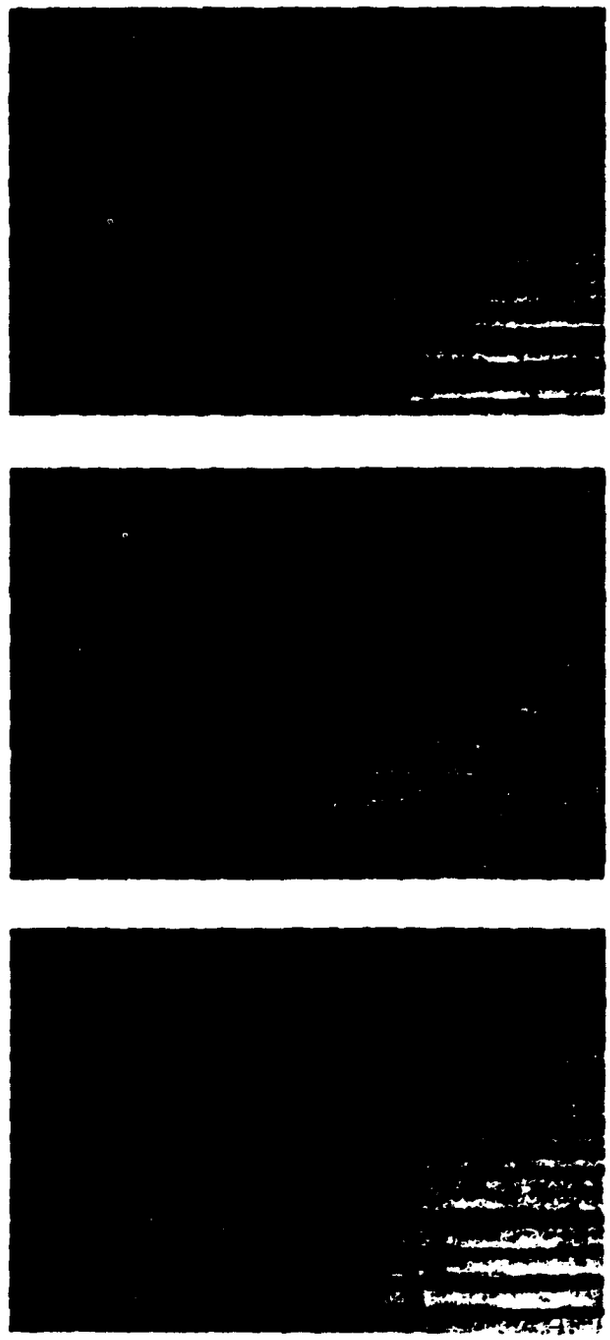

Figure 3 Optical micrographs of the [001] plate, BTG 10/13 crystal: (a) ~283 K; (b) ~210 K; (c) ~283 K, after passing through the low-temperature phase transition. The dark area visible in the upper section of the photographs is the thermocouple.

often scarce. In general in the 3/16 sample, the domains occurred along the edges of the sample, or where it was cracked. Kimura *et al.* (1976) detwinned a BTG sample at 973 K with a compressive stress of 100 kg/cm^2 applied along [010]. Detwinning was not possible in the BTG 10/13 crystal upon application of a compressional stress up to 823 K, possibly because of the great number of twins, or because the temperature was too low.

Upon increasing the temperature the number of 90° twins decreased, until at ~ 1123 K none were visible. Above this temperature a uniaxial figure was observed, thus confirming the prototypic crystal system as tetragonal. Similar behavior was found previously by Kimura *et al.* (1976). After cooling below 1123 K the ferroelastic domains reappeared, and as is common in ferroic phase transitions, they did not reappear in the same location.

The reapparance of the domains in different positions observed on passing through the high-temperature phase transition is in contrast to the behavior found at the low-temperature transition. Figure 3 shows three photographs of the [001] BTG 10/13 plate; Figure 3a was taken at 283 K, Figure 3b at 213 K, and Figure 3c back at 283 K after the crystal had gone through the phase transition at the upper end of its thermal hysteresis. It is immediately evident that the domains have returned to the same position after cycling through the phase transition. Another feature observed is the very small number of 90° twins found in the low temperature phase, indicating that the ferroelastic twins are not stable in the low-temperature phase. Observation of the first-order phase transition is quite dramatic; a "wave" quickly sweeps across the sample, shifting and moving the domain walls. The thermocouple holds the sample down, and the effect this has on the domain structure of the crystal is unclear.

Previous workers (Kimura *et al.* 1973) have reported that the domains found in the [001] plates were the only ones observed. This observation is consistent with the symmetry assigment of mm2 to BTG. However, in the BTG 10/13 crystal another set of twins were found. In one of the {110} plates (the same sample that was susceptible to thermal shocking) wavy irregular twins were observed. These twins often begin or stop at the cracks associated with thermal shocking. The angle of extinction between the two twins is approximately 3°. The other {110} plate does not show this twinning (nor is it susceptible to thermal shocking). These may represent stress twinning, such as those occasionally found in quartz. An attempt was made to anneal the twins, to see if the twins could be eliminated, or their number reduced. Annealing at 773 K showed a slight decrease in the number of twins, and a further reduction in the size and number of twins was seen by annealing at 973. This type of behavior implies that the twins are stress-related. The twins could conceivably be annealed out, although it would require long annealing times and high temperatures. The counterpoint is the question of why the other {110} plate doesn't show this feature. The absence may be related to the fact that the former plate is along the growth direction. The twins in this plate reappear in a different position after the high-temperature phase transition is passed. If the twins are not related to the highly stressed state of the sample, then the symmetry of the BTG 10/13 crystal may be lower than mm2.

The remaining samples, the [100] and [010] plates, did not show any twinning. They did show features that were interpreted as birefringence striations, such as those

observed in silicon (Lederhandler, 1959) and K(Ta, Nb)O_3 (Scheel and Sommerauer, 1983). Striations such as these are attributed to impurity segregation, or temperature instability during crystal growth, which leads to a strain-induced birefringence. In silicon they are commonly found perpendicular to the growth direction, and this aspect is consistent with observations in the BTG 10/13 crystal.

4 X-RAY PRECESSION PHOTOGRAPHY

Experimental

Precession photography, employing Zr-filtered Mo radiation, was used to examine the room-temperature BTG structure. For both the 3/16 and 10/13 BTG crystals [001] plates were cut from the boules and examined under a polarizing microscope. Areas without ferroelastic domains were clearly visible in both samples, and so small crystals were cut from these areas. The BTG 10/13 piece was approximately $100 \times 100 \times 50\,\mu m$ in size, while the BTG 3/16 sample size was approximately $200 \times 200 \times 100\,\mu m$. These pieces were mounted on drawn glass fibers with nail polish and placed in a standard goniometer. For both crystals *hk*0, *hk*1/2 (this photograph involves the level at 1/2 c in the Cmm2 cell), *hk*1, 0*kl*, 1*kl*, 2*kl*, *h*0*l*, *h*1*l*, and *h*2*l* photographs were taken.

In addition to giving an undistorted view of the reciprocal lattice, the precession technique has a reasonably open experimental apparatus. This aspect was utilized to design a device that allowed the crystal to be examined at low-temperatures. The principle is to use a nozzle to blow cold nitrogen gas onto the sample and to cool through conduction. The design of the nozzle is similar to that of Post, Schwartz and Frankuchen (1951). Additional features were gleaned from the excellent book by Rudman (1976). To minimize ice formation, a stream of warm (room temperature) nitrogen gas flowed around the cold stream. The interior of the nozzle was coated with air-dried silver paint to aid in insulation. The apparatus was capable of reaching and maintaining temperatures as low as 200 K without appreciable ice formation. As is common in nozzles of this design the temperature gradients both across the opening and in depth are extreme. Care was taken to center the nozzle on the crystal and not to move it during the exposure. To accommodate the large temperature gradient the μ angle was set at 10°. Unfiltered Mo radiation was utilized in order to shorten the exposure times. The shortened exposure time also allowed for more efficient use of N_2 gas. Although a thermocouple was not built into the nozzle, it was possible to insert a thermocouple into the gas-stream near the crystal. The experiments were commonly run at ~ 210 K. The temperature stability was good, although this feature was not critical because of the thermal hysteresis associated with the phase transition. Only the BTG 10/13 crystal was investigated with the low-temperature experiment, and *hk*1/2, *hk*1, 2*kl* and *h*1*l* photographs were taken. The geometry of the camera, and the placement of the nozzle, prevented zero-level photographs at low-temperatures from being taken.

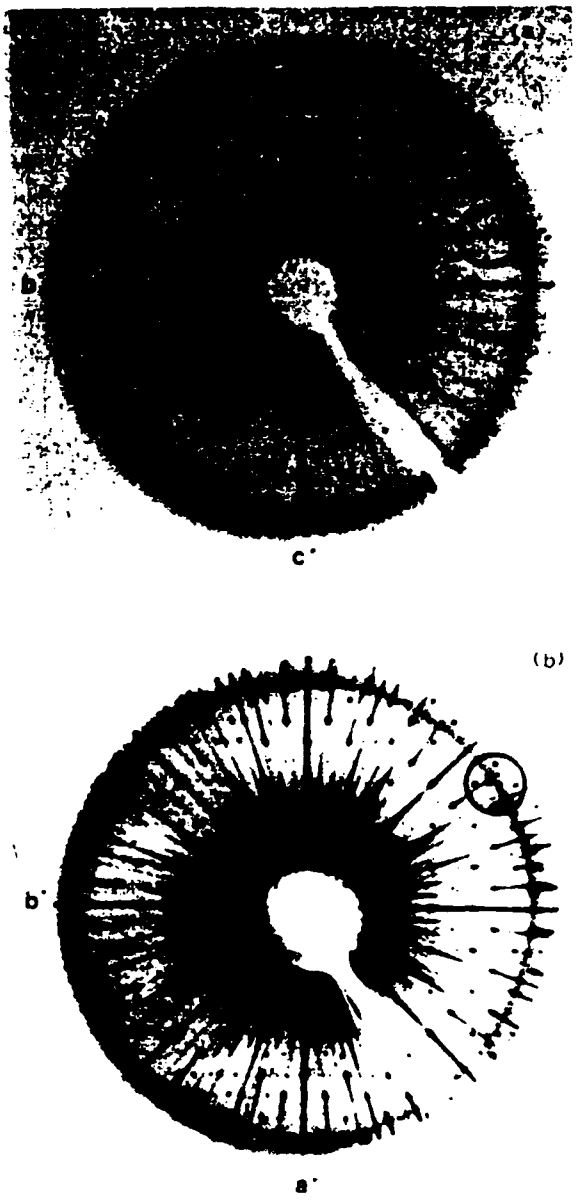

Figure 4 Precession photographs of the zero-level reciprocal net of the BTG 10/13 crystal: (a) 0*kl*; (b) *hk*0. The circled area show some of the superlattice reflections.

Room-Temperature Results

Figure 4 presents the 0*kl* and *hk*0 reciprocal lattice photographs for the BTG 10/13 crystal. These two photographs show the orthorhombic symmetry of the crystal as well as the peculiar superlattice reported by Kimura *et al.* (1973). It should be noted that although at first glance the precession photographs appear tetragonal, the presence of the superlattice and the observed ferroelastic domains rule out a tetragonal assignment.

Ignoring the superlattice for a preliminary analysis, the 10/13 crystal may be assigned to space group Cmm2 (extinction rules: $h + k = 2n + 1$), as reported by Iijima *et al.* (1981) and Schmid *et al.* (1978). This space group assignment is consistent with the orientation of the domains in relation to the tetragonal prototype. There is no evidence in the photographs, i.e. intensity variations across pseudo-mirror planes, that the crystal is of lower than orthorhombic symmetry.

Attention is now turned to the superlattice. The zero-level photographs (Figure 4) show the superlattice along **b*** only. Schematics representing the approximate distances between the reflections, as measured on the films, are given in Figure 5. (Note: for precession photographs $d = F\lambda/g$, where g is the value presented in Figure 5. F in this case is 60 mm and λ is 0.7107 Å). Densitometer readings on these photographs would be helpful in the interpretation; one was not available. The zero-level case is shown in Figure 5a. A distance of 6.9 mm is equivalent to the translation from h, k, l to $h, k + 2, l$ in the Cmm2, $b = 12.246$ Å, structure. No second order satellite reflections were observed around the superlattice reflections. Figure 6 presents a three-dimensional view of the observed reciprocal lattice framework for BTG.

Another feature observed on the precession photographs is the coupling of the superlattice along **b*** to the halving of the c^* parameter. The doubling of c relative to the prototypic structure was reported by Kimura *et al.* (1973), and discounted by Schmid *et al.* (1978). It is best shown in a 1*kl* (or a 2*kl*) photograph (Figure 7). Most (or at least the strongest) of the superlattice reflections occur in the **c***/2 zones, and *only* superlattice reflections occur in this zone. Figure 5b presents a schematic of the superlattice in relation to the non-superlattice reflections for zones **c***/2 and **c***. Within the **c*** zones the values reported are the same as those observed in the zero-level photographs. However, along the **c***/2 zones the distance from the non-superlattice reflection (absent in this case) to the superlattice reflection is ~2.2 mm, whereas in the **c*** zones this distance is ~2.55 mm.

If the superlattice in the **c***/2 and **c*** zones arise from the same structural distortion, and they are not considered incommensurate, the b cell parameter is on the order of 120-130 Å. This cell parameter agrees with the cell parameter of 135 Å reported by Kimura *et al.* (1973), and represents a cell multiplier of 11. The assignment of space group Iba2 by these workers is then intimately connected with the superlattice, and with the choice of 11 as the multiple. In their assignment of Iba2, the "systematic absences of the superlattice" are treated as part of the systematic absences of the crystal. This aspect is shown by comparing Figures 5b and 5c, which shows the predilection for a "set" of superlattice reflections to occur about an unobserved Cmm2 "reflection". This feature was undoubtedly interpreted by Kimura *et al.* (1973)

as a systematic absence rule. Utilizing this observation, and a b cell parameter of ~ 135 Å, the BTG 10/13 crystal follows the condition $h + k + l = 2n$, the condition for body-centering.

Such a large cell parameter is relatively uncommon in inorganic crystals, although not impossible. Another possibility is that the superlattice falls into the incommensurate family: incommensurate or commensurate. To describe a crystal in the conventional way, three independent vectors are used ($\mathbf{a}^*, \mathbf{b}^*, \mathbf{c}^*$). For incommensurate materials a fourth vector is needed, the modulation vector. In general this modulation vector, $\mathbf{q}^*$, may be evaluated as:

$$q^* = (1 \pm \delta)p^*n$$

where p^* is a reciprocal lattice cell parameter without a superlattice, δ is the distortion factor (dimensionless) describing whether the superlattice is commensurate, $\delta = 0$; or incommensurate, $\delta \neq 0$, and n is the fractional multiplier (e.g. 1/4, 2/3, 1/2) that describes the commensurate superlattice.

The difficulty of an incommensurate-type of superlattice in BTG is finding a model that fits both the $\mathbf{c}^*$ and $\mathbf{c}^*/2$ zones. Along the $\mathbf{c}^*$ zones a superlattice of $b^*/4$ fits very well, with the distortion factor approximately 0.02.

In the upper-level precession photographs the superlattice observed along $\mathbf{c}^*/2$ (see Figure 5b and c) does not fit the $b^*/4$ model very well. Another alternative is suggested from the consistent appearance of the values 2.2 and 2.55 mm found in the $\mathbf{c}^*/2$ zones. These same values occur in the $hk1/2$ photograph (Figure 8; Figure 5d for the schematic). The distance of 2.2 mm taken from the film is very close to a fraction of 2/3 (0.636, $\delta = 0.04$). The value of 1.275 (2.55/2), found in the $hk1/2$ photograph, is near the fraction 1/3. This suggests that the modulation vector could better be described using a $b^*/3$ modulation. The appeal of this model is that the shift between the superlattices from one $\mathbf{a}^*$ zone to the next, ~ 0.95 mm (Figure 5d), can be explained as due to the incomensuration. If, or when, the lattice modulation locks-in these reflections would line up at 1/3 and 2/3, and in a like manner the superlattice reflections in the $\mathbf{c}^*$ and $\mathbf{c}^*/2$ zones would possibly line up.

It appears that there are several possible explanations available for the observed superlattice. The first is that the superlattice represents a unit cell of $12.24 \times 135 \times 10.7$ Å. The second explanation involves two modulation vectors in the description of the superlattice, with the first equation describing the (near) commensurate superlattice along the $\mathbf{c}^*$ zones, and the second equation describing the incommensurate modulation in the $\mathbf{c}^*/2$ zones:

$$q^* = (1 \pm \delta)b^*/4$$

$$q^* = (1 \pm \delta)b^*/3 + c^*/2.$$

The final possibility is that the second equation describes both the $\mathbf{c}^*$ and $\mathbf{c}^*/2$ superlattice reflections, with the apparent differences being found in the incommensurate nature of the crystal, i.e. the δ factor. Evidence from the low-temperature precession photographs favor this model. However, utilizing only precession photographs it is difficult to categorically state which is the correct model.

The ferroelastic twinning in BTG can be described as adjacent twins with

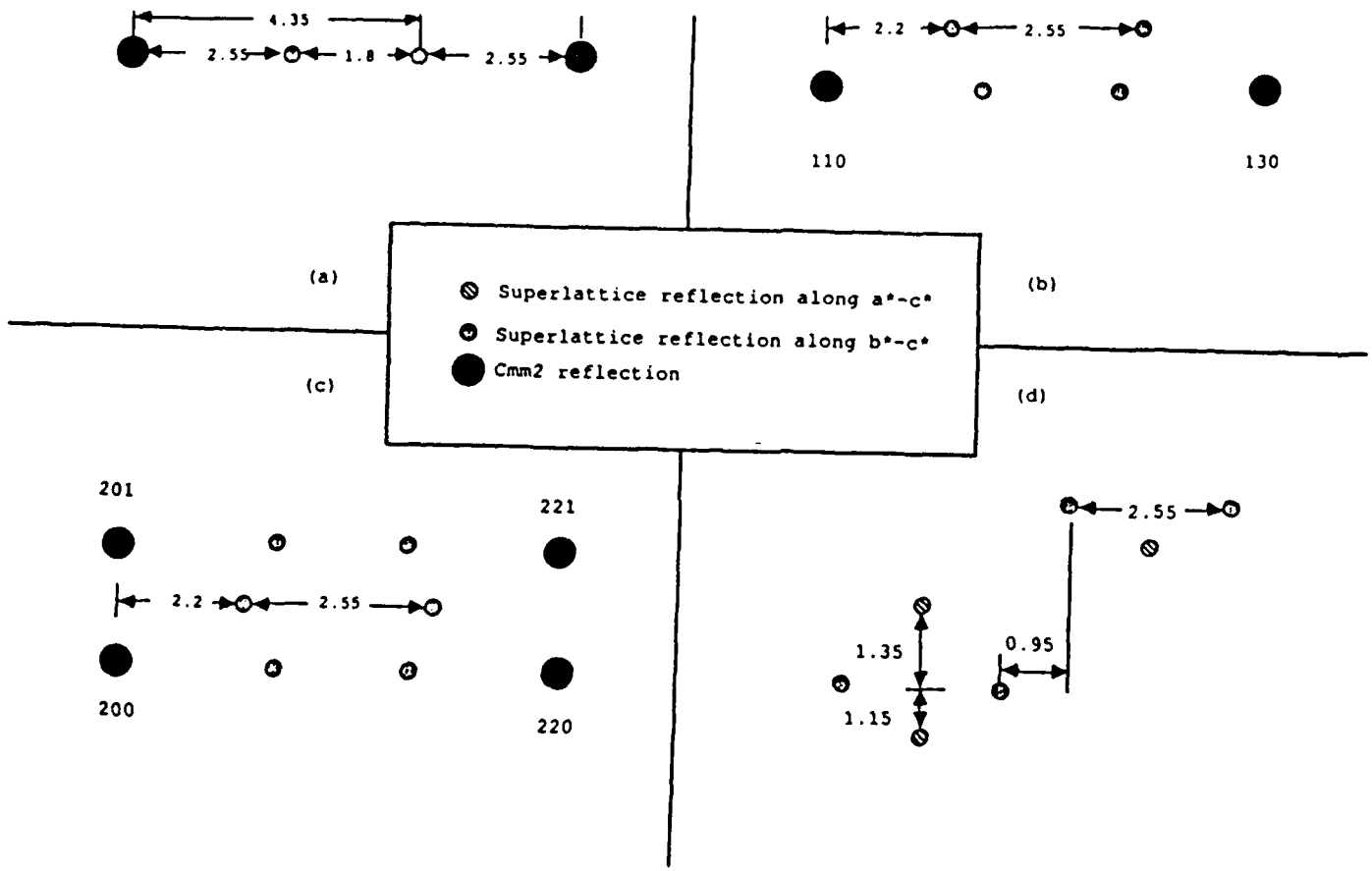

Figure 5 Schematic diagram of the superlattice and nonsuperlattice reflections with approximate distances for the BTG 10/13 crystal. All measurements in millimeters. (a) $0kl$; (b) $1kl$; (c) $2kl$; (d) superlattice reflections in $hk1/2$ photograph.

interchanged **a** and **b** axes. This type of twinning would have the effect of averaging the intensities and positions of the Cmm2 reflections, essentially making the crystal appear tetragonal. Therefore it is difficult to discern with x-ray photographs if the crystal is twinned, and to what extent. Because the superlattice reflections show the greatest difference between the **a** and **b** axes, twinning would be readily observed in these reflections. Figure 8 shows the *hk*1/2 photograph for the BTG 10/13 crystal. All reflections in this level are superlattice derived. The circled area on Figure 8 also shows very weak superlattice reflections along **a***, where they were not expected. Therefore, without the possibility of the 90° ferroelastic twinning, this would indicate that the **a*** axis was also modulated. No evidence of the twinning is seen in any other photographs, and this is unexpected if the crystal was twinned. Evidence from the low-temperature precession studies indicate that the superlattice along **a*** is not because of the presence of ferroelastic domains.

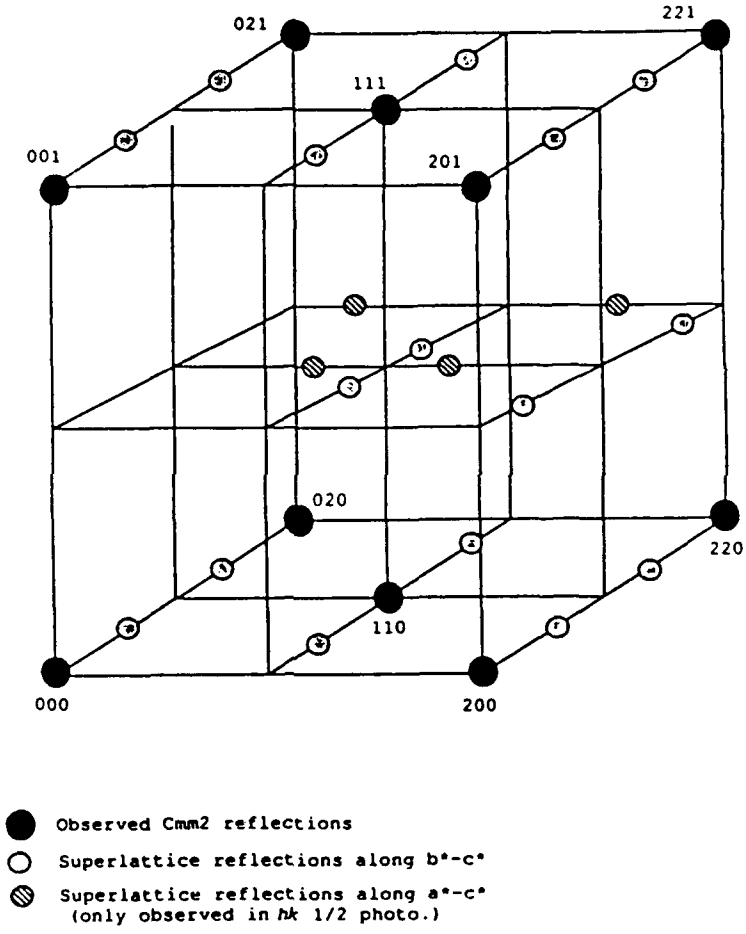

Figure 6 Three-dimensional view of the observed reciprocal lattice framework found in BTG crystals at room-temperature.

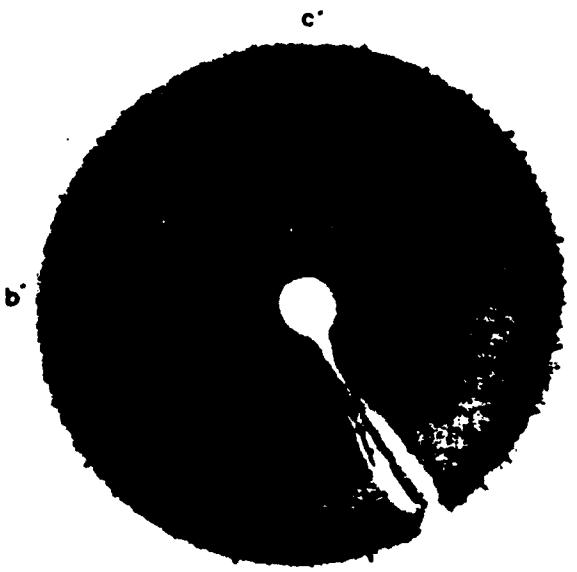

Figure 7 Precession photograph of the *1kl* reciprocal net of the BTG 10/13 crystal. The circled area shows the superlattice in the c*/2 zone. See figure 5b for a schematic enlargement with measurements.

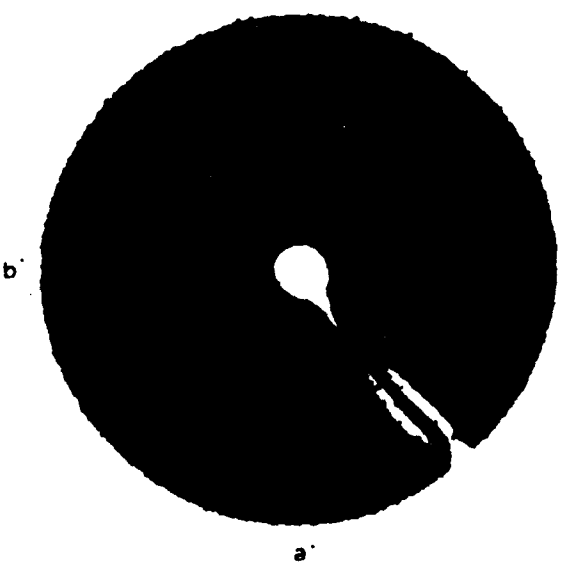

Figure 8 Precession photograph of the *hk*1/2 level of the BTG 10/13 crystal at 298 K. The circled area shows several weak superlattice reflections along a*. Figure 5d shows a schematic.

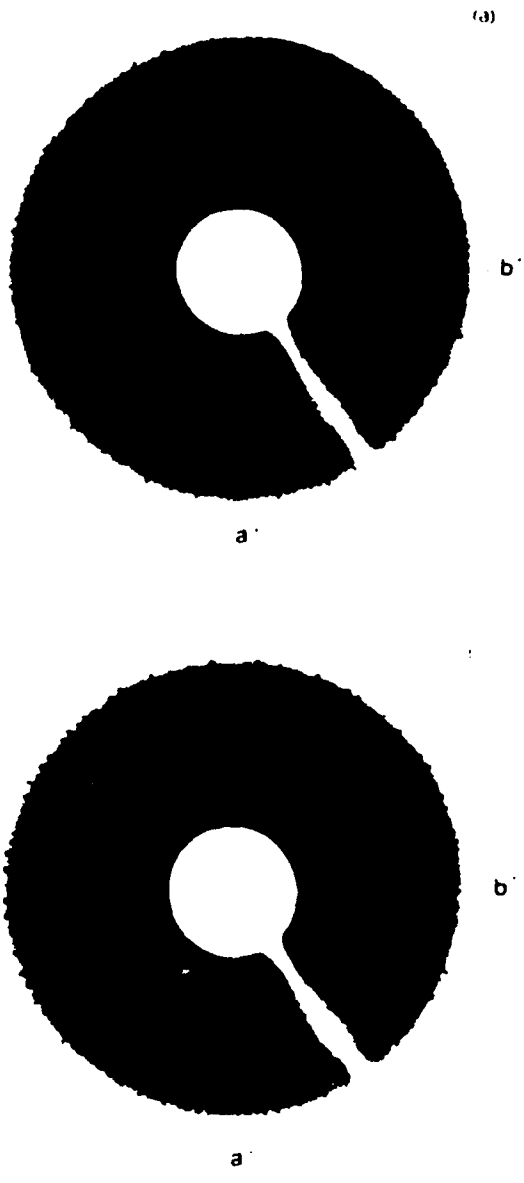

Figure 9 Precession photographs of the *hk*1/2 reciprocal net of the BTG 10/13 crystal taken at (a) 298 K and (b) ~210 K.

The average distances between the **a*** superlattice at room-temperature are the same as those in the **b*** superlattice (*hk*1/2 photograph). As shown in Figure 5d these are ~2.55 and 0.95 mm. Another observation made is that the superlattice along **a*** is not exactly centered with the **b*** zones, and that the asymmetry shown in Figure 5d is not affected by the mirror plane across {010}.

Another circumstantial piece of evidence against the twin model explanation for the superlattice along **a*** is found in the precession photographs of the BTG 3/16 sample. The BTG 3/16 boule does not show the pervasive twinning found in the BTG 10/13 boule. Yet the (*hk*1/2) precession photograph for the 3/16 samples show the superlattice in the **a*** direction. This observation is certainly *not* conclusive proof that this superlattice is not due to twinning.

The same suite of precession photographs taken for the BTG 10/13 crystal was also examined for the BTG 3/16 sample. The two crystals gave essentially identical precession photographs.

Low-Temperature Results

Low-temperature precession photographs were recorded on the same BTG 10/13 crystal used in the room-temperature study. As mentioned previously, because of the geometry of the technique only upper-level photographs were recorded. The 2*kl* and *h*1*l* low-temperature photographs are essentially identical to the room temperature ones. Both the superlattice reflections and the non-superlattice reflections show no measurable change in position or intensity, and the angular relations remains ≅90°.

The most significant change is found in the *hk*1/2 and *hk*1 photographs. Figure 9 shows two *hk*1/2 photographs: one taken at room-temperature and the other taken at low-temperatures (~210 K). In the room-temperature photograph (Figure 9a) the superlattice along **a*** is very weak, yet in the low-temperature photograph it is nearly equal, if not greater in intensity to the superlattice along **b*** (Figure 9b). These photographs display the orthorhombic **a*** and **b*** axes, and at 45° the prototypic tetragonal axes. Notice that in the room-temperature photograph the crystal appears to be orthorhombic; the {110} plane is not a mirror plane. However, in the low-temperature case the {110} plane does appear to be a mirror plane, giving the crystal a tetragonal appearance. It must be emphasized that this suggested mirror plane occurs only with the *hk*1/2 photographs. The average distances between the "sets" of superlattice reflections in the **a*** direction have decreased at low-temperatures to ~2.37 and ~1.12 mm. As discussed previously, these values are consistent with a commensurate superlattice of 1/3. Another unusual feature is that the asymmetry noted in Figure 5d shifts the other way in low-temperature phase.

Upon entering into the low-temperature phase a change was noticed in the *hk*1 precession photograph. On passing through the phase transition the superlattice is observed occurring along **a***, as shown in the circled region in Figure 10b. No superlattice is observed along **a*** at room-temperature. Although the superlattice reflections observed along **b*** in the room-temperature photograph (Figure 10a) appear to have become unobservable in the low-temperature photograph, they are in fact there, but weaker relative to the room-temperature intensity. The critical observation is that the superlattice along **a*** is now commensurate with a divisor of

1/3. In relation to the superlattice along **b***, the distance between superlattice reflections in **a*** is greater, from ~1.8 mm in **b*** to ~2.3 mm in **a***. These measurements (along with the observations in the low-temperature *hk*1/2 photograph) suggest the appearance of a commensurate superlattice along **a***, while the superlattice along **b*** remains incommensurate.

5 DISCUSSION

The goal of this study was to gain some understanding of the low-temperature phase transition occuring in $Ba_2TiGe_2O_8$. The phase transition is unusual for several reasons. It shows a strong signal in the pyroelectric coefficient p_3, yet only a slight signature in the dielectric data. It has a relatively rare polar-to-polar symmetry change. The material is ferroelastic, and the ferroelasticity is coupled with the appearance of a superlattice (Iijima *et al.*, 1981). The low-temperature phase transition is evidently composition dependent, as some samples show it, while others do not.

The dielectric data collected as a function of temperature show the transition in all three crystallographic directions (Markgraf, 1987). However, the transition does not produce peaks in the permittivity or dissipation (which are common in ferroelectric transitions), just discontinuities. In addition, hysteresis loops were not observed in either the room-temperature phase or the low-temperature one. These observations lead to the conclusion that the low-temperature phase transition does not involve ferroelectricity. The pyroelectric data are consistent with mm2 symmetry, both at room-temperature and low-temperature.

The average structure presented by Iijima *et al.* (1981) was confirmed on data taken on the BTG 3/16 crystal (Markgraf, 1987). The BTG 10/13 crystal was of insufficient quality for structure refinement (presumably because of the growth striations), but strong evidence (*precession photographs and MULTAN results*) leads to the conclusion that it too is in space group Cmm2. The oxygen atoms in the pyrogermanate groups show evidence of positional disorder. Iijima *et al.* (1981) have shown that the oxygen atoms around (at least) one of the germanium tetrahedra are prone to positional disorder. The oxygens in the refinement of Iijima *et al.* (1981) showed extreme anisotropic behavior.

As pointed out by Iijima *et al.* (1981) in their English summary, the modulated structure is most likely derived from the disorder in the skewed Ge_2O_7 groups. This modulation involves a "bending" of the Ge_2O_7 groups at the 1123 K transition. The bent nature of the Ge_2O_7 groups shifts the O(2) and O(5) atoms off their special positions (although for an average structure analysis they remain at this site), and thus skews the pyrogermanate members. Evidently this flexing also causes shifts in the O(3) and O(6) oxygens (see Figure 2) in the [001] direction, and leads to the observed doubling of the *c* lattice parameter. Disorder in the pyrogermanate groups explains the coupling of the superlattice in **b*** and **c***. There are in fact two different Ge_2O_7 groups in BTG, one oriented along **b*** and the other along **a***, and therefore a superlattice along **a*** is plausible. Arguments pro and con on the possibility of

ferroelastic twinning as a cause for the superlattice along **a*** have been discussed above, but there is one other point to be made. If the superlattice along **a*** was a result of twinning it should disappear in the low-temperature phase, because the ferroelastic domains are unstable in this phase. In fact the reflections become stronger, and are present in the low-temperature *hk*1 photograph. This observation implies that BTG is modulated in all three-dimensions, making it a very complex crystal.

The model suggested for the low-temperature phase transition from the analysis of the precession studies is an incommensurate to commensurate lock-in transition. Only the modulation along **a*** locks-in at a value of 1/3; the superlattice along **b***

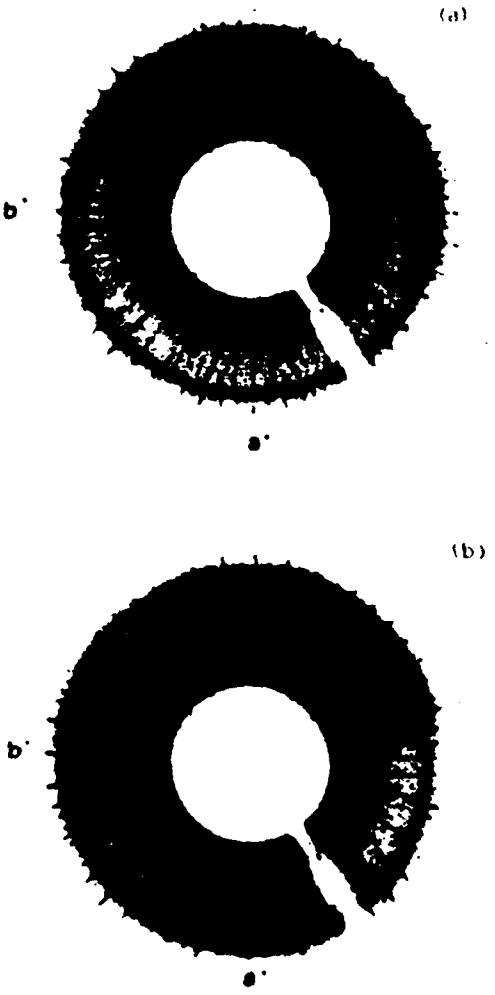

Figure 10 Precession photographs of the *hk*1 reciprocal net of the BTG 10/13 crystal taken at (a) 298 K and (b) ~ 210 K. The circled region shows the superlattice along **a***.

remains incommensurate. Lock-in transitions have recently received much attention, both theoretically and experimentally. Several of the unusual characteristics of the low-temperature phase transition in BTG may be satisfactorily explained by invoking a lock-in transition. Attention is now turned to those features.

The first indication that modulation vectors were involved in the low-temperature phase transition was in the ultrasonic velocity experiments (Markgraf, 1987). Most modes sampled did not show a strong anomaly upon passing through the phase transition. The longitudinal velocity in the [001] direction showed a slight inflection, as did the shear modes in the basal plane. But these signatures are small in comparison to the effect of the phase transition on the shear modes propagating down **a**, and/or **b**, and polarized in the **c** direction (Figure 11). It is not possible, because of the multi-domain nature of the sample, to ascertain whether one direction was undergoing a larger change at the transition; much information was lost because of the averaging effect of the twinning. The velocity data show that these modes stiffen at the low-temperature phase transition.

The ultrasonic velocity data in our studies (Figure 11) show the thermal hysteresis observed by Halliyal *et al.* (1985) in the piezoelectric properties. In compounds that are not modulated, the presence of thermal hysteresis at a phase transition generally indicates a volume change across the phase transition. This volume change means that the process in going from one phase to the other involves nucleation and growth, with the former being the more important parameter (Parsonage and Staveley, 1978). In a like manner a nucleation and growth process has been suggested for the observed thermal hysteresis in lock-in transitions. A model reviewed by Hamano (1986) suggested that an incommensurate crystal is composed of commensurate areas separated by discommensurations. Discommensurations are "domain walls" where the phase of the modulation changes abruptly. In cases where the incommensurate-commensurate transition leads to a ferroelectric commensurate phase, these discommensurations become the ferroelectric domain walls. In the discommensuration model the discommensurations are distributed throughout the incommensurate phase, approximately equal distances apart. When the commensurate crystal is heated above the lock-in temperature the discommensurations must nucleate on the underlying commensurate crystal. This nucleation process requires an activation energy, hence the thermal hysteresis. If this model holds for BTG, with a thermal hysteresis of ~ 45 K, the activation energy must be rather high.

This model for the thermal hysteresis at an incommensurate-commensurate lock-in transition is an intrinsic effect. Defects may also contribute to the thermal hysteresis by pinning the discommensurations (Hamano, 1986). Evidence that defects affect the low-temperature transition in BTG is found in the variation of the transition temperature. Often the transition temperature will vary by ± 5 K in successive dielectric and pyroelectric runs. Another feature attributed to defects in incommensurate crystals is the fixing of the incommensuration. Addition of impurities (i.e. defects) often fixes the incommensuration. No lock-in transition occurs in this "impure" crystal, whereas in the "pure" crystal it does. A good example of this dopant effect is found in the system $(Rb_{1-x}K_x)_2ZnCl_4$ (Hamano, Ema and Hirotsu, 1981). This may be why the BTG 3/16 crystal does not show the low-temperature phase transition.

This point cannot be discussed further without a better understanding of the impurities in both the BTG 3/16 and BTG 10/13 crystal, and so remains speculative. However, this model would explain the observation of the superlattice along **a*** in the BTG 3/16 crystal without the low-temperature phase transition.

The ferroelastic domains in BTG appear as a result of the 1123 K phase transition. This phase transition also stabilizes the modulated structure. In spite of the apparent coupling between the superlattice and the ferroelastic domains (a very rare occurrence), the instability of the domains in the low-temperature phase (Figure 3) was an unexpected result. The instability of these domains indicates a rise in the point-group symmetry of the crystal, the most likely candidate being tetragonal symmetry. Unfortunately the poor optics of the microscope used in these experiments prevented an interference figure from being obtained.

If the low-temperature phase was tetragonal, it would place BTG in the very rare class of compounds that have a low-symmetry phase sandwiched between two higher symmetry phases. The most widely known case is the ferroelectric Rochelle salt, $NaKC_4H_4O_8 \cdot 4H_2O$, which goes from $P2_12_12$ to $P2_1$ at 297 K, and then back to $P2_12_12$ at 255 K (Mason and Shirane, 1962). $Ba_2NaNb_5O_{15}$ (hereafter denoted as BNN) shows a suggested phase transition sequence of 4 mm to mm2 at ~573 K, and then back to 4 mm at 110 K (Schneck, Primot, Von der Mühll and Ravez, 1977). The key observation in this case was the disappearance of the ferroelastic domains in the crystal at 110 K. By way of comparison, the low-temperature phase transition in BNN shows very little change in the dielectric properties (which are much larger than BTG) and has thermal hysteresis. Also, the phase transition is very sample dependent, with quite a few BNN crystals not showing it (Schneck and Paquet, 1978). Laue photographs of BNN crystals taken at 80 K and room-temperature are similar

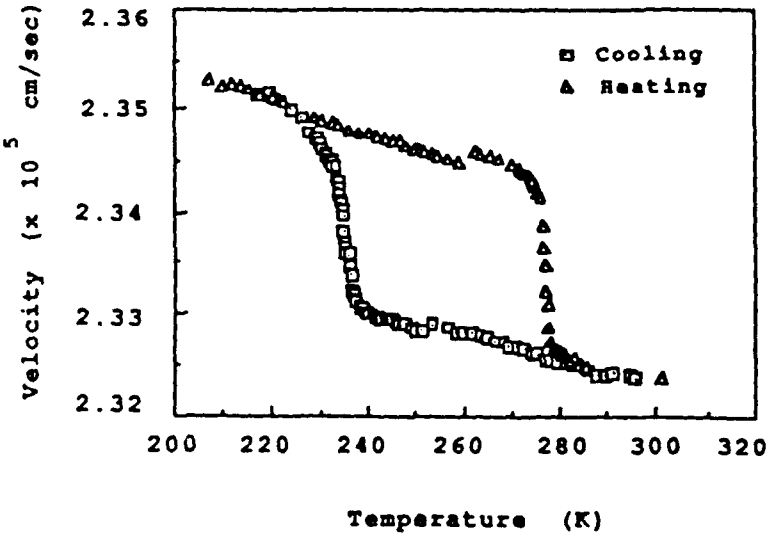

Figure 11 Ultrasonic velocity vs. temperature for shear wave propagating along an orthorhombic axis and polarized along c for heating and cooling run. BTG 10/13 crystal.

(Schneck *et al.*, 1977), indicating that only small displacements are involved in the phase transition. These aspects are similar with the observations in BTG. The work on the low-temperature phase transition in BNN, however, pre-dated the discovery of its incommensurate modulation (Tolédano, Schneck and Errandonéa, 1986, and references therein). Its role in the phase transition remains unclear.

In the results section for the low-temperature precession studies it was pointed out that, as preliminary analysis, {110} appeared to be mirror planes. Close examination of the intensities of the superlattice reflections rules out this mirror plane. There are several cases where the intensity mismatch across the {110} pseudo-mirror planes are quite noticeable. Figure 10b also shows an intensity inequality in the superlattice reflections between $\mathbf{a}^*$ and $\mathbf{b}^*$. The variation in the intensities implies that the crystal is not tetragonal.

The disappearance of the domains in the low-temperature phase remains an unexplained feature of the BTG crystal. Evidently the strong appearance of the superlattice along $\mathbf{a}^*$ leads to their instability. The explanation why a lock-in transition causes these domains to disappear is unclear. Lock-in transitions do not generally involve a change in the average crystal structure, although one case is known where a change in the average symmetry occurs. In $\{N(CH_3)_4\}_2CuCl_4$ the lock-in transition leads to a symmetry change of orthorhombic to monoclinic (Sawada, Sugiyama, Wada and Ishibashi, 1980).

Several aspects of the low-temperature phase transition in the 10/13 BTG crystal have been satisfactorily explained by postulating a lock-in transition along $\mathbf{a}^*$. What has not been addressed is the peculiar "memory" effect observed in the domain studies. Figure 3 shows that ferroelastic domains return to the same position after the low-temperature phase transition. An explanation, very speculative in nature, is that this behavior is similar to the "memory" effect observed in BNN (Tolédano *et. al.*, 1986) and Rb_2ZnCl_4 (Unruh, 1983). The model presented by these authors is that crystal imperfections at a temperature (called the annealing temperature, T_A) will stabilize the modulation vector and the associated discommensurations; that is, pin the modulation. The crystal then returns to that same defect pattern when it returns to that temperature. This model does not include any contribution from the underlying lattice pinning the domain structure. In particular, when the incommensurate phase is stable at T_A, passing from the commensurate phase to the incommensurate phase on heating will result in the reoccurrence of the same discommensuration pattern. The crystal in effect remembers its defect structure. In the case of the BTG crystal, T_A is (approximately) room-temperature, and the domains are pinned by the defects to the same position prior to the low-temperature phase transition. This explanation is speculative, and the low-temperature phase transition in BTG still has many aspects unresolved.

Acknowledgements

We would like to thank Z. P. Chang, R. E. Newnham, C. A. Randall, D. K. Smith, and J. K. Yamamoto for critical readings of this paper. Dr. Chang graciously provided a BTG crystal, and Dr. Smith made available his precession camera; we thank them for efforts made in our behalf. This study was funded in part by grants from the National Science Foundation and the Office of Naval Research.

References

Abrahams, S. C., and E. T. Keve (1971). Structural basis of ferroelectricity and ferroelasticity. *Ferroelectrics*, **2**, 129-154.

Alfors, J. T., M. C. Stinson and R. A. Matthews (1965). Seven new barium minerals from eastern Fresno County, California. *Am. Mineral.*, **50**, 314-340.

Drafall, L. E., and K. E. Spear (1976). Czochralski growth of $Ba_2Ge_2TiO_8$. *J. Cryst. Growth*, **33**, 180-182.

Halliyal, A. (1984). *Study of the Piezoelectric and Pyroelectric Properties of Polar Glass-Ceramics*. Ph.D. Thesis, The Pennsylvania State University, University Park, PA.

Halliyal, A., A. S. Bhalla and L. E. Cross (1985). Phase transitions, dielectric, piezoelectric and pyroelectric properties of barium titanium germanate $Ba_2TiGe_2O_8$ single crystals. *Ferroelectrics*, **62**, 3-9.

Hamano, K., K. Ema and S. Hirotsu (1981). Effect of impurities on the incommeensurate-commensurate phase transitions in Tb_2ZnCl_4, K_2ZnCl_4, and Rb_2ZnBr_4. *Ferroelectrics*, **36**, 343-346.

Hamano, K. (1986). Thermal hysteresis phenomena in incommensurate systems. In R. Blinc and A. P. Levanyuk (eds.), *Modern Problems in Condensed Matter Sciences, Vol. 14.2: Incommensurate Phases in Dielectric Materials*, North-Holland, Netherlands, Chap. 9, pp. 365-383.

Haussühl, S., J. Eckstein, K. Recker, and F. Wallrafen (1977). Growth and physical properties of fresnoite $Ba_2TiSi_2O_8$. *J. Cryst. Growth*, **40**, 200-204.

Iijima, K., F. Marumo, M. Kimura and T. Kawamura (1981). Structure of a ferroelastic crystal $Ba_2TiGe_2O_8$ and its thermal phase transition (in Japanese with English summary). *J. Chem. Soc. Jpn.*, **10**, 1557-1563.

Iijima, K., F. Marumo, M. Kimura and T. Kawamura (1982). Synthesis and crystal structures of compounds in the system $Ba_2TiGe_2O_8$-$Ba_2TiSi_2O_8$. *Mineral. J.*, **11**, 107-118.

Jona, F., and G. Shirane (1962). *Ferroelectric Crystals*, Peragamon Press, Inc., New York, NY.

Kimura, M., K. Doi, S. Nanamatsu and T. Kawamura (1973). A new piezoelectric crystal: $Ba_2Ge_2TiO_8$. *Appl. Phys. Lett.*, **10**, 531-532.

Kimura, M., K. Utsumi and S. Nanamatsu (1976). Ferroelastic behavior in $Ba_2Ge_2TiO_8$. *J. Appl. Phys.*, **47**, 2249-2251.

Lederhandler, S. R. (1959). Infrared studies of birefringence in silicon. *J. Appl. Phys.*, **30**, 1631-1638.

Markgraf, S. A. (1987). *Structure-Property Relations and Phase Transitions in Fresnoite-type Crystals*. Ph.D. Thesis, The Pennsylvanis State University, University Park, PA.

Masse, R., and A. Durif (1967). Spectrogramme d'absorption infrarouge de la fresnoite. Donnes cristallographiques du pyrogermanate isomorphe $Ba_2TiGe_2O_8$. *Bull. Mineral.*, **90**, 407-408.

Masse, R., J.-C. Grenier and A. Durif (1967). Structure cristalline de la fresnoite. *Bull. Mineral.*, **90**, 20-23.

Moore, P. B., and J. Louisnathan (1967). Fresnoite: unusual titanium coordination. *Science*, **156**, 1361-1362.

Moore, P. B., and J. Louisnathan (1969). The crystal structure of fresnoite, $Ba_2(TiO)Si_2O_7$. *Z. Kristallogr.*, **130**, 438-448.

Parsonage, N. G., and L. A. K. Staveley (1978). *Disorder in Crystals*, Oxford University Press, New York.

Post, B., R. S. Schwartz and I. Fankuchen (1951). An improved device for x-ray diffraction studies at low-temperatures. *Rev. Sci. Instrum.*, **22**, 218-219.

Rudman, R. (1976). *Low-Temperature X-ray Diffraction*, Plenum Press, New York, NY.

Sawada, A., J. Sugiyama, M. Wada and Y. Ishibashi (1980). Evidence of incommensurate-ferroelastic (commensurate) phase transition in $\{N(CH_3)_4\}_2CuCl_4$ crystal. *J. Phys. Soc. Jpn.*, **48**, 1773-1774.

Scheel, H. J. and J. Sommeraur (1983). Crystal growth and characterization of "striation-free" $KTa_{1-x}Nb_xO_3$ ($x = 0.26$) solid solutions. *J. Cryst. Growth*, **62**, 291-298.

Schmid, H., P. Genequand, H. Tippmann, G. Pouilly and H. Guedu (1978). Pyroelectricity and related properties in the fresnoite pseudobinary system $Ba_2TiGe_2O_8$-$Ba_2TiSi_2O_8$. *J. Mater. Sci.*, **13**, 2257-2265.

Schneck, J., J. Primot, R. Von der Mühll and J. Ravez (1977). New phase transition with increasing symmetry on cooling in barium sodium niobate. *Solid State Commun.*, **21**, 57-60.

Schneck, J., and D. Paquet (1978). Low temperature behavior of barium sodium niobate. *Ferroelectrics*, **21**, 577-578.

Tolédano, J. C., J. Schneck and G. Errandonéa (1986). Incommensurate phase of barium sodium niobate. In R. Blinc and A. P. Levanyuk (eds.), *Modern Problems in Condensed Matter Sciences, Vol. 14.2: Incommensurate Phases in Dielectric Materials*, North-Holland, Netherland, Chap. 17, pp. 233-252.

Unruh, H.-G. (1983). Pinning effects in incommensurately modulated structures. *J. Phys. C*, **16**, 3245-3255.

APPENDIX 53

ELASTIC ANOMALY IN FRESNOITE ($Ba_2TiSi_2O_8$) SINGLE CRYSTAL

Z.P. CHANG and A.S. BHALLA
Materials Research Laboratory, The Pennsylvania State University, University Park, PA 16802, USA

Received 28 August 1989

Ultrasonic velocities in fresnoite single crystal along several directions were measured from room temperature to above 200°C at 20 MHz. It was observed that an elastic anomaly occurs near 160°C. One of the shear mode velocities showed an anomaly at about 130°C. The anomalies may be attributed to a commensurate–incommensurate phase transition.

1. Introduction

Recently anomalous behaviors in the dielectric, piezoelectric and pyroelectric properties of a fresnoite ($Ba_2TiSi_2O_8$) single crystal were reported [1]. The dielectric constant, planar coupling coefficient and pyroelectric coefficient show a maximum value at 160°C and the frequency constant reaches a minimum at the same temperature. The sign of the pyroelectric coefficient, which is positive at room temperature, becomes negative at 190°C.

The possibility of a structural phase transition as the cause of the anomaly was tested by X-ray powder diffraction patterns taken from room temperature up to 400°C at intervals of 50°C. No significant changes in either *d*-spacings or intensities were detected [2]. An analysis of the intensity data at 24°C and 300°C also did not reveal any change in the crystal symmetry or space group of the crystal [2]. The origin of the anomaly is probably neither dielectric nor piezoelectric as described in ref. [1]. It will be interesting to investigate the elastic behavior as a function of temperature near 160°C.

2. Experimental

2.1. Growth of BTS single crystals

Single crystals of BTS were grown from the melt by the Czochralski pulling method. Starting materials were $BaCO_3$, SiO_2, and TiO_2 in stoichiometric proportion. SiO_2 was obtained from silicic acid $SiO_2 \cdot nH_2O$, in which the weight percent of SiO_2 was determined in a preliminary test by heating the silicic acid powder at 250°C for 3 h to remove the hydration water. The mixture of $BaCO_3$, SiO_2, and TiO_2 powders were calcined at 1090°C for 12 h for the first run but at 1250°C for the later runs. X-ray powder diffraction pattern confirmed the complete reaction of BTS after calcination at 1250°C. The growth conditions were: pulling rate 0.8–1.8 mm/h, crystal rotation 20–25 rpm, and the crucible being stationary.

In the first run, growth was initiated from a Pt wire, and the growth direction was close to [110]. For later runs, seeds along [100] and [110] were also used. The [100] direction has a slower growth rate. The grown crystals are colorless and transparent, about 1.7 cm in diameter and 3.5 cm in length for the first one, and smaller for the others. Facets of (001) and (110) were noticeable.

2.2. Ultrasonic wave velocity measurements

Ultrasonic velocity measurements were made using the pulse superposition method developed by McSkimin [3]. A quartz transducer with a resonance frequency of 20 MHz was bonded with Nonaq stopcock grease to one face of a pair of parallel faces. Constructive interference between the train of input pulses and the echos reflected from the other face leads to the determination of the transit time. The phase velocity is then calculated from the transit time

0167-577x/89/$ 03.50

and the thickness of the sample corrected for the thermal expansion [4]. Measurements were made in the temperature range from room temperature to above 200°C. A thermocouple for the temperature measurement was in direct contact with the sample. Typical rate of increase of the temperature was about 15–20°C/h. Satisfactory coupling for ultrasonic wave propagation can be obtained with Nonaq in the temperature range of the experiment, and in one of the runs, up to 250°C.

Fresnoite is tetragonal at room temperature. In the crystallographic [100], [110] and [001] directions, there are three pure modes of propagation: one longitudinal and two shear, the shear modes in the [001] direction are degenerate. For the ultrasonic measurements, samples with parallel faces normal to the [100], [110] and [001] directions were prepared. All the measurements were made on samples cut from boule no. 1. Because of the smaller size of boule no. 2, only a sample with [001] faces was prepared and used as a check at room temperature. Both the longitudinal and shear velocities agree very well between the two boules. The discrepancy is 0.13% for the former and 0.07% for the latter.

3. Results and discussion

The velocities as a function of temperature along the [100], [110] and [001] directions are shown in fig. 1. It is seen that anomalies also appear in the elastic property. For the longitudinal waves (curves a, b, and c), with increasing temperature from room temperature, the velocities decrease to a minimum at about 160°C. After that a rapid increase of about 4% in 60°C occurs for the [100] and [110] waves (curves b and a), whereas only a shallow maximum appears for the [001] wave (curve c). For the shear waves, the one propagating in the [100] and polarized in the [010] direction also showed large anomaly (curve d). However, the minimum occurs at about 130°C. A repetition of this run gave the same result. Good contact between the thermocouple and the sample was confirmed after the run, thus excluding the possibility of any wrong temperature reading. For the other shear waves in [001] and [110] directions, no anomaly was observed (curves e, f, and g).

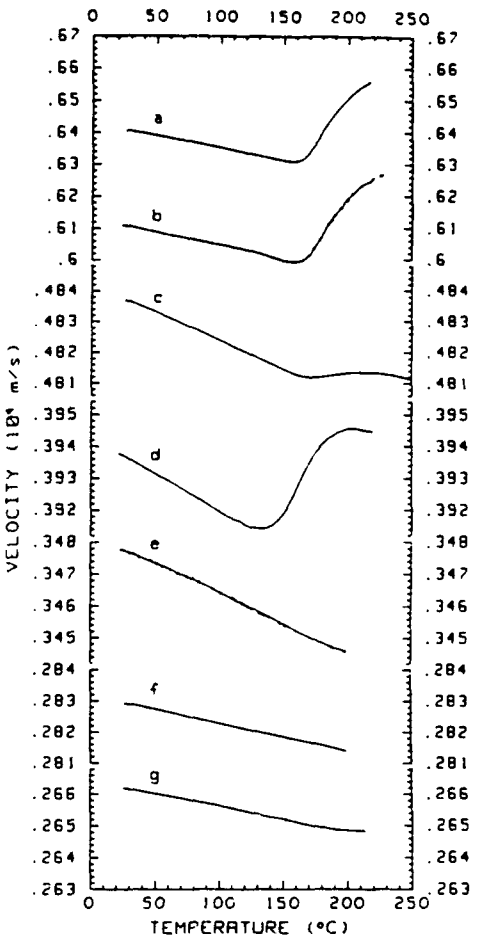

Fig. 1. Ultrasonic velocities for 7 modes in BTS versus temperature. (a) $L\|110$; (b) $L\|100$; (c) $L\|001$; (d) $T\|100$, $P\|010$; (e) $T\|110$, $P\|1\bar{1}0$; (f) $T\|110$, $P\|001$; (g) $T\|001$, $P\|100$. L and T indicate the propagation direction of longitudinal and transverse waves respectively, P indicates the direction of polarization. Measurements were made on heating. For runs b and e, data were also taken during cooling (indicated by dots).

Thus large anomalies indeed were observed in some of the ultrasonic velocities, indicating that the cause of the anomaly is probably in the elastic property. In some runs (curves b and e) in which data were successfully taken during decreasing temperature as indicated by the solid dots in fig. 1, no hysteresis was observed in the velocity versus temperature behavior, indicating that the change is reversible.

Recent studies using transmission electron mi-

croscopy suggest a commensurate–incommensurate phase transition near 160°C [5].

It is not clear why the shear wave propagating in the [100] direction and polarized in the [010] direction has a minimum at about 130°C which is different from the minimum at 160°C for the three longitudinal waves. More studies on the lattice vibration using Raman spectroscopy will be of interest.

The modes of wave propagation used in the present investigation show clearly the elastic anomalies. However, in order to obtain the complete set of elastic constants, two more propagation directions for the sound wave are needed. This due to the piezoelectric stiffening of the crystal. As a result, the piezoelectric constants also enter into the expressions for the sound velocities. Thus, a total of nine unknowns, six elastic and three piezoelectric constants, has to be determined simultaneously from the velocities. Presently, samples for propagation directions 45° and 60° away from the *c* axis in the *ac* plane are being prepared. The results will be reported later.

References

[1] A. Halliyal, A.S. Bhalla, S.A. Markgraf, L.E. Cross and R.E. Newnham, Ferroelectrics 62 (1985) 27.
[2] S.A. Markgraf, A. Halliyal, A.S. Bhalla, R.E. Newnham and C.T. Prewitt, Ferroelectrics 62 (1985) 17.
[3] H.J. McSkimin, J. Acoust. Soc. Am. 33 (1961) 12.
[4] A.S. Bhalla, *unpublished*.
[5] S.A. Markgraf, private communication.

APPENDIX 54

PYROELECTRIC AND DIELECTRIC PROPERTIES OF HEMIMORPHITE, $Zn_2Si_2O_7(OH)_2 \cdot H_2O$ *

S.A. MARKGRAF and A.S. BHALLA

Materials Research Laboratory, The Pennsylvania State University, University Park, PA 16802, USA

Received 24 March 1989

Pyroelectric, dielectric and other properties have been measured on naturally occurring hemimorphite $Zn_2Si_2O_7(OH)_2 \cdot H_2O$ crystals. Hemimorphite has a strong pyroelectric coefficient ($-45\ \mu C/m^2\ ^\circ C$ at room temperature), low permittivity and loss, and weak piezoelectricity, making it an appealing sensor material. Dehydrated hemimorphite is also polar, and selected properties of this material are presented.

1. Introduction

The investigation of polar crystals for use in a variety of sensor applications is a very active field. Commonly, ferroelectric materials are used for pyroelectric detectors, but there is some interest in non-ferroelectric (polar) crystals with large pyroelectric coefficients. These materials in general have low permittivity, small dielectric loss, weak piezoelectricity and do not show again effects common to ferroelectric materials. Several oxide crystals that fall into this class of compounds are $M_2TiX_2O_8$ (M: Ba, Sr; X: Si, Ge), M_2XO_3 (M: Li, Na; X: Si, Ge), $M_2X_2O_5$ (M: Li, Na; X: Si, Ge), and MB_4O_7 (M: Li, Pb, Sr, Ba). Historically hemimorphite ($Zn_2Si_2O_7(OH)_2 \cdot H_2O$) has been known to show strong polar properties [1], yet there are no modern quantitative measurements of the property coefficients. In this paper we report on the dielectric, pyroelectric, and related properties of single crystals of hemimorphite. Hemimorphite dehydrates at 450°C. At still higher temperatures hemimorphite undergoes two oriented conversions until willemite (Zn_2SiO_4) is obtained [2]. The $Zn_2Si_2O_7(OH)_2$ phase, because it has the same structure as hemimorphite minus the water molecule, should be polar.

* Dedicated to Professor Robert E. Newnham on the occasion of his sixtieth birthday.

2. Structure

The structure of hemimorphite has been the subject of a number of investigations. Both X-ray [3] and neutron [4] structure determinations have been performed. Hemimorphite consists of a three-dimensional framework of three-membered rings of one SiO_4 tetrahedron and two $ZnO_3(OH)$ tetrahedra oriented perpendicular to (010). This linkage creates three types of cavities: four-, six-, and eight-membered units parallel to (001) (fig. 1). The water molecule is located close to the center of the large

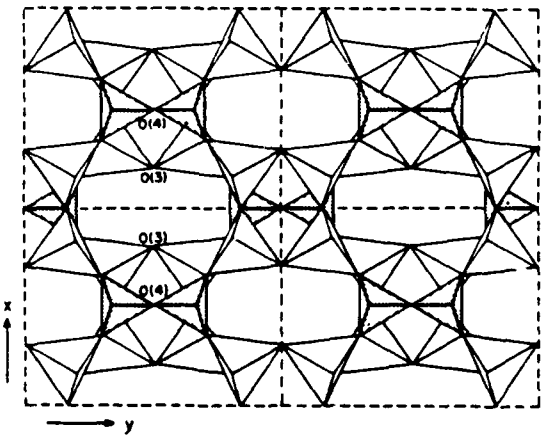

Fig. 1. (001) projection of four unit cells illustrating the $Zn(OH)O_3$ and SiO_4 (stippled) tetrahedral framework. After ref. [3].

0167-577x/89/$ 03.50 © Elsevier Science Publishers B.V.
(North-Holland Physics Publishing Division)

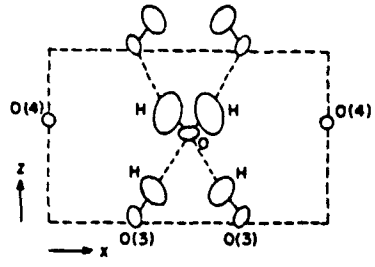

Fig. 2. (010) projection at $y=0.0$ showing the location of the water molecule. After ref. [4].

cavity, and is oriented parallel to (010) through hydrogen bonding with the hydroxyl groups (fig. 2). We would like to reiterate a point made by Hamilton and Finney [5] that compounds with zinc and silicon in tetrahedral coordination are often acentric. Further investigation into the acentric-related properties of these materials may be rewarding.

3. Experimental

The hemimorphite crystals used in this study were obtained from the Smithsonian Institute (Sample No. 147796), and were collected at the Potosi Mine, Santa Eulalia, Mexico. They occurred as large (between 1 and 3 cm) clear single crystals, with [001] as the growth direction. X-ray diffraction patterns showed only hemimorphite.

In order to examine the dielectric and pyroelectric properties a part of the crystal was cut into a thin [001] plate, polished, and electroded with sputtered gold. The dielectric constant and dissipation factor in the [001] direction was measured as a function of temperature (200 to 500 K) using an automated capacitance technique, and the pyroelectric constant was determined with a Byer–Roundy [6] technique. Both measurements were performed with a heating/cooling rate of 4°C/min, and have an accuracy of ± 5%. The piezoelectric d_{33} coefficient was measured with a Berlincourt d_{33} meter. This apparatus is intended for strongly piezoelectric materials, and was used merely to confirm that hemimorphite is a relatively weak piezoelectric. The planer electromechanical coupling coefficient was measured with standard resonance techniques. The second harmonic signal was tested with the Kurtz and Perry powder method [7] on powdered samples. A dehydrated sample of hemimorphite was obtained by heating the sample at 500°C for 12 h. The resulting crystal was opaque and fragile.

4. Results and discussion

The room-temperature pyroelectric coefficient for hemimorphite is -45 μC/m² °C. The pyroelectric coefficient is exceptionally high for a non-ferroelectric crystal. Fig. 3 presents the pyroelectric coefficient as a function of temperature on both heating and cooling runs. There is very little hysteresis. The dielectric constant (K_{33} at 1 MHz) was 11.8, and the tangent delta was in the range 0.002 to 0.004. A piezoelectric d_{33} coefficient of approximately 7 pC/N was measured, and a planer coupling coefficient of 10% was obtained. The same sample gave a second harmonic signal ten times that of quartz. Table 1 summarizes the as measured properties for hemimorphite. The pyroelectric properties are quite attractive for infrared devices.

Pyroelectric materials are useful as uncooled detectors of a wide variety of wavelengths (infrared being the most common; for a recent review see ref. [8]). There are many different designs and applications for these detectors (fast laser pulse detectors, pyroelectric vidicons, intruder detectors, fire alarms, etc.), and many different materials are available for these detectors: $LiTaO_3$, triglycine sulphate (TGS),

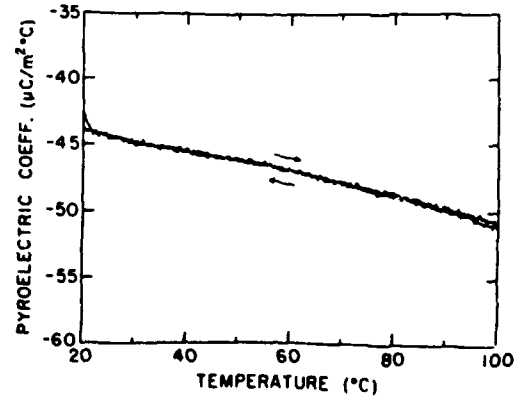

Fig. 3. Pyroelectric coefficient versus temperature for hemimorphite.

Table 1
Properties of hemimorphite and $Zn_2Si_2O_7(OH)_2$

	Hemimorphite	$Zn_2Si_2O_7(OH)_2$
pyroelectric coefficient (p_3; $\mu C/m^2\,^\circ C$)	−45	−10
piezoelectric coefficient (d_{33}; pC/N)	7	≈0
planer coupling coefficient (k_p; %)	10	-
SHG signal (times quartz)	10	
dielectric constant (K_{33})	11.8	7.2
tangent delta	0.003	0.001

$Sr_{0.5}Ba_{0.5}Nb_2O_6$, modified lead-zirconate ceramics. It is difficult to draft a figure of merit that covers all the applications and designs available. Aspects of the *material* properties of hemimorphite that are appealing to the design engineer are: weak piezoelectricity (weak microphony), no ferroelectricity (and hence no poling or aging), small dielectric constant (good for large area detectors) and low loss tangent (improved signal/noise ratio), and flat pyroelectric coefficient (thermal stabilization is not a serious factor). Although the pyroelectric coefficient in hemimorphite is smaller the figure of merit is quite competitive to the best materials currently in use. Also coming into consideration in detector design, but not discussed here, are thermal characteristics, and cost/availability.

Selected properties of dehydrated hemimorphite are also included in table 1. The loss of the water molecule results in a drop in pyroelectric coefficient by a factor of approximately 4. It is interesting to note that the strong pyroelectric properties are associated with the OH group.

5. Summary

Hemimorphite is a non-ferroelectric phase with a large pyroelectric coefficient. It has several appealing aspects for potential use as a pyroelectric detector, and because it is not ferroelectric will not depole or age. $Zn_2Si_2O_7(OH)_2$ is also polar, but with a much smaller pyroelectric coefficient.

Acknowledgement

We would like to take this opportunity to thank Professor Newnham for the many helpful discussions he has held with us over the years. We wish him a happy sixtieth birthday, and many more. We would also like to thank John White and the Smithsonian Institute for the hemimorphite crystals.

References

[1] S.B. Lang, Sourcebook of pyroelectricity (Gordon and Breach, New York, 1974).
[2] H.F.W. Taylor, Am. Mineral. 47 (1962) 932.
[3] W.S. McDonald and D.W.J. Cruickshank, Z. Krist. 124 (1967) 180.
[4] R.J. Hill, G.V. Gibbs, J.R. Craig, F.R. Ross and J.M. Williams, Z. Krist. 146 (1977) 241.
[5] R.D. Hamilton and J.J. Finney, Min. Mag. 49 (1985) 91.
[6] R.L. Byer and C.B Roundy, Ferroelectricity 3 (1972) 333.
[7] S.K. Kurtz and T.T. Perry, J. Appl. Phys. 39 (1968) 3798.
[8] R.W. Whatmore, Rept. Progr. Phys. 49 (1986) 1335.

DISTRIBUTION LIST

Scientific Officer Code: 1131
Wallace A. Smith
Office of Naval Research
800 North Quincy Street
Arlington, Virginia 22217-5000

Administrative Grants Officer
Office of Naval Research
Resident Representative N66005
Administrative Contracting Officer
The Ohio State University Research Center
1314 Kinnear Road
Columbus, OH 43212-1194

Director, Naval Research Laboratory
Attn: Code 2627
Washington, DC 20375

Defense Technical Information Center
Building 5, Cameron Station
Alexandria, Virginia 22314